H24/3660

MONASH UNIVERSITY
THESIS ACCEPTED IN SATISFACTION OF THE
REQUIREMENTS FOR THE DEGREE OF
DOCTOR OF PHILOSOPHY
ON..... 18 May 2004.....
.....[redacted].....
Sec. Research Graduate School Committee

Errata

1. Page 30, 3rd paragraph, 1st line, ignore repeated word "recently"; line should read "Recently, PEMFC technology has received...".
2. Page 38, 2nd paragraph, 2nd line should read "...three principal types of...".
3. Page 77, 2nd paragraph, 2nd line should read "...$Na_6Ru(SO_3)_4$ was prepared...".
4. Page 82, 1st paragraph, the company name in the 1st, 2nd, 4th and 5th lines should read "ADInstruments".
5. Page 95, 7th line should read "...in the case where platinum is immersed in...".
6. Page 120, 2nd paragraph, 4th line should read "...an important benefit...".
7. Page 121, 1st paragraph, 4th line should read "The chemical formula of the ruthenium...".
8. Page 140, 2nd line from the bottom should read "...to evolve from...".
9. Page 190, 2nd line from the bottom should read "...potentiodynamic cyclic scans between...".

ELECTRODEPOSITION OF PLATINUM-BASED CATALYSTS FOR POLYMER ELECTROLYTE MEMBRANE FUEL CELLS

A thesis submitted to the Faculty of Engineering, Monash University, in fulfillment of the requirements for the degree of *Doctor of Philosophy*

Scott Damon Thompson

B.Sc. (Hons)

School of Physics and Materials Engineering

Monash University

Australia

June 2003

Abstract

Within the present dissertation, some alternative approaches have been investigated for preparing catalysts for the polymer electrolyte membrane fuel cell (PEMFC). Typically, 80-90% of the noble metal catalyst, usually platinum, contained in PEMFC electrodes is not utilised in the electrochemical reactions. A more efficient utilisation of catalyst should enable reductions in PEMFC cost, which is the primary concern for the commercialisation of these systems. Electrodeposition of platinum and ruthenium has been the focus of this work, with the intention of achieving dispersed catalysts having high surface area-to-mass ratios. Another aim was to place these catalyst particles at the optimal interfacial sites where reactions readily occur.

An investigation into the electrochemistry of $H_3Pt(SO_3)_2OH$ is reported. Platinum was electroreduced from a solution of this complex acid onto glassy carbon (GC) in preliminary experiments and then onto carbon-black (CB) based electrodes as used in PEMFCs. During electrodeposition the platinum is thought to be poisoned by a sulphide (or retained sulphite species) that limits the growth of platinum particles during electrodeposition. Platinised electrodes were electrochemically cycled between the hydrogen and oxygen evolution potentials in H_2SO_4 solution in order to activate the platinum and obtain a reproducible surface area. Strong oxidation and reduction currents were observed during the potentiodynamic cycling treatments indicating gradual removal of the poisoning species. For a comparison, the poisoning effect of sulphite was investigated on both smooth platinum and Pt/GC electrodes using a $NaHSO_3$ solution. The Pt and Pt/GC electrodes were instantly deactivated in $NaHSO_3$ solution and were cleaned in a manner akin to the Pt/GC electrode prepared from electroreduction of $H_3Pt(SO_3)_2OH$. The platinum redox behaviour and surface area of these sulphite-poisoned electrodes was fully recoverable using the same potentiodynamic cycling treatment.

The electrochemistry of $H_3Ru(SO_3)_2OH$ was also investigated. Ru is an important alloying metal in fuel cell catalysts, particularly for operation on fuels such as hydrogen containing carbon monoxide, or methanol. Ruthenium was electroreduced from $H_3Ru(SO_3)_2OH$ solution onto GC and CB-based electrodes. It was found that the ruthenium surface was also poisoned, probably via a sulphide or sulphite species, in the same way as the Pt electroreduced from $H_3Pt(SO_3)_2OH$. Cleaning the Ru surface proved difficult via electrochemical cycling, since the metal electrodissolves at potentials less than those required to oxidise the poisoning species. The electrodeposition of Ru onto Pt electrodes and the co-electrodeposition of PtRu catalysts was also investigated.

A novel electrodeposition technique for platinising the catalyst layer of a PEMFC was also developed. This method is believed to deposit platinum particles in the necessary three-phase reaction zones (essential for catalysis in fuel cells), facilitating increased utilisation of platinum in comparison to conventional systems. This method consists of a two-step procedure involving the impregnation of platinum ions into a preformed catalyst layer (via an ion-exchange into the Nafion polymer electrolyte), followed by a potentiostatic reduction. The concentration of Nafion within the catalyst layer was found to have a significant bearing on the size of the platinum deposits. The preparation of catalyst layers containing a desired platinum loading should also be possible using this method.

Declaration

This thesis contains no material that has been accepted for the award of any degree or diploma at any university or other institution and, to the best of the author's knowledge, contains no material previously published or written by another person, except where due reference has been made in the text.

Scott Thompson

June 2003

Table of Contents

Chapter One *Introduction*

Chapter Two *Experimental Theory*

Chapter Three *Experimental Methodology*

Chapter Four *Platinum Poisoning During Electrodeposition*

Chapter Five *Ruthenium and PtRu Electrodeposition*

Chapter Six *Catalyst Deposition via Impregnation/Electroreduction*

Chapter Seven *Conclusions and Future Work*

List of Figures

List of Tables

Abbreviations

3PRZ	Three Phase Reaction Zone
AAS	Atomic Absorption Spectroscopy
ABARE	Australian Bureau of Agricultural and Resource Economics
ABS	Australian Bureau of Statistics
ADL	Arthur D. Little, Inc.
AFC	Alkaline Fuel Cell
CARB	California Air Resources Board
CB	Carbon-Black
CE	Counter Electrode
CTFE	Chlorotrifluoroethylene fluoropolymer
CV	Cyclic Voltammetry
DMFC	Direct Methanol Fuel Cell
EDXS	Energy Dispersive X-ray Spectroscopy
EPA	Environment Protection Agency
ESA	Electrochemical Surface Area
EV	Electric Vehicle
EVAA	Electric Vehicle Association of the Americas
EW	Equivalent Weight
GC	Glassy Carbon
GDE	Gas Diffusion Electrode
HER	Hydrogen Evolution Reaction
HOR	Hydrogen Oxidation Reaction
ICE	Internal Combustion Engine
IEA	International Energy Agency
IEE	The Ion-Exchange/Electroreduction Method (Chapter Six)
IISE	The Impregnation and *In Situ* Electroreduction Method (Chapter Six)
IPCC	Intergovernmental Panel on Climate Change
IPCS	International Programme on Chemical Safety
LANL	Los Alamos National Laboratory

MEA	Membrane-Electrode Assembly
NASA	National Aeronautics and Space Administration
OER	Oxygen Evolution Reaction
ORR	Oxygen Reduction Reaction
PAFC	Phosphoric Acid Fuel Cell
PEM	Polymer Electrolyte Membrane
PEMFC	Polymer Electrolyte Membrane Fuel Cell
PTFE	Teflon®, poly(tetrafluoroethylene)
RE	Reference Electrode
SCE	Saturated Calomel Electrode
SEM	Scanning Electron Microscopy
SHE	Standard Hydrogen Electrode
SOFC	Solid Oxide Fuel Cell
UNESCO	United Nations Educational, Scientific and Cultural Organization
WE	Working Electrode
WHO	World Health Organisation
ZEV	Zero Emission Vehicle

Nomenclature

ε	Efficiency
η_i	Polarisation
ρ	Density
C_{dl}	Double-layer capacitance
d	Particle diameter
E°	Standard potential
E_i	Initial potential
E_l	Lower potential
E_{red}	Electroreduction potential
E_u	Upper potential (scanned to in a CV or linear sweep)
i_{dl}	Current due to the charging of the electrical double-layer (between an electrode surface and the solution)
j	Current density (relative to the geometric area of the electrode)
j_a	Anodic current density (positive, e.g. from an oxidation process at the WE surface)
j_c	Cathodic current density (negative, e.g. from an reduction process at the WE surface)
j_{dl}	Current due to the charging of the electrical double-layer between the electrode surface and the solution
Pt/C	Platinum supported on carbon
Pt-H_{ads}	Protons adsorbed on a platinum surface
Pt-O_{ads}	Platinum surface oxides
S	Specific surface area (i.e. surface area per mass, e.g. $m^2\ g^{-1}$)
-SO_3H	A sulphonic acid group of the Nafion® PEM
V_{SCE}	Voltage with respect to the SCE
V_{SHE}	Voltage with respect to the SHE
W	Loading (i.e. mass/electrode surface area, e.g. $mg\ cm^{-2}$)

Acknowledgments

I am very grateful for having received a Monash University Departmental Scholarship (from the former Department of Materials Engineering) during my PhD candidature. I have also become indebted to a vast number of people for friendships and help (scientific and otherwise) both during the initial stages and throughout:

Firstly, to my principal supervisor, Prof. Maria Forsyth, not only for guidance throughout, but also for managing to keep so much in perspective (and having a seemingly unending well of optimism, regardless of the circumstances or lack of coffee)!

Secondly, to my provisional supervisor, Prof. Barry Muddle, for helping greatly, particularly in the early stages, and for being one of the prime movers in developing the whole inter-departmental project.

Special thanks to Dr. Larry Jordan, Dr. Neil Avery, Tom Berhsing and Prof. Ashok Shukla.

Thanks also for the support from the Chemistry/Mat. Eng. "Electrolytes Group," in particular Dr. Kate Nairn, Dr. Peter Newman and Prof. Doug MacFarlane.

Thanks to the School of Physics and Materials Engineering (SPME) staff, workshops and postgrads for experimental aid and for many enjoyable years. Cheers also to Dr. Tony Trueman and Steven Knight at DSTO.

Of course, the HUGEST thanks go out to those most dear to me- Katy, my family, Katy's family and my friends (yeah, it's pretty clichéd, I know).

Also, thanks (and apologies!) to all those who learnt not to ask, "So how's the thesis coming along?" too often (or at least choosing your words *very* carefully)...

to Katy

Chapter One

Introduction

As society becomes more industrialised there is an increasing need to develop sustainable, more efficient power sources. Non-renewable sources such as fossil fuels provide the bulk of our present electrical energy, as they have since the Industrial Revolution. However, not only is the eventual demise of fossil fuel reserves inevitable, but the increasing quantity of carbon dioxide and pollutants released from these materials in power generation has become a major concern for the well-being of both humanity and earth's ecosystems. Air pollution is directly linked to respiratory disease and acid rain, whilst CO_2 is a major contributor to global warming.

The development and widespread usage of efficient, environmentally sustainable power sources, i.e. those operating on renewable energy sources, has therefore become a significant aspiration. Renewable energy sources include hydro-electric, geothermal, solar, wind, tidal and wave energy. The storage of surplus energy obtained from these sources is also an important consideration. One promising option is the conversion of renewable energy to hydrogen, for later conversion to electricity via a fuel cell. A fuel cell is essentially an electrochemical device that enables the conversion of chemical energy at much higher efficiencies and in a more environmentally acceptable manner *cf.* most conventional power sources.

Affordability is probably the main limiting factor towards the widespread commercialisation of fuel cell technology. A considerable amount of research has been undertaken on material cost reduction and ways of improving the operating performance of fuel cells for everyday applications. A major area for continued research is the reduction in the amount of expensive catalyst material (e.g. platinum) used in the low-temperature fuel cells. For the high-temperature fuel cells, a reduction in the operating temperature is desired (or else the development of superior materials to withstand the corrosion and thermal expansion problems at ~ 1000 °C). Once fuel cells become financially equivalent or superior (e.g. via improved fuel efficiency) to conventional power sources, a widespread fuel distribution infrastructure is expected to arise as a result of supply-and-demand.

Over the last two decades, the capabilities of fuel cells have been improved to the extent that many fuel cell types are now comparable to existing technology. This is particularly true in the case of the polymer electrolyte membrane fuel cell (PEMFC) and the internal combustion engine. In most ways, the PEMFC is comparable in performance to the conventional car engine, and in some ways they are far superior (particularly in fuel efficiency and lack of undesirable emissions). This fuel cell technology is predicted to be commercially available in vehicles from as early as 2010, according to General Motors [*Burns, 2002*], and possibly even by 2004, according to DaimlerChrysler [*Kable, 1999*]. In December 2002, Honda and Toyota separately released the first few 'market ready' hybrid electric vehicles (EVs), powered by a battery and a PEMFC, for testing under typical driving conditions in California [*Hydrogen Fuel Cell Letter, 2002*]. The demonstration of such prototype PEMFC and hybrid-powered EVs by the major auto-makers illustrates the rise of the PEMFC as a highly viable candidate for future power generation.

This dissertation seeks to minimise the amount of platinum-based catalysts used in PEMFCs via alternative preparation methods, to aid in making these fuel cells more affordable.

1.1 Energy

Energy is required by all life-forms. Plants harness solar energy. Animals obtain energy from chemically breaking down molecules in foodstuffs. During the last 30-40 000 years, humans have discovered how to harness an increasing number of energy sources. Today, the global demand for energy is forever increasing due to the continual growth in population and the technological advancement of all societies.

One of the earliest forms of energy harnessed by primitive humans was fire. The chemical reaction between oxygen and a carbonaceous material releases heat and light. Dried plant materials such as wood may 'burn': the combined chemical energy

of the reactants (carbon and oxygen) is higher than that of the product (CO_2), and the difference in energy is released (in this case as heat and light). For a chemical reaction to occur spontaneously, it is essential that the total energy of the products is less than that of the reactants; Fig. 1-1 illustrates this general process. In more recent centuries, energy has been extracted from more complex carbonaceous substances, such as fossil fuels, which have much higher energy densities.

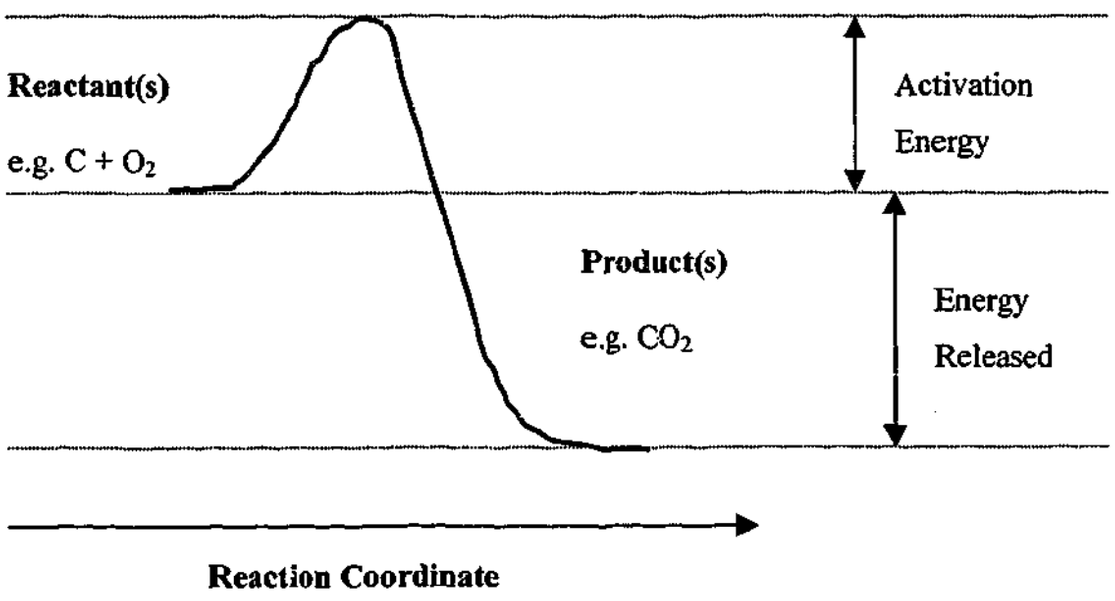

***Fig. 1-1** A schematic representation of the release of energy in an exothermic reaction. In most cases, it is preferable for the released energy to be greater than the energy required to initiate the reaction (the activation energy).*

Another form of commonly available energy is 'potential energy', which is derived from the Earth's gravitational field. Potential energy is determined from the mass of an object, the gravitational force and the height of the object above the earth's surface (for most typical situations). The force of gravity is utilised in producing hydro-electric power, where the natural flow of water to a lower altitude is

harnessed by turbines. The potential energy of the water is converted to 'kinetic energy' (which is determined from its mass and velocity) as it is allowed to flow through the turbines. The turbines are linked to a generator that converts this energy to electrical power. Hydro-electric power is considered a 'renewable' energy source, since its operation does not involve the consumption or conversion material resources and it is potentially available in unlimited quantities. Of course, the use of hydro-electric power generally involves the damming of a river valley, and this may cause the loss of considerable land area and also destroy the habitat of many species, so it is not necessarily a particularly environmentally-friendly solution. Furthermore, most dams fill up with silt after 20 to 50 years [*Lomborg, 2001*].

Other renewable energy sources include tidal, wave and wind energy, Table 1-1. Power generation from these sources involves harnessing the kinetic energies of water or wind and the subsequent conversion of these sources to electrical energy. An increasing number of such power stations are being built in many locations around the world. The other major renewable energy sources include solar energy (radiation from the sun) and geothermal energy (heat from the earth in volcanically active regions). Solar and geothermal energy may be used for either thermal or electrical power generation. Photovoltaic arrays are used to convert solar radiation energy to electricity. Solar radiation also plays a role in atmospheric fluctuations (along with effects from the earth's rotation) and thus is also partially responsible for wind energy.

All of these renewable energies sources can be used to produce electricity (in fact, any energy source can be converted to electricity), and this electricity may then be used or stored in batteries or capacitors for later use. Similarly, chemical energy may be converted in a fuel cell to electrical energy (however, so far these power sources have experienced use only in specialist applications such as in the space industry and remote area power). Renewable electricity could be used to produce H_2 and O_2 by the electrolysis of water for later re-conversion back to electricity via a fuel cell. The production of H_2 and O_2 could also be performed by electrolysis from conventionally attained electricity in off-peak times, to be later converted back to

electricity via fuel cells to either increase the efficiency of coal or nuclear power plants, or to help with peak energy requirements. The storage of energy as H_2 is predicted by many as the form of energy storage and transportation in the future: the 'hydrogen economy'. Unfortunately, some energy is always lost during the conversion of 'fuels'- batteries and fuel cells can never attain 100% conversion efficiency, although if the energy is gained from renewable resources then this method remains advantageous. Further, for power in remote locations (where fuel cells are presently being utilised in small quantities) this energy loss is less than that which would result in the transmission of electricity over several hundred kilometers.

The conversion of chemical energy to heat, light or electricity is the other major source of energy used globally. This includes the combustion of fossil fuels (oil, natural gas and coal) and 'combustible renewables and waste' (CRW), Table 1-1. CRW is defined by the International Energy Agency as comprising a range of various substances such as solid and liquid biomass (including plant matter and animal waste) to municipal and industrial waste, Table 1-2 [*IEA, 2002*].

Atomic or nuclear energy is utilised in some countries, which harnesses some of the energy within atomic nuclei (by the splitting of e.g. uranium nuclei). The heat generated in nuclear fission is used to create steam, which then rotates turbines, creating electrical power. There are presently more than 420 nuclear reactors around the world, in particular ~ 104 in the US, ~58 in France, ~52 in Japan, ~35 in the UK, and ~29 in the former USSR [*Commons et al., 1999*].

ENERGY SOURCE	*ADVANTAGES*	*DISADVANTAGES*
Coal	Large Australian Reserves; Low Cost; Easily Mined; Export Income	Non-renewable; Higher Pollution *cf.* Oil and Natural Gas
Oil	Some Australian Reserves; Ease of Transportation; Many Uses	Non-renewable; Limited Global Supply; Pollution
Natural Gas	Some Australian Reserves; Moderate Cost; Efficient Source of Domestic Heat	Non-renewable; Pollution (but Least of all Fossil Fuels)
Nuclear	Large Australian Reserves; High Energy Output per Fuel Mass; Low Accident Rate; Export Income	Non-renewable; Radioactive Waste Disposal; Severity of Accidents; Security Risks
Hydro-Electricity	Renewable; Low Operating Costs; Minimal Pollution	Limited Sites; Dam Construction Destroys Local Habitats
Solar	Renewable; Low Operating Costs; Efficient Heating; Minimal Pollution	Weather Dependency; Need for Large Collector Areas (Low Utilisation of Solar Rays: 10-14% efficient)
Wind	Renewable; Low Operating Costs; Minimal Pollution	Weather Dependency (> than 5 m s^{-1} needed; Limited Sites
Tidal/Wave	Renewable; Low Operating Costs; Minimal Pollution	Weather and Tidal Time Dependency; Limited Sites
Geothermal	Renewable; Low Cost; No Pollution; Heating at 30- 80 °C	Limited Sites; Deep Digging required
CRW*	Renewable; Biogas uses Waste	Limited Supply; Low Efficiency

Table 1-1 *Advantages and disadvantages of a range of energy sources; taken from Commons et al., 1999 and James et al., 2000.*
**CRW (combustible renewables and waste) is defined in Table 1-2.*

CRW FUEL CATEGORY	*DEFINITION*
Solid Biomass and Animal Products	Wood, vegetal waste, animal materials/wastes, sulphite lyes (black liquor), and other solid biomass including charcoal.
Gas/Liquids from Biomass	Combustible biogas derived from the anaerobic fermentation of solid wastes.
Municipal Waste	Wastes produced in the residential, commercial and public service sectors, including hospital waste.
Industrial Waste	Solid and liquid products e.g. tyres that are combusted directly in specialised plants.

Table 1-2 *The fuel sources constituting combustible renewables and waste (CRW); definitions taken from the International Energy Agency [IEA, 2002]. 97% of CRW is considered as biomass, both commercial and non-commercial [IEA, 2002]. All categories of CRW may be combusted directly to produce heat and/or power, in some cases the fuels may be converted into other forms before combustion.*

1.1.1 Global Energy Use

The combustion of non-renewable fossil fuels to provide heat and/or electricity accounted for nearly 80% of the World Total Primary Energy Supply (TPES) in the year 2000, Table 1-3. Oil comprises more than one-third of the global energy use. "Constituting 1.6% of global GDP, oil is today the most important and most valuable commodity of international trade" [*Lomborg, 2001*]. Nuclear energy is the other major non-renewable energy source used globally, accounting for ~ 7% of the global TPES, Table 1-3. In the countries with nuclear power, around 20% of energy is obtained from this source [*ibid.*].

Fuel	*Share of World TPES (%)*	*Share of World Electricity Production (%)*
Oil	34.8	8.0
Coal	23.5	39
Gas	21.1	17
Renewables	13.8	19
Nuclear	6.8	17

Table 1-3 *The fuel shares of the global Total Primary Energy Supply (TPES) and of the global electricity production during the year 2000; data taken from the International Energy Agency [IEA, 2002].*

Renewable fuels constitute a considerable proportion of global energy sources (~ 14%, Table 1-3), and of these, CRW represents almost 80%, Table 1-4. Hydro-electric power also makes up a large amount of globally used renewable energy, at 16.5%. The remaining renewables (geothermal, solar, wind and tidal power) constitute less than 0.5% of the global TPES (or 3.7% of all renewables).

For global electricity production, coal is the main source, at 39%, followed by renewables (19%), and gas and nuclear (both at 17% each), Table 1-3. Of the renewables accounting for electric power, 92% of all renewables was generated from hydro-electric sources, 5% from CRW and less than 3% from geothermal, wind and solar combined [*IEA, 2002*]. Oil is used much more heavily in transportation, hence the difference in TPES and electricity production with oil.

Breakdown of Renewables	*Share of Renewable TPES (%)*	*Share of World TPES* (%)*
CRW*	79.8	11.0
Hydro-Electric	16.5	2.3
Geothermal	3.27	0.44
Solar	0.298	0.039
Wind	0.192	0.026
Tide	0.030	0.004

Table 1-4 *The breakdown of renewable energy sources and the share of each in terms of total renewables and of the global Total Primary Energy Supply (TPES) during the year 2000; data taken from the International Energy Agency [IEA, 2002].*
** CRW= combustible renewables and waste.*

The annual growth in the global TPES has been at 2.1% over the last 30 years, which is identical to the growth in the total renewables supply [*IEA, 2002*]. However, over this time scale, the annual global growth of CRW was slightly lower, at 1.8%, and that of hydro-electric power a little higher, at 2.7% [*IEA, 2002*]. For the remaining 'new' renewables (*viz.* geothermal, solar, wind and tidal power) the accumulated annual global growth was recorded at 9.4%, a considerable increase in comparison [*IEA, 2002*]. Of these new renewables, wind and solar power experienced the fastest

development, with 52.1 and 32.6% annual growth[i], respectively [*IEA, 2002*]. These last figures are promising for the proliferation of future 'clean' power sources, however for this to occur, the price of energy from these sources will need to be competitive with that from fossil fuel and nuclear power. This may be realised via either governmental subsidies of these new sources, or higher costs placed on energy derived from fossil fuels (e.g. similar to carbon taxes, to penalise the causes of pollution), and the efficiencies resulting from the greater development of these new technologies.

Already the cost of wind and solar power has decreased by 94- 98% over the last 20 years [*Lomborg, 2001*] however, even by 2020 wind may remain 20% more expensive *cf.* the least expensive electricity available from gas. Lomborg believes that half of the world's energy needs could realistically be covered by windmills (about 100 million required). Windmills are viewed by some as noisy, and of poor aesthetics, however these problems are solved if placed out at sea, where windmills may become 50% more efficient [*ibid.*]. A Greenpeace-related website even claims: "There is enough wind resource spread across the six continents to meet the entire energy consumption of the world roughly four times over" and that "enough sunlight strikes the earth each hour to meet all human needs for a year" [*Choose Positive Energy URL*]. Lomborg suggests that solar radiation is equivalent to about 7000 times our global energy consumption, and that a 220 000 km^2 area (e.g. 2.6% of the Sahara Desert) could harvest all of our global energy needs using the conventionally available 15- 20% efficient solar cells. Unfortunately, despite the fact that the wind and solar energy are 'free' sources, the energy source does not constitute the bulk of the cost. For example, in 1995, the fuel price of fossil fuels only constituted about 16% of the electricity cost [*Lomborg, 2001*]. Additionally, fossil-fueled power sources have been in use for a much longer time, and have been highly refined and made more efficient over time.

[i] It should be noted that this growth remains a great deal less *cf.* the slower percentage growth of conventional energy use, e.g. oil expanded at 2% between 1990-8 (*cf.* 22% for wind) however, the energy derived from oil was ~ 320 times greater than that of wind in 1998 [*Lomborg, 2001*].

Over the next 30 years, the International Energy Agency predicts that if the OECD[ii] governments implement a "new range of energy and environmental policies now under consideration," that non-hydro renewables could grow at an annual growth of 4% (in the IEA's 'alternative policy scenario') [*IEA, 2002*]. The share of renewables in the TPES would be 40% greater than without governmental intervention nor technological breakthroughs (i.e. *cf.* the 'reference scenario') [*IEA, 2002*]. By 2030, the 'reference scenario' forecasts that the world share of total renewables could drop from 13.8% (in Table 1-3) to 12.5%, largely due to a shift from the use of biomass in developing countries to fossil fuels [*IEA, 2002*]. There is no doubt a large amount of energy is available in renewable sources- the question is whether the driving forces are strong enough to promote such a dramatic change in our energy infrastructure.

Developing countries account for 73% of renewables at present; by 2030 the use of these renewables (mostly biomass for cooking and heating) may have decreased by 12%. The growing use of power derived from fossil fuels in developing countries is not necessarily a concern in itself, since pollution resulting from biomass can also be considerable for a given amount of energy. However, once a strong fossil fuel infrastructure is implemented in developing countries it will be difficult to change and increased energy usage (and thus more pollution) may more readily eventuate. It may be worthwhile for e.g. the OECD nations to help instigate renewable power (other than CRW and hydro-electric) in the developing world. This could be greatly beneficial to all- while the developed nations phase out their usage of fossil fuels, they could also help other nations in bypassing the 'fossil fuel stage'.

[ii] Organisation for Economic Cooperation and Development. 30 nations including: Australia, Austria, Belgium, Canada, Czech Republic, Denmark, Finland, France, Germany, Greece, Hungary, Iceland, Ireland, Italy, Japan, Korea, Luxembourg, Mexico, Netherlands, New Zealand, Norway, Poland, Portugal, Slovak Republic, Spain, Sweden, Switzerland, Turkey, United Kingdom, and the United States.

1.1.2 Energy Use in Australia

In the year 2000, Australia's energy supply was about 2.1% of the TPES for the rest of the OECD nations (and ~ 1.1% of the global TPES), Table 1-5. 6.3% of our total energy supply was derived from renewable sources, which is roughly equivalent to the OECD average but under half that of the world's total. However, the share of 'renewables excluding CRW' of the TPES in Australia was half that of either the global or OECD average in 2000. This last statistic shows that Australia is lagging behind the majority of the OECD nations in the use of non-CRW derived renewable energy, and as a result a higher proportion of our renewable energy is contributing to pollution. However, the proportional usage of non-CRW renewables in Australia is roughly equivalent to the combined global usage (of the total renewables).

Region	*TPES (Mtoe)**	*Renewables (%)*	*Renewables-CRW (%)*
Australia	110.2	6.3	1.4
OECD	5316.9	6.2	2.8
World‡	9957.5	13.8	2.8

Table 1-5 *A comparison of the Total Primary Energy Supply (TPES), the share of renewables, and the share of renewables excluding combustible renewables and waste (CRW) during the year 2000 in different regions; data taken from the International Energy Agency [IEA, 2002].*
**Mtoe stands for 'million tonnes of oil equivalent' (1 toe = 41.868 GJ).*
‡ The world includes all nations (i.e. OECD also).

The Australian Bureau of Agricultural and Resource Economics (ABARE) has predicted that over the next 20 years, "Australia's reliance on imported crude oil is expected to increase significantly" (in the absence of major discoveries), and that coal and oil will continue to supply the bulk of Australia's energy needs [*Dickson et al., 2001*]. The consumption of fossil fuels provided most of the energy and electricity in Australia during 1998-99 (with shares greater than 90% for each) and

this is not expected to change significantly by 2020, Table 1-6. This share of fossil fuel derived power in Australia is considerably higher than that in the global TPES (compare Tables 1-3 and 1-6). In particular, almost twice the amount of coal is used in Australia (both in overall energy consumption and in electricity generation), reflecting our large coal reserves (8% and 15% of the global black and brown coal known world reserves, respectively [*ABS, 2001*]). In addition, the lack of nuclear power in Australia helps to account for the comparatively large share of fossil fuel derived power.

Fuel	*Primary Energy Consumption (%)*		*Electricity Generation (%)*	
	1998-99	2019-20	1998-99	2019-20
Black Coal	28.2	24.8	54.8	52.3
Brown Coal	13.2	9.4	24.5	18.8
Oil	34.8	35.6	1.1	1.2
Natural Gas	18.0	23.9	10.7	18.3
Renewables	5.9	6.3	8.9	9.4
Biomass	4.5	4.8	0.6	2.0
Biogas	0.2	0.3	0.2	0.6
Hydro-Electric	1.2	0.9	8.1	5.9
Solar	0.1	0.1	0.0*	0.8*
Wind	0.0	0.1	0.0	0.1

Table 1-6 *The primary energy consumption and electricity generation by fuel in Australia over 1998-99 and a 20-year prediction; data taken from the Australian Bureau of Agricultural and Resource Economics [Dickson et al., 2001].*
**Numbers missing from the ABARE conference paper [Dickson et al., 2001], determined here from the remaining percentage.*

On 1 April 2001 the Australian government's Mandatory Renewable Energy Target commenced, requiring an additional generation of 9500 GWh of renewable electricity per year by 2010 [*Dickson et al., 2001*]. Interim targets were implemented (e.g. 300 GWh required in 2000). 9500 GWh (or 0.82 Mtoe) corresponds to about half of the renewable electricity generated in 1998-99, or about one-third of that predicted by the ABARE study for 2019-20. This is a promising initiate, although the actual forecast for renewable electricity growth (2.6% p.a.) trails the large annual growth forecast for natural gas (4.9%). Some compensation may be found in the fact that natural gas is responsible for much less pollution *cf.* coal, and electricity generation from both black and brown coal is predicted to decrease in Australia over the next 20 years, Table 1-6. In 2009-10, biomass (mainly bagasse) is forecast to constitute ~ 42% of the renewable electricity, with wind (26%), new hydro (17%) and biogas (11%) comprising the remainder [*Dickson et al., 2001*]. The major increase in renewable energy use in Australia over the next 20 years is therefore expected to take place in the electricity generation sector.

A brief overview of the breakdown of energy use in different sectors is also useful. In 1998-99, the largest energy consuming sectors in Australia were transport (40.5%) and manufacturing (31.7%), followed by residential (12.6%) [*Dickson et al., 2001*]. These were not forecast to change significantly by 2020. Around 97% of the fuel mix in transportation comprised liquid fuels derived from oil products [*Dickson et al., 2001*], as is the case in the US [*Kreith et al., 1999*]. Road transport (65% passenger cars, 35% road freight) accounted for 78% of the total transportation energy consumption; air transport was the second largest consumer at 14%. The high share of energy consumption by the transportation sector is very important in terms of total pollution. In fact, as Section 1.1.3.2 illustrates, a large proportion of the air pollution in major cities originates from vehicular exhaust, particularly particulate matter from diesel engines. Many other dangerous toxins are also produced from vehicles, for example, in the US automobiles account for nearly 80% of the CO emissions [*Kreith et al., 1999*], a toxic gas that has recently been linked to asthma in children.

1.1.3 Reasons for Alternative Power Generation Technologies

Energy security, pollution and global warming are the most significant issues that may be solved by the use of renewable energy sources and alternative technologies such as fuel cells. These issues are discussed in the following sections.

1.1.3.1 Renewable Fuels and the 'Hydrogen Economy'

Indeed, the reserves of fossil fuels are limited, just like all material resources on earth. It is unlikely that the global fossil fuel supply will ever be completely depleted, rather, supply will eventually fall, forcing prices to rise and allowing alternative energies to become competitive. Alternative fuels, particularly renewable fuels are the logical energy progression for the 'fossil free age', but whether these fuels will be required due to a dwindling fossil fuel supply, or from other driving forces (e.g. pollution and/or global warming effects- see the next section) is yet to be observed.

It has been widely predicted that the current oil reserves will be depleted[iii] in the next 40-60 years, and this will have a significant impact, particularly on transportation. Some studies have even estimated that the world oil-supply will fail to meet demand as early as 2010 [*Hatfield, 1997 and Kerr, 1998*], causing a dramatic increase in the price of petroleum. In a recently published book [*Kreith et al., 1999*], 12 oil experts provided estimates of when the global oil supply will peak, and all estimates (made between 1995 and 1999) were in the range 2000- 2025, with the average year being 2012. Reserves of coal are expected to last a great deal longer (~ 240 years, *cf.* only ~ 60 more years for natural gas) at present rates [*Commons et al., 1999*]. Thus, there is little concern in the electricity generation sector, with coal remaining relatively plentiful. Coal may continue to comprise a large share of

[iii] Many people question predictions of this nature, due to poor forecasting in the past. A group of scientists in the 1970s forecast that oil would be depleted by around the year 2000. However, the scientists responsible (whom worked in the solar energy field) were not experts in the oil or gas industries and may have had a conflicting interest in promoting solar energy [*Kreith et al., 1999*].

electricity generation both globally (~ 40%) and in Australia (~ 80%). However, since such a high percentage of oil is used in the transportation sector, research into alternative power generation technologies such as fuel cells (which may readily operate on renewable fuels) has increased considerably in recent years.

The commonly-held belief that the global oil supply is in rapid decline has been recently challenged by Bjørn Lomborg[iv]. Lomborg argues that the scarcity of a substance is usually determined from its price, and the price of oil has remained roughly constant over the last 100 years (aside from a few anomalies, including the OPEC oil crisis in the 1970s). Rising oil prices have merely increased prospecting, and correspondingly, more reserves have been found. Mining technology is continually being improved, but nevertheless more than half of the oil remains in the ground with today's techniques [*Lomborg, 2001*]. Lomborg believes that oil will last for a long time yet. Tar sands and shale oil also contain a vast amount of the world's oil. It is possible to increase the global oil reserves if the price of oil rises: a 50% increase could be achieved if the price rises to US$30 barrel^{-1} (up from $27 in 2000); if the price increased to US$40 barrel^{-1}, this could enable the exploitation of ~ five times the present oil reserves [*ibid.*]. It is actually estimated that there exists ~ 240 times more shale oil *cf.* conventional oil reserves, which at our present energy consumption could last for more than 5000 years [*ibid.*]. Of course, the cost of extracting oil in more difficult minerals and regions may be the deciding factor, and the cost of other energy sources will become more comparable. Lomborg also believes there is sufficient coal resources for "well over 1500 years," and that the amount of natural gas remaining at present consumption rates (60 years) could be doubled by the exploitation of methane in coal beds.

In fact, if the price of oil rises too high research into extracting fuel sources from other reserves, e.g. oil shales and tar sands, will be increased, along with promotion of renewable energy sources. Eventually, as the price of oil rises to an uneconomic

[iv] Whilst it is noted that Lomborg was accused of scientific dishonesty and use of selective data [*Pianin, 2003; McMichael, 2002*]. Lomborg was not found to be grossly negligent by the Danish Committees on Scientific Dishonesty and has not formally found to be scientifically dishonest [*Pianin, 2003*].

level a new energy source will take its place. The transition may well be seamless. As Sheik Ahmed Zaki Yamani, the former oil minister for Saudi Arabia said in June 2000, "The Stone Age came to an end not because we had a lack of stones, and the Oil Age will come to an end not because we have a lack of oil" [*Yamani, 2000*]. Even the Greenpeace organisation appears to agree: "...we are in a second world oil crisis. But in the 1970s the problem was a shortage of oil. This time round the problem is that we have too much" [*Greenpeace URL*].

Yamani also told Britain's Sunday Telegraph newspaper that he believed "...that after five years there will be a sharp drop in the price of oil. The price will stay high for the moment because of high demand". Successful oil exploration and the development of new technologies that did not use oil, such as fuel cells, were cited by Yamani as the main reasons for the predicted fall in oil prices. In addition, oil-derived fuels are being utilised at much higher efficiencies with advancing technologies, enabling the extraction of more energy from an equivalent amount of fuel. "The hybrid engines will cut gasoline consumption by something like 30 percent," Yamani was quoted as saying. In the past, the "average US car has improved its mileage by 60% since 1973" [*Lomborg, 2001*].

Additionally the possibility of political instability in the Middle East, where more than half of known oil reserves are located [*Lomborg, 2001*], is concerning for most governments due to the oil reliance of most developed nations. The US is one of the world's largest oil users and relies heavily on oil imports (around 56% of oil consumed in 2000 was estimated to have been imported- over US$50 billion [*Kreith et al., 1999*]), which is not only an issue for energy security, but also represents a large cost to the US economy. Australia has a similar reliance on oil imports, with estimates that by 2020, 52% of all the oil consumed in Australia will originate from imports [*Dickson et al., 2001*]. However, considering the range of other energy options being developed, including a great deal of renewable power, this 'reliability' point may be valid only in the short term.

Regarding nuclear power, enough uranium-235 (U^{235}) is estimated to remain for about 100 years, however, with fast breeder[v] reactors, Lomborg believes there could be enough for 14000 years. Aside from the production of radioactive waste (some materials with half-lives of more than 100 000 years), the safety of nuclear reactors, and security concerns (e.g. the use of plutonium in nuclear weapons), the actual energy efficiency of nuclear power is around double that of fossil fuels [*Lomborg, 2001*]. The development of fusion remains a future possibility, and if it ever proves to be successful, fusion could drastically alter the energy picture. The hydrogen isotope deuterium (H^2) is a likely fusion fuel, and is economically available in sea-water.

Any rise in oil prices or reduction in reliability will act to promote more research into (and greater use of) renewable fuels. Renewable fuels such as CRW or renewable electricity (from solar, hydro, CRW, geothermal, tidal/wave sources etc.), do not necessarily have to be utilised within alternative power generation technologies such as fuel cells. It is conceivable that conventional power stations and the internal combustion engine could be modified to operate on the combustion of many different fuels (or else these fuels could be modified to suit the power stations/engines). Any electricity generated could, of course, be stored in batteries for later use. However, by far the most promising alternative is the conversion of these renewable fuels or electricity to hydrogen for later re-conversion back to electricity via fuel cells. The PEMFC is the most promising candidate of the various fuel cell types, being particularly suited for either vehicular power and also for localised combined-heat-and-power generation in residential situations. Fuel cells will be discussed in more detail later.

[v] In the operation of these reactors, the more commonly available uranium-238 isotope is also placed in the reactor core. Some of the radiation produced during the fission of uranium-235 converts the uranium-238 to plutonium-239, another nuclear fuel.

1.1.3.2 Air Pollution

Air pollution (from all sources) is believed to cause about 5% of all annual deaths [*WHO, 2001*]. Health effects such as respiratory diseases, asthma and lung cancer are also related to air quality. Air pollution is by far the most serious type of pollution in the interests of human health. One of the simplest ways to express the degree of air pollution on health has been to estimate the cost of air pollution per capita. In both the US and the UK, the most significant of the pollutants is particulate matter (i.e. smoke and soot) constituting ~ 82% of the present cost [*Lomborg, 2001*]. PM_{10} and $PM_{2.5}$ refer to small particles of less than 10 or 2.5 microns in diameter respectively, which are believed to pass deep into the lungs and alter normal functioning [*ibid.*]. Other air pollutants with a significant bearing on health include sulphur dioxide (SO_2), ozone (O_3), lead, nitrogen oxides (NO and NO_2, collectively 'NO_X') and carbon monoxide (CO) [*ibid.*]. Appendix B outlines the adverse health effects of common air pollutants.

A considerable amount of energy is consumed by transportation, and correspondingly, vehicles produce a significant proportion of pollution. In fact, the World Health Organisation (WHO) believe that "motor vehicles account for about 30% of emissions of nitrogen oxides, 50% of hydrocarbons, 60% of lead and 60% of carbon monoxide in cities of developed countries" [*WHO, 2001*]. Around 14% of the total CO_2 present in the atmosphere is believed to have been contributed by vehicles [*IPCS, 1992*]. Polycyclic aromatic hydrocarbons (PAHs), ozone (O_3), and particulate matter are also released from diesel and internal combustion engines.

Pioneering governmental actions in California during the 1990s have proved groundbreaking in both increasing air pollution restrictions and in encouraging cleaner vehicular technologies. In 1990, the US Federal "Clean Air Act" provided a number of programs requiring cleaner fuels and also paved the way for the Californian air restrictions [*US EPA, 1994*]. The California Air Resources Board (CARB) passed regulations in 1990, requiring carmakers to put small demonstration fleets of zero-emission vehicles (ZEVs) on the road in the 1990s, and then begin

major ZEV production and marketing by 2003 [*CARB, 2001*]. It was mandated under the CARB regulations that 2% of the biggest selling car manufacturers' fleets (General Motors, Chrysler, Ford, Toyota, Nissan, Honda and Mazda) be zero-emitting by 1998 [*Kreith et al., 1999*]. Following CARB studies and reports from auto-makers, in 1995 CARB recognised that the "current battery technology and vehicle technology fall short of that necessary to produce a car that meets consumer expectations and acceptance," and the 1998 ZEV target was suspended [*Kreith et al., 1999*]. However, the mandate for 10% of new car sales be zero-emitting by 2003 remained. The CARB regulations also anticipate that the requirement for ZEVs will be raised gradually to 16% by 2018 [*CARB, 2001*].

Los Angeles, in particular, has been notorious for high levels of smog (a petrochemical haze formed from the reaction of hydrocarbons and NO_x with sunlight) in past decades. During the 1970s, Los Angeles commonly had 100 or more Stage 1 smog alerts per year. These alerts were greatly reduced over time-there were no Stage 1 smog alerts in 1999 nor in 2000, yet more than 95% of Californians lived in areas that failed to meet federal or state air quality standards [*CARB, 2001*]. About 50% of smog-forming pollutants still come from petrol and diesel fuelled vehicles [*CARB, 2001*], and auto emissions account for 90% of the state's CO and 77% of its NO_x [*Motavalli, 2000*]. Although cars currently sold in California are 98% cleaner than those sold 30 years ago [*CARB, 2001*], the CARB regulations were implemented in response to air pollution levels that may get out of control again due to continued population growth and increased driving rates.

Incentives for purchasing/leasing and using ZEVs in California and many other US states [*EVAA, 2002*] have been provided, since these are not as affordable as conventional vehicles. Such incentives have included the use of carpool lanes, free parking in certain places, discounts towards electricity used to recharge ZEV batteries and services to help with the use and maintenance of ZEVs [*CARB, 2002*]. Federal initiatives include the elimination of a luxury tax on alternative fuel vehicles and tax credits.

Electric vehicles such as battery and fuel cell-powered cars are generally considered ZEVs. At present, all ZEVs are battery-powered (excluding a very small number of fuel cell prototypes- refer to Section 1.3.5). A PEMFC operating on pure hydrogen produces water as the only emission, and is considered a ZEV. For an EV to really be 'zero-emitting' the origination of the electricity or hydrogen needs to be produced from a non-polluting source (e.g. nuclear, hydroelectric, solar, wind, etc.).

1.1.3.3 Global Warming

A phenomenon known as 'global warming' is generally believed to be occurring, although the future possibilities of this are very difficult to predict. Generally, most scientific reports suggest that the global temperature has increased over the last 1000 years, and especially during the last 100 (by 0.4- 0.8 °C [*Lomborg, 2001*]). Rajendra K. Pachauri, the Chairman of the UN's Intergovernmental Panel on Climate Change (IPCC), recently delivered a keynote address on global warming at the recent World Summit on Sustainable Development (Johannesburg, 2002). Pachauri outlined some of the main findings from the IPCC's Third Assessment Report, with predictions that global warming might have on agricultural practices. "Increasing global surface temperatures are very likely to lead to changes in precipitation and atmospheric moisture," Pachauri said, which is expected to cause "an increase in annual precipitation in high- and mid-latitudes and most equatorial regions" and "a general decrease of annual precipitation in the sub-tropics" [*Pachauri, 2002*]. The sub-tropics, where more droughts are likely to be achieved, include areas such as the Sahel, the Middle East, China and Western Australia. In addition, Pachauri said the report forecast an "increased frequency of heavy rainfall events" are expected with global warming, however, even the changes in annual precipitation are expected to be small up to 2080 "when compared with natural multi-decadal variability."

The difficulties in predicting future changes in weather patterns, global temperatures and other related phenomena such as ocean levels has made such forecasts either very broad in outcomes (such as the 40 possible scenarios presented in the IPCC report [*IPCC, 2001*]), or highly unreliable with so many unknown factors and interrelated systems. Some of the main findings of IPCC's Third Assessment Report are presented in Table 1-7.

The main issues, in terms of human prosperity, are (i) to what extent have recent industrial practices affected global warming? (i.e. how much effect does CO_2 have on the temperature) and (ii) what may be done to alleviate any future global warming? Additionally, modeling the possible greenhouse scenarios is important, although such forecasting is very complicated and potentially unreliable.

The influence on temperature[vi] of the man-made 'greenhouse gases' (which trap heat, thus contributing to global warming) have been apportioned by the IPCC as follows: 60% CO_2, 20% methane, 14% halocarbons such as CFCs, and 6% N_2O (as reported in [*Lomborg, 2001*]). Carbon dioxide is by far the most significant of these gases, and ~ 80% of the additional CO_2 is believed to arise from the combustion of fossil fuels (the remainder from e.g. deforestation) [*ibid.*]. Oceans and forests re-absorb ~ 55% of this extra CO_2, with the rest remaining in the atmosphere [*ibid.*]. Since pre-industrial times, the atmospheric concentration of CO_2 is believed to have increased by about 31% [*ibid.*].

The IPCC's Summary for Policymakers (taken from the IPCC's Third Assessment Report, 2001) states the following in regards to future opportunities for reducing vulnerabilities to climate change [*IPCC, 2001*]: "Greenhouse gas emissions, as well as local and regional pollutants, could be reduced through more efficient use of energy and increasing the share of lower carbon-emitting fossil fuels, advanced

[vi] In fact, the extent of global warming that may be directly attributed to greenhouse gases is difficult to ascertain. Substantial fluctuations in the global temperature are believed to have occurred throughout the last 10 000 years, with possible swings of up to 8 °C over a 1500 year time-scale [*Lomborg, 2001*]. In addition, other factors including sunspot activity, clouds, water vapour, and sulphate particles are also considered to have a significant bearing on global temperature modeling [*ibid.*].

fossil-fuel technologies (e.g., highly efficient combined cycle gas turbines, fuel cells, and combined heat and power) and renewable energy technologies (e.g., increased use of environmentally sound biofuels, hydropower, solar, wind- and wave-power)."

IPCC Robust Finding*
The 1990s was very likely the warmest decade in instrumental record.
CO_2, CH_4, N_2O and tropospheric O_3 increased substantially since the year 1750.
Some greenhouse gases have long lifetimes (e.g. CO_2, N_2O and halocarbons).
Most of the observed warming over the last 50 years is likely due to increases in greenhouse gas concentrations due to human activities.
CO_2 concentrations increasing over 21st century are virtually certain to be mainly due to fossil fuel emissions.
Nearly all land areas are very likely to be warm more than the global average, with more hot days and heat waves.
Rise in sea level during 21st century that will continue for further centuries.
The adverse impacts of climate change are expected to fall disproportionately upon developing countries and the poor persons within countries.
Ecosystems and species are vulnerable to climate change and other stresses, and some will be irreversibly damaged or lost.
In some mid- to high-latitudes, plant productivity would increase with small increases in temperature. Plant productivity would decrease in most regions of the world for warming beyond a few °C.
Many physical systems are vulnerable to climate change (e.g. the impact of coastal storm surges will be exacerbated by sea-level rise, and glaciers and permafrost will continue to retreat).
Greenhouse gas emission reduction (mitigation) actions would lessen the pressures on natural and human systems from climate change.

***Table 1-7** Some selected 'robust' findings of climate change by the IPCC, taken from the Summary for Policymakers [IPCC, 2001].*
** The term 'Robust Finding' is used by the IPCC to denote a finding that "holds under a variety of approaches, methods, models and assumptions and one that is expected to be relatively unaffected by uncertainties."*

1.2 Fuel Cells

The fuel cell is an alternative power technology that may operate on a wide range of fuels. As mentioned before, fuel cells may operate on fuels from renewable energy sources including, *inter alia*, methanol or hydrogen produced from biomass and hydrogen electrolysed from water (using renewable electricity). Fuel cells also enable increased power generation efficiencies from fossil fuels. Fuel cells offer increased versatility compared with battery technologies in many applications, particularly via flexibility in fuel type and fuel storage, greater longevity and higher power densities. At present fuel cell technologies are not economically competitive with existing power sources, and are undergoing considerable development. The following section will outline the operation, components, types and potential uses of fuel cells.

1.2.1 Fuel Cell Technology

A fuel cell is an electrochemical power source, similar in operation to a battery, except with an external reactant supply. Hydrogen is the simplest fuel and oxygen the simplest oxidant (but air is commercially more feasible). Unlike a battery, a fuel cell does not require recharging, and will continue to produce power (direct current) as long as the reactants are supplied. Sir William Grove demonstrated the first fuel cells in 1839, consisting of platinum electrodes in an aqueous acid electrolyte, operating on hydrogen and oxygen[vii]. However, little fuel cell development transpired over the next one-hundred years, until the potential of fuel cells in space applications was realised.

[vii] Francis Bacon is recognised for building the first practical fuel cell unit in the 1950s, incorporating aqueous KOH electrolyte between porous nickel electrodes [*Austin, 1967*]. The Bacon cell could generate ~ 6 kW of power [*Kreith et al., 1999*].

The typical electrochemical process of fuel cell operation is shown in Fig. 1-2. In this case the electrolyte is an acid (a polymer membrane; a liquid acid could also be used). Hydrogen is oxidised into protons and electrons at the anode, Eq. 1-1. The protons migrate through the polymer electrolyte to react with oxygen at the cathode, along with the electrons passing through the external circuit, Eq. 1-2. These electrons may be used for electric power. The overall reaction of a fuel cell operating on these simple reactants is shown by Eq. 1-3.

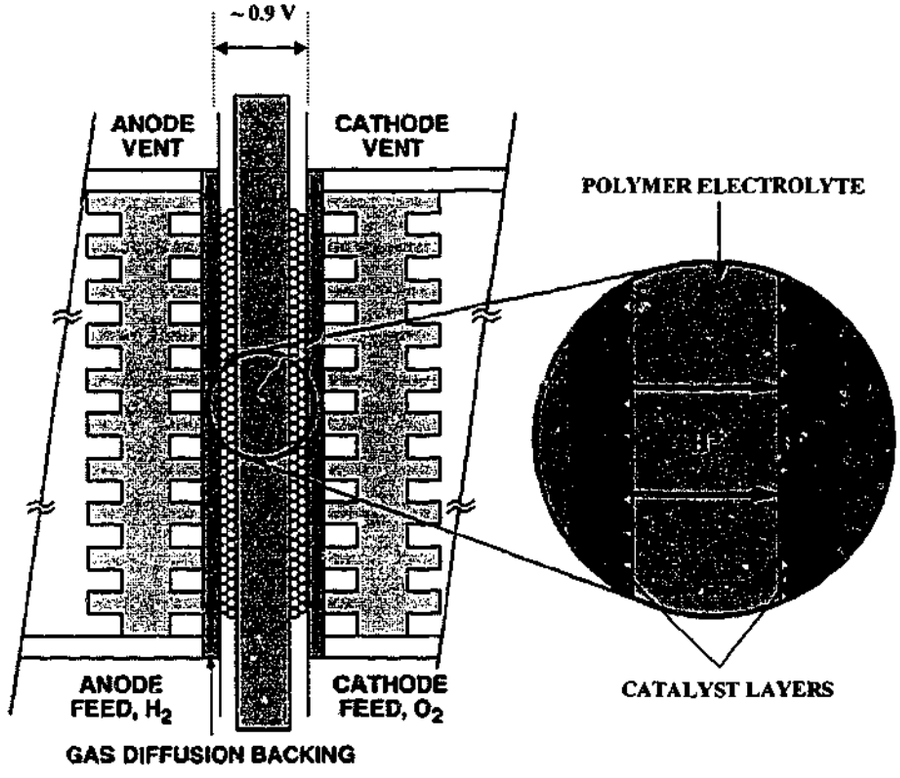

Fig. 1-2 The electrochemical operation in a PEMFC. Modified from Gottesfeld [Los Alamos National Laboratory URL].

$$H_2 \rightarrow 2H^+ + 2e^- \qquad (1\text{-}1)$$

$$O_2 + 4H^+ + 4e^- \rightarrow 2H_2O \qquad (1\text{-}2)$$

$$2H_2 + O_2 \rightarrow 2H_2O \qquad (1\text{-}3)$$

The general electrochemical process is similar for all types of fuel cells, except for in fuel cells with alkaline electrolyte or with anionic conducting species, the main charge carriers move in the opposite direction through the electrolyte (towards the anode). Fuel cell operation and catalysis is described in more detail later, with an emphasis on the PEMFC (Section 1.3).

The five main types of fuel cells, are normally distinguished by electrolyte: Polymer Electrolyte Membrane Fuel Cells (PEMFCs), Alkaline Fuel Cells (AFCs), Phosphoric Acid Fuel Cells (PAFCs), Molten Carbonate Fuel Cells (MCFCs) and Solid Oxide Fuel Cells (SOFCs). Table 1-8 illustrates the main properties of these devices.

Characteristic	*PEMFC*	*AFC*	*PAFC*	*MCFC*	*SOFC*
Electrolyte	Polymer Electrolyte	30% Aqueous KOH	H_3PO_4	Na/K/Li Carbonates	Y_2O_3 and ZrO_2
Conducting Species	H^+	OH^-	H^+	CO_3^{2-}	O^{2-}
Operating Temperature (°C)	80	90	220	*ca.* 650	*ca.* 1000
Fuels	H_2, Methanol	Pure H_2	Natural Gas	Any Hydro-Carbon	H_2, Any Hydrocarbon
Efficiency* (%)	55%*	Up to 55%	55%**	55-65%**	55-65%**
Present Cost* (£ kW^{-1})	~ 2500-5000	~ 1500-2500	~ 2000	N.A.	N.A.

Table 1-8 *Characteristics of the five main types of fuel cells.*
** Figures from Hamman et al., 1998. Efficiency is of the cell alone.*
‡ Both Toyota [Kreith et al., 1999] and DaimlerChrysler [DaimlerChrysler URL] report up to 60% efficiency for their PEMFC EVs.
*** PAFC drops to 40% efficient with a reformer; MCFC and SOFC units may still attain 55% efficiency with reformers [Hamman et al., 1998].*

A subset of the PEMFC (sometimes also called PEFC, 'proton-exchange fuel cell') is the Direct Methanol Fuel Cell (DMFC). The DMFC, as the name implies, operates on a methanol solution (without conversion to H_2, as may be performed for use in a PEMFC). It should also be noted that PEMFCs are sometimes referred to as DHFCs (or 'Direct Hydrogen Fuel Cells). H_2 may be prepared from a large number of sources, such as electrolysis from renewable (e.g. wind, solar, etc.) or non-renewable sources such as conventional coal or nuclear power stations. Hydrogen may also be produced from the 'reforming' (i.e. conversion) of other fuels, e.g. via the 'water-gas shift' reaction of methanol at *ca.* 300 °C, Eq. 1-4. Methanol may be produced from biomass (e.g. the fermentation of wood pulp) or from conversion of methane (e.g. from biomass or from natural gas).

$$CH_3OH + H_2O \rightarrow 3H_2 + CO_2 \qquad (1\text{-}4)$$

As may be observed in Table 1-8, the various fuel cells may use a range of different reactants, the type of which depends largely on the operating temperature of the cell. AFCs are the most limited type, since they may only operate on pure reactants. In particular, AFCs are intolerant to carbon and sulphur oxides, thus excluding the direct use of air (unless the air is scrubbed free of CO, CO_2 and SO_2), since these species form insoluble precipitates in the alkaline electrolyte. The SOFC, in contrast, can operate on just about any carbonaceous fuel (bypassing the need for reforming), enabling utilisation at higher efficiencies *cf.* conventional power sources (due to both the higher operating temperatures, and the efficiency of electrochemical processes).

Fuel cells and batteries convert the chemical energy of a fuel into electrical energy and high efficiencies may be attained, since these devices do not have to obey the 'Carnot Cycle'. The Carnot Cycle is a measure of the efficiency of a thermo-mechanical system such as the internal combustion engine, where only part of the obtained energy is converted into mechanical work. For example, in a coal-fired

power plant the standard steam temperature at the turbine inlet is 540 °C, and the exhaust is at 150 °C [*McEvoy URL*]. Thermodynamics describes the limiting efficiency of such a system, by Eq. 1-5, where T_1 and T_2 correspond to the initial and final (exhaust) temperatures, respectively. The steam cycle is more closely represented by the Rankine formulation, Eq. 1-6, from which the typical conversion efficiency (ε) of a coal-fired power plant (35%) is obtained [*McEvoy URL*].

$$\varepsilon_{carnot} = 1 - (T_2/T_1) = 1 - (423\ K/\ 813\ K) = 48\% \qquad (1\text{-}5)$$

$$\varepsilon_{rankine} = 1\text{- (mean condenser temp (K)/mean boiler temp (K))}$$
$$= 1 - (361/557) = 35\% \qquad (1\text{-}6)$$

The electrochemical processes within fuel cells are essentially isothermal (a small amount of heat is produced during the electrochemical reactions) and also, due to entropy constraints, not all of the available energy is transferred to electrical energy. The efficiency of the process will therefore be given by Eq. 1-7 [*McEvoy URL*], where ΔG_T is the free energy of the fuel oxidation process at the operating temperature of the cell, and ΔH_o is the standard reaction enthalpy value. The maximum theoretical efficiency of a fuel cell is typically considered to be ~ 90%. At present, most of the fuel cell types are achieving almost two-thirds of this maximum efficiency, due to polarisation losses (explained later, in Section 1.3.1.2). Further, since it is impossible to operate a fuel cell to exact stoichiometry, not all the fuel in the gas stream is oxidised (up to 10% is often combusted in an afterburner [*McEvoy URL*], which may be used to power other components). On comparison, an internal combustion engine may achieve up to ~ 20- 25% (and can fall to 10% in normal city driving), a diesel engine ~ 30- 45% and a steam turbine ~ 30- 40% conversion efficiency [*Oniciu, 1976*].

$$\varepsilon_{\text{fuel cell}} = (\Delta G_T/\Delta H_o) \qquad (1\text{-}7)$$

1.2.2 The Present Status of Fuel Cells

Currently PAFCs are the most highly developed of the fuel cell types with several hundred PAFC units in operation worldwide. By 1985 around fifty 40 kW PAFCs had been tested around the world, and two 4.8 MW power stations were established in New York and Tokyo [*UNESCO, 1985*]). PAFCs are known to have a very high reliability, and are often marketed for applications requiring un-interruptible power generation [*Cameron, 1997*], and are used in hospitals, office buildings and schools in the US. These units are most commonly sold in 200 kW units (enough power for about 40 houses) [*Kreith et al., 1999*], although prototypes of up to 11 MW have been constructed [*Hamman et al., 1998*]. PAFCs, along with PEMFCs, are the most likely candidates for vehicular power, resulting from their low operating temperatures (and PAFCs have been used to power fuel cell buses [*Kreith et al., 1999*]). However, PAFC components are more expensive *cf.* PEMFCs and reforming is expensive, but nevertheless, efficiencies of 40- 45% are expected (refer to Table 1-8- PAFC drops to 40% efficient with a reformer [*Hamman et al., 1998*]), *cf.* efficiencies of 36- 39% for small diesel engines [*Kreith et al., 1999*].

Several demonstration units of MCFCs have been tested over the last five years in a number of stationary applications, but material selection must be considered for these systems (corrosion is significant at the high operating temperatures with the alkaline electrolyte). MCFCs promise high fuel efficiencies and also the ability to operate on coal-based fuels and prototypes of up to 1 MW are in construction [*Hamman et al., 1998*]. CO_2 is required in the MCFC cathode reaction, and is normally re-circulated from the anode waste gas. The higher operating temperatures of MCFCs increase their 'start-up' time, but much less expensive catalysts are required at such temperatures.

SOFCs are presently the least developed and are undergoing considerable research. Commercialisation is presently limited by the high operational temperatures and expensive production of the ceramic electrolytes. Along with corrosion problems at these elevated temperatures, problems with thermal expansion are significant. In fact, some SOFCs may not be cooled or stopped once started, due to delamination of components. Prototype (experimental) stacks are currently in the order of only a few kW [*Hamman et al., 1998*]. However, SOFCs promise the potential of achieving the highest operational efficiency of all the fuel cell types and could be used in large high-power applications. These may be used in stationary power applications for large buildings, and possibly even as power sources for trucks and trains.

PEMFCs and AFCs were developed for the American Space Program (their development dating from the early 1950s). The PEMFC (developed for the Gemini Spacecraft by General Electric) was superseded by the AFC (in the Apollo missions by Pratt and Whitney Aircraft) for increased power levels [*Hamman et al., 1998* and *Austin, 1967*] (AFCs have faster oxygen reduction kinetics due to the alkaline conditions, enabling higher power densities). These systems were very expensive, relying on pure hydrogen and oxygen (cryogenically stored), but they had superior power-to-weight characteristics *cf.* batteries, and the product water was available for astronaut consumption. Through the 1950s to the 1980s, PEMFC cell fabrication technologies were steadily improved. Liquid electrolytes were contained more effectively and some polymer electrolytes (such as polystyrene-divinylbenzene sulphonic acid) were developed. A particularly important development was the use of porous electrodes (or 'gas diffusion' electrodes) to help increase the electrolyte-catalyst contact. In addition, the manufacturing of fuel cell 'stacks' (i.e. a number of cells connected in series, like a battery) was improved, using thin bipolar interconnecting plates with enhanced corrosion resistance.

Recently, PEMFC technology has recently received a large investment by most international auto-makers, and a wide range of prototype systems have been developed (refer to the following section). This has occurred particularly in recent years, following increasing restrictions on vehicular pollutants in certain areas,

particularly in the US (refer to Section 1.1.3.2). AFCs have not undergone widespread commercial development (other than in space, and in small units of up to ~ 100 kW [*Hamman et al., 1998*]), largely due to their inability to run on air (carbon dioxide intolerance) and requirements for high-purity hydrogen. In addition, the solid polymer in a PEMFC is both a lighter and safer electrolyte for vehicular and other applications *cf.* the corrosive potassium hydroxide in an AFC. However, AFCs can utilise less expensive catalysts such as nickel (although normally platinum is used), and may also use low cost electrolytes (e.g. potassium hydroxide). AFCs and PEMFCs are also ideal for military traction, being silent and having a low thermal signature. On comparison with the internal combustion engine, the PEMFC is more than twice as fuel efficient (in typical city traffic- at high speeds there is not as much difference), and both PEMFCs and AFCs have the advantage of fewer moving parts, potentially reducing any maintenance required *cf.* internal combustion engines. Further, the low operating temperature of these cells enables fast starting, which is important for vehicular power. Small commercial PEMFC units (of up to 500 kW) are available [*Hamman et al., 1998*].

For the commercial viability of fuel cells, a number of factors must be considered. Issues such as weight and cold-start time are not as big a concern when the application is for stationary power generation. These systems (e.g. PAFCs, MCFCs, and SOFCs) may be built to any volume, have large amounts of fuel stored on-site (or transported via pipeline), and run at high temperatures. The oxidant is typically oxygen from the atmosphere. The major concerns are the expense and lifetime of materials. At lower temperatures the cost of materials remains an issue, but the lifetime is generally much longer. For small-scale power generation (e.g. PEMFCs, DMFCs) the cost of materials is quite high (in particular the polymer electrolyte membrane and the noble metal catalysts). The polymer membrane is expected to substantially reduce in price with increased levels of production (i.e. by 'economies of scale'). The cost of platinum is limited by world supply, and if a large number of low temperature fuel cells with acidic electrolytes (i.e. PEMFCs and DMFCs, the most likely candidates for vehicular traction) are produced the price of Pt and Pt group metals may rise.

Weight and volume are very important issues for vehicular power and these considerations will affect decisions in terms of the type and amount of fuel stored on board, and the type of system used (e.g. PEMFC-battery hybrid vehicles, H_2 stored in cylinders, or converted from methanol, etc.). If reformers are used (e.g. to convert methanol or ethanol to hydrogen on board), then parasitic power losses must be taken into account. Parameters such as the operational temperature and reactant pressure also have a significant impact on the performance of the fuel cell (and hence commercial acceptability), but the resulting energy penalties must be evaluated.

The modularity of fuel cell stacks is a big advantage *cf.* other power sources- similar to batteries, fuel cell stacks may be added together for greater power, e.g. "from 10 kW for a house to a 1000 kW for a locomotive" [*Burns, 2002*]. Fuel cell stacks may also be made into any shape to suit the application (for best use any available space). Generally, on-board EVs, stacks consist of several hundred very thin cells, each of maximised area (voltage is increased by the number of cells in series, and the current density is increased by large electrode surfaces). These PEMFC stacks can be situated beneath the seats of the EV, or could even consist of several separate stacks distributed in different areas where space is less important.

1.2.3 Recent Developments: Towards the 'Fossil Free Age'

Other than the PAFC, which has experienced only limited commercial success so far, the PEMFC appears to be initiating a new energy infrastructure, referred to by some people as the 'hydrogen economy'. This is an area in which significant improvements may be made in the health of the average citizen, whilst helping to limit the dependence on the dwindling oil supply and also possibly limit the global warming phenomenon. However, as with the introduction of most new technologies, acceptance by society is paramount for the success of the product. The abovementioned issues are expected to facilitate the widespread integration of fuel cells, initially in vehicles and eventually in other areas of power generation.

The presence of PEMFC technology in prototype vehicles from most of the major auto-makers is a very promising sign for their continued development and integration. The general public is becoming increasingly aware of these new developments in hybrid, battery and fuel cell-powered vehicles through a considerable amount of positive publicity. Most auto-makers are endeavouring to either meet strict emissions levels, or increase fuel efficiency (or both) whilst maintaining typical vehicle expectations such as acceleration, top speed, and driving range. For widespread acceptance, it is likely that other than being environmentally-friendly, PEMFC-powered EVs must also drive like conventional vehicles. Larry Burns (GM's vice president of R&D) believes, "to make fuel cell cars attractive they must match current lifetime expectations of 150 000 miles or more." Burns is optimistic of this aspect: "the only moving parts will be the wheels, the suspension and the compressor, so it should have a pretty good life" [*Burns, 2002*]. PEMFCs and the closely related DMFCs may also be used as remote power sources, or in small portable electronics, however the driving force for these fuel cells is in the transportation sector. Burns believes that the 55 million cars produced each year may increase to 70 million by 2010 [*Burns, 2002*], so even if a small proportion of new cars are powered by PEMFC or PEMFC-hybrid systems, this would represent a considerable breakthrough in the technology (and promote further reductions in fuel cell cost and also a greater understanding in the community).

Ballard Power Systems of Vancouver (one of the world leaders in PEMFC technology) have had their PEMFC stacks integrated into most fuel cell and hybrid EV prototypes. DaimlerChrysler, Ford, GM and Toyota have invested ~ US$750 million in a partnership with Ballard Power Systems [*Kreith et al., 1999*] (and all four auto-makers have announced plans to have fuel cell EVs commercially available by 2004 [*CARB URL, 2002*])[viii]. Three Ballard PEMFC-powered buses are presently operating in a demonstration program in Chicago [*Kreith et al., 1999*], others have been operating in Vancouver since 1997 [*Cameron, 1997*].

[viii] Refer to Appendix C for a more detailed description of the present status of PEMFC-powered prototype EVs from the main auto-makers.

Partnerships between governmental bodies and companies around the world are encouraging fuel cell vehicle trials. 10 European cities are involved in the 'CUTE' (Clean Urban Transport for Europe) project, with 30 fuel cell buses linking the cities. CUTE commenced in November 2002 [*Hydrogen Fuel Cell Letter, 2002*]. In the US the most significant program is the California Fuel Cell Partnership- a collaboration between the major auto-makers, fuel providers, fuel cell manufacturers and governmental bodies (founded by the California Air Resources Board, CARB). This partnership is actively demonstrating fuel cell EVs under normal driving conditions and demonstrating the viability of an alternative fuel infrastructure. The partnership plans to place "up to 70 fuel cell vehicles on the road by 2003" [*CARB URL, 2002*].

An increasing number of hydrogen refueling stations have opened up around the world. As at November 2002, eight H_2 stations were in existence in North America. The stations typically use electric power to generate hydrogen from water via electrolysis [*Hydrogen Fuel Cell Letter, 2002*].

1.3 Polymer Electrolyte Membrane Fuel Cells (PEMFCs)

1.3.1 PEMFC Operation

1.3.1.1 Choice of Fuel: Hydrogen or Methanol?

Hydrogen is the fuel of choice for PEMFCs in the short term, since it undergoes an extremely facile oxidation reaction at a platinum surface, yielding high energy densities. However, the on-board storage of H_2 in cylinder form presents two serious issues in terms of weight and safety. The mass of pressurised hydrogen in a cylinder may be only ~ 1% of the total cylinder weight, which is an unnecessary weight addition to a vehicle, and results in a lower vehicle range compared to vehicles using liquid fuels. Higher storage densities are being developed, including storing the hydrogen as an adsorbed species (e.g. metal hydrides).

The use of methanol as a fuel in PEMFCs has created considerable interest, dating back to the beginnings of fuel cell research for the NASA space program. Methanol is a relatively plentiful fuel, which is easily handled, stored, and transported. It is also a potentially renewable fuel source which may be produced from hydrocarbons such as methane (e.g. from biomass) and natural gas. The energy density of methanol approaches that of hydrogen, and methanol does not require heavy pressurised cylinders for storage. A further advantage of methanol-fueled vehicles (compared to using hydrogen) is the safer storage of methanol on-board a vehicle, and also the potential use of the existing petrol station infrastructure.

A petrol reformer was developed in late 1997, by the Boston-based Arthur D. Little, New York's Plug Power and the US Department of Energy [*Motavalli, 2000*]. This could enable a more rapid integration of PEMFCs, using the existing petrol infrastructure. Sulphur is removed from the fuel before it gets to the cell, with a device similar to a catalytic reformer. However petrol is a very complex fuel, and the extra weight and cost this reformer could add to an EV may yet make this unfeasible.

Pure hydrogen remains the best fuel for maximum PEMFC performance, and unless significant improvements in DMFC performance ensue, H_2-powered PEMFCs will most likely be the chosen power source for EVs. Whether this hydrogen is generated on-board from methanol or stored in cylinders at high pressure is uncertain. DMFCs may find niche applications in portable electronics (e.g. battery replacement), where simplicity is important and low power is not an issue.

If carbon monoxide is present in the fuel stream (e.g. from reformed methanol or other hydrocarbons), the platinum catalyst may become poisoned. Typically, CO is adsorbed onto the platinum surface, forming intermediate Pt-CO_{ads} species that block the catalyst surface. Poisoning is a major problem on platinum catalysts, due to the slow kinetics of CO-oxidation, and high potentials are normally required to oxidise CO on a Pt catalyst. For PEMFC operation, reformed H_2 mixtures must have a CO concentration well below 100 ppm [*Hamman et al., 1998*], and generally less than 10 ppm is preferred for CO-poisoning not to have a detrimental effect. The

presence of CO_2 in reformate is of minimal concern for PEMFC operation, other than diluting the fuel stream by around a quarter.

Platinum-ruthenium catalysts are often used in PEMFCs to enable operation on reformed mixtures having CO concentrations of up to 250 ppm (without degradation of cell performance, other than that resulting from the diluted fuel stream). Sometimes a small amount of O_2 or H_2O_2 may be introduced into a reformed fuel stream, to allow toleration of CO levels of up to 500 ppm, but these oxidants also consume some of the hydrogen. Bifunctional PtRu catalysts are also used in the anodes of DMFCs, to lower the potential of methanol oxidation. Methanol is oxidised in a few steps, passing through a stage where an adsorbed COH or similar species remains. This COH_{ads} species poisons a Pt catalyst in a similar fashion to CO. The Ru metal helps to adsorb oxygen-containing species at low potentials, facilitating the oxidation of the COH_{ads} or CO_{ads} species, Eq. 1-8.

$$Pt\text{-}CO_{ads} + RuOH \rightarrow Pt + Ru + CO_2 + H^+ + e^- \qquad (1\text{-}8)$$

DMFCs operate in a similar fashion to PEMFCs and often consist of the same basic cell materials. The methanol in aqueous solution reacts directly at the PtRu catalyst (at the anode), Eq. 1-9. Product CO_2 is liberated from the anode as a gas. The cathode reaction (Eq. 1-10) is similar to that in a PEMFC (Eq. 1-2), except that three moles of oxygen are required per two moles of methanol.

$$CH_3OH + H_2O \rightarrow CO_2 + 6H^+ + 6e^- \qquad (1\text{-}9)$$

$$1.5O_2 + 6H^+ + 6e^- \rightarrow 3H_2O \qquad (1\text{-}10)$$

$$CH_3OH + 1.5O_2 \rightarrow 2H_2O + CO_2 \qquad (1\text{-}11)$$

The thermodynamic reversible cell potential for DMFC operation, E° = 1.21 V (Eq. 1-11), is close to the 1.23 V for the hydrogen/oxygen fuel cell (Eq. 1-3). Complete methanol oxidation (Eq. 1-9), however, is considerably slower than the oxidation of hydrogen (Eq. 1-1), due to the requirement for a six-electron transfer per mole of methanol, and the slow oxidation of intermediate carbonaceous species. Consequently, much lower power densities are obtainable from DMFCs *cf.* PEMFCs at present. However, apart from decreased fuel processing issues (and less concerns with methanol safety and weight on-board a vehicle), DMFC operation has an important advantage over PEMFCs- external humidification[ix] is not required. The high level of water production in a DMFC (Eq. 1-11) combined with the aqueous methanol solution supplied to the anode is adequate for maintaining the membrane moisture content, enabling power savings. This allows for a much simpler system *cf.* the PEMFC, with DMFCs not requiring humidifiers or fuel reformers. Additionally, DMFCs may operate at temperatures as low as 1 °C, promoting their use in low power applications at room temperature, where compressed H_2 or reforming is not practical.

However, DMFCs are not nearly as developed *cf.* PEMFCs. The power outputs of DMFCs are around 30% of a PEMFC system at best. Other than slow methanol oxidation kinetics, performance is also limited in DMFCs due to a phenomenon known as 'methanol crossover'. This occurs when polymer electrolytes (such as Nafion®[x]) allow a high rate of methanol to pass through the membrane to the cathode, where it is oxidised. For motion within Nafion, protons need to be hydrated (hence the 'humidification') and typically, 2- 5 water molecules pass over to the cathode with each proton [*Ren and Gottesfeld, 2001*]; this is known as 'electro-osmotic drag'. Methanol molecules are similarly taken across to the

[ix] Humidification of the gas streams is usually required in PEMFCs (particularly at the anode) to prevent the polymer membrane from drying and the associated reduction in ionic (proton) conductivity this causes. To achieve this, the gas streams (especially hydrogen) are usually bubbled through water at an elevated temperature, e.g. 60- 80 °C, so that water vapour is supplied to the PEMFC, along with the reactant gases.

[x] Nafion is a registered trademark of DuPont de Nemours.

cathode, often severely poisoning the platinum-based catalyst and resulting in considerable efficiency and power losses. For continued development of DMFCs, a new polymer membrane is required, which would ideally be conductive and stable at higher temperatures, and also have a low permeability to methanol. Higher operating temperatures (e.g. up to 200 °C) are known to enhance reaction kinetics and depress platinum poisoning (by adsorbed CO and related species), but at present, higher operating temperatures require more complicated pressurised systems (due to water evaporation within membranes such as Nafion). At present, achievable power densities in experimental DMFCs have been reported in the range 0.2- 0.4 W cm^{-2} (at operating temperatures between 95- 130 °C) [*Ren et al., 1996; Shukla et al., 1998*]. Some studies continue to investigate the use of a liquid sulphuric acid electrolyte (a return to original designs), to move away from using expensive Nafion membranes that also have significant methanol-crossover problems [*McNicol et al., 1999*].

1.3.1.2 Polarisation

Polarisation (or overpotential) is the magnitude of potential loss from the ideal thermodynamically reversible voltage upon drawing current. There are three principle types of polarisation in fuel cell operation, each dominating a section of the curve in Fig. 1-3. At low current densities 'activation polarisation' dominates due to slow electron transfer reactions, particularly at the cathode (oxygen reduction reaction). 'Ohmic polarisation' arises from electrical resistances across the electrolyte and electrodes, and is apparent in the central region of the polarisation curve (by the linear slope). At high current densities 'concentration polarisation' occurs where reactants are unable to move to the catalyst sites fast enough to sustain the high rates of reaction- a sharp decrease in voltage is typically observed due to this mass-transfer limitation of reactions (this phenomenon is not shown in Fig. 1-3). Concentration polarisation is also exacerbated by the slow removal of products (e.g. water) and other species (e.g. N_2 from air), which limits the reaction rate, particularly at the cathode. Cathodes are usually designed to minimise 'water

flooding' by wet-proofing agents. For the hydrogen/oxygen PEMFC, the ideal situation would be to attain a voltage of 1.23 V at all current densities (i.e. the open circuit potential, Fig. 1-3).

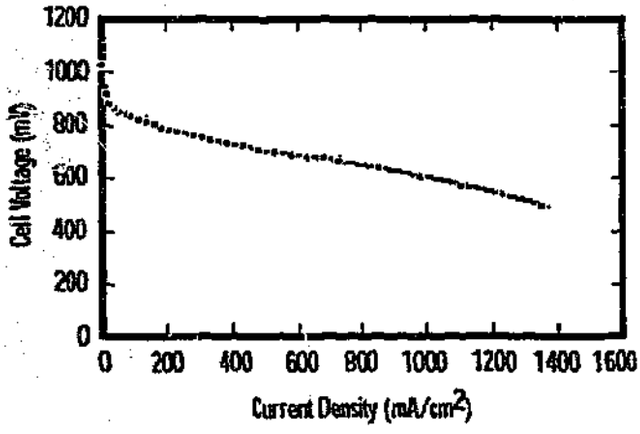

Fig. 1-3 PEMFC Polarisation [Thomas and Zalbowitz, from Los Alamos National Laboratory URL].

Power density (W cm^{-2}) is the first indication of fuel cell performance, which is dependent on the current density (A cm^{-2}) at a particular voltage (power being the product of current and voltage). Vehicular applications require high power densities at low costs, which is usually obtained at high current densities. For stationary power generation, lower current densities are preferable (higher cell voltages) allowing higher efficiencies (and less heat losses). The current at which the power density is a maximum is somewhere between these two extremes. The maximum power obtainable from a cell is iE°, where E° is the reversible cell potential at 20 °C. The electrochemical or voltage efficiency is calculated from E_c/E°. The overall potential of the cell, may be expressed by Eq. 1-12, where iR is the potential drop across the electrolyte, η is the polarisation, and E_n is the equilibrium cell voltage, given by the Nernst equation, Eq. 1-13. In Eq. 1-13, R_g is the universal gas constant (8.314 J K^{-1} mol^{-1}), T is the absolute temperature, z is the number of electrons transferred in the reaction, F is the Faraday constant (96485 coulombs per mole

electrons), a_1 is the activity of reactant gas dissolved in water, and a_2 is the activity of reactant gas ions. When the polarisation losses are large (greater than 50- 100 mV at room temperature) the polarisation is given by Eq. 1-14, where i is the current density, i_o is the exchange current density, and α is the transfer coefficient (a number between 0 and 1).

$$E_c = E_n - \eta - iR \qquad (1\text{-}12)$$

$$E_n = E^\circ + (R_g T/zF)\ln[a_1/a_2] \qquad (1\text{-}13)$$

$$\eta = (2.3\,RT/\alpha zF)\log i - (2.3\,RT/\alpha zF)\log i_o \qquad (1\text{-}14)$$

The power density of a fuel cell may be improved by reducing the individual polarisation losses. For example, if activation polarisation is found to be extreme, both electrodes could be compared to a reference electrode to determine which one is being heavily polarised. Operating the cell at higher temperatures, increasing the reactant concentration, or increasing the catalyst surface area may then reduce these activation losses. Ohmic polarisation can be tested using an AC-bridge or a current-interruption method. These losses may then be minimised by increasing the electrode-electrolyte interfacial area, and by using thinner or more conductive electrolytes. When mass-transfer processes are causing polarisation losses, the diffusion of reactant species into the affected electrode may be improved through redesigning the electrode or by increasing the reactant concentration (if in solution) or partial pressure (if gaseous).

1.3.1.3 Cell Components

The basic apparatus for a single-cell PEMFC or DMFC is shown in Fig. 1-4. The membrane-electrode assembly (MEA) is shown in the centre of the figure,

incorporating the polymer membrane and both electrodes (in a 'sandwich-type' structure). The catalyst layers may be applied to either the membrane or the gas-diffusion electrodes (GDEs).

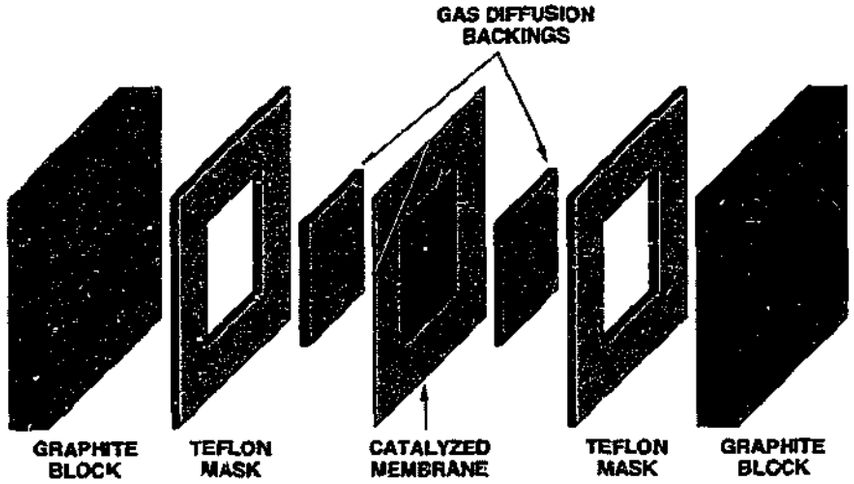

Fig. 1-4 The components of a single PEMFC, including the membrane-electrode assembly (MEA) in the centre (from LANL URL).

The GDE typically consists of two parts- an outer carbon paper (or cloth) and an inner layer of carbon-black. The inner diffusion layer acts as a micro-porous support for the catalyst layer and prevents penetration of the catalyst into the macro-porous carbon paper [*Jordan et al., 2000*]. The outer carbon paper consists of long, interwoven carbon fibres that provide a rigid support for the inner diffusion and catalyst layers. Both gas diffusion layers are commonly wet-proofed, e.g. with Teflon® (PTFE)[xi]. The combined diffusion layers act to enhance the inward diffusion of fuel cell reactants into the catalyst layer and aid in the removal of any products such as water or carbon dioxide (wet-proofing also helps to prevent bubble formation).

[xi] PTFE is chemically inert and helps to maintain a hydrophobic gas pathway to the catalyst layer. In addition, PTFE helps to bind the gas-diffusion layer and provides structural integrity.

Carbon-black (most commonly Vulcan) is used in the gas-diffusion and catalyst layers of PEMFCs. These high surface area carbon powders have both macroscopic and microscopic porosity, and may be made into thin layers with very high internal areas available for catalysis. Additionally, carbon-black is electrically conducting (essential for supporting electrochemical catalysis), chemically stable, lightweight and inexpensive. Acetylene blacks (with more open structures than the Vulcan 'furnace blacks') have also been used in catalyst layers, and these allow higher efficiencies at higher current densities [*Appleby, 1996*].

The ion-exchange or polymer electrolyte membranes used in PEMFCs are normally those containing strong acidic or basic end groups, as these will have the least ion association (and therefore the highest ionic conductivities). The choice of polymer backbone is also of vital importance, in terms of its mechanical strength, thermal and chemical stability, and porosity. The thickness of the membrane needs to be sufficient to reduce gas diffusion and provide strength, whilst remaining thin enough to minimise internal resistance.

The most common polymer used in PEMFCs is Nafion, which is a polymeric perfluorosulphonic acid. Nafion has both hydrophilic (SO_3H) and hydrophobic (C-F) functionalities (as represented in Fig. 1-5). Complete fluorination is required for chemical stability. When solvated, the proton in the sulphonic acid (SO_3H) group becomes mobile and may readily pass through the polymer as H_3O^+, $H_5O_2^+$, etc. (the proton is typically hydrated by between two to five water molecules, at temperatures of 15 and 130 °C, respectively [*Ren and Gottesfeld, 2001*]). Apart from exhibiting high ionic conductivities, it is also essential for the polymer membrane to be free of pores, to maintain separation of reactants. The membrane also acts as an electrical insulator between the anode and cathode.

Due to the hydrophobic/hydrophilic nature of Nafion, a complex network of inverse micelles joined by channels develops on hydration (see Fig. 1-6). The Teflon backbone of the polymer exists outside these micelles, whilst the $-SO_3^-$ groups line the insides. Hydrated protons (or other cations) may readily pass from one micelle

to the next, however a similar transport of anions is prevented by repulsion from the $-SO_3^-$ groups within the channels. (The transport number for protons, t_{H^+}, is almost 1.0, i.e. essentially all of the ionic conductivity is due to proton conduction).

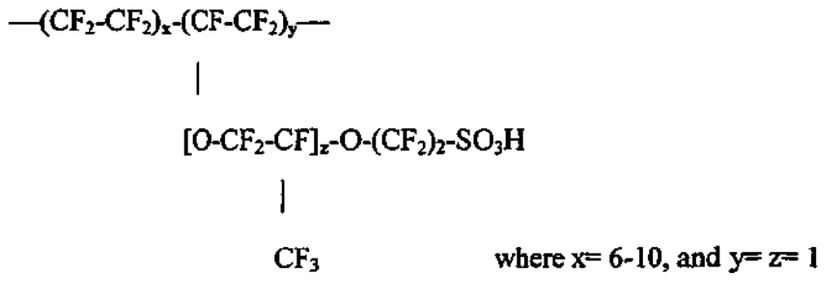

Fig. 1-5 The structure of DuPont's Nafion® [Savadogo, 1998].

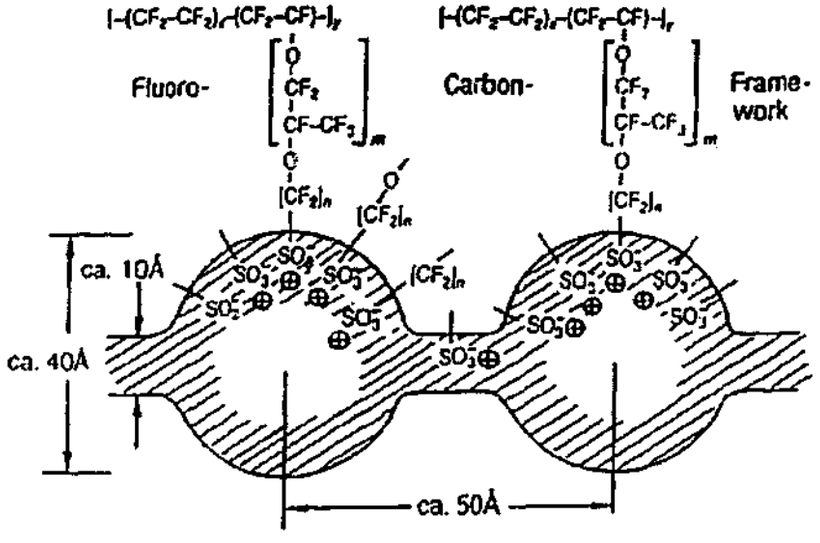

Fig. 1-6 The internal structure of Nafion (taken from Hamann et al., 1998).

In PEMFCs, the commonly used membranes are Nafion 117 (175 μm) and Nafion 112 (50 μm), both with an equivalent weight of 1100 (ratio of the polymer mass to the moles of $-SO_3^-$ sites), and a specific conductance (conductivity/film thickness) of 0.081 $(\Omega\ cm)^{-1}$. The 112 form is preferred in PEMFCs, being thinner and therefore allowing higher power densities (less ohmic resistance), but it is more fragile than Nafion 117. In DMFCs the 117 film is generally used, because it is thicker and does not allow as much methanol crossover. The major disadvantages with Nafion electrolytes are the moisture requirements, limiting the operating temperature range to *ca.* 5-90 °C (the fuel and oxidant gases are usually humidified by passing these through water at an elevated temperature), and the high cost.

Currently the cost of a PEMFC power system is largely dominated by the cost of the PEMFC stack (i.e. the collection of cells joined in series; the stack expense constitutes *ca.* 80% of a typical 50 kW system [*ADL, 2000*]). In turn, the price of a typical PEMFC stack is dominated by the cost of the MEA materials and preparation (*ca.* 76% of the stack [*ADL, 2000*]). In 2000, the cost of a MEA (materials and production) was *ca.* US$ 236 m^{-2}, [*ADL, 2000*]. The Arthur D. Little study was based on high-volume production estimates (500,000 units per year) and assumed a cost of US$ 55 m^{-2} for the Nafion PEM, whereas the price of Nafion in 1999 was around US$ 750 m^{-2}. Almost half of the MEA cost is from the platinum-based catalysts on each electrode (around 47% of the MEA cost in 2000).

1.3.2 The Catalyst Layer: The Heart of the PEMFC

The catalyst layer is the region where the fuel cell reactions take place. Reactant species pass into this layer and react at the surface of a catalyst particle, in the so-called 'three-phase reaction zone' (explained in Section 1.3.2.2). To achieve fast rates of reaction a high catalyst surface area is generally desirable. At the same time, the catalyst layer should be as thin as possible to facilitate quick diffusion of reactant gas (and removal of any products); thinner layers are also less resistive. The nature of the various components in this layer (e.g. hydrophobicity or hydrophilicity,

catalyst type and particle size) is also very important, and may significantly affect fuel cell performance.

Typically, PEMFC and DMFC catalyst layers are largely comprised of 1- 2 nm sized platinum particles 'supported' on ~ 30 nm carbon-black particles (Pt/C). Polymer electrolyte is usually used to bind these layers and also provide a H^+ pathway to most of the catalyst particles. Sometimes PTFE is also used for binding the catalyst layer; PTFE may also be useful e.g. for increasing the hydrophobicity of the cathode to minimise flooding. The preparation of these layers is extremely important for maximised catalyst utilisation- typical preparation methods are outlined later (in Section 1.3.3).

1.3.2.1 Catalysis

A catalyst is a material that enhances the rate of a particular reaction without appearing in the final products. It accelerates both the forward and reverse reactions equally, by lowering the activation energy required for a reaction. A catalyst has no effect on the position of equilibrium (e.g. platinum or nickel may be used as both hydrogenation and dehydrogenation catalysts). The Pt-based catalysts used in fuel cells enable the hydrogen and oxygen reactions to readily occur at low temperatures (e.g. ~ 80 °C in a PEMFC).

The catalysis within fuel cells is called 'heterogeneous catalysis' (sometimes called 'contact' or 'solid' catalysis), since the reaction occurs at the interface of two phases. Five elementary steps usually describe a heterogeneous reaction [*Moore, 1983*]: (i) diffusion of reactants to the catalyst surface, (ii) surface adsorption, (iii) chemical reaction (i.e. transfer of electrons), (iv) desorption, and (v) diffusion of products away from the catalyst surface. The chemical reaction step is normally rate limiting. The rate of reaction is proportional to the surface fraction covered by reactant. In catalysis, chemisorption is generally the type of reactant adsorption on a substrate (as opposed to physisorption).

The exchange current density, j_o, is the rate of electron transfer across an electrode at equilibrium, where the current densities of anodic and cathodic (j_a and j_c) reaction directions are equal, Eq. 1-15 [*Moore, 1983*]. Platinum electrodes typically have a high j_o for most reactions, allowing a high flow of charge between the electrode and solution for an increased potential difference across the electrode (i.e. a shift in equilibrium). Such electrodes may exhibit very little polarisation.

$$J_o = j_a = j_c \qquad (1\text{-}15)$$

Platinum is the most abundant of the noble metals (or the 'platinum group metals'- Pt, Pd, Rd, Ru, Ir, Os) and has been studied the most extensively; uses of platinum range from applications where corrosion resistant surfaces are required (including, *inter alia*, electrochemistry and medicine) to applications in catalysis (e.g. catalytic converters in vehicles and hydrogenation/dehydrogenation reactions). For hydrogen oxidation, platinum, gold, nickel, and even tungsten carbide are suitable catalysts; platinum and nickel are also reasonably effective catalysts for the reduction of oxygen, as is silver [*Hamann et al., 1998*]. For PEMFCs however, the only suitable catalyst materials found to date are platinum and alloys of some of the platinum-group metals (including ruthenium in particular). Platinum is chemically stable in acid solution, and readily catalyses fuel cell reactions at low temperatures (yielding much higher current densities than any other catalyst). The main disadvantage in using platinum for catalysis is the high cost, but at present this is unavoidable. Many studies have therefore attempted to reduce the total amount of platinum required in PEMFCs.

As outlined in Section 1.3.1.1, platinum surfaces become poisoned during operation on fuels containing CO (or during the direct electrochemical oxidation of methanol, which breaks down to a similar carbonyl species). The alloying of a second metal (or

an 'ad-atom') with platinum can greatly enhance catalysis, and ruthenium is typically used in such situations.

Generally, PtRu has been the best performing catalyst system for CO and methanol oxidation. A number of other catalyst formulations have been investigated, including binary, ternary and quaternary systems using the elements of tin, tungsten, molybdenum, osmium, iridium, rhodium, and palladium. Recently, a Pt-Ru-Os-Ir system has been shown to perform slightly better *cf.* PtRu for methanol oxidation [*Reddington et al., 1998*]. However preparation of ternary and quaternary systems is often more complicated and likely to be more expensive due to the additional elements, so a significant improvement in catalysis is necessary for these systems to be commercially viable. Other catalyst alternatives have been attempted by intercalating platinum into perovskites [*White and Sammells, 1993*], and incorporating platinum into polyacrylonitrile foams [*Ye, 1996*] and conducting films such as polypyrrole [*Hepel, 1998*].

For DMFCs operating on a typical methanol solution concentration of 5 molar, the optimal catalyst ratio is 7-30% Ru:Pt, with higher Ru content necessary at low temperatures [*Fujiwara et al., 1999*]. In the case of PEMFC operation on CO/H_2 mixtures, a 50-50 ratio of Ru to Pt is often preferable.

The Langmuir-Hinshelwood surface reaction (or the 'bifunctional mechanism') is generally the accepted oxidation mechanism for methanol and carbonaceous species at the binary PtRu catalyst. This mechanism (i.e. Eq. 1-8) involves the adsorption of oxygen-containing species on the ruthenium surface (at lower potentials than on the platinum surface), which aid in the oxidation of $Pt–COH_{ads}$ species, thus fastening the rate-determining step. Ru adsorbs OH^- species at ~ 0.2 V (vs. RHE), possibly even from 0.16 V [*Szabó and Bakos, 1987*], *cf.* ~ 0.4 V for platinum. There may also be a small electronic, or 'ligand' mechanism occurring (from the overlap of platinum and ruthenium electron orbitals) that also gives rise to the enhanced catalysis of PtRu *cf.* catalysis on either metal. [*Tremiliosi-Filho et al., 1999*].

It follows that PtRu deposits situated in the electrochemically active regions of fuel cell electrodes (i.e. at the 'three-phase reaction zones') should, as in the case of platinum catalysts, ideally be prepared as small as possible. For platinum deposits, 1 nm has been calculated as the smallest 'energetically stable' particle size [*Stonehart, 1990*]. Generally PtRu particles can be prepared at a smaller size *cf.* pure platinum particles, and thus PtRu catalysts < 1 nm in diameter may be feasible.

1.3.2.2 Catalyst Utilisation

A major challenge for the cost reduction (and improved performance) of PEMFCs is to increase the utilisation of the noble metal catalysts[xii] within the electrodes. For a high catalyst utilisation (i.e. the amount of platinum surface area available for reactions relative to the mass of platinum) it is essential to prepare platinum deposits of maximum specific surface area. Accordingly, platinum particles are usually deposited onto a high surface area carbon-black to limit particle agglomeration.

A highly utilised catalyst is the most desirable from a cost perspective, and also since using less catalyst generally allows thinner catalyst layers with better gas diffusion properties. A high utilisation requires most of the catalyst atoms to be actively involved in the reaction of interest. It is well known that surface area is inversely proportional to particle size (for a given mass of substance). Eq. 1-16 illustrates how the platinum particle diameter, d (in m), may be calculated, if homogeneously dispersed, spherical particles are assumed [*Kinoshita, 1988; Gloaguen, 1997*] (where the density of platinum, ρ, is 21.4×10^6 g m^{-3}, and specific surface area, S, is in m^2 g^{-1} units). In general, the highest specific surface area (surface area per mass of catalyst) is preferred. In fact, an 'ideal' platinum catalyst could be imagined as consisting of 1 nm (10 Å) supported particles (with a specific surface area of *ca.* 280 m^2 g^{-1} Pt), where every atom is a surface atom and is available for catalysis (i.e.

[xii] Largely Pt and Pt-based catalyst systems.

100% utilisation) [*Kinoshita and Stonehart, 1977*]. One of the most commonly used catalysts, 20 wt% Pt/C from E-TEK Inc., has a particle size range of 2- 5 nm. However, the actual surface-area available in a PEMFC may be a lot less, resulting in a low platinum utilisation. To date, the best platinum utilisations have been typically no more than ~ 20% [*Appleby, 1995*], which also takes into account platinum particles lacking ionic contact.

$$d = 6 / S\rho \qquad (1\text{-}16)$$

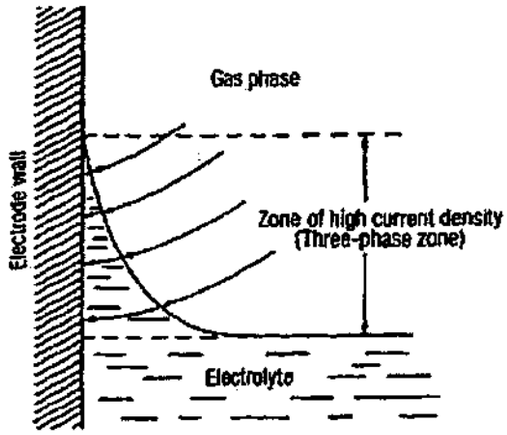

Fig. 1-7 *The three-phase reaction zone. The electrolyte must come into contact with the catalyst (in the electrode), but be thin enough to allow rapid mass transport [from Hamann et al., 1998].*

For a high platinum utilisation it is essential that these small catalyst particles are located in particular regions of the catalyst layer. Ideally, the whole platinum surface-area within a PEMFC catalyst layer would be active for the hydrogen oxidation and oxygen reduction reactions. For this to be the case, the fuel or oxidant must react at the interfacial region between the polymer electrolyte (eg. Nafion) and the platinum catalyst. This is known as the three-phase reaction zone (3PRZ), Fig. 1-7. The electrode should be suitably fashioned to allow fast access of the reactant into this zone and furthermore, for a reaction to occur, the

electrolyte/catalyst interface must enable the transfer of both protons and electrons. Fig. 1-8 illustrates two possible routes for low catalyst utilisation- catalyst lacking either proton or electrical conduction pathways.

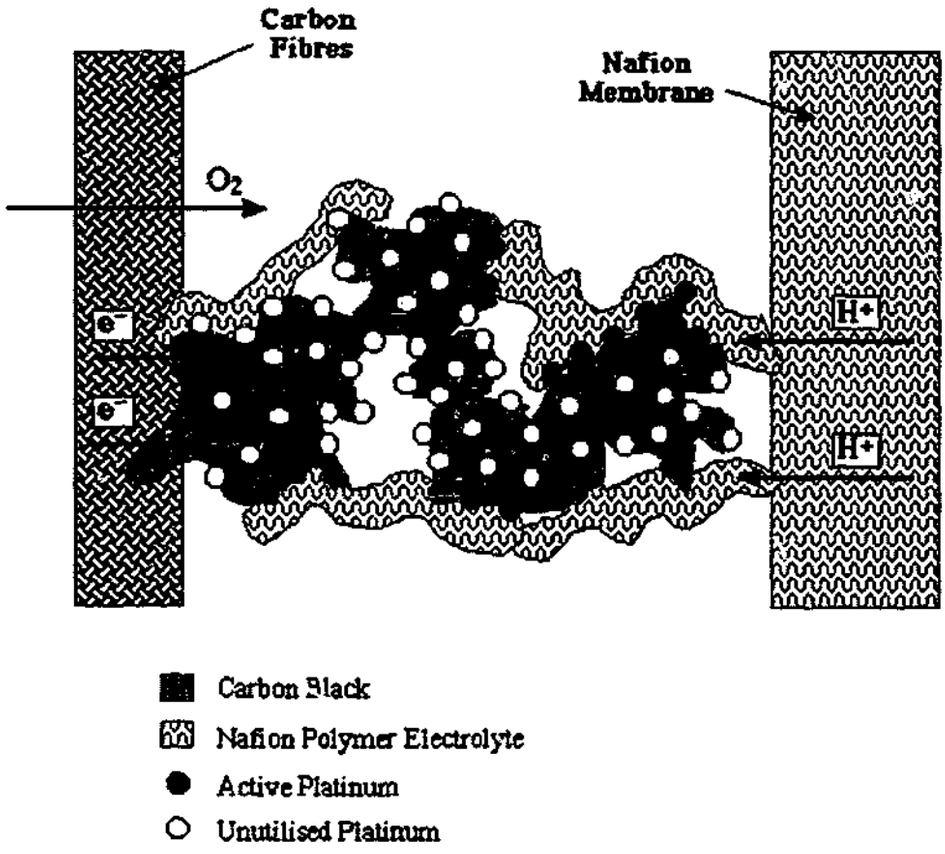

Fig. 1-8 A schematic diagram illustrating the active and non-active platinum particles in a PEMFC catalyst layer. The cathode catalyst layer is used as an example. The polymer electrolyte is Nafion which is typically impregnated into the catalyst layer (refer to the text).

Hence, it is necessary for the polymer electrolyte (in the catalyst layer) to be ionically connected to the membrane between anode and cathode, to facilitate proton passage. It is also necessary for the catalyst to be electrically connected (through the carbon particles) to the current collectors, so that the electrons may pass through the external circuit. If these 3PRZ conditions are not satisfied then reactions will not take place (i.e. the catalyst will not be active for PEMFC catalysis).

1.3.3 Catalyst Layer Preparation

This discussion will focus on platinum catalysts, since they have been primarily used in PEMFCs. The PtRu binary system has, until more recently, been used almost exclusively with DMFCs (and these fuel cells have had less commercial focus). Nevertheless, the same issues of catalyst utilisation remain for PtRu catalysts (i.e. catalyst size and placement are equally important). A section outlining Ru and PtRu catalyst preparation methods follows (Section 1.3.3.5).

1.3.3.1 Historical Development

The initial PEMFC catalysts developed for the Space Program used high loadings (4 mg cm^{-2}) of platinum-black (finely divided platinum particles, without carbon support) for the catalyst layer. This platinum had a very low utilisation, about 0.1% [*Appleby, 1996*], and resulted in very expensive electrodes (*ca.* US$ 400 kW^{-1} [*Taylor et al., 1992*]). The platinum-supported-on-carbon (Pt/C) technology developed for PAFCs (to enable the preparation of smaller platinum particles) was then adopted for use in PEMFCs. The Teflon-bound Pt/C catalyst layer used in PAFCs was not entirely suited to a solid polymer electrolyte, which could not flood throughout the catalyst layer. Appleby (in 1986), and Raistrick (in 1989) patented techniques, describing methods for incorporating Nafion ionomer into PAFC and PEMFC catalyst layers, respectively[xiii]. This addition of Nafion into the catalyst layer (via brushing/spraying ionomer solution onto the electrode surface) enabled equivalent performance with one-eighth of the platinum loading (0.5 mg cm^{-2}) compared to state-of-the-art Pt-black electrodes. However, platinum utilisation remained low (at only *ca.* 10%) in the early 1990s [*Appleby, 1995; Wilson et al., 1995; Srinivasan, et al., 1991*].

[xiii] On drying, the Nafion ionomer is recast, and helps to bind the catalyst layer, removing the need for using a Teflon binder.

The next major advancement involved mixing Nafion ionomer with the Pt/C particles before forming the catalyst layer. This technique was developed by Uchida *et al.* in 1995, to extend the interfacial area of polymer electrolyte throughout the catalyst layer (i.e. to increase the three-phase reaction zone). This method enabled further improvements in fuel cell performance, and is now the most commonly used method for preparing the catalyst layer. Platinum loadings of about 0.5 mg Pt cm^{-2} are conventional, but loadings down to 0.05 mg Pt cm^{-2} (i.e. 50 μg cm^{-2}) have been reported, usually at the hydrogen anode (although these ultra-low loadings can prove limiting at high current densities).

1.3.3.2 Conventional Preparation

The preparation of very small platinum particles has been extensively investigated in other work, particularly via chemical or colloidal precipitation techniques. For example, platinum particles with a diameter of 2.5- 3 nm, supported on carbon, are commercially available in the commonly used 20 wt% Pt/Vulcan XC-72R (from E-TEK, Inc. [*E-TEK, 1996*]). Supporting Pt nanoparticles onto high surface-area carbons was found to limit Pt particle agglomeration (and thus helped maintain small Pt particle sizes). Yet, the utilisation of such particles also depends on the fabrication of the catalyst layer (i.e. whether the 3PRZ conditions are satisfied).

A common method for platinising electrodes is via the chemical reduction of readily available platinum salts such as H_2PtCl_6 or $Pt(NH_3)_4Cl_2$ by $NaBH_4$. Platinum has been deposited onto or into the polymer electrolyte membrane to produce Pt/PEM electrodes using the impregnation-reduction method [*Delime et al., 1998; Sheppard et al., 1998; Millet et al., 1995; 1989; Liu et al., 1992*]; generally, large platinum particles and films are produced using this method. $NaBH_4$ has also been used to reduce H_2PtCl_6 [*Rogers, 1983*] and reduce thermally decomposed H_2PtCl_6 [*Shukla, 1992*] onto activated carbon surfaces. Unsupported platinum alloy particles have also been prepared by borohydride reduction [*Ley et al., 1997*], whereby the

particles are precipitated out of solution and may be made into an electrode using the decal transfer process [*Wilson and Gottesfeld, 1992, in J. Appl. Electrochem.*].

Another common way of preparing platinum-supported-on-carbon (Pt/C) with a high specific surface area is via a colloidal method such as the 'sulphite route' [*Stonehart, 1990; Petrow and Allen, 1977*]. In an early stage of this method, chloride is removed from H_2PtCl_6 by converting this platinum salt into $Na_6Pt(SO_3)_4$. The removal of chloride species from PEMFC catalysts is necessary since chloride is known to poison platinum and decrease the adsorption of oxygen, methanol [*Bagotzky et al., 1970*], and glucose [*Skou, 1973*]; chloride is even believed to corrode platinum in acidic media [*Chemodanov and Kolotyrkin, 1970*]. Meta-stable platinum oxide colloids are then prepared from $Na_6Pt(SO_3)_4$, which precipitate onto suspended carbon-black particles, followed by chemical reduction, e.g. by H_2, to produce the supported Pt/C catalyst [*Petrow and Allen, 1977*]. An average platinum particle diameter of 1.5- 1.8 nm may be prepared via the sulphite route, although even with particles this small only half of the platinum atoms are at the surface [*Stonehart, 1990*] and available to participate in reactions. Furthermore, for high utilisation the 3PRZ conditions must be satisfied, i.e. proper fabrication of the catalyst layer is paramount.

Wilson and co-workers modified the procedure of catalyst layer fabrication to maintain high performance with low platinum loadings [*Wilson et al., 1995; Wilson and Gottesfeld, 1992, in J. Appl. Electrochem; 1992 in J. Electrochem. Soc.*]. The Los Alamos group impregnated phosphoric acid-style electrodes with solubilised polymer electrolyte (usually Nafion®) [*Raistrick, 1989*], and eventually replaced all the PTFE in the catalyst layer with Nafion [*Wilson and Gottesfeld, 1992, in J. Appl. Electrochem; 1992 in J. Electrochem. Soc.*]. The procedure involved mixing with the supported Pt/C catalyst particles, and then drying this 'ink' onto the polymer membrane; this remains the most commonly used method today. Nafion acts as a binder for the catalyst layer and more importantly, increases the 3PRZ area throughout the layer. Before polymer electrolyte was mixed throughout the catalyst layer the 3PRZ was restricted to the approximately two-dimensional region where

the catalyst layer connects to the polymer membrane (eg. Nafion). This was not problematic in phosphoric acid fuel cell (PAFC) systems because the hot H_3PO_4 electrolyte was able to penetrate the Teflon-bound catalyst layers.

1.3.3.3 Shortcomings of Conventional Catalyst Layers

The utilisation of platinum within conventional Nafion-modified catalyst layers often remains low (e.g. up to 20% [*Appleby, 1995*]), largely due to poor ionic contact. However, the maximisation of ionic conductivity and 3PRZ area throughout catalyst layers is in direct conflict with the overall fuel cell performance. It is usually preferable to minimise the amount of Nafion within the catalyst layer, typically to about 10- 20 wt%[xiv], since high concentrations increase the *iR*-drop across the cell (and can also decrease the transport of reactant/product gases). Additionally, minimisation of Nafion usage is desirable for reduced electrode cost. A certain percentage of platinum particles will thus exist in catalyst layer regions lacking access to the sulphonic acid (SO_3H) groups of Nafion (depending on the amount of Nafion used). This platinum will not be accessible.

1.3.3.4 Alternative Preparation Methods

A number of different preparative approaches for fuel cell catalyst layers have been explored. The electrodeposition of catalysts has been investigated the most extensively, although other methods (generally involving a chemical reduction step) have also been investigated.

Electrodes have been successfully platinised via the chemical reduction of readily available platinum salts such as H_2PtCl_6 or $Pt(NH_3)_4Cl_2$ by $NaBH_4$. For example, $NaBH_4$ was used to reduce H_2PtCl_6 [*Rogers, 1983*] and reduce thermally

[xiv] Loadings of up to 25 wt% are sometimes used, but whether these will be economically feasible is uncertain.

decomposed H_2PtCl_6 [*Shukla, 1992*] onto activated carbon surfaces. Unsupported platinum alloy particles were also prepared by borohydride reduction [*Ley et al., 1997*], whereby the particles were precipitated out of solution and made into an electrode using the 'decal transfer' process [*Wilson and Gottesfeld, 1992*].

Platinum has also been deposited onto or into the polymer electrolyte membrane to produce Pt/PEM electrodes using an impregnation-reduction method [*Delime et al., 1998; Sheppard et al., 1998; Millet et al., 1995; 1989; Liu et al., 1992*]. There are a number of variations of the impregnation-reduction method, but essentially Pt/PEM electrodes were prepared by cation-exchanging $Pt(NH_3)_4^{2+}$ for the protons in Nafion, followed by an *in situ* chemical reduction with e.g. $NaBH_4$. Low platinum loadings were possible in some of these methods (*ca.* 0.5 mg cm^{-2}), but a small proportion of platinum was lost as isolated particles within the Nafion membrane. In these studies [*Delime et al., 1998; Millet et al., 1995; Liu et al., 1992*], platinum particles were generally deposited into the surface 0.5 μm of the polymer, forming a porous conducting layer, and in most cases large platinum particles and films are produced using these methods.

The electrodeposition of platinum has been studied by a number of researchers, with the main intention of depositing small platinum particles at the polymer electrolyte/electrode interface; increased platinum utilisation in PEMFC electrodes was also a typical objective. The most common method of electrochemical reduction (for PEMFC catalysts) employs the electroreduction of catalyst ions from an electrolytic solution into the catalyst layer. The other alternative is an electroreduction of catalyst ions that have been impregnated into either the polymer electrolyte, or the surface groups on the carbon support. Electrochemical reduction is commonly performed potentiostatically (at a constant potential), but galvanostatic reduction (constant current) has also been used. Reducing potentials have been applied in pulses, enabling greater ion diffusion to the deposition sites. Potential sweeping (e.g. via cyclic voltammetry) has also been used for deposition. In addition, the surface activities of electrochemically-deposited platinum are known to be similar to those of chemically-reduced platinum [*Hogarth et al., 1994*].

Platinum has been electroreduced from solution onto glassy carbon substrates [*Mikhaylova et al., 2000; Ye and Fedkiw, 1996; Shimazu, et al., 1988; 1987; Lin-Cai and Pletcher, 1983*], at carbon/Nafion interfaces [*Gloaguen et al., 1997; Verbrugge, 1994; Taylor, et al., 1992; Vilambi et al., 1992; Itaya et al., 1986*], and into PEMFC electrodes [*Choi et al., 1998; Gloaguen et al., 1997; Verbrugge, 1994; Hogarth et al., 1994; Taylor, et al., 1992; Vilambi et al., 1992*]. Under certain conditions, electrodeposition may enable accurate control over the platinum loading deposited onto an electrode. Loadings of 10 μg cm^{-2} or lower [*Mikhaylova et al., 2000; Gloaguen et al., 1997; Shimazu et al., 1988; 1987; Itaya et al., 1986*] and loadings of up to 750 μg cm^{-2} [*Mikhaylova et al., 2000; Gloaguen et al., 1997; Ye and Fedkiw, 1996; Verbrugge, 1994; Taylor et al., 1992; Vilambi et al., 1992; Shimazu et al., 1988; 1987; Itaya et al., 1986*] have been successfully prepared.

Platinum particle size may also be limited during electrodeposition; particles of less than 20 nm have been electrodeposited from $PtCl_6^{2-}$ solutions [*Mikhaylova et al., 2000; Choi et al., 1998; Gloaguen et al., 1997; Ye and Fedkiw, 1996; Shimazu et al., 1988; Itaya et al., 1986*]. Most notable of these studies is the work of Choi *et al.* [*Choi et al., 1998*], who reported the deposition of ~ 1.5 nm platinum particles into a preformed electrode, using a pulse electrodeposition technique. However, similar to the case of conventionally prepared electrodes, these pulse-platinised electrodes may face the same problem of poor polymer contact.

The cationic platinum salt, $Pt(NH_3)_4^{2+}$, has been used by a few researchers for selectively depositing platinum. Verbrugge [*Verbrugge, 1994*] investigated platinum electrodeposition from dilute $Pt(NH_3)_4Cl_2$ solutions into preformed catalyst layers and succeeded in depositing most platinum in a ca. 10 μm region at the Nafion membrane/electrode interface. Verbrugge attempted to utilise the unique chemistry of the carbon/Nafion interface in order to electroreduce platinum only at carbon particles in the vicinity of Nafion (i.e. in the 3PRZ areas). An indication of platinum particle size or dispersion was not given, so the possible utilisation of the platinum deposited via this method is uncertain. Taylor *et al.*

[*Taylor, et al., 1992; Vilambi et al., 1992*] electrodeposited a cationic platinum species into electrodes from solution through a Nafion film, and a particle size of 2- 3.5 nm was achieved. A tenfold increase in mass activity was reported on comparison to an E-TEK platinum colloid, which was believed to result from an increase in platinum utilisation.

In another variation on the use of ion-exchanged platinum, Kinoshita [*Kinoshita and Stonehart, 1977; Kinoshita, 1988*] impregnated $Pt(NH_3)_4^{2+}$ into the surface oxide species of a pre-oxidised carbon-black. The highly alkaline $Pt(NH_3)_4(OH)_2$ platinum species was used to adjust the pH of solution and increase the extent of ion-exchange. The electrode was then heated in air to produce platinum oxide particles. The PtO_2 was subsequently electroreduced, resulting in high surface-area platinum deposits (*ca.* 100 $m^2\ g^{-1}$). However, if polymer electrolyte contact is insufficient low platinum utilisation may still result in PEMFC electrodes platinised via this method.

1.3.3.5 PtRu Catalyst Preparation

Further to the above, a brief outline of PtRu electrode catalysation is provided here. Generally, the most common methods used to prepare PtRu/C are extensions of Pt/C preparation methods. As outlined in Section 1.3.1.1, alloying Pt with other elements (usually Pt group metals) can improve the catalysis of certain fuels. For operation on methanol or CO-containing H_2 (in a DMFC or PEMFC respectively), the PtRu binary catalyst system is typically used.

Similar to Pt/C preparation, PtRu/C supported catalysts are usually prepared via chemical deposition. The 'sulphite route' is a well-known example (see Section 1.3.3.2), where $Na_6Pt(SO_3)_4$ and $Na_6Ru(SO_3)_4$ species are prepared [*Stonehart, 1990; Petrow and Allen, 1977*], then oxidised into an unstable colloid which then precipitates onto suspended carbon-black particles. Other variations on this method have been investigated [*Castro Luna et al., 2000*]. Reduction of Pt and Ru species

from solution has also been studied, with either a slow addition of $NaBH_4$, or via formic acid-treated carbon powder [*Castro Luna et al., 2000*].

Again, as in the case of preparing Pt/C catalysts and platinising electrodes, electrodeposition of PtRu/C has probably been the major alternative to conventional preparation approaches. Co-electroreduction of PtRu from a mixed solution of Pt and Ru species is generally the most common approach. In addition, a number of more fundamental studies have investigated the electrodeposition of Ru onto a range of electrode surfaces. The commonly available $RuCl_3$ species is predominantly used.

Ru has been electrodeposited onto Pt [*Vigier et al., 2001; Lin et al., 1999; Cramm et al., 1997; Vukovic, 1990; Lezna et al., 1983*], Au [*Souza et al., 1997*], glassy carbon [*O'Connell, 1998*] and at a Nafion-Pt interface [*Shiroishi et al., 2001*]. Koponen *et al.* investigated the potentiostatic deposition of $RuCl_3$ onto a Pt/C + Nafion layer on a gold electrode [*Koponen et al., 2000*]. The Pt-H_{ads} region was found to decrease and the double-layer charging response increase with higher Ru loadings (i.e. Ru was electroreduced onto Pt sites). Koponen also found that Ru was deposited onto carbon, since some Pt crystallites were less accessible. Ru is known to preferentially reduce onto Pt sites of a smooth Pt electrode, rather than onto deposited Ru particles [*Koponen et al., 2000*].

Some researchers have investigated the 'spontaneous' or 'electroless' deposition of Ru from $RuCl_3$ solution, where an electrode such as Pt [*Szabó and Bakos, 1987*] or Au [*Strbac et al., 2001*], is immersed in the ruthenium solution and is ruthenised at the open circuit potential (i.e. without the application of potential). Sometimes a Pt electrode is first cathodically polarised and then allowed to stabilise under open circuit conditions before introducing the $RuCl_3$ solution [*Szabó and Bakos, 1987*]. Ruthenium species are adsorbed onto the Pt electrode, displacing adsorbed H species. Care must be taken to avoid the deposition of ruthenium oxide at higher potentials (for fuel cell catalysts). Another method investigated for depositing Ru

has involved impregnating $RuCl_3$ solution into graphite cloth before drying and heating in either N_2 or H_2 at 500 °C [*Williams and Mahmood, 1980*].

A number of researchers have co-electrodeposited binary PtRu alloys onto Pt [*Frelink et al., 1995; Beden et al., 1981*] and Au [*Cattaneo et al., 1999; Richarz et al., 1995; López de Mishima et al., 1995*] substrates, for fundamental investigations (e.g. surface/bulk fractions and electrocatalysis). To date, no studies have investigated the electrodeposition of PtRu binary catalysts into 'fuel cell type' electrodes. It is expected that the utilisation of such catalysts might be improved in a similar fashion to that of Pt, as was described in Section 1.3.3.4.

1.4 Summary & Aims

As outlined in Section 1.2, PEMFCs and DMFCs have candidate applications in portable electronics, stationary power and, most significantly at present, in electric vehicles. However, cost has been the primary limitation to any widespread commercialisation of PEMFCs and DMFCs (even despite significant cost reductions since the use of PEMFCs in space).

Eventually, automation of PEMFC cell and stack construction is anticipated, and with this a large reduction in PEMFC fabrication costs is expected. High-volume PEMFC (and DMFC) production is expected to facilitate a significant reduction in the fabrication costs of individual components [*ADL, 2000*]. However, the platinum-based catalysts are expected to constitute a significant proportion of the MEA cost, even in high-volume production estimates- these catalysts may constitute around 50% of the total MEA cost (i.e. ~ 36% of the total PEMFC cost) [*ADL, 2000*].

This work has investigated new methods for the catalysation of DMFC and PEMFC electrodes. The main objective was to enhance the utilisation of the Pt and PtRu catalysts in the catalyst layers of these electrodes. As discussed in Section 1.3.2.2, the utilisation of a catalyst may be improved via either preparing smaller catalyst

particles (i.e. with a higher specific surface area), or by increasing the proportion of platinum in the 3PRZ regions of the electrode (where fuel cell reactions are known to occur).

It was hypothesised that catalyst utilisation within fuel cell electrodes might be improved if the catalyst is electrodeposited directly into the electrode. Under certain conditions, the electrodeposition of catalyst ions into pre-formed fuel cell electrodes may enable the selective deposition of small platinum particles at the three-phase reaction zones (refer to Section 1.3.2.2). Placement of catalysts in 3PRZ regions of the electrode is difficult using conventional methods. Other methods were investigated to prepare small catalyst particles.

1.5 Outline of the Dissertation

Chapter Two provides a background to general electrochemical theory, since electrocatalysis and electrochemical analysis of catalysts are a major focus in the present work. In particular, the technique of cyclic voltammetry (CV) is outlined. In Chapter Three, the chemicals and materials used are provided, along with descriptions of experimental apparatus and methods.

An investigation into the poisoning of platinum deposits during electrodeposition is presented in Chapter Four as a potential electrode catalysation method. In Chapter Five a similar poisoning approach is trialled during the electrodeposition of ruthenium. Chapter Six investigates the selective electrodeposition of platinum into fuel cell electrodes following platinum-impregnation. Conclusions and some recommendations for future work in each of the three areas of investigation are then provided in Chapter Seven.

Chapter Two

Experimental Theory

2.1 Chapter Overview

Chapter Two outlines general electrochemical theory and concepts. Section 2.2 is provided to help familiarise the reader with electrochemical cells and basic electrode phenomena in solution. General aspects of electrodeposition are discussed in Section 2.3. Section 2.4 outlines cyclic voltammetry (CV), a common electro-analytical tool (CV is a major analytical technique employed in this work).

2.2 Electrochemistry

2.2.1 Electrochemical Cells

The mobility of electrons in a metal and ions in an electrolyte may be utilised for transferring charge, such as in an electrochemical cell. A simple example of an electrochemical cell comprises two dissimilar metals (electrically connected) in an electrolyte. Fig. 2-1 shows a diagram of such a cell, consisting of a zinc electrode immersed in a zinc sulphate solution connected to a copper electrode in a copper sulphate solution. The electrical (or external) circuit is completed via a resistor (which could be e.g. a light bulb).

In the case of Fig. 2-1, zinc is more reactive than copper so zinc atoms lose electrons (i.e. are oxidised), and Zn^{2+} ions pass into solution, Eq. 2-1. The electrons pass through the external circuit to the copper electrode. To balance charge, a net motion of cations develops between the zinc and copper electrodes. The salt bridge may be an electrolyte, such as K_2SO_4, contained within an agar gel, cloth or filter paper. A salt bridge allows the migration of ions between 'half-cells' to balance charge. In Fig. 2-1, K^+ ions move towards the $Cu|CuSO_4$ half-cell. Eq. 2-2 describes the reaction occurring at the copper electrode, where the Cu^{2+} cations accept electrons and are 'electrodeposited' (or 'electroplated' or 'electroreduced') as copper atoms.

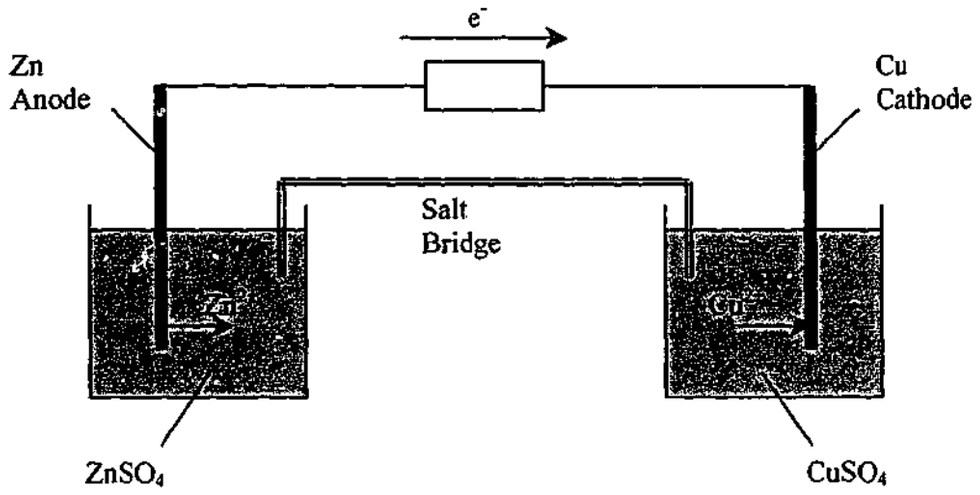

***Fig. 2-1** A simple electrochemical cell.*

$$Zn \rightarrow Zn^{2+} + 2e^- \qquad (2\text{-}1)$$

$$Cu^{2+} + 2e^- \rightarrow Cu \qquad (2\text{-}2)$$

$$Zn + Cu^{2+} \rightarrow Zn^{2+} + Cu \qquad (2\text{-}3)$$

In this Fig. 2-1, the zinc electrode is called the anode, since it is where oxidation occurs (the anode is sometimes defined as the electrode towards which anions travel). The copper electrode is the cathode, where reduction occurs. In a 'galvanic' cell[i], such as Fig. 2-1, the cathode becomes positively charged, and it accepts electrons. Eq. 2-3 describes the overall 'redox' reaction of Fig. 2-1 (Eqs. 2-1 and 2-2 are the two half-equations and occur simultaneously). Redox reactions involve the transfer of electrons. The word 'redox' is derived from reduction and oxidation. The chemical energy stored in the reactants is transformed into electrical energy. A

[i] i.e. a type of electrochemical cell, sometimes called a 'voltaic' cell; apparatus used to generate electricity from a spontaneous chemical reaction.

series of such cells could be connected (by joining oppositely charged terminals) to form a battery.

'Potential difference,' 'voltage' or 'electromotive force' are often used to describe the output of an electrochemical cell, which is the amount of electrical energy passing between two points of a circuit per unit of charge. The potential difference, E, is measured in volts (V), and is defined as the passages of one joule (J) of energy per coulomb of charge. Electrical current, i, is defined as the amount of charge, Q, (in coulombs, C) flowing for a given time, t. An ampere (A) is the standard unit of current and is equivalent to a coulomb of charge per second. The relationship between i and E is described by Ohm's Law (Eq. 2-4), where R is the resistance of the conductor (in Ohms, Ω).

$$E = iR \qquad (2\text{-}4)$$

2.2.2 Standard Potentials and the Electrochemical Series

Electrode potential may be considered as the ability of a galvanic cell to produce an electric current. Between two half-cells, this potential arises from competition for electrons. The half-cell with the stronger affinity for electrons (i.e. that with the greater reduction potential) will undergo reduction. 'Reduction potential' is defined as the tendency of an oxidant (i.e. species being reduced) in a half-cell to accept electrons.

The reduction potentials of half-cells are measured in comparison to the standard hydrogen half-cell, or the Standard Hydrogen Electrode (SHE). The SHE consists of a high surface-area platinum electrode in a 1.0 M H^+ solution, with H_2 gas bubbling across the electrode. The SHE is assigned a reduction potential, $E°$, of 0.0 V under standard conditions (25 °C, 1.0 M H^+ ion concentration and 1.0 atmosphere of H_2).

Eq. 2-5 describes the equilibrium between proton reduction and hydrogen oxidation.

$$2H^+ + 2e^- \leftrightarrow H_2 \qquad E^\circ = 0.0\ V \text{ (by definition)} \qquad (2\text{-}5)$$

The standard cell potential (E°_{cell}) is the potential difference between two half-cells, under standard conditions (i.e. 1.0 M concentrations of reacting ions, pressures of 1.0 atm, and at 25 °C). E°_{cell} may be calculated using Eq. 2-6 and a Table of 'Standard Reduction Potentials' such as Table 2-1. These tables are sometimes known as 'The Electrochemical Series'. Half-cells with high E° values are likely to undergo reduction reactions.

$$E^\circ_{cell} = E^\circ_{oxidant} - E^\circ_{reductant} \qquad (2\text{-}6)$$

In the galvanic cell example of Fig. 2-1, Zn is oxidised (the 'reductant') and Cu is reduced (the 'oxidant'). A possible cell voltage of 1.1 V may thus be generated (0.34 + 0.76 V, Table 2-1). In the case of the hydrogen-oxygen fuel cell (with acidic electrolyte), O_2 is the stronger oxidant, being reduced and oxidising H_2. This yields a maximum E°_{cell} of 1.23 V.

2.2.3 The Electrolytic Double-Layer

When a metal is immersed in an electrolytic solution the chemical equilibrium is altered and a chemical reaction must occur to minimise the free energy of the system. All systems (solutions, interfaces, etc.) will internally adjust into the lowest possible energy state. For example, if a copper electrode is brought into contact with a solution containing Cu^{2+} ions, then the equilibrium described by Eq. 2-7 will be set

up. Either the forward reaction (dissolution of copper ions into the solution) or the reverse reaction (deposition of copper ions onto the metal) must occur at the surface.

Increasing Oxidising Strength →

Reduction Reaction	*E° (V)*
$F_2 + 2e^- \leftrightarrow 2F^-$	+ 2.87
$H_2O_2 + 2H^+ + 2e^- \leftrightarrow 2H_2O$	+ 1.75
$Cl_2 + 2e^- \leftrightarrow 2Cl^-$	+ 1.36
$O_2 + 4H^+ + 4e^- \leftrightarrow 2H_2O$	+ 1.23
$O_2 + 2H^+ + 2e^- \leftrightarrow H_2O_2$	+ 0.68
$O_2 + 2H_2O + 4e^- \leftrightarrow 4OH^-$	+ 0.40
$Cu^{2+} + 2e^- \leftrightarrow Cu$	+ 0.34
$S + 2H^+ + 2e^- \leftrightarrow H_2S$	+ 0.14
$2H^+ + 2e^- \leftrightarrow H_2$	0.00*
$Zn^{2+} + 2e^- \leftrightarrow Zn$	- 0.76
$2H_2O + 2e^- \leftrightarrow H_2 + 2OH^-$	- 0.83
$Li^+ + e^- \leftrightarrow Li$	- 3.05

***Table 2-1** Standard reduction potentials for selected species.*

**By definition.*

$$Cu \leftrightarrow Cu^{2+} + 2e^- \qquad (2\text{-}7)$$

The dissolution of copper will occur if the chemical potential of the copper metal exceeds that of the Cu^{2+} ions and electrons [*Hamman et al., 1998*]. Conversely, deposition of copper will occur if the chemical potential of Cu^{2+} ions and electrons exceeds that of the copper metal. Both reactions involve the passage of electrical charge, and this is accompanied by the formation of a potential difference between the electrode and electrolyte [*Hamman et al., 1998*].

Continuing with the example above, the surface of the electrode will acquire a negative charge if the forward reaction occurs, as electrons are lost by Cu^{2+} ions passing into solution. Cations will then be attracted to the negatively charged electrode surface, setting up a charged 'double-layer'. The potential difference across the double-layer then prevents further dissolution of the Cu. Similarly, the surface of the electrode will acquire a positive charge if the reverse reaction occurs, as electrons are accepted by Cu^{2+} ions (via electrodeposition onto the metal). Anions are then attracted to the positively charged electrode surface, producing a double-layer and inhibiting further copper deposition.

The double-layer at the electrode/electrolyte phase boundary may be considered as two parallel charged layers of opposite polarity. This simple model is known as the 'Helmholtz layer', and it acts as a capacitor. The distance between the layers is taken as half the diameter of the ions (which may be larger solvated species) in the solution layer. Beyond the Helmholtz layer (i.e. passing further away from the electrode) is a region known as the 'diffuse' or 'Goüy-Chapman' double-layer, which takes into account thermal motions of ions [*Hamman et al., 1998*]. Again, oppositely charged ions are found in excess within this 'diffuse' layer region (moving between the Helmholtz and diffuse layers). These layers are shown schematically in Fig. 2-2.

If an electric current is passed between this electrode (known as the working electrode, WE) and a counter electrode (CE) immersed in the same solution, the equilibrium potential at the WE will be disturbed. Correspondingly, the double layer charging in the WE will be altered. The term 'overpotential' (or 'overvoltage') is defined as "the difference between the equilibrium potential and the potential at an electrode at which an appreciable current flows" [*Hamman et al., 1998*]. An electrode potential may be 'polarised', by forcing it beyond the equilibrium potential until the desired reaction occurs (or appreciable current flows) and/or a substance is decomposed.

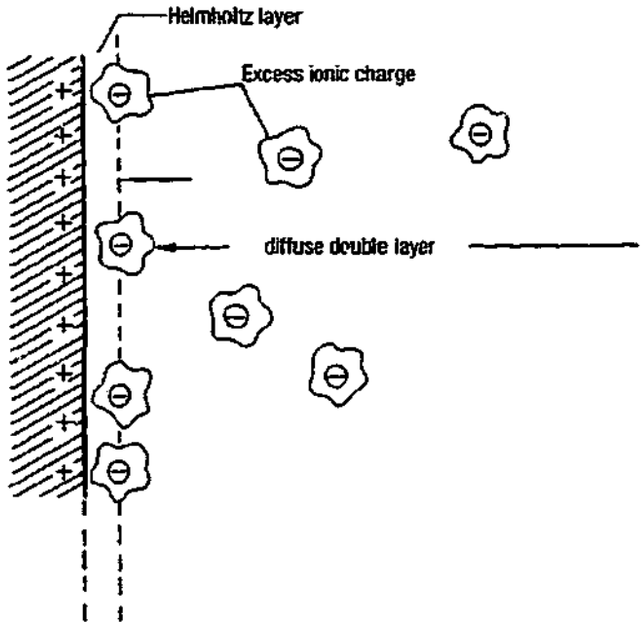

Fig. 2-2 A schematic representation of the double-layer at an electrode/electrolyte interface (from Hamman et al., 1998).

2.3 Electrodeposition

If a galvanic cell such as that shown in Fig. 2-1 is operated in reverse, i.e. if a sufficient voltage is applied between the electrodes to force electrons to travel in the opposite direction, an 'electrolytic' cell is achieved. The Zn electrode will then become the cathode (negative in this case) and will be electroplated by Zn^{2+} cations from solution. The Cu electrode (anode, positive) will be oxidised, releasing Cu^{2+} cations into solution. This is similar to the recharging process of a battery, i.e. applying electrical energy to convert chemicals back to a reactive state (in the context of the cell). Hence, electrical energy may be stored 'chemically'.

Electrodeposition is a commonly used industrial technique (where it is usually called 'electroplating'). Materials may be electrochemically coated with a thin metal layer for corrosion protection (e.g. zinc galvanisation of steel roofs, or tin coating of iron in cans), improved electrical contact (e.g. gold plating) and also to improve an item's

appearance (e.g. silver plating of kitchenware). Electrodeposition is also commonly used to recharge batteries. In addition, electrodeposition is widely used in metal processing, such as purification of copper and in the extraction of reactive metals (such as sodium and aluminium) from their ores.

In catalyst electrodeposition it is generally desirable that $E°$ or E_{red} is greater than that of hydrogen evolution (0.0 V_{SHE}) so that the amount of electroreduced metal may be estimated from coulometry. Coulometry is an electroanalytical technique that is founded on the direct relationship between the mass of a substance undergoing an electrochemical reaction and the amount of charge passed. If the current yield is 100% then Eq. 2-8 defines this relationship [*Hamman et al., 1998*], where m and M are the mass and molar mass of a substance, n is the number of electrons transferred per mole of substance and F is the Faraday constant (96485 coulombs per electron)]. Side reactions (e.g. hydrogen evolution and oxygen reduction, at the low potentials typical of electrodeposition) should be avoided for efficiencies approaching 100%.

$$Q = \int i.dt = m/(M/nF) \qquad (2\text{-}8)$$

2.4 Cyclic Voltammetry (CV)

Cyclic voltammetry (CV) is the major technique used for electrode characterisation in this work. CV is a versatile electroanalytical technique that enables the study of chemical reactions at an electrode-solution interface. Essentially, the potential of the electrode being studied (the working electrode) is cycled over time, and the current response is measured. Particular reactions take place on the WE surface at certain potentials, and these may be monitored from the resulting currents produced.

The amount of charge passed in a given reaction and reaction kinetics may be calculated from CV scans. By convention, the current density produced during an anodic reaction (i.e. oxidation) is taken as positive. Electrons from an oxidation reaction at the WE pass through the external circuit to the counter electrode, CE, at the surface of which a cathodic (i.e. reduction) reaction occurs with an equal and opposite charge. Conversely, during a cathodic reaction at the WE, electrons pass from CE to WE, and a negative current is recorded on the CV scan. For example, during platinum electroreduction from a Pt^{2+} species, the most likely reaction on the CE to balance the charge of the WE is the electro-oxidation of water, yielding oxygen (assuming experiments are performed under nitrogen). In this case the reaction at the WE (Pt^{2+} reduction to Pt) consumes the electrons produced at the CE.

Cyclic voltammograms are usually performed by scanning the WE potential from an initial value (E_i) to an upper or lower potential (E_u or E_l) and then back to E_i, which in this case is also the final potential (E_f). The WE potential is scanned linearly and the limits between scanning directions are known as the 'switching potentials' [*Mabbott, 1983*]; a triangular *E-t* waveform is thus imposed on the WE. In this way any number of CV scans may be performed. More complex CV experiments are possible where several switching potentials are used, and E_f does not necessarily have to be equivalent to E_i. In aqueous electrolyte the switching potentials are usually chosen to lie between the hydrogen and oxygen evolution potentials, so that a wide potential range is obtained and also because these processes help to remove any adsorbed impurities from the WE surface [*Hamman et al., 1998*].

Platinum Electrodes

Platinum electrodes are widely used in electrochemistry due to the high stability of platinum in a range of electrolytes and pH extremes. Platinum exhibits a wide electrochemical 'window' (i.e. voltage range) between the hydrogen and oxygen evolution regions where the metal is chemically stable. The strong catalytic nature of platinum is another reason for its use as a WE, enabling the study of reactions in a

convenient potential range and aqueous electrolyte. Moreover, the platinum WE surface is usually completely recoverable (e.g. by potentiodynamic cycling the electrode between the potentials of hydrogen and oxygen evolution).

The cyclic voltammograms in Fig. 2-3 illustrate the typical surface electrochemistry of platinum between the potentials of hydrogen and oxygen evolution in acidic electrolyte (0.5 M H_2SO_4)[ii]. By definition, the hydrogen evolution reaction (HER, i.e. the forward reaction of Eq. 2-5) occurs at 0.0 V vs. SHE. The oxygen evolution reaction (OER), Eq. 2-9, occurs at 1.23 V vs. SHE. The potentials reported in Fig. 2-3 are relative to the saturated calomel electrode (SCE), on which Eqs. 2-5 and 2-9 occur at – 0.242 V and + 0.988 V, respectively[iii]. The SCE is a commonly used reference electrode, containing a $Hg|Hg_2Cl_2|KCl(sat.)$ half-cell. Since the SCE reference electrode is used in this work, all potentials will be given in this scale.

$$2H_2O \rightarrow O_2 + 4H^+ + 4e^- \qquad (2\text{-}9)$$

$$Pt + H^+ + e^- \rightarrow Pt\text{-}H_{ads} \qquad (2\text{-}10)$$

$$Pt\text{-}H_{ads} \rightarrow Pt + H^+ + e^- \qquad (2\text{-}11)$$

$$Pt + 2H_2O \rightarrow PtO_2 + 4H^+ + 4e^- \qquad (2\text{-}12)$$

$$PtO_2 + 4e^- + 4H^+ \rightarrow Pt + 2H_2O \qquad (2\text{-}13)$$

[ii] The present dissertation is concerned only with electrodes in acidic electrolyte, primarily 0.5 M H_2SO_4. This concentration of sulphuric acid provides high ionic conductivity and has a pH of 0.0. This pH value is commonly used in electrochemistry, being equivalent to 1.0 mol L^{-1} of H^+ ions. Other commonly used electrolytes (in other work) include 1.0 M HCl or 1.0 M $HClO_4$ (both 1.0 M H^+ equivalents).

[iii] In Fig. 2-3, strong current densities from the OER are not observed until much higher potentials due to the large overpotential for this reaction on Pt in acidic media. By comparison, the HER on Pt is facile at low pH, as is evidenced by the small overpotential.

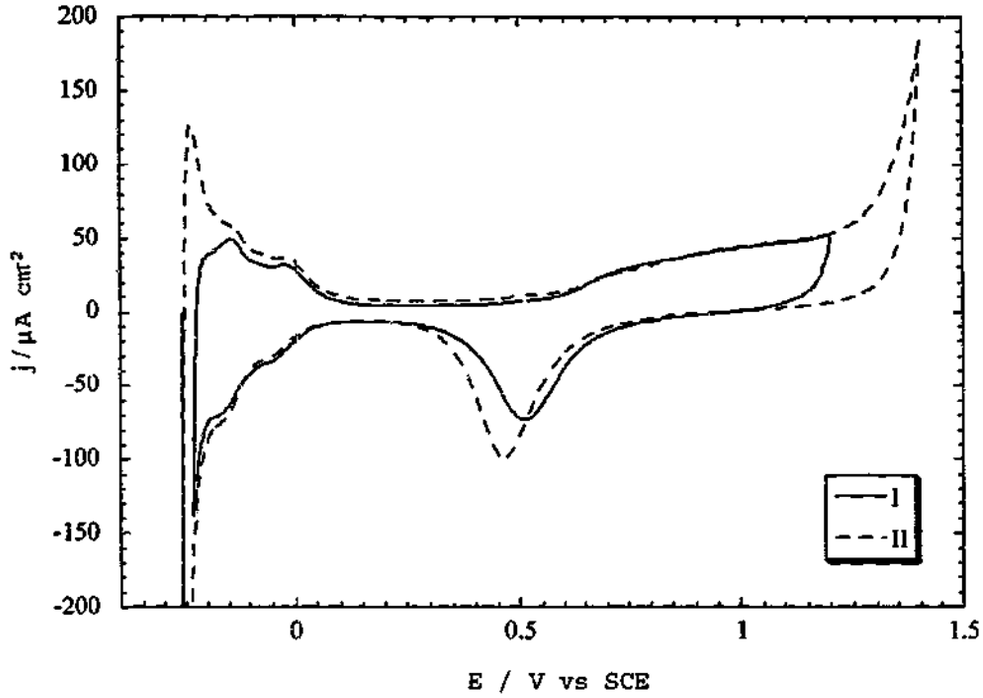

Fig. 2-3 Potentiodynamic analysis of a polycrystalline platinum electrode in 0.5 M H_2SO_4 (at 20 °C, under N_2). Cyclic voltammograms of Pt performed over a typical potential range (Curve I) and across a wider potential range (Curve II). Scan rate: 0.05 V s^{-1}.

A number of reactions take place on the platinum surface in the potential range between the HER and OER regions, in acidic media. Curve I in Fig. 2-3 was recorded after *ca.* 150 scans over a similar range. Pt CV scans are normally reproducible after *ca.* 10 consecutive scans between an E_i of – 0.232 V and an upper potential, E_u, of + 1.2 V (such as in Curve I)[iv]. If the Pt electrode is scanned over a wider potential range (e.g. Curve II) strong anodic current densities, j_a, for the OER and strong cathodic current densities, j_c, for the HER will be observed at the potential extremes. The kinetics of these reactions increase as the potential of the WE is swept to more extreme values (i.e. to greater overpotentials). Curve II commenced from an E_i of – 0.26 V to illustrate this point. Following the evolution of H_2 at low potentials, an additional anodic spike is observed on forward scanning (towards more positive potentials) at *ca.* – 0.25 V, representing the oxidation of H_2.

[iv] In the case of a platinum electrode in 0.5 M H_2SO_4 electrolyte, an E_i slightly above the HER onset by 0.01 to 0.05 V (i.e. – 0.232 to – 0.192 V vs. SCE) is usually employed.

This phenomenon is only observed in sufficiently fast scans, where molecular hydrogen (produced by Eq. 2-5, at low potentials) close to the platinum surface is oxidised.

Nitrogen is usually bubbled through the electrolyte and a nitrogen atmosphere maintained during electrochemical experiments to remove any gases (especially oxygen) from solutions. If dissolved oxygen is present, the oxygen reduction reaction (ORR, i.e. the reverse of Eq. 2-9) is likely to occur at the WE at low potentials and the cathodic currents produced may interfere with currents resulting from other reactions of interest. Usually solutions are 'degassed' for at least 15 min before experimentation.

In the potential region – 0.242 to + 0.15 V, the platinum electrode has a surface layer of adsorbed hydrogen atoms, where 1 H atom is chemisorbed to each surface platinum atom (Pt-H_{ads}). The j_c for this process, Eq. 2-10, may be observed by two or three steps in the cathodic shoulder, before the HER onset. This hydrogen monolayer is oxidised, Eq. 2-11, on scanning the Pt WE potential to more positive values, (and the anodic current response may be observed by two or three steps in the range – 0.242 to + 0.15 V) at slightly more positive potentials *cf.* the cathodic steps for Pt-H_{ads} formation. The region between ~ + 0.15 V and + 0.3 V is known as the "double-layer" region, where no chemical reactions take place on the platinum surface. The current densities observed in this region result from the capacitance of the platinum-electrolyte electrical double-layer, C_{dl}.

When scanning the Pt WE to more positive potentials, the formation of a 'hydrated-platinum-oxide' surface layer occurs, Eq. 2-12. This is essentially a thin, surface layer of platinum oxide. On continuing the positive potential CV sweep, the oxygen evolution reaction (OER, Eq. 2-9) takes place. On the reverse CV sweep (towards negative potentials) the platinum oxide layer is electroreduced, Eq. 2-13, in the region + 0.8 V to + 0.4 V. Finally, on scanning the WE potential back through the double-layer region towards the E_i (- 0.232 V), Pt-H_{ads} forms again, Eq. 2-10.

The scanning rate of 0.05 V s^{-1} is quite commonly used since it provides a reasonably rapid indication of both the roughness and cleanliness of the platinum surface. The surface of platinum is susceptible to the adsorption of minute traces of impurities such as organic species (particularly CO), sulphur-containing species (especially sulphide and sulphite) and certain anions (especially halogen ions, but also HSO_4^- and others to a lesser extent). For this reason, platinum electrodes are usually scanned between the HER and OER onset potentials several times to acquire a reproducible, clean electrode surface; generally scans are considered reproducible if constant over 10 min of potential cycling (i.e. roughly 10 CVs between the HER and OER onset potentials at 0.05 V s^{-1}) [*Will, 1965*].

Since there may be only one hydrogen atom adsorbed per surface platinum atom (and bridging of hydrogen atoms over two platinum atoms is unlikely) it is possible to calculate the surface area of a platinum electrode from the charge passed during either the formation (Eq. 2-10) or oxidation (Eq. 2-11) of Pt-H_{ads}. This is sometimes called the electrochemical surface-area (ESA) of platinum, and may be calculated using Eq. 2-14, where i is the current (A) excluding the electric double-layer (i-i_d), dE is the potential interval (V) between current data points in the CV scan and ν is the scanning rate (V s^{-1}). $\int i.dE$ is the integration of the area under the Pt-H_{ads} formation/oxidation current peaks and Q_H is the charge of forming/oxidising Pt-H_{ads} (210 μC cm^{-2}). The specific surface area, S (m^2 g^{-1}), of a platinum electrode may be calculated from the ESA:Pt-loading ratio, Eq. 1-16 (Chapter One).

$$\text{Pt ESA} = \int i.dE/\nu.Q_H \qquad (2\text{-}14)$$

Chapter Three

Experimental Methodology

3.1 Chapter Overview

Chapter Three is primarily concerned with the methods used in this work to prepare electrode substrates, deposit catalysts and analyse catalysed electrodes. A description of all chemicals and materials used is provided in Section 3.2. The preparation of reproducible working electrodes (platinum, glassy carbon and carbon-black based) is discussed in Section 3.3. Section 3.4 outlines the general methods used in this work to electrodeposit catalysts and the electrochemical apparatus and conditions typically employed. The more specific methods of catalysation developed in this work are explained in Chapters Four, Five and Six. Section 3.5 pertains to the instrumental methodology used to analyse the catalysed electrodes.

3.2 Chemicals and Materials

$H_2PtCl_6.xH_2O$ (hydrogen hexachloroplatinate (IV) hydrate, 99.995%), $Pt(NH_3)_4Cl_2.xH_2O$ (tetraammineplatinum (II) chloride hydrate, 99.99%) and $RuCl_3.xH_2O$ (ruthenium (III) chloride hydrate) were purchased from Aldrich. 0.01 M solutions of these platinum and ruthenium species were prepared by dissolution in 0.5 M H_2SO_4 (A.R. Grade) in the fume cupboard for electrodeposition experiments.

$Na_6Pt(SO_3)_4$ was prepared from $H_2PtCl_6.xH_2O$ according to US Patent 4,044,193 [*Petrow and Allen, 1977*]. Eq. 3-1 illustrates the overall reaction in the commonly called 'sulphite-complex' route for the preparation of $Na_6Pt(SO_3)_4$ [*Ravikumar and Shukla, 1996*]. Essentially, $Na_6Pt(SO_3)_4$ is produced with careful adjustments of the pH of solution in a fume cupboard (SO_2 in particular is released). The insoluble white salt was copiously rinsed with warm Milli-Q water to remove any probable impurities such as chloride ions [*Stonehart, 1990*]. $Na_6Pt(SO_3)_4$ was then dissolved in 0.5 M H_2SO_4 producing the complex platinum sulphite acid, $H_3Pt(SO_3)_2OH$

[*Petrow and Allen, 1977*]. A solution of 0.01 M $H_3Pt(SO_3)_2OH$ in 0.5 M H_2SO_4 was thus prepared.

$$H_2PtCl_6 + Na_2CO_3 + NaHSO_3 \rightarrow Na_6Pt(SO_3)_4 \qquad (3\text{-}1)$$

$$RuCl_3 + HCl + Na_2CO_3 + NaHSO_3 \rightarrow Na_6Ru(SO_3)_4 \qquad (3\text{-}2)$$

$Na_6Ru(SO_3)_4$ was prepared from $RuCl_3.xH_2O$ in a similar way to $Na_6Pt(SO_3)_4$, using US Patent 4,044,193 [*Petrow and Allen, 1977*]. Again, $Na_6Ru(SO_3)_4$ is prepared in the fume cupboard, Eq. 3-2 [*Ravikumar and Shukla, 1996*]. A solution of 0.01 M $H_3Ru(SO_3)_2OH$ in 0.5 M H_2SO_4 was also prepared. The confirmation of the chemical formulae of these ruthenium species is further discussed in Chapter Five.

Ultrapure water (resistance of ~ 18.2 MΩ) was prepared by filtration through a Milli-Q water treatment system and was used throughout for all solutions and rinsings.

A carbon-black (Vulcan XC-72R), commonly used in both the gas-diffusion and catalyst layers of PEMFCs, was purchased from Multichem. Vulcan has a primary particle size of ~ 30 nm, and comes in aggregates with diameters of ~ 250 nm (about 79 particles per aggregate) [*Kinoshita, 1988*]. The Vulcan particles have many surface irregularities and defects, and have a surface area of 254 $m^2 g^{-1}$ [*ibid.*].

Toray TGPH-120 carbon-paper (25 wt% wetproofed carbon fibres, thickness 0.3 mm) was purchased from E-TEK, Inc. This provides a rigid backing for the electrode, and also acts as part of the gas-diffusion component. A 20 wt% Pt/C 'standard' catalyst (commonly used in PEMFCs) was purchased from E-TEK for comparing catalysts. This has a platinum particle size range of 2- 5 nm supported on Vulcan XC-72R.

A 5 wt% Nafion ionomer solution (in low molecular weight alcohols and water) was purchased from Aldrich. A Nafion 117 polymer membrane was also purchased (from DuPont Australia Ltd.) and has a thickness of ~ 175 μm. Both Nafion varieties had an equivalent weight of 1100 (grams polymer/moles SO_3H groups).

Most electrochemical apparatus was obtained from Bioanalytical Systems (BAS Inc.), including 3 GC electrodes (3 mm diameter, embedded in a CTFE[i] cylinder) and 2 platinum electrodes (2 mm diameter, also embedded in CTFE). Felt polishing pads, 1, 3 and 15 μm diamond suspensions, 0.05 μm Al_2O_3 suspension, a support tube (similar to a Luggin capillary) and a glass electrochemical cell (~ 20 cm diameter) with a Teflon sealing lid to house the electrodes were purchased from BAS Inc. 2 saturated calomel reference electrodes (SCEs, $Hg/HgCl_2$) were purchased from Radiometer Pacific Pty Ltd.

Other chemicals used in this work include A.R. Grade HCl solution, $NaHSO_3$, isopropyl alcohol (isopropanol), methanol, cyclohexane and a 60.1 % PTFE suspension in water (Aldrich). High purity nitrogen, oxygen and hydrogen were purchased from BOC Gases; nitrogen was used in all electrochemical de-aeration.

3.3 Electrode Preparation

3.3.1 Platinum Electrodes

The platinum working electrodes were polished with a series of grits, e.g. from a 2 μm diamond suspension down to the 0.05 μm alumina suspension. The electrode surface was held flat on the polishing felt and circular or 'figure of 8' polishing patterns were carried out. Electrodes were then ultrasonically cleaned in Milli-Q water for 1-2 minutes at room temperature before each experiment. Sometimes electrodes were also rinsed with methanol before the ultrasonication step. The

[i] Chlorotrifluoroethylene fluoropolymer.

typical platinum redox behaviour was confirmed via cyclic voltammetry (as described in Section 2.4) and used to determine the surface purity of the electrode. Electrochemical cycling (or polarising) was used in most cases to clean the Pt surface (Section 2.4).

3.3.2 Glassy Carbon (GC) Electrodes

GC electrodes were used in preliminary platinum electrodeposition investigations, since GC allows the preparation of a readily reproducible, low surface-area carbon support. GC electrodes were polished in a similar fashion to the Pt working electrodes (often only requiring the 0.05 μm Al_2O_3 suspension) and the typical GC redox behavior was confirmed via cyclic voltammetry.

Baseline cyclic voltammograms of the polished GC electrodes were then recorded in 0.5 M H_2SO_4 to ensure a smooth, reproducible surface (i.e. unchanged over 10 cyclic voltammograms at 50 mV s^{-1}) without any evidence of platinum or surface oxide functionalities. These electrodes were extensively scanned in the range – 0.23 to + 1.2 V[ii] and repolished, if necessary. The GC electrodes were then repolished and ultrasonically cleaned before checking via cyclic voltammetry. At this final stage only 5 baseline CV scans were performed so as to avoid oxidation of the GC surface (and the upper voltage was not allowed to exceed + 0.4 V for the same reason).

3.3.3 Carbon-Black (CB) Based Electrodes

'Fuel cell type' electrodes consisting largely of carbon-black (CB) were prepared using the present state-of-the-art PEMFC electrode design, as described in Section 1.3.3. The electrodes ranged from 1 to 5 cm^2 in geometric area.

[ii] All potentials are reported on the SCE scale (refer to Chapter Two), unless otherwise stated.

These electrodes consist of a catalyst layer supported on a diffusion layer, which is in turn supported on porous carbon paper (Section 1.3.1.3). The catalyst layer is essentially a thin, composite film of polymer electrolyte and carbon-black, which, in the case of the present electrodeposition work, is uncatalysed.

A backing layer paste or 'ink' was prepared by suspending 10 wt% PTFE (from a 60.1 wt% PTFE dispersion in water) and Vulcan XC-72R carbon-black in cyclohexane. Care was required in preventing drying of the Teflon dispersion, and water was usually added quickly after weighing the desired amount. This 10 wt% PTFE/C ink was ultrasonically homogenised for ~ 30 minutes, and a loading of 0.7 mg cm^{-2} was applied to the wet-proofed carbon paper (Toray TGPH-120). The electrodes were dried at ~ 75 °C to constant weight, and then sintered at 350 °C for 30 minutes.

Catalyst layer inks were prepared from a 5 wt% Nafion solution and Vulcan XC-72R carbon-black. The ink comprised 10 wt% Nafion(dry mass)/C in isopropyl alcohol and water, and was ultrasonically homogenised (at 50 Hz) prior to application. 2.3 mg cm^{-2} of this ink was applied via pipette to the sintered backing layers, before drying the electrodes to constant weight. The electrodes were allowed to dry at room temperature and were then heated at 90 °C for 1.0 h (in air) to ensure that all the solvent had evaporated. Baseline CV scans of the CB electrodes were performed in 0.5 M H_2SO_4 (presented later, in Section 2.4).

Some 'conventional' electrodes were also prepared for comparison. These were prepared in the same fashion, using either a commercially available 20 wt% Pt/C catalyst (from E-TEK Inc.), or by an in-house preparation of Pt/C or PtRu/C supported catalysts (see below). The carbon-black support for these catalysts is of the Vulcan XC-72R variety. These catalysed carbon particles are, of course, used in place of the uncatalysed carbon-black in the electrodeposited electrodes.

3.4 Catalyst Electrodeposition

3.4.1 Three-Electrode Cell Arrangement

All electrochemical experiments were performed in a three-electrode cell at room temperature. The cell consisted of a working electrode (Pt, GC or CB), a Pt wire counter electrode (immersed ~ 2 cm in solution), and a saturated calomel reference electrode (SCE).

The SCE was separated from the cell by a support tube similar to a Luggin capillary, which was filled with the supporting electrolyte, usually 0.5 M H_2SO_4. Luggin capillaries are used to prevent any ions from the reference electrode from interfering with reactions at the WE. The capillary is similar to a salt bridge, allowing the transfer of ions, and thus determination of the potential difference between the WE and RE (in this case the SCE). Current flows between the WE and CE, and thus the end of the Luggin capillary is placed immediately in front of the WE. The RE is generally at a very high impedance so that most current flows between the WE and CE (the potential drop between capillary tip and RE is negligible, since only extremely low currents pass, e.g. less than 10^{-12} A [*Hamman et al., 1998*]).

The highly concentrated electrolyte helps to minimise conductivity variations (i.e. the non-uniformities in current flow) throughout the solution. The glass frit at the base of the SCE tube was spaced at a distance roughly twice its diameter from the working electrode surface, since distances of less than this can cause inhomogeneous current distributions due to screening of the WE [*Hamman et al., 1998*].

All potentials are reported in the SCE scale (– 0.242 V vs. SHE) unless otherwise stated. High purity nitrogen was used to flush gases from all solutions for at least 15 minutes before use and usually remained bubbling for the duration of each experiment (to minimise diffusion limitations and maintain an oxygen-free solution).

E-Chem software (version 1.3.2, AD Instruments) was used for cyclic voltammetry and linear-sweep experiments; Chart (version 3.6, AD Instruments) was used for all potentiostatic experiments. All experiments were programmed via a Macintosh computer platform, interfaced with a ML500 (8 channel) Powerlab Recorder (AD Instruments), connected to a ML160 Potentiostat (AD Instruments).

3.4.2 General Electrodeposition of Catalysts

Before any noble metal electrodeposition was studied, the electrochemical characteristics of the working electrodes were investigated in 0.5 M H_2SO_4 solution. The reproducibility in producing new surfaces on the GC and Pt electrodes by the polishing procedure and in preparing clean CB-based electrodes (refer to Section 3.3) was also investigated.

The electrochemistry of each platinum and ruthenium species was first studied on GC electrodes using CV and/or linear potential sweeps. Scans/sweeps were usually performed in the range – 0.232 V to + 0.4 V (vs. SCE); in some cases potential extremes of up to ± 1.0 V were used. Generally for electrodeposition, E_i, was chosen as 0.4 V and scans proceeded towards more negative potentials (to monitor the electroreduction onset for the noble metal species). Since oxidation of the GC surface occurs readily at potentials positive to + 0.4 V, scanning above this potential was avoided if possible. Higher catalyst loadings were usually produced potentiostatically, where a suitable potential was chosen to readily enable the reduction of the noble metal. In most cases, catalyst electrodeposition was investigated onto all three types of working electrodes, from 0.01 M solutions of the noble metals in 0.5 M H_2SO_4.

The analysis of these electrodeposited catalysts was then carried out (as is outlined in the next section), particularly via electrochemical means.

3.5 Catalyst Analysis

Cyclic voltammetry is the major technique used for characterising the electrodes in this work. Refer to Section 2.4 for a more detailed outline of CV theory. Atomic absorption spectroscopy (AAS) was used to determine the platinum loadings deposited into the CB-based electrodes. Morphological evaluation of the catalyst layers was achieved via scanning electron microscopy (SEM). Energy dispersive X-ray analysis was also used to help confirm the composition of the noble metal deposits.

3.5.1 Cyclic Voltammetry (CV)

In most cases following the catalyst deposition experiments, the platinised/ruthenised electrodes were rinsed in Milli-Q water and placed in 0.5 M H_2SO_4 for an initial investigation. The same three-electrode cell described in Section 3.4.1 was used for all electrochemical analyses (primarily CV) of the catalysed electrodes. The conditions were also again at room temperature, and under a nitrogen atmosphere (all experiments following de-aeration of solutions for at least 15 min). Again, all potentials reported in this dissertation are with reference to the SCE (– 0.242 V SCE = 0.0 V SHE).

A few cyclic voltammograms of the catalysed electrodes were performed at 0.05 V s^{-1} from – 0.232 to + 1.2 V to check for any presence of platinum or ruthenium. In some cases, especially with ruthenised electrodes, lower upper potentials were used (Chapter Five). The E_l of – 0.232 V was used to avoid any current interference from the evolution of hydrogen on both Pt and Ru electrodes at potentials ≤ – 0.242 V.

The electrodes were then potentiodynamically cycled from – 0.232 to + 1.4 V at 0.05 V s^{-1} (or occasionally up to 0.5 V s^{-1}) for 10-50 scans. Again, in the case of Ru-containing electrodes, care was taken to use lower E_u values. Following these cycling

treatments, electrodes were again investigated. This two-step procedure was repeated until reproducible platinum or ruthenium surfaces were acquired (i.e. from observing the redox characteristics of the catalyst metal).

High flow rates of nitrogen were used to purge solutions of any possible gases produced during either the deposition or electrochemical analysis stages. In situations where the catalysed electrodes appeared highly poisoned, the 0.5 M H_2SO_4 solution was changed and the electrodes and cell were rinsed at several stages throughout the cycling procedures.

3.5.2 Scanning Electron Microscopy (SEM) and Energy Dispersive X-Ray Spectroscopy (EDXS)

The platinised CB-based electrodes were also investigated by scanning electron microscopy (SEM) on a JEOL-840A instrument at an accelerating voltage of 20 kV. The dispersion of the platinum nuclei was evident from this analysis, and an average platinum particle size estimated. An X-ray source was connected to the SEM, enabling the energy dispersive X-ray spectroscopy (EDXS) technique. EDXS was used to confirm the platinum or ruthenium composition of the deposits.

The high atomic masses of platinum and ruthenium (195.1 and 101.1 g mol^{-1}, respectively) cause these elements to appear as bright regions during secondary electron derived SEM images, relative to the carbon-black substrate [*Passalacqua et al., 1998*]. The other typical elements contained in the Nafion-bound CB electrodes have relatively low atomic masses in comparison, e.g. 1, 12, 16 and 32 g mol^{-1} for hydrogen, carbon, oxygen and sulphur, respectively. Thus a high contrast between catalysed and non-catalysed electrode regions is typically observed.

3.5.3 Atomic Adsorption Spectroscopy (AAS)

Quantitative elemental analysis is possible by using Atomic Absorption Spectroscopy (AAS). In this technique, ionised atoms absorb light of a certain wavelength characteristic of that element. An accurate solution is prepared from a known mass of sample, and this is introduced into the ionising flame at a temperature adequate for ionising the element of interest. An elemental lamp for the particular element under analysis is used. For quantitative analysis, the instrument must be calibrated using solutions with known concentrations of the element to be analysed. Exact concentrations of an element are then calculated from relative absorption intensities.

AAS was used to quantify the amount of platinum present in the platinised CB-based electrodes prepared. Electrodes were extensively washed with water and heated in 0.5 M H_2SO_4 (at 80 °C for 1.0 h) before AAS analysis, to ensure that any remaining platinum ions, if any, were removed. AAS analyses were performed externally by Global Environment Corporation Pty Ltd (Melbourne).

3.5.4 PEMFC Test Station

4 cm^2 CB-based electrodes (2 cm x 2 cm) were prepared, as described in Section 3.3.3, either conventionally with Pt/C catalysts, or platinised via an electrodeposition method. A thin layer of Nafion was applied to the catalysed electrode surface by pipette from a 1 wt% Nafion solution (diluted in water or isopropyl alcohol from a 5 wt% solution) onto the surface in stages, drying (at 80- 90 °C) to constant weight. In this way, 0.5 mg cm^{-2} of dried Nafion film was applied to each electrode surface.

The reasons for applying this additional Nafion are two-fold. Some of the Nafion electrolyte penetrates into the catalyst layer, further increasing the three-phase reaction zone and thus increasing the utilisation of the noble metal catalyst particles.

The second benefit is that the thin Nafion film enables physical bonding of the electrode to the Nafion membrane (e.g. 112 or 117) during the hot-pressing stage, which enhances the ionic conductivity between the anode and cathode.

The membrane-electrode assembly (MEA) was prepared by hot pressing two Nafion-coated CB-based electrodes onto either side of a clean Nafion membrane (the membrane was previously cleaned by boiling in 30% H_2O_2 for 1 h followed by boiling in 0.5 M H_2SO_4 for 1-2 h to remove any impurities). The MEA was placed between grease-proof paper and laminated at 110 °C (between two thin aluminium sheets, with roughly 3- 4 passes through the laminator). The MEA was then pressed (under ~ 50 kg cm^{-2}) at 125 °C under for 2 min. The MEA was slowly cooled (e.g. 5 °C min^{-1}) under load, then removed.

The MEA was inserted into the PEMFC test station and allowed to equilibrate for several hours. During equilibration the fuel cell was usually maintained at around 60 °C, and the humidifiers (through which N_2 or O_2 bubbled) were set to ~ 80 °C. The general operating conditions involved the fuel cell at ~ 80- 85 °C, the hydrogen humidifier at ~ 60 °C and the oxygen humidifier at ~ 20 °C. Gas flow rates were around 100 cm^3 min^{-1}. An HP Electronic Load controlled the desired potential and consumed the current generated.

Chapter Four

Platinum Poisoning During Electrodeposition

4.1 Introduction

The utilisation of platinum in a PEMFC or DMFC electrode depends on both the placement and size of the platinum particles, as outlined in Chapter One. In this chapter, the inhibition of the growth of electrodeposited platinum (during electrodeposition) was investigated for the preparation of small platinum particles.

Electrodeposition has been shown to enable selectivity in the placement of platinum deposits in desired areas of carbon-black (CB) based electrodes used in these lower temperature fuel cells (refer to Chapter One). However, maintaining a small particulate size is an issue with this technique, since platinum will preferentially reduce onto a platinum surface rather than carbon. Particulate growth may be inhibited by the adsorption of substances or 'poisons' on the surface of an electrodeposited metal during electrodeposition- thus discouraging any further reduction of metal ions onto the metal deposit.

In this chapter, the electrodeposition of a platinum precursor in the 'sulphite route', $H_3Pt(SO_3)_2OH$, was investigated. The resulting electrochemical behaviour of the Pt deposits proved interesting and electrodeposition from this species was thus explored for possible benefits in preparing fuel cell catalysts. The $H_3Pt(SO_3)_2OH$ compound was initially chosen for platinising electrodes because all chloride ions[i] are removed during its preparation [*Petrow and Allen, 1977*] and this should enable the preparation of a 'cleaner' platinum catalyst with a higher chemical stability. Surprising results were found, however, in preliminary $H_3Pt(SO_3)_2OH$ electrodeposition experiments, where the resulting platinum deposits appeared to be poisoned. It was then postulated that the species adsorbing on the platinum deposits might, in fact, limit the growth of these particles during the electrodeposition step.

[i] Chloride is a known Pt poison [*Bagotzky et al., 1970*], refer to Section 1.3.3.2 of Chapter One.

4.2 Platinum Deposited from $H_3Pt(SO_3)_2OH$ Solution

4.2.1 Potentiodynamic Studies of $H_3Pt(SO_3)_2OH$

The electroreduction of $H_3Pt(SO_3)_2OH$ onto glassy carbon from a 0.01 M $H_3Pt(SO_3)_2OH$ + 0.5 M H_2SO_4 solution is shown by Curve II in Fig. 4-1. The platinum sulphite acid reduces onto GC at potentials negative to – 0.4 V when sweeping the electrode potential towards more negative values (Curve II). For comparison, Curves III and IV illustrate GC platinisations from 0.01 M solutions of $Pt(NH_3)_4Cl_2$ and H_2PtCl_6 in 0.5 M H_2SO_4 via similar potentiodynamic sweeps. The existence of platinum deposits on the electrodes was confirmed in later analyses from the typical platinum CV 'fingerprint' scans in sulphuric acid [*Will, 1965*] and also by EDXS, as described later in this chapter.

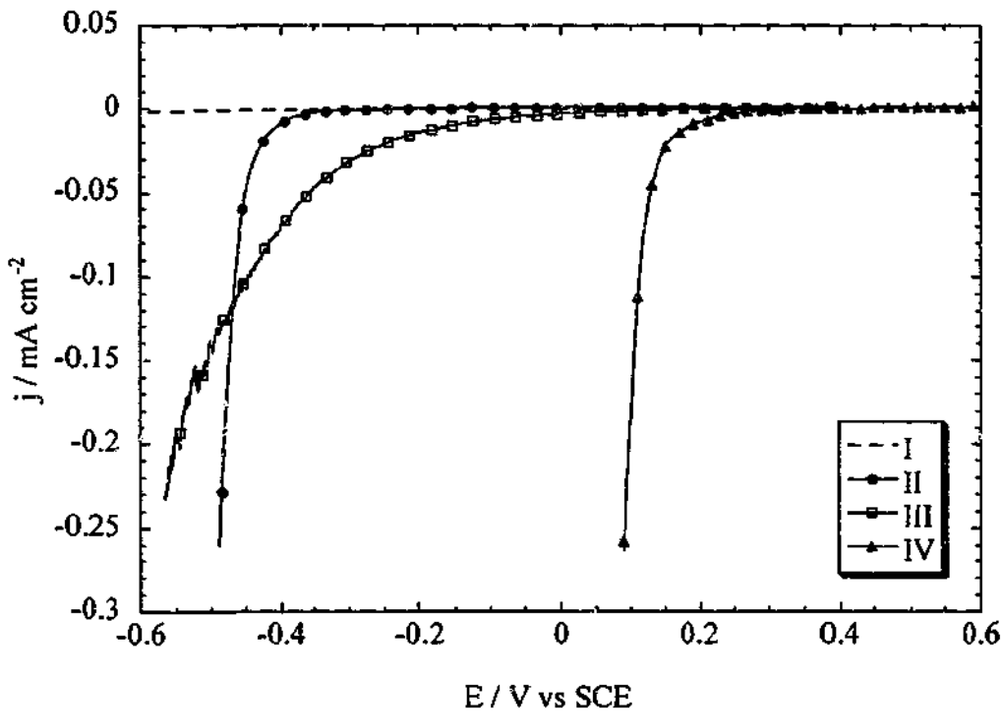

Fig. 4-1 *Linear-sweep electroreduction of platinum from aqueous solutions onto glassy carbon (GC) electrodes. Curve I is the GC baseline in 0.5 M H_2SO_4. Curves II to IV show the initial sweeps of platinum electroreduction onto GC from 0.01 M solutions of $H_3Pt(SO_3)_2OH$, $Pt(NH_3)_4Cl_2$ and H_2PtCl_6 in 0.5 M H_2SO_4, respectively. Sweep rate: 0.001 V s^{-1}.*

$H_3Pt(SO_3)_2OH$ appears to be very stable in comparison with the other two platinum species. $PtCl_6^{2-}$ is readily electroreduced onto GC at potentials negative to + 0.2 V (Curve IV in Fig. 4-1), in agreement with the literature [*Itaya et al., 1986; Ye and Fedkiw, 1996*]. The $Pt(NH_3)_4^{2+}$ species has not been studied as extensively as chloroplatinic acid and the electroreduction of this species is known to be slow [*Penven et al., 1992*] but $Pt(NH_3)_4^{2+}$ appears to reduce at potentials below 0.0 V (Curve III). The substitution of ammonia ligands for chlorides is known to increase the stability of platinum species [*Bard, 1976*]. The complexing ability of sulphite probably contributes to the high chemical stability observed for $H_3Pt(SO_3)_2OH$.

Numerous studies reported in the literature have investigated the electroreduction of platinum from $PtCl_6^{2-}$ solutions onto carbonaceous substrates [*Itaya et al., 1986; Ye and Fedkiw, 1996*]. It is well documented that once platinum nuclei have been deposited, further platinum deposition will take place onto existing platinum nuclei since this facilitates reduction at a lesser overpotential in comparison with the carbon substrate. This leads to a positive shift in the onset potential for $PtCl_6^{2-}$ reduction in CV sweeps following the initial reduction sweep, as demonstrated by Curves II to IV in Fig. 4-2. In this Figure, the onset for $PtCl_6^{2-}$ reduction in the second sweep (Curve III) has shifted positively by ~ 0.15 V *cf.* that in the initial reduction sweep (Curve II). Curve IV in Fig. 4-2 was performed after 10 CV reduction scans to – 0.2 V, during which time a considerable amount of platinum was deposited on the electrode ($PtCl_6^{2-}$ reduction current densities as low as – 16 mA cm^{-2} were obtained). Curve IV displays an increase in the $PtCl_6^{2-}$ electroreduction onset potential of ~ 0.4 V *cf.* the initial sweep (Curve II). This shift in the onset potential is comparable to the ~ 0.3 V positive shift reported elsewhere [*Itaya et al., 1986; Ye and Fedkiw, 1996*]. It is likely that, in Curve IV, $PtCl_6^{2-}$ predominantly reduces onto the existing platinum deposits, whereas in Curve III $PtCl_6^{2-}$ was probably electroreduced onto both platinum deposits and the remaining GC surface (i.e. the platinum deposited during Curve II is likely to be much less than a monolayer).

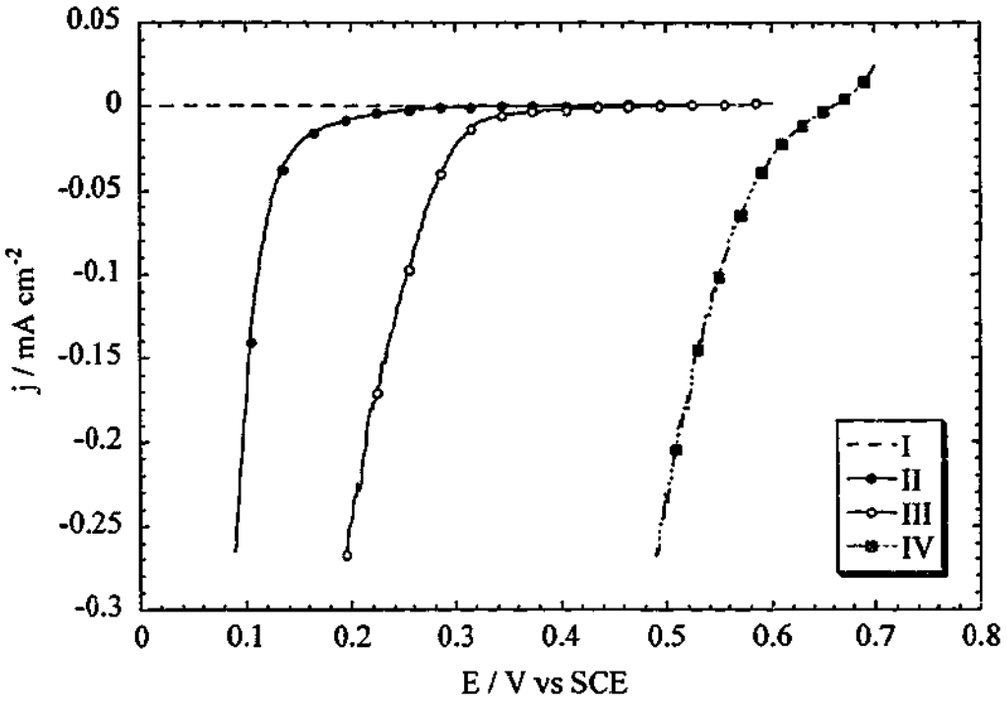

Fig. 4-2 *Consecutive linear-sweep electroreduction curves on a GC electrode in a 0.01 M H_2PtCl_6 + 0.5 M H_2SO_4 solution. Curve I is the GC baseline in 0.5 M H_2SO_4. Curves II and III are the first and second sweeps in H_2PtCl_6 solution. Curve IV was performed after many linear-sweeps and considerable platinum deposition. Sweep rate: 0.001 V s^{-1}.*

In contrast to platinum electroreduction from $PtCl_6^{2-}$ solutions, no significant shift in the onset potential is observed when platinising GC from $H_3Pt(SO_3)_2OH$ solution, as is illustrated by Curves II to IV in Fig. 4-3. In Curve III, the second sweep, $H_3Pt(SO_3)_2OH$ electroreduction commences at a potential roughly 0.03 V more positive *cf.* the onset observed in the initial electroreduction sweep (Curve II). The shift in the electroreduction onsets of Curves III and IV is again positive, but of a lesser magnitude (~ 0.015 V). Furthermore, the electroreduction onset potential was not observed to change significantly regardless of the number of sweeps performed in the $H_3Pt(SO_3)_2OH$ solution. Instead, a scatter of ~ 0.05 V is typically observed across consecutive electroreduction sweeps, which is likely to have arisen from currents produced by other reactions on the surface of the electrodes during the sweeps. The relatively constant onset potential for consecutive electroreduction

sweeps suggests that $H_3Pt(SO_3)_2OH$ does not reduce onto platinum deposits formed from the same platinum species.

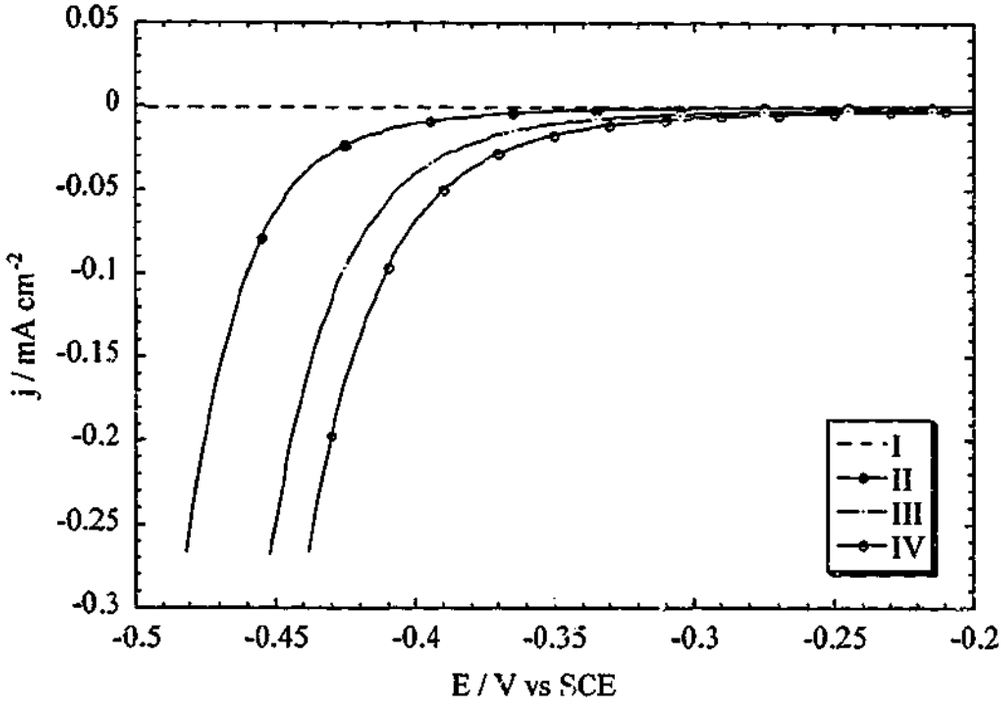

Fig. 4-3 Consecutive linear-sweep electroreduction curves on a GC electrode in a 0.01 M $H_3Pt(SO_3)_2OH$ + 0.5 M H_2SO_4 solution. Curve I is the GC baseline in 0.5 M H_2SO_4. Curves II, III and IV are the first, second and third respective sweeps in $H_3Pt(SO_3)_2OH$ solution. Sweep rate: 0.001 V s^{-1}.

In another experiment, the electroreduction of $H_3Pt(SO_3)_2OH$ onto pure platinum was attempted. Curve I in Fig. 4-4 shows the first CV of a smooth platinum electrode in 0.01 M $H_3Pt(SO_3)_2OH$ + 0.5 M H_2SO_4 solution. As the electrode was scanned from + 0.4 V towards – 0.25 V (before scanning back to + 0.4 V), a strong cathodic current density, j_c, is observed below 0.0 V. In comparison with the CV scans of the cleaned platinum electrode before or after the scans in $H_3Pt(SO_3)_2OH$ solution, this j_c occurs in the same potential region for Pt-H_{ads} formation, and with greater magnitude (*cf.* Curve IV, the cleaned platinum electrode scanned in 0.5 M H_2SO_4 after Curves I to III were performed). The j_c may correspond to charge passed for the reduction of $H_3Pt(SO_3)_2OH$ in addition to that passed during Pt-H_{ads}

formation. However, as Fig. 4-5 illustrates, the smooth platinum electrode does not appear to have been further platinised by the scans in $H_3Pt(SO_3)_2OH$ solution. Note that the anodic current density, j_a, at low potentials is greater for the scans in the platinum sulphite solution *cf.* Curve IV. This is most likely due to the lower potentials used in Curves I to III, enabling hydrogen evolution and oxidation on some of the platinum surface, contributing to a larger j_a.

4.2.2 Activation of Poisoned Platinum

The CV scans in Fig. 4-5 were performed at the usual 0.05 V s^{-1}, which allows greater clarity of the Pt-H_{ads} region *cf.* scans performed at lower speeds (such as the scans in Fig. 4-4); refer to Section 2.4 of Chapter Two for a more detailed explanation. In contrast, greater accuracy in the obtained j_c is achieved when scanning at slower rates, such as those in Fig. 4-4. Curve I in Fig. 4-5 shows a scan of the platinum electrode in 0.5 M H_2SO_4 before the attempted platinisation, with the well-defined CV shape typical of a clean platinum electrode [*Will, 1965*]. Curve II is the first scan in 0.5 M H_2SO_4 which was performed immediately after the scans in $H_3Pt(SO_3)_2OH$ solution. This scan is clearly lacking the typical platinum CV shape, in particular not exhibiting any Pt-O_{ads} reduction at around + 0.5 V (*cf.* the strong cathodic peak in Curve IV of Fig. 4-5). The current densities in the H_{ads} region (below 0.1 V) are also reduced on comparison with those in Curve IV. This provides strong evidence that the electrode is 'poisoned' (i.e. that the electrode has a species strongly adsorbed to the surface preventing normal reactions on the platinum surface) following the scans in $H_3Pt(SO_3)_2OH$ solution.

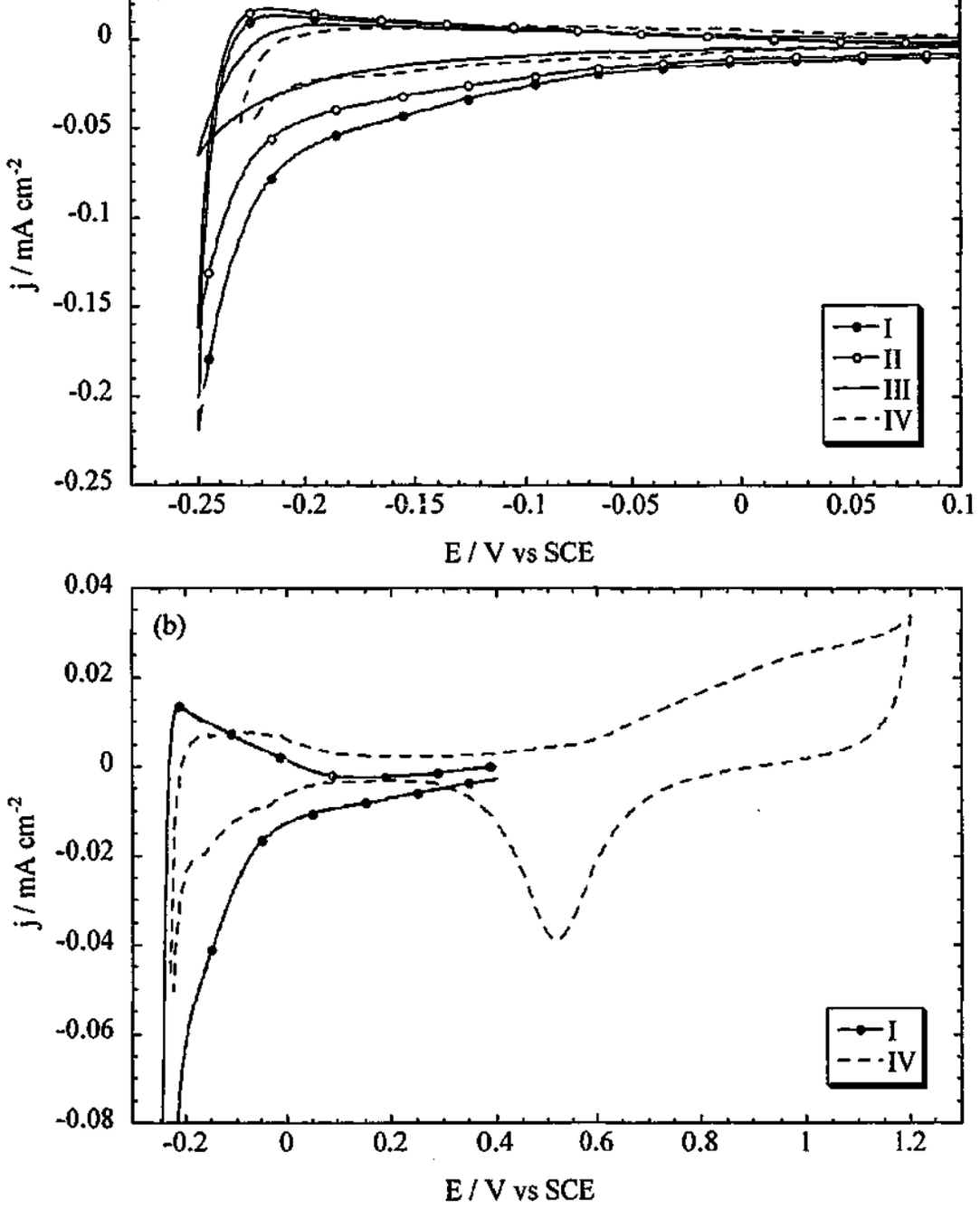

Fig. 4-4 *An attempted platinisation of a smooth platinum electrode via $H_3Pt(SO_3)_2OH$ electroreduction. (a) Curves I to III show CV scans in 0.01 M $H_3Pt(SO_3)_2OH$ + 0.5 M H_2SO_4 solution. Curve IV is a CV scan of the same Pt electrode in 0.5 M H_2SO_4 following Curves I to III (and following potentiodynamic cycling in the H_2SO_4 solution). The entire potential range is displayed for two of the scans, Curves I and IV, in (b). Scanning rate: 0.02 V s^{-1}.*

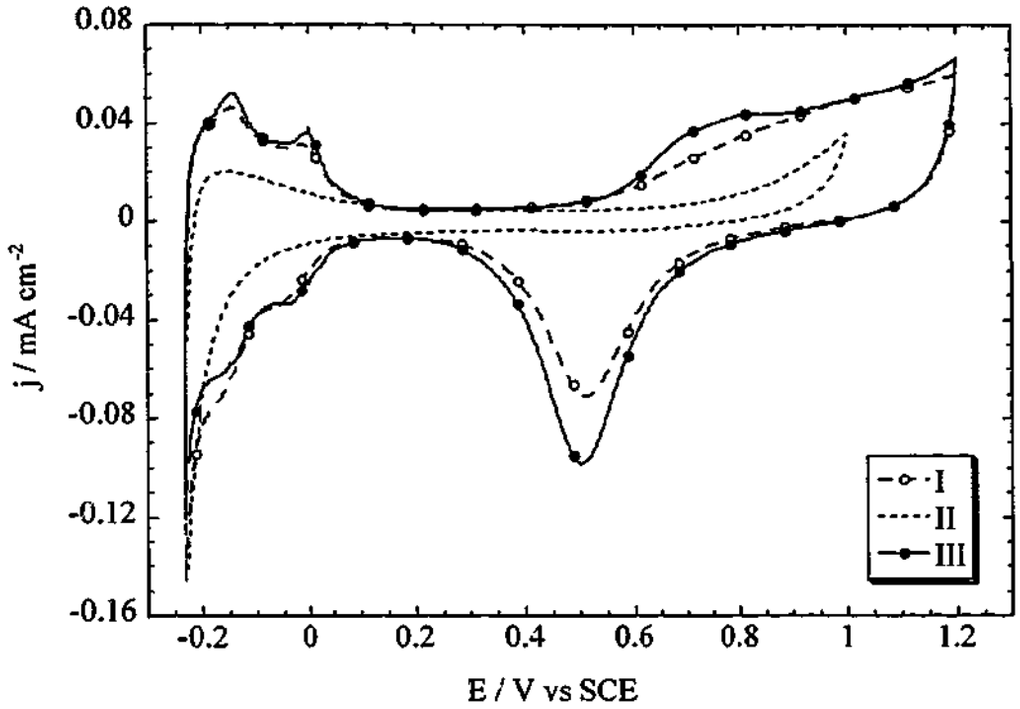

Fig. 4-5 *Cyclic voltammograms of a platinum electrode before, during and after scans in a 0.01 M $H_3Pt(SO_3)_2OH$ + 0.5 M H_2SO_4 solution. Curve I is the Pt baseline in 0.5 M H_2SO_4. Curve II is a scan of the Pt electrode in $H_3Pt(SO_3)_2OH$ solution following an attempted platinisation in the same solution (see text). Curve III shows the restored platinum surface (in 0.5 M H_2SO_4) following considerable electrochemical cycling of the electrode. Scanning rate: 0.05 V s^{-1}.*

After a number of 'analysis' scans similar to Curve I of Fig. 4-5, the scans appeared more typical to those of a platinum CV, and finally the electrode was completely 'cleaned' of impurities, as shown by Curve III of Fig. 4-5. It is a common practice to cycle platinum electrodes between the hydrogen and oxygen evolution potentials in 0.5 M H_2SO_4 to remove any undesired species (e.g. adsorbed from the laboratory atmosphere), until a reproducible CV is obtained [*Will, 1965*]. Normally, only 10 to 20 scans are required to achieve this, but in the case were platinum is immersed in $H_3Pt(SO_3)_2OH$ solution, a great number of CV scans appear necessary before the usual platinum behaviour is observed. Hence, from the lack of increased platinum surface area (as observed in Fig. 4-5 by the nearly equivalent areas of the Pt-H_{ads} formation and oxidation peaks in Curves I and III), the j_c in Curves I to III of Fig. 4-4 does not appear to have corresponded to any significant $H_3Pt(SO_3)_2OH$

electroreduction. This difficulty in electroplating platinum from the $H_3Pt(SO_3)_2OH$ species onto a platinum substrate could prove to be useful in the electrodeposition of fuel cell catalysts. For example, once a platinum particle is deposited onto a non-platinum surface, such as a carbon fuel cell electrode, any further reduction of platinum atoms from the $H_3Pt(SO_3)_2OH$ species onto this particle may be prevented, or at least limited.

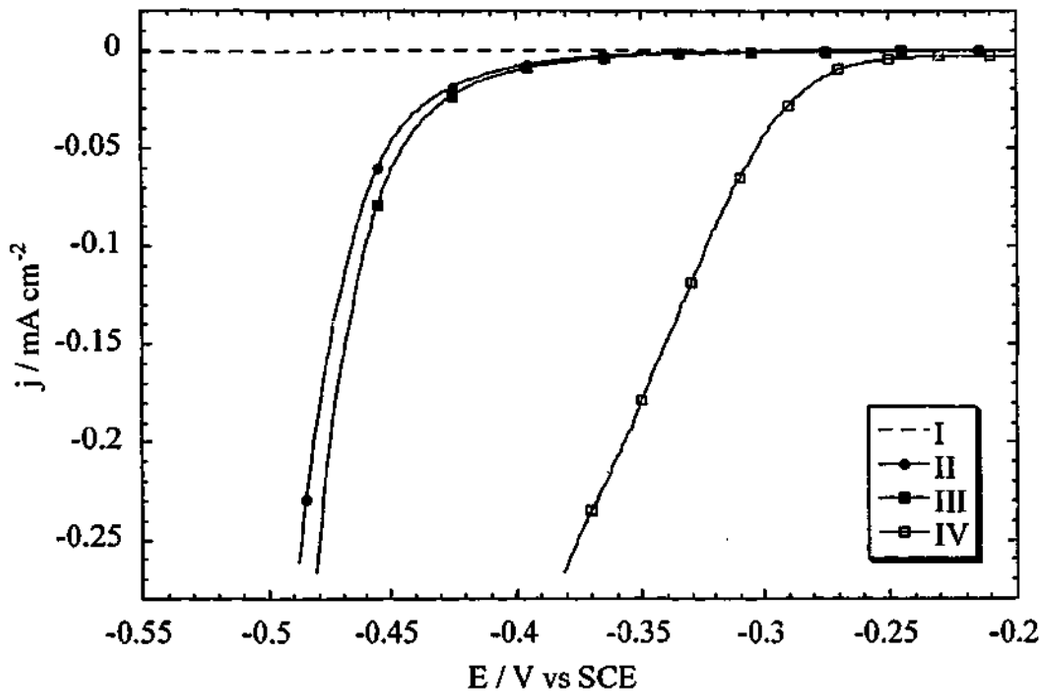

Fig. 4-6 Potentiodynamic sweeps of three GC electrodes in sulphuric acid and platinum sulphite solutions. Curve I is a GC baseline in 0.5 M H_2SO_4. Curves II to IV show the initial linear-sweeps of separately prepared GC electrodes, GC-1, GC-2 and GC-3, respectively, in a 0.01 M $H_3Pt(SO_3)_2OH$ + 0.5 M H_2SO_4 solution. Sweep rate: 0.001 V s^{-1}.

A small degree of scatter (~ 0.12 V) was observed between the $H_3Pt(SO_3)_2OH$ electroreduction onset potentials on different GC electrodes. Curves II to IV in Fig. 4-6 show the initial platinum reduction sweeps onto three separately prepared GC electrodes in 0.01 M $H_3Pt(SO_3)_2OH$ + 0.5 M H_2SO_4 solution. Curve II in Fig. 4-7 shows $H_3Pt(SO_3)_2OH$ electroreduction onto a CB based electrode, on which the reduction commences at potentials negative to – 0.4 V, similar to the reduction

onsets of Curves II and III in Fig. 4-6. Stronger current densities are observed in Fig. 4-7 because the rough CB-based electrode has a considerably larger real surface area *cf.* that of the smoothly polished GC surface. The scatter in the $H_3Pt(SO_3)_2OH$ electroreduction potentials may be explained by the effects of other reactions occurring simultaneously with the reduction in both the initial GC sweeps (Fig. 4-6) and in the subsequent GC sweeps (Fig. 4-3). The hydrogen evolution reaction, HER, is expected to cause the most significant interference, since a strong j_c is typically observed on pure platinum electrodes in acidic solutions at these reduction potentials. Hydrogen evolves at potentials negative to – 0.242 V_{SCE} (i.e. versus SCE) on platinum in 1.0 M H^+ solutions (e.g. in 0.5 M H_2SO_4) and any hydrogen evolution on the initial platinum deposits could significantly obscure the $H_3Pt(SO_3)_2OH$ electroreduction currents. Similarly, the by-products of $H_3Pt(SO_3)_2OH$ electroreduction might cause other interfering reactions. If the electroreduction of the platinum sulphite species is described by Eq. 4-1, sulphite ions (SO_3^{2-}) would be liberated. At potentials negative to – 0.011 V sulphite ions are reduced to sulphide (S^{2-}) in accordance with Eq. 4-2 [*Valensi et al., 1975*]. Since Eq. 4-1 occurs at potentials much more negative (Curve II in Fig. 4-1) *cf.* Eq. 4-2, any liberated sulphite ions from Eq. 4-1 would be immediately reduced (Eq. 4-2), thus contributing to the j_c observed in $H_3Pt(SO_3)_2OH$ electroreduction sweeps.

Sulphide is a known platinum poison [*Chin and Howard, 1986; Gerischer, 1975; Loucka, 1971*], and the production of sulphide or other sulphur-containing species during platinisation may lead to the poisoning of platinum nuclei. In addition to possibly causing an interfering j_c, the concomitant reduction of sulphite to sulphide could poison platinum immediately after deposition. Poisoning may help to explain the relatively constant onsets for $H_3Pt(SO_3)_2OH$ reduction in consecutive sweeps, as illustrated in Fig. 4-3, if the $H_3Pt(SO_3)_2OH$ species are unable to reduce onto poisoned platinum deposits.

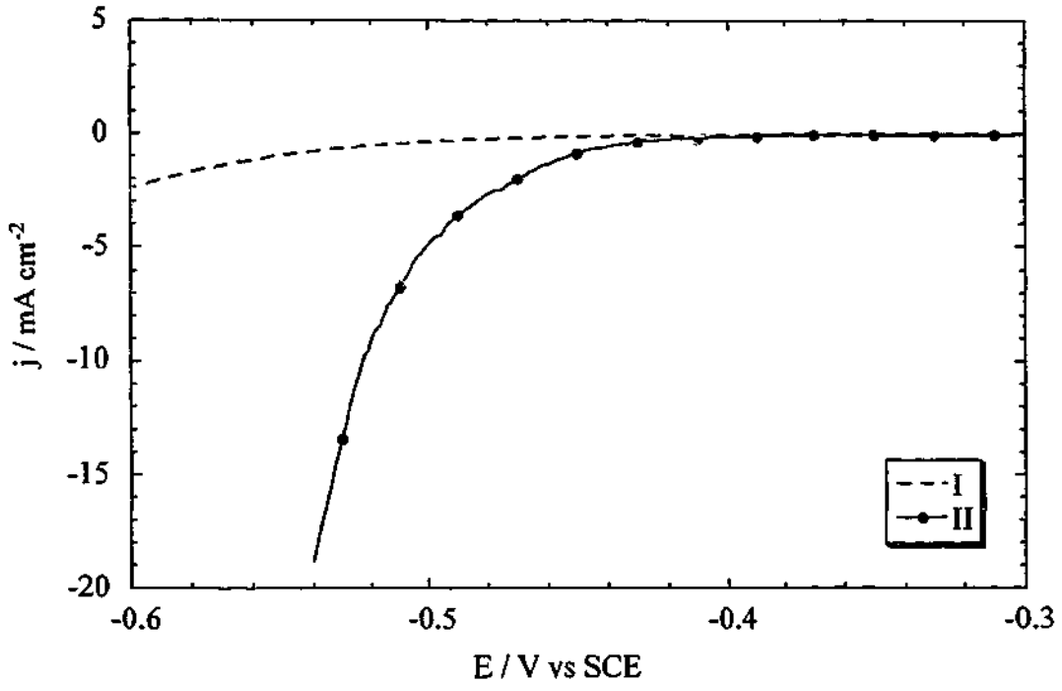

Fig. 4-7 *Potentiodynamic sweeps of carbon-black (CB) based electrodes in sulphuric acid and platinum sulphite solutions. Curve I is a baseline sweep of a CB-based electrode in 0.5 M H_2SO_4. Curve II shows the initial linear-sweep of a CB-based electrode, CB-1, in a 0.01 M $H_3Pt(SO_3)_2OH$ + 0.5 M H_2SO_4 solution. Sweep rate: 0.001 V s^{-1}.*

$$Pt(SO_3)_2^{2-} + 2e^- \rightarrow Pt^0 + 2SO_3^{2-} \qquad (4\text{-}1)$$

$$SO_3^{2-} + 6e^- + 6H^+ \rightarrow S^{2-} + 3H_2O \qquad (4\text{-}2)$$

It was also found that the electroreduction onset potential was very sensitive to minute traces of platinum remaining on the GC electrodes after polishing. Even if CV scans of polished GC electrodes displayed no platinum oxidation/reduction behaviour nor hydrogen adsorption/desorption reactions, linear-sweep baselines such as Curve I, Fig. 4-1 were performed in 0.5 M H_2SO_4. Trace amounts of platinum will result in a strong j_c most likely due to hydrogen evolution, and if $H_3Pt(SO_3)_2OH$ is reduced onto such electrodes slightly higher onset potentials are observed. This most likely results from a slight catalysis of both the $H_3Pt(SO_3)_2OH$

and sulphite electroreduction reactions by the remaining Pt deposits. This is similar to the scans of Fig. 4-4, where a greater j_c was observed in the $H_3Pt(SO_3)_2OH$ solution, *cf.* the Pt electrode in sulphuric acid, and since the platinisation of platinum surfaces is negligible (see discussion for Fig. 4-4) it is probable that a large proportion of this j_c results from other reactions such as the electroreduction of sulphite to sulphide.

In the case of platinum electrodeposition onto GC from $H_3Pt(SO_3)_2OH$ solution, electrochemical features typical for platinum were only observed when scanning to low potentials. For example, in Fig. 4-4 peaks in the Pt-H_{ads} region appeared after scanning the poisoned electrode from potentials below – 0.242 V, where the evolution of hydrogen evolution may have cleaned some of the platinum surface enabling the adsorption and subsequent oxidation of protons. In contrast, during platinisation from K_2PtCl_6 + H_2SO_4 solution, Pt-H_{ads} oxidation peaks were observed on the return sweep of all CV scans [*Itaya et al., 1986; Ye and Fedkiw, 1996*].

Decreased redox behaviour for platinum was also observed in the initial analyses (in 0.5 M H_2SO_4) of Pt/GC electrodes prepared from the electroreduction of $H_3Pt(SO_3)_2OH$. Fig. 4-8 displays the post-platinisation analysis of a Pt/GC electrode that was platinised by five sweeps similar to those shown by curves II and III in Fig. 4-6. Curve I is the first CV which scans to 1.4 V (starting at – 0.232 V), and does not show any Pt-H_{ads} oxidation nor reduction currents as observed in typical platinum CV scans (e.g. Fig. 2-3 in Chapter Two). Instead, Curve I exhibits a strong j_a around 1.4 V and also a strong j_c at – 0.1 V, but neither is indicative of the presence of any platinum on the electrode. In the third consecutive scan (Curve II), the strong current densities at the potential extremes have decreased slightly, and a slight shoulder is observed in the positive sweep at ~ 1.2 V in the region for the formation of platinum surface oxides (Pt-O_{ads}). On the return sweep, a small cathodic peak is observed at + 0.35 V, in the region for the reduction of Pt-O_{ads}. Curve II also exhibits j_c between + 0.25 and – 0.23 V, representing the reduction of some species. A cathodic peak is observed at – 0.08 V, in the region for the formation of Pt-H_{ads}. The peaks in the potential regions for the formation and reduction of Pt-O_{ads} may be seen

with more clarity by the sixth consecutive scan (Curve III in Fig. 4-8), and finally appear typical of a platinum electrode CV in Curve IV (after around one hundred further scans over the same potential range). The anodic peak representing the oxidation of Pt-H_{ads} becomes significant only after the extensive potentiodynamic cycling which results in Curve IV. The behaviour of CB-based electrodes is discussed later since a large electrical double layer dominates the electrochemistry of such high surface-area electrodes (and higher platinum loadings are consequently necessary).

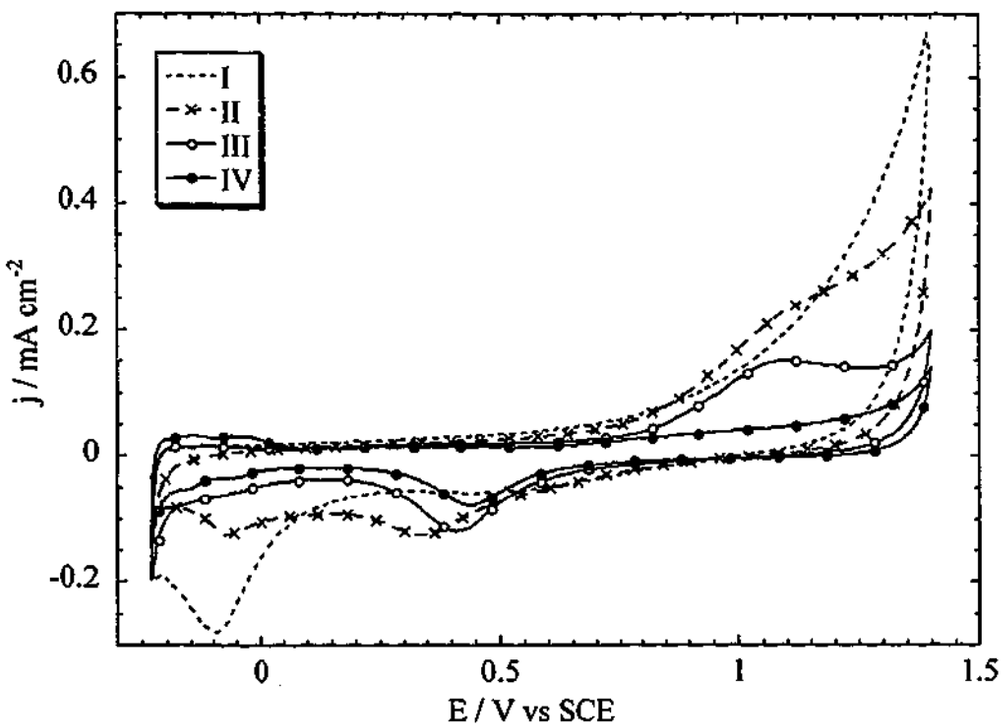

Fig. 4-8 *Typical potentiodynamic cleaning in 0.5 M H_2SO_4 of a Pt/GC electrode platinised in $H_3Pt(SO_3)_2OH$ solution. This electrode was platinised by 5 linear-sweeps (similar to those shown in Fig. 4-6) in a 0.01 M $H_3Pt(SO_3)_2OH$ + 0.5 M H_2SO_4 solution. Curve I shows the initial CV scan of the poisoned Pt/GC electrode scanning to an upper potential, E_u of 1.4 V. Curves II and III show the third and sixth consecutive CV scans of the Pt/GC electrode following Curve I. Curve IV was performed after approximately 100 similar CV scans. Scanning rate: 0.05 V s^{-1}.*

4.2.3 Potentiostatic Pt/GC and Pt/CB Electrode Preparation

Figs. 4-9 and 4-10 show current density-time (*j-t*) transients for the potentiostatic reduction of $H_3Pt(SO_3)_2OH$ onto both GC (Curves I and II, Fig. 4-9) and CB based (Curve I, Fig. 4-10) electrodes at – 0.45 V. This relatively low potential was used because at this potential the reduction of $H_3Pt(SO_3)_2OH$ appears significant (i.e. compare Curves I and II in Fig. 4-1). The three *j-t* curves in Figs. 4-9 and 4-10 (in $H_3Pt(SO_3)_2OH$ solution) have an unusual appearance on comparison with previous studies of $PtCl_6^{2-}$ electroreduction [*Gloaguen et al., 1997; Hogarth et al., 1994*], where the long term reduction current has been shown to be constant over time. On the other hand, a marked increase in j_c over time is displayed in the *j-t* transients in Figs. 4-9 and 4-10, which suggests other reactions are occurring simultaneously with the platinum electroreduction. Additional j_c may have arisen from hydrogen evolving on the deposited platinum (whereas in the work of other researchers [*Gloaguen et al., 1997; Hogarth et al., 1994*], more positive potentials were used, avoiding hydrogen evolution). Another likely reaction at – 0.45 V is the reduction of sulphite to sulphide (Eq. 4-2), which could contribute to the cathodic currents along with platinum reduction and hydrogen evolution. Again, the CB based electrode (Fig. 4-10) exhibits stronger current densities (by a factor of ~ 20) as a result of the much greater surface area of this electrode *cf.* the GC electrode.

Fig. 4-11 shows the CV analysis of Electrode Pt/GC-5 that was platinised as shown by Curve II in Fig. 4-9. Longer reduction time was allowed compared with Curve I to facilitate a higher platinum loading. Curve I in Fig. 4-11 shows the second cyclic voltammogram in 0.5 M H_2SO_4 which was scanned to an upper potential, E_u, of + 1.4 V. Several scans were performed prior to the measurement shown in Curve I with E_u less than + 1.4 V but these did not show any evidence of characteristic platinum surface reactions (apart from a sharp cathodic spike followed by an anodic peak when scanning into the hydrogen evolution region, as observed in curves I to III of Fig. 4-4). Curve I (in Fig. 4-11) appears similar to Curves II and III in Fig. 4-8, exhibiting clear signs of $Pt\text{-}O_{ads}$ reduction (at + 0.4 V) and a strong anodic peak between + 0.6 and + 1.3 V, in the potential range for $Pt\text{-}O_{ads}$ formation. The strong

j_a > 0.8 V is believed to represent the oxidative removal of the poisoning species, which occurs in the range of oxide formation on the platinum surface, Pt-O_{ads}. The decrease in j_a in Curve I to Curve III in Fig. 4-11 appears to be related to the decrease in j_c of the Pt-O_{ads} reduction peak at ~ 0.4 V. This reduction peak may comprise of j_c from the reduction of Pt-O_{ads} species and also the reduction of remaining adsorbed species and/or partially oxidised adsorbed species. Curve I also exhibits a strong j_c between + 0.25 and – 0.23 V (similar to those in Curve II of Fig. 4-8).

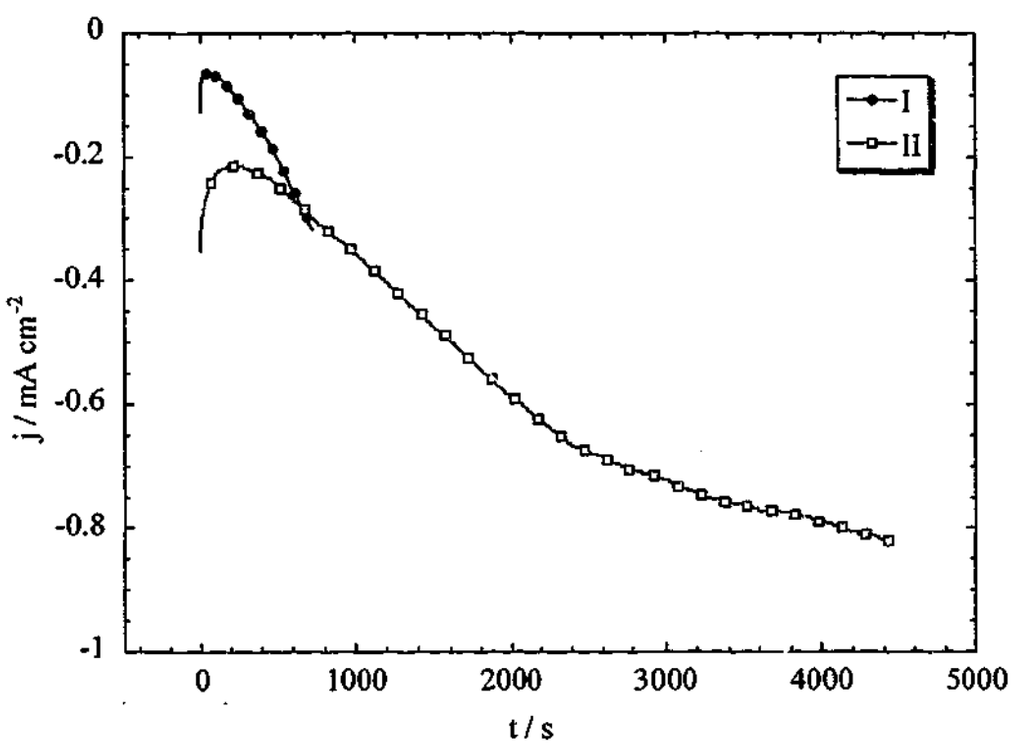

Fig. 4-9 *Current density-time (j-t) transients for the potentiostatic reduction of platinum at – 0.45 V from a 0.01 M $H_3Pt(SO_3)_2OH$ + 0.5 M H_2SO_4 solution onto GC-4 (Curve I) and GC-5 (Curve II). Curves I and II were obtained under identical conditions onto separately polished GC electrodes, and highlight the reproducibility issues of $H_3Pt(SO_3)_2OH$ electrodeposition.*

Curve II in Fig. 4-11 displays the fifth consecutive cyclic voltammogram scanned to an upper potential of + 1.4 V of Electrode Pt/GC-5. The magnitude of the strong oxidation and reduction current densities observed in Curve I have somewhat receded in subsequent scans (i.e. in Curve II) and the Pt-H_{ads} formation/oxidation

peaks between – 0.23 and + 0.1 V are also visible at this time. Curve III in Fig. 4-11 shows a CV scan of the completely cleaned Pt/GC-5 which was performed after a further 50 scans (the final 10 scans of which were performed the following day after the electrode was rested for ~ 12 h in mQ water). Curve III was considered to be completely free of poisoning species since it exhibits the typical platinum CV 'fingerprint' and all of the hydrogen and oxygen reactions on the platinum surface are clearly visible (and no additional peaks were observed). Further, after continued cycling of Pt/GC-5, no further increase in the platinum surface area was observed (in comparison with Curve III). Instead, during this cycling procedure, the current density due to the electrical double-layer charging on the electrode (j_{dl}) gradually increased along with anodic and cathodic peaks at around + 0.35 V, representing the oxidation and reduction of surface functionalities on the glassy carbon.

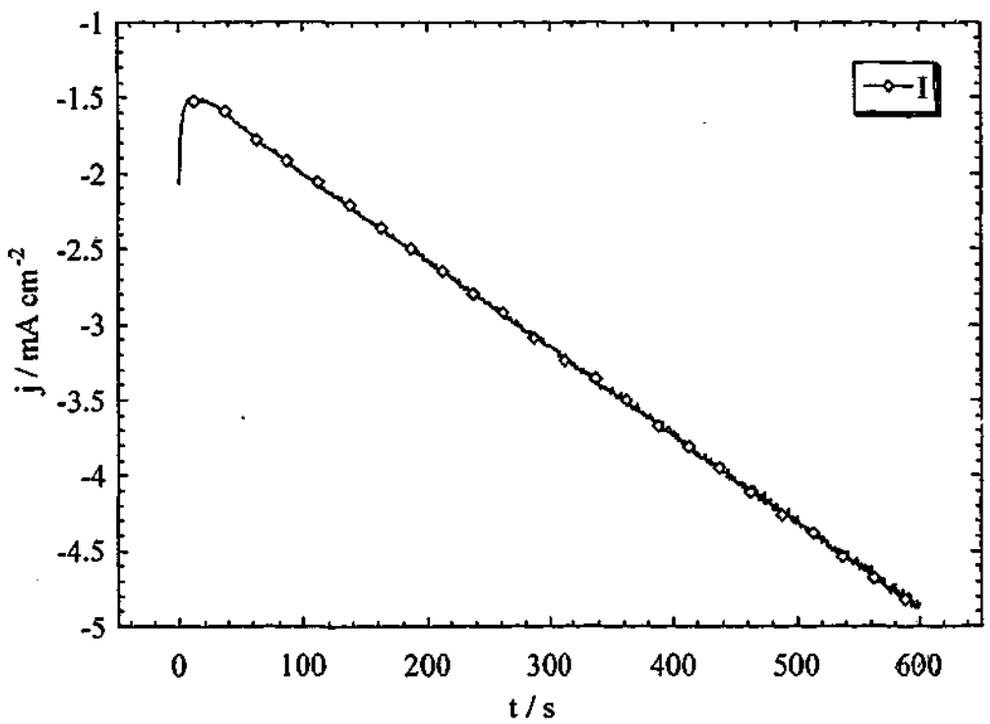

Fig. 4-10 *Current density-time (j-t) transient for the potentiostatic reduction of platinum at – 0.45 V from a 0.01 M $H_3Pt(SO_3)_2OH$ + 0.5 M H_2SO_4 solution onto a CB-based electrode, CB-2 (Curve I).*

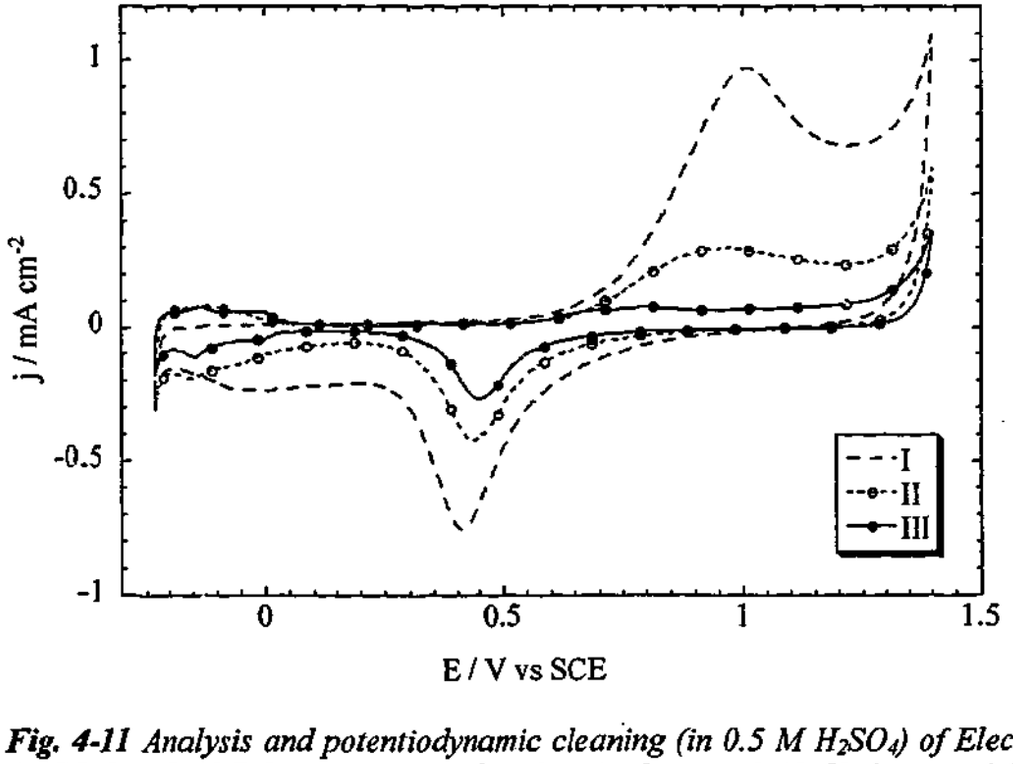

Fig. 4-11 *Analysis and potentiodynamic cleaning (in 0.5 M H_2SO_4) of Electrode Pt/GC-5. Pt/GC-5 was previously platinised at – 0.45 V from a 0.01 M $H_3Pt(SO_3)_2OH$ + 0.5 M H_2SO_4 solution, as shown by Curve II in Fig. 4-9. Curve I shows the second CV scanned to an E_u of 1.4 V; Curve II shows the fifth consecutive scan. Curve III was performed after ca. 50 similar CV scans, and after resting in mQ water for 12 h, and shows the cleaned Pt surface of Pt/GC-5. Scanning rate: 0.05 V s^{-1}.*

The behaviour of CB-based electrodes, e.g. Pt/CB-2 (platinised as shown by Curve I in Fig. 4-10) was also investigated. Curve I in Fig. 4-12, scanned to + 1.2 V in sulphuric acid, displays negligible platinum redox features. Only the j_c at potentials negative to 0.0 V and the j_a at potentials greater than about + 0.8 V suggest any platinum presence. In the second CV scanned to + 1.4 V (Curve II), j_a peaks in the regions for Pt-O_{ads} formation and reduction are apparent, and small peaks in the Pt-H_{ads} formation and oxidation regions are just visible. Curve III in Fig. 4-12 shows the cleaned Pt/CB electrode after 25 similar scans. The faster cleaning of Pt/CB-2 compared with that of Pt/GC-5 may be explained by less time for the potentiostatic deposition and possibly less time for the deposited platinum to be poisoned in the case of Pt/CB-2. The different carbon substrates may also have had an effect- the greater surface-area and possibly the less ordered, graphitic nature of the CB-based

electrode, *cf.* GC, may have also led to enhanced oxidative removal of the poisoning species. Continued cycling was again performed on Pt/CB-2 after Curve III (*cf.* the previous discussion for Pt/GC-5) but no further increase in the platinum surface area was observed; the additional scans merely caused an increased j_{dl} and large carbon oxidation and reduction peaks at about + 0.35 and + 0.25 V, respectively. The platinum electrochemical 'fingerprint' is shown in Curve III of Fig. 4-12 (slightly obscured by the large j_{dl} of the CB-based substrate). The Pt-O_{ads} reduction peak at + 0.4 V merges with the reduction peak of the oxidised GC surface groups in Curve III. These separate cathodic peaks can be seen with more clarity in a CV scan of another Pt/CB electrode, Pt/CB-3 (Curve IV, Fig. 4-12). Pt/CB-3 was platinised from $H_3Pt(SO_3)_2OH$ solution in the same fashion as Pt/CB-2 (i.e. 600 s of potentiostatic reduction at – 0.45 V), except this electrode experienced a 2 h immersion time in the same 0.01 M $H_3Pt(SO_3)_2OH$ + 0.5 M H_2SO_4 solution prior to the reduction.

Fig. 4-13 displays a typical SEM micrograph of the cleaned Pt/CB-2. The bright particles throughout this image were confirmed to be platinum by EDXS analysis. The average platinum particle diameter is approximately 50 nm, which is considerably larger than desired. However, it may be possible to reduce this particle size under optimised conditions. These particles observed in the SEM micrograph may actually be aggregates of smaller platinum particles as found by Ye and Fedkiw in similar work using Nafion-coated GC electrodes [*Ye and Fedkiw, 1996*].

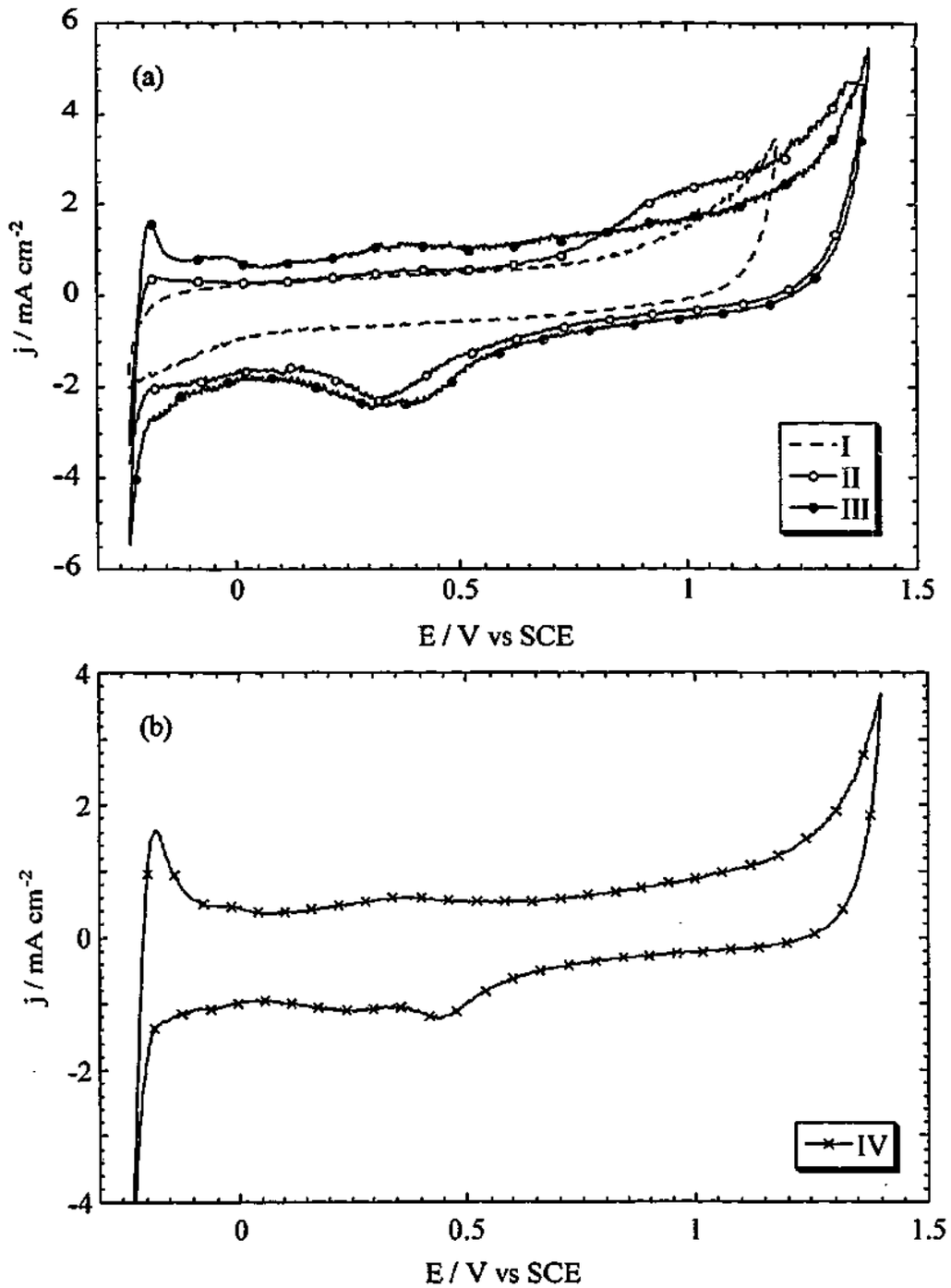

Fig. 4-12 *Analysis and potentiodynamic cleaning (in 0.5 M H_2SO_4) of Pt/CB electrodes. (a) Electrode Pt/CB-2, which was previously platinised at – 0.45 V in a 0.01 M $H_3Pt(SO_3)_2OH$ + 0.5 M H_2SO_4 solution, as shown by Curve I in Fig. 4-10. Curve I shows the second CV scanned to an E_u of 1.2 V; Curve II shows the second CV scanned to 1.4 V. Curve III was performed after ca. 25 similar CV scans and shows the cleaned Pt/CB-2 electrode. (b) Electrode Pt/CB-3, which was platinised in a similar fashion to Pt/CB-2, apart from experiencing 2 h of immersion in the 0.01 M $H_3Pt(SO_3)_2OH$ + 0.5 M H_2SO_4 solution prior to the 600 s potentiostatic reduction at – 0.45 V. Curve IV shows a CV scan of the cleaned Pt/CB-3. Scanning rate: 0.05 V s^{-1}.*

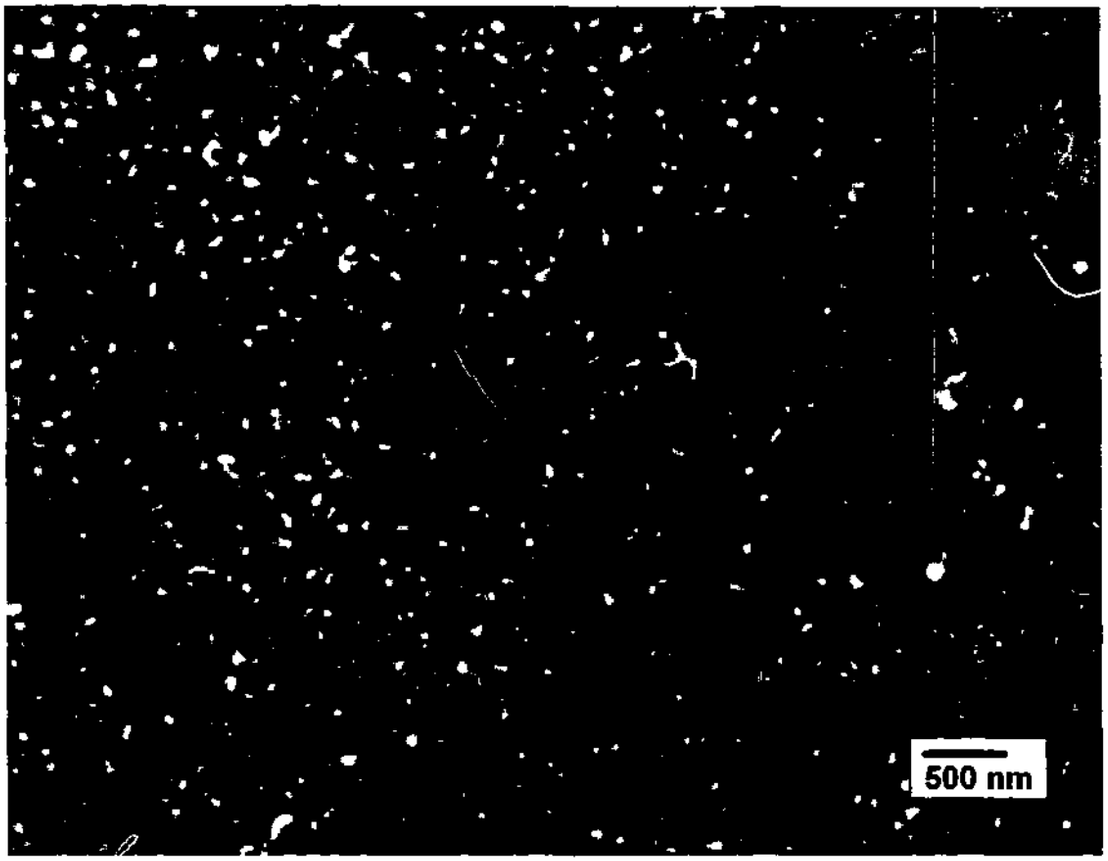

Fig. 4-13 *SEM image of Electrode Pt/CB-2. This electrode was previously platinised in a 0.01 M $H_3Pt(SO_3)_2OH$ + 0.5 M H_2SO_4 solution, at – 0.45 V for 600 s, as shown by Curve I in Fig. 4-10. The electrochemical analysis of this electrode is shown in Fig. 4-12 (Curves I to III). The highly dispersed, bright particles are platinum as determined by EDXS.*

Table 4-1 shows the characteristics of the GC and CB based electrodes which were platinised potentiostatically from a $H_3Pt(SO_3)_2OH$ solution at – 0.45 V. As one can observe in this table, the specific surface areas (*S*) are quite low, and the estimates of the platinum particle diameters (*d*) are very large. In fact, the estimated platinum particle size for Pt/CB-2 is around 20 times greater than the 50 nm approximate size observed in the SEM image of Fig. 4-13. On comparison with the Pt/GC electrodes, the *d* estimates appear up to two orders of magnitude greater than these particles observed in the CB based electrode. Unfortunately, SEM analysis was not possible with these platinised GC electrodes since removing such small deposits proved

impossible (and cutting the electrodes shattered the GC surface). As discussed before, the deposition charge, Q_r, is thought to contain significant contributions from parasitic processes such as sulphite reduction and hydrogen evolution, and this may account for the large discrepancy. If an average platinum particle size of 50 nm is assumed, then an S value of 5.6 $m^2\ g^{-1}$ would be more representative of these electrodes. This value is still low compared to e.g. 180 $m^2\ g^{-1}$ (i.e. around 1.6 nm Pt particles) possible in commercially available catalysts [*Stonehart, 1990*].

Electrode	A_g (cm^2)	t_{red} (s)	Q_r (C)	W (μg)	A_r (cm^2)	R_f	S ($m^2\ g^{-1}$)	d (μm)
Pt/GC-4	0.071	720	0.008	8.0	0.022	0.31	0.28	1.0
Pt/GC-5	0.071	4450	0.18	180	0.082	1.2	0.046	6.1
Pt/CB-2	1.0	600	1.8	1870	6.2	6.2	0.33	0.85

Table 4-1 *Characteristics of the electrodes platinised from a 0.01 M $H_3Pt(SO_3)_2OH$ + 0.5 M H_2SO_4 solution at − 0.45 V, where A_g is the geometric area of the electrodes; t_{red} is the time for potentiostatic reduction; Q_r is the charge passed; W is the platinum loading determined from the charge transferred (assuming a 2 electron transfer per platinum atom deposited); A_r is the electrochemical surface area of the cleaned platinum determined from the charge passed in oxidising a full monolayer of adsorbed hydrogen, Pt-H_{ads} (assuming Q_H = 210 μC cm^{-2}); R_f is the roughness factor of the platinum deposits (i.e. the ratio of A_r to A_g); S is the specific surface area (i.e. the ratio of A_r to W); d is the estimate of the platinum particle diameter, assuming homogeneously dispersed spherical deposits, Eq. 1-16 in Chapter One.*

On comparing the platinised GC electrodes, the particle size does appear to increase with an increase in the platinum loading, which suggests the poisoning process may not completely prevent particle growth (although the calculation of d is dependent on W which is unlikely to be accurate given the above discussion). Indeed, from Fig. 4-13 some particle growth is evident. The lower S value for Pt/GC-5 compared to Pt/GC-4 is also uncertain, since one cannot be sure how much of the deposition charge is from platinum reduction. The platinum surface area (A_r) of Pt/GC-5 is not

much larger than that of Pt/GC-4. It is possible that if Pt/GC-5 was well platinised and poisoned, and could therefore not facilitate further platinum reduction, then the remaining charge could have arisen largely from other reactions such as hydrogen evolution.

Since the platinum loadings calculated from the *j-t* transients are prone to overestimation, the roughness factor provides more information on the platinum deposits. The R_f of 6.2 for Pt/CB-2 compares favourably with the work of Gloaguen *et al.* [*Gloaguen et al., 1997*], where platinum loadings into Nafion-bound CB electrodes ranged between 3 and 39 μg cm^{-2} with roughness values between 1.9 and 5.9 respectively.

Attempts were made to deposit $H_3Pt(SO_3)_2CH$ onto both GC and CB electrodes at more positive potentials, without much success. Potentials chosen were + 0.1, 0, – 0.1, – 0.2 and – 0.35 V. The Pt/CB prepared from potentiostatic deposition at – 0.35 V was similar to the electrode shown in Fig. 4-12, although even less evidence of platinum redox behaviour was observed. Again the *j-t* curve displayed an increase in the j_c (towards more negative current densities) with time. Of more interest is the possibility of depositing platinum from the $H_3Pt(SO_3)_2OH$ species at potentials more positive *cf.* the HER. Only very minor evidence of deposited platinum was found on electrodes held at + 0.1, 0 and - 0.1 V in $H_3Pt(SO_3)_2OH$ solution; no Pt-H_{ads} adsorption/oxidation peaks were visible, but j_c similar to that of hydrogen evolution was observed on scans to potentials as low as – 0.3 V.

Fig. 4-14 shows the potentiostatic deposition of platinum onto Electrode GC-6 at – 0.2 V for 1 h, from a 0.01 M $H_3Pt(SO_3)_2OH$ + 0.5 M H_2SO_4 solution. At this potential, the observed j_c is very low (in μA) and, as was discussed earlier for Figs. 4-9 and 4-10, not all the current passed necessarily results from the electroreduction of $H_3Pt(SO_3)_2OH$. In Fig. 4-14 however, the possibility of any current produced by the HER has been eliminated (the potential being more positive than – 0.242 V), so the electroreduction of $H_3Pt(SO_3)_2OH$ and/or SO_3^{2-} are the most significant possible causes of the j_c. A very slight increase in current density

(towards more negative values) is observed in this figure, but it is not as significant as the gradients in Curves I to III of Figs. 4-9 and 4-10. This slight increase in current may have arisen from the reduction of sulphite to sulphide, after some platinum had been reduced.

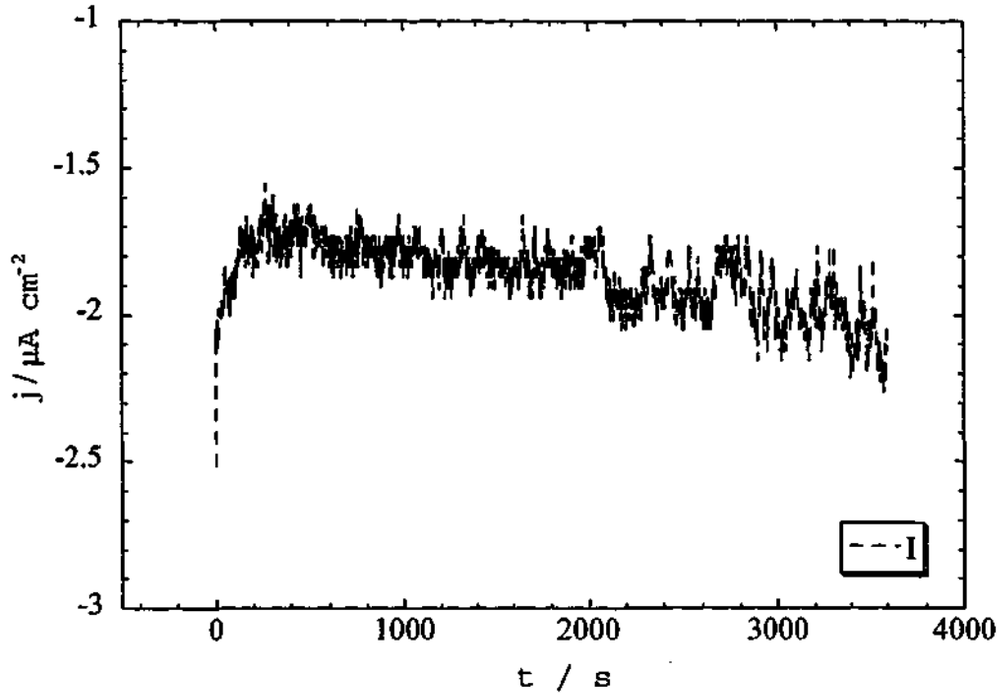

Fig. 4-14 *Current density-time (j-t) transient for the electroreduction of platinum onto Electrode GC-6 from a 0.01 M $H_3Pt(SO_3)_2OH$ + 0.5 M H_2SO_4 solution at – 0.2 V.*

Fig. 4-15 displays the analysis of this electrode in 0.5 M H_2SO_4, at a number of scanning rates. At a fast scanning rate such as 0.5 V s^{-1}, the typical platinum surface reaction characteristics may be observed with some clarity (Curve III). The lack of stronger current densities for the platinum surface reactions at lower scanning rates is suggestive of low platinum loading. However, it appears possible to electrodeposit at higher potentials, where the HER is not a competing reaction. Longer electroreduction times would be expected for an equivalent mass of deposited platinum. In addition, avoiding the evolution of hydrogen on the deposits may prove to be beneficial in further limiting particulate growth during

electrodeposition. Hydrogen evolution may actually aid in the removal of poisoning species, if they are reducible (e.g. by reducing sulphur to H_2S). Conversely, evolving hydrogen on deposits during electrodeposition may act to inhibit further reduction onto deposits; a sponge-like deposit of high surface-area may form under such conditions. [*Moore, 1983*].

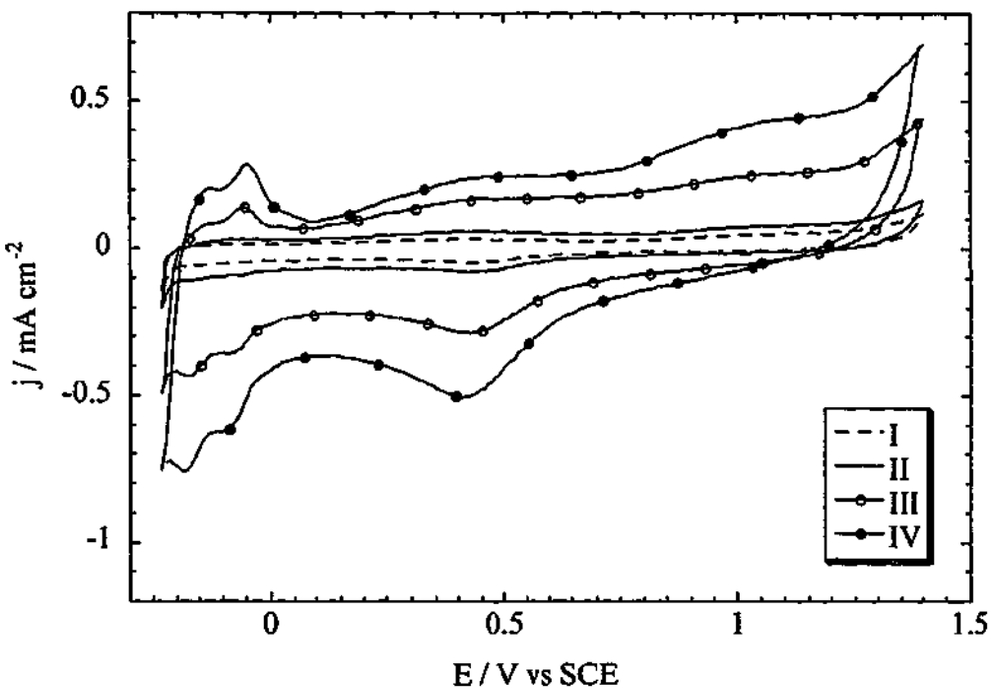

***Fig. 4-15** Analysis of Electrode Pt/GC-6 in 0.5 M H_2SO_4 solution. Pt/GC-6 was platinised as shown in Fig. 4-14 and cleaned via potentiodynamic cycling. Curve I was performed after 130 CV scans over the same range and shows the cleaned electrode, scanning rate: 0.05 V s^{-1}. Curves II, III and IV were performed at a rate of 0.1 V s^{-1}, 0.5 V s^{-1} and 1.0 V s^{-1} respectively, and illustrate the effect of scanning rate.*

The gradual increase in the platinum surface area (as represented by the Pt-H_{ads} oxidation peak during the potentiodynamic cycling between – 0.23 and + 1.4 V) indicates the activation of the platinum surface. In addition, the strong j_a and j_c in the regions of + 1.0 and + 0.2 V, respectively, in Figs. 4-8 and 4-11 were observed to decrease with further potential cycling and this is also representative of the gradual cleaning of the platinum surface. Similar oxidation and reduction currents have

been observed with sulphide-poisoned platinum electrodes in both H_2SO_4 and H_3PO_4 solutions [*Chin and Howard, 1986; Loucka, 1971*]

4.2.4 Platinum Poisoning with $NaHSO_3$ Solution

Hence, from the various phenomena observed throughout this $H_3Pt(SO_3)_2OH$ electrodeposition study and, in particular, the unaltered onset for reduction and the required activation of the deposited platinum via potential cycling, we can conclude that a passivation process occurs on the platinum deposited from $H_3Pt(SO_3)_2OH$ solution. It is suggested that the deposited platinum retains some sulphite ligands or has adsorbed these after reduction. According to Eq. 4-2 and with the platinum deposition being undertaken at these low potentials, the adsorbed species is likely to be sulphide. To confirm this hypothesis, the effect of sulphite ions on both smooth platinum and Pt/GC electrodes was investigated in separate experiments using a 1.0 M $NaHSO_3$ solution. Platinum poisoning was evident in the first CV scans of each electrode by the complete lack of hydrogen adsorption and oxidation peaks, as shown by Curves II and III of Fig. 4-16. The electrodes remained passivated after rinsing in Milli-Q water and being transferred to sulphuric acid solution for analysis.

Curves III and IV in Fig. 4-17 show the first and second analysis scans towards negative potentials in 0.5 M H_2SO_4 following a number of scans in the $NaHSO_3$ solution similar to Curves I in Figs. 4-16 and 4-17. The j_c in the initial sweep (scanning towards negative potentials) of Curve III appear strong compared to the clean platinum baseline (Curve I), and it is interesting to note the similarity between this current density and that also observed in the negative-potential sweeps of Curves I and II in each of Figs. 4-8 and 4-11. In all three figures this probably represents the reduction of an adsorbed sulphur-based species. The cathodic peak between – 0.05 and – 0.1 V is common to both Fig. 4-8 (Curves I and II) and Fig. 4-17 (Curve III), and is in the potential region where weakly-bound protons are adsorbed on the platinum surface (Pt-H_{ads}). This could be a coincidence, and the peak may have instead resulted from the reduction of sulphite to sulphide, according

to Eq. 4-2. Any number of reactions, including possibilities such as Eqs. 4-3 or 4-4 may have caused the cathodic peak.

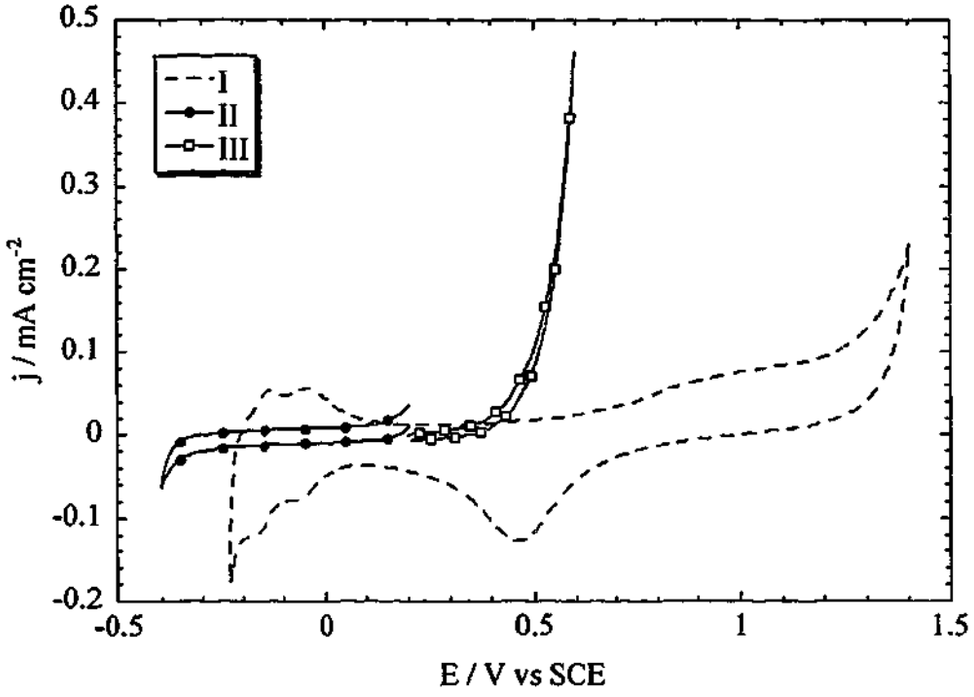

Fig. 4-16 Passivation of platinum in sulphite solution. Curve I shows a typical CV of a clean Pt electrode in 0.5 M H_2SO_4. Curves II and III show CV scans of the same platinum electrode in 1.0 M $NaHSO_3$ solution. Scanning rate: 0.05 V s^{-1}.

Again, the reduction of sulphite to sulphide is likely to have occurred during these experiments in $NaHSO_3$ solution where the electrodes were scanned to – 0.23 V. Whilst cycling the poisoned electrodes in 0.5 M H_2SO_4, oxidation and reduction current densities similar to those in Figs. 4-8 and 4-11 were observed. However, after 10 sweeps in the – 0.23 to + 1.2 V range, the platinum surface had almost completely recovered as observed from the restoration of the typical platinum CV 'fingerprint'. Similar to the previous discussion, the additional j_a and j_c is believed to correspond to the oxidative/reductive removal of the adsorbed species which in this case is either sulphite or sulphide ions.

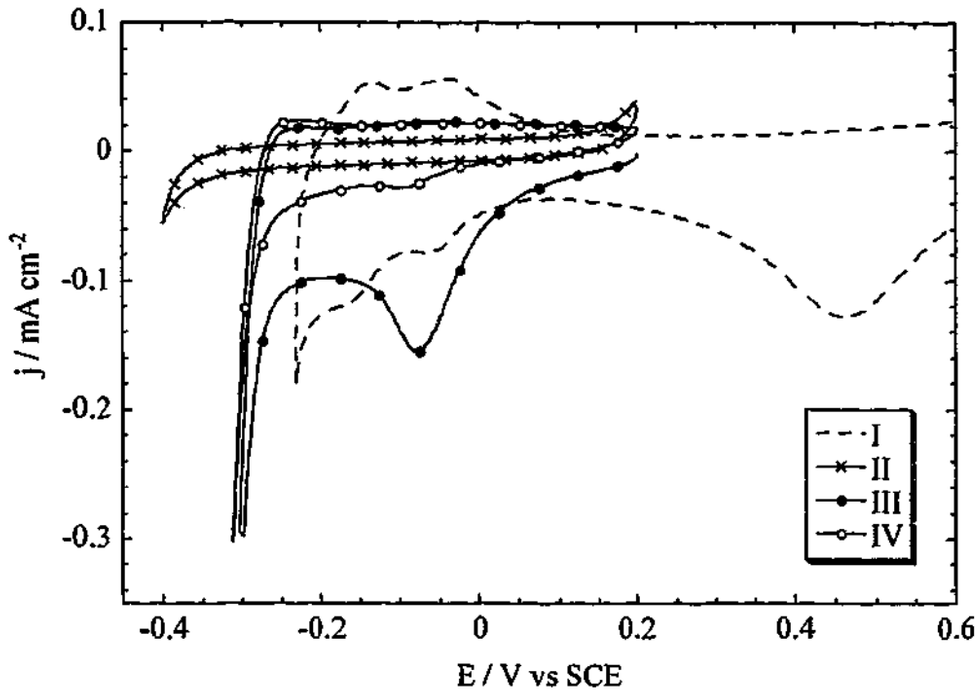

***Fig. 4-17** Analysis of a platinum electrode passivated in a 1.0 M $NaHSO_3$ solution. Curve I shows a typical platinum CV scan in 0.5 M H_2SO_4 (identical scan to Curve I of Fig. 4-16). Curve II shows a scan of the passivated electrode in $NaHSO_3$ solution. Curves III and IV show the first and second CV scans of the poisoned platinum electrode in 0.5 M H_2SO_4 following many scans in the $NaHSO_3$ solution. Scanning rate: 0.05 V s^{-1}.*

$$Pt\text{-}S^-_{ads} + 3H^+ + 2e^- \rightarrow Pt\text{-}H_{ads} + H_2S \qquad (4\text{-}3)$$

$$Pt\text{-}S^-_{ads} + 2H^+ + e^- \rightarrow Pt + H_2S \qquad (4\text{-}4)$$

Fig. 4-18 illustrates the potentiodynamic cleaning of another platinum electrode which was also poisoned by scanning in 1.0 M $NaHSO_3$ solution, except without any scanning to potentials negative to + 0.4 V. This was performed in order to determine whether sulphite ions could adsorb onto the clean platinum surface and passivate the electrode, without converting sulphite to sulphide (a known platinum poison [*Chin and Howard, 1986; Gerischer, 1975; Loucka, 1971*]), at potentials below – 0.11 V, according to Eq. 4-2. Curve I shows the second CV scan in 0.5 M

H_2SO_4, in which the platinum electrode has clearly been passivated. The electrode was again cleaned in a similar fashion to the other $NaHSO_3$ poisoned platinum electrodes and the Pt/GC and Pt/CB electrodes prepared from $H_3Pt(SO_3)_2OH$ electroreduction (i.e. via potentiodynamic cycling). Again strong current densities are observed at the potential extremes in the CV scans. It appears that sulphite does in fact adsorb onto, and passivates, the surface of platinum. Whether sulphite is converted to sulphide and whether electrodes platinised by the electroreduction of $H_3Pt(SO_3)_2OH$ are passivated by sulphide or sulphite has not been ascertained, but it is clear that a sulphur-containing species is responsible.

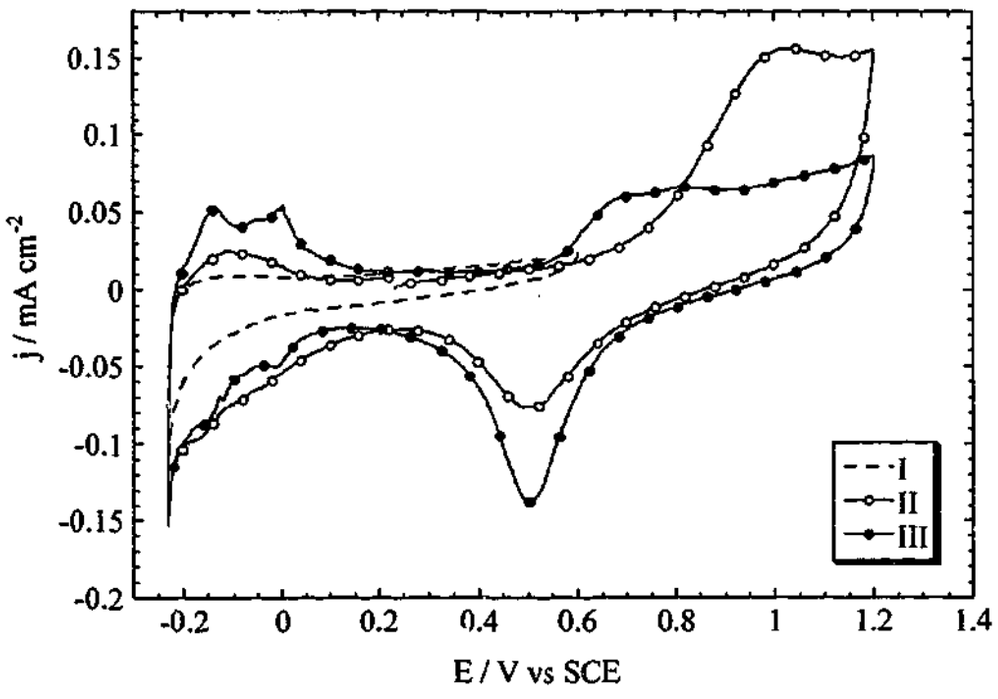

Fig. 4-18 *Analysis of a platinum electrode passivated in a 1.0 M $NaHSO_3$ solution. Curve I shows the second CV scan in 0.5 M H_2SO_4 following passivation in sulphite solution by scans similar to Curve III in Fig. 4-16. Scans were limited to potentials > 0.4 V. Curve II shows an initial cleaning scan of the passivated platinum electrode (in 0.5 M H_2SO_4), the first CV to be scanned to 1.2 V. Curve III shows the cleaned platinum electrode after ca. 90 potentiodynamic cycles similar to Curve II. Scanning rate: 0.05 V s^{-1}.*

The potentiodynamic cycling of the electrodes platinised from $H_3Pt(SO_3)_2OH$ solution was found to be the most effective method for platinum activation, compared with either static potential approaches or heating the platinised electrodes. A minor improvement was observed in the Pt-H_{ads} oxidation peak area after applying potentials of + 1.0 or + 1.2 V to the Pt/GC electrode for 5-10 minutes. However, sweeping from – 0.23 to + 1.2 V at 0.05 V s^{-1} for the same duration appeared to clean platinum more rapidly. Potentiostatic holds at – 0.2 or – 0.3 V for the same time yielded negligible improvement. Similar findings have been observed in the work of Loucka [*Loucka, 1971*] who attempted to oxidise a poisoning sulphur species from platinum by holding the electrode potential at 1.35 V for 10 minutes. Loucka found that the sulphur was not completely removed from the electrode even though the currents for sulphur oxidation had fallen to zero and cycling was required for complete platinum activation. Alternating polarisation approaches have also been used to activate platinum, e.g. switching the potential of a platinum electrode between + 0.07 and + 1.27 V in presence of sulphite ions [*Rosental' and Veselovskij, 1953*]. In addition, no effect was found in this work from heating Pt/GC electrodes poisoned in $NaHSO_3$ solution, even when electrodes were heated for up to 15 h in air at 100°C.

Furthermore, cleaning was observed to occur more rapidly when an upper potential of + 1.4 V was used whereby the maximum oxidation of the poisoning species is attained in each cycle. The oxidation probably proceeds via the formation of Pt-O_{ads}, where strong j_a are observed at potentials positive to + 0.6 V (e.g. Curve I in Fig. 4-11). It is known that sulphide adsorbs onto platinum and may be removed by being initially oxidised to elemental sulphur followed by further oxidation by oxygen evolution to SO_4^{2-}, $S_2O_6^{2-}$, and $S_2O_3^{2-}$ ions [*Gerischer, 1975*] or to SO_4^{2-} and SO_3 species [*Loucka, 1971*]. The Pt electrode remains passivated due to a thin oxide layer and must then be reduced. At high surface coverages of adsorbed sulphur, it is necessary to repeat these oxidation and reduction steps, i.e. to cycle the electrode potential in order to completely remove all of the poisoning species.

Faster scanning rates, e.g. 0.5 V s^{-1}, were found to slightly enhance the cleaning time of the platinised electrodes (most probably since a greater number of oxidation-reduction cycles could be performed in a given time). However, scanning at rates faster than 0.5 V s^{-1} or to potentials greater than + 1.4 V was avoided since this resulted in an apparent loss in the platinum surface area, i.e. a decrease in the Pt-H_{ads} oxidation peak area. In the work of Loucka [*Loucka, 1971*] the rate of potential scanning was found to have no effect on the cleaning of sulphide-poisoned platinum, where scanning rates were varied between 6.7 x 10^{-3} V s^{-1} and 30 V s^{-1}. Cycling to potentials cathodic to – 0.3 V was also avoided in this work since this merely resulted in a large amount of evolved hydrogen and negligible improvement in activating the platinum deposits. It should also be noted that these activated Pt/GC and Pt/CB electrodes were analysed again a day later and several weeks later after resting in Milli-Q water and the final platinum surface area was reproducible. Any faceting or roughening caused by the electrochemical cycling is therefore discounted and the increase in platinum surface area is believed to be wholly due to the cleaning process.

4.3 Summary

Hence, platinum was successfully electrodeposited from the $H_3Pt(SO_3)_2OH$ species onto both GC and CB-based electrodes. The resulting platinum deposits were found to be poisoned, possibly by a sulphide or similar species. It was possible to remove the strongly-bound poisons from the deposited platinum surface via potentiodynamic cycling. This platinum 'poisoning' technique could be utilised in the catalysation of PEMFC electrodes if further optimised. Refer to Chapter Seven for more extensive conclusions of this chapter and also possibilities for future studies on related work.

Chapter Five

Ruthenium and PtRu Electrodeposition

5.1 Introduction

Whether methanol or hydrogen produced from reformed methanol is eventually used as the fuel of choice in PEMFCs or DMFCs, the catalytic requirements are similar. As outlined in Chapter One, fuel cell operation on either methanol or a H_2 + CO (reformate) mixture requires the use of a slightly more advanced catalyst, due to poisoning of platinum by CO_{ads} species. The PtRu catalyst system has been proven to be the most active for both methanol and CO-containing hydrogen fuels. The conventional preparation of these catalysts is similar to that of the platinum catalysts (i.e. by chemical reduction or colloidal precipitation), and the resulting PtRu particles suffer from a similar low utilisation in the fuel cell electrodes.

The majority of work in this dissertation is based upon the central idea that catalyst utilisation in PEMFC and DMFC electrodes may be improved via the electrochemical preparation of such electrodes. The electrochemical deposition of a known amount (or 'loading') of catalyst into fuel cell electrodes is readily achievable, and the placement of these deposits may be manipulated under well-controlled conditions. It is possible that smaller PtRu catalyst particles could be prepared via electrodeposition, thus increasing the surface area-to-mass ratio of the particles and enabling greater 'catalyst atom' utilisation. More significant improvements in catalyst utilisation could even be achieved if PtRu particles were selectively deposited at the necessary places throughout the electrode (i.e. at the three-phase reaction zones where fuel cell reactions take place). Electrodeposition has a much greater potential in the ability to selectively place catalyst atoms in these desired zones within preformed fuel cell electrodes compared to conventional preparation methods (where the Pt/C and PtRu/C supported catalysts are made first and then formed into an electrode- refer to Chapter One). Following improvements in catalyst utilisation, lower noble metal loadings are required in electrodes, thus reducing electrode cost and enabling the manufacture of more compact electrodes and correspondingly lighter DMFC stacks.

In the previous chapter, a catalyst-poisoning process was observed during electrodeposition of platinum from the $H_3Pt(SO_3)_2OH$ species. The poisoning of the Pt deposits by a sulphite or related species was believed to limit the growth of Pt particles from further $H_3Pt(SO_3)_2OH$ electroreduction. Since ruthenium exhibits similar electrochemistry to platinum, electroreduction of the $H_3Ru(SO_3)_2OH$ species may result in poisoned Ru particles onto which further Ru deposition is limited or even prevented. If the particulate growth of Ru is limited during $H_3Ru(SO_3)_2OH$ electroreduction, then growth of PtRu particles during co-electroreduction (e.g. from a binary solution containing one or both of the sulphite species) might also be limited, which is highly desirable in the preparation of catalyst particles with a high surface area : mass ratio. Co-electrodeposition of PtRu particles into preformed fuel cell electrodes may also lead to higher catalyst utilisations under certain conditions. Additionally, as in the case of the $H_3Pt(SO_3)_2OH$ studies, the $H_3Ru(SO_3)_2OH$ species was initially trialled in electrodeposition experiments because chloride is removed in its preparation.

5.2 Ruthenium Electrodeposition and Analysis

A ruthenium sulphite species was prepared (from $RuCl_3$) in a similar way to the $H_3Pt(SO_3)_2OH$ species investigated in Chapter Four, according to US Patent 4,044,193 [*Petrow and Allen, 1977*]. Refer to Chapter Three for a more detailed description of the preparation. Again, in a similar fashion to $H_3Pt(SO_3)_2OH$, a important benefit in using the ruthenium sulphite species for fuel cell catalysts is the removal of chloride ions during its preparation. For PtRu catalyst preparation the removal of Cl^- is essential since Cl^- acts as a complexing species to Pt [*Bagotzky et al., 1970*], causing dissolution in acidic conditions [*Chemodanov and Kolotyrkin, 1970*]. Ruthenium is also known to corrode in chloride-containing solutions, at low pH [*Bard, 1976*]. Additionally, to the knowledge of this author the electroreduction of the ruthenium sulphite species has not been published before.

In the preparation of the ruthenium sulphite species, the chlorides in $RuCl_3$ are replaced with sulphite (SO_3^{2-}) ligands, most probably forming the $Na_6Ru(SO_3)_4$ species. The grey-blue $Na_6Ru(SO_3)_4$ powder is then dissolved in 0.5 M H_2SO_4, producing a dark blue solution. The chemical structure of the ruthenium sulphite species is believed to be $H_3Ru(SO_3)_2OH$, being prepared in an almost identical fashion to $H_3Pt(SO_3)_2OH$ (refer to Chapter Three); ruthenium and platinum exhibiting similar chemistry. This would signify a valence of Ru^{II}, which is a rare form of ruthenium. The most common oxidation state for ruthenium is IV [*Pourbaix, 1966*], and in acid media the usual valences are Ru^{III} and Ru^{IV} [*Bard, 1976*]. However, aqueous solutions of Ru^{III} and Ru^{IV} are yellow and red-brown in colour respectively, whereas divalent ruthenium (or 'ruthenous') solutions appear blue [*Bard, 1976; Pourbaix, 1966*]. No other ruthenium valences reported in literature yield blue solutions; the less common Ru^{VI}, Ru^{VII} and Ru^{VIII} species dissolve to form orange or green (RuO_4^{2-}, RuO_2^{2+}), green (RuO_4^-) and golden yellow (H_2RuO_5, $HRuO_5^-$) solutions respectively [*Pourbaix, 1966*]. Since blue is also the colour of the 0.01 M $H_3Ru(SO_3)_2OH$ + 0.5 M H_2SO_4 solution used in this work it is likely that $H_3Ru(SO_3)_2OH$ is indeed the correct chemical formula.

Ru^{II} solutions are reported to be barely stable and easily oxidised to Ru^{III} or Ru^{IV} [*Bard, 1976*], however the sulphite ligands are thought to stabilise the Ru^{II} in this species. Furthermore, the coordination number of Ru^{II} species is usually 6 [*Bard, 1976*], which is in agreement with the six ligands in the $H_3Ru(SO_3)_2OH$ structure. Only Ru^{IV} species and lower valences may be cathodically deposited [*Bard, 1976*]. Complexing agents have been used before in ruthenium electrodeposition to prepare deposits of high quality and thickness. Amine sulphonic acid, nitrosyl chloride and nitrosyl sulphamate solutions have been used to successfully complex and electroplate ruthenium [*Bard, 1976*]. The sulphite ligands in the $H_3Ru(SO_3)_2OH$ species may also enable the formation of high quality Ru electrodeposits.

Initially, the ruthenisation of glassy carbon electrodes in $H_3Ru(SO_3)_2OH$ solution was studied, despite the fact that ruthenium alone is not a suitable catalyst for PEMFCs or DMFCs. These Ru/GC electrodes were prepared to gain some insight

into the electrodeposition of the sulphite species (in comparison to platinum species with which it may eventually be alloyed). The preparation of Ru/CB electrodes was briefly pursued to determine whether it was possible to electrodeposit this ruthenium species into 'fuel cell type' electrodes, and also for surface analysis (SEM and EDXS) purposes. After establishing the electrodeposition conditions of $H_3Ru(SO_3)_2OH$, preparation of the binary PtRu catalyst was investigated.

5.2.1 Potentiodynamic Studies of $H_3Ru(SO_3)_2OH$

The electroreduction of $H_3Ru(SO_3)_2OH$ onto glassy carbon from a 0.01 M $H_3Ru(SO_3)_2OH$ + 0.5 M H_2SO_4 solution is shown by Curves II to IV in Fig. 5-1. The current density for the reduction of the ruthenium sulphite species becomes significant at potentials negative to + 0.2 V. The deposition potential for $H_3Ru(SO_3)_2OH$ has not been quoted in literature, however the reduction potential of the Ru^{II} species has been calculated from thermodynamic data, Eq. 5-1 [*Bard, 1976; Pourbaix, 1966*]. Ruthenium (from a 0.01 M Ru^{II} solution) is therefore expected to be electroreduced at ~ 0.154 V_{SCE} (0.396 V_{RHE}) and lower potentials. This is in close agreement with the electroreduction of the Ru^{II} sulphite species in this work; there may be a small amount of $H_3Ru(SO_3)_2OH$ reduction at potentials slightly above this. For comparison, the electroreduction potential of the commonly available ruthenium chloride species has been theoretically calculated as 0.438 V_{SCE}, Eq. 5-2 [*Bard, 1976*], suggesting greater chemical stability of the $H_3Ru(SO_3)_2OH$ species compared to $RuCl_3$. This higher stability is believed to result from the sulphite ligands in the $H_3Ru(SO_3)_2OH$ complex.

$$Ru^{II} + 2e^- \rightarrow Ru \qquad E^\circ = 0.213 + 0.0295\log(Ru^{2+})\ V_{SCE} \qquad (5\text{-}1)$$

$$RuCl_3 + 3e^- \rightarrow Ru + 3Cl^- \qquad E^\circ = 0.438\ V_{SCE} \qquad (5\text{-}2)$$

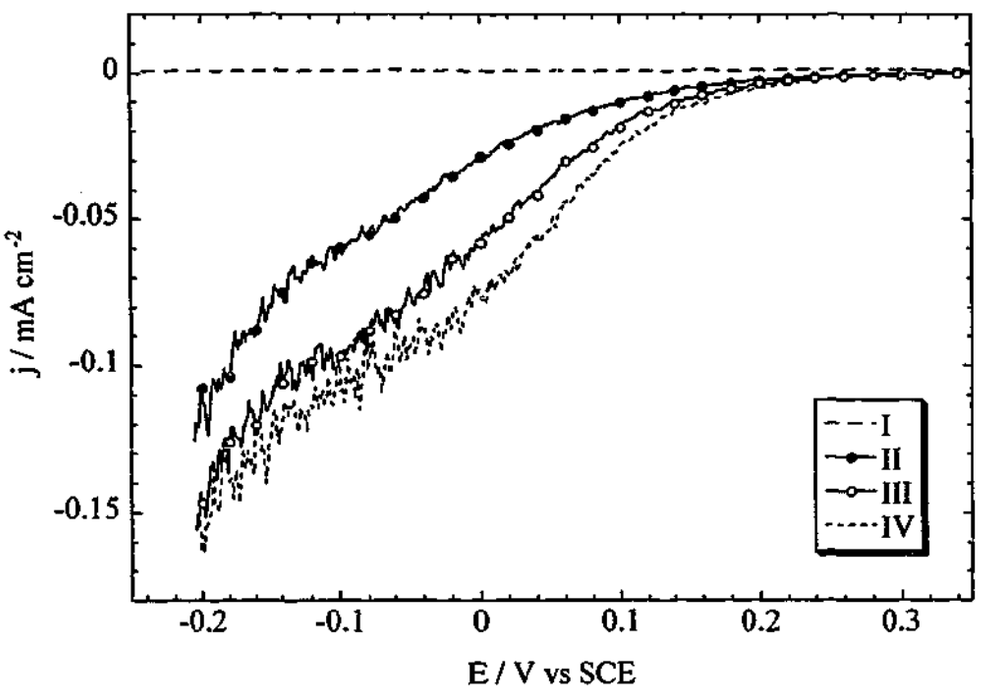

Fig. 5-1 *Linear-sweep electroreduction of ruthenium from a 0.01 M $H_3Ru(SO_3)_2OH$ + 0.5 M H_2SO_4 solution onto glassy carbon. Curve I is a GC baseline in 0.5 M H_2SO_4. Curve II shows the first ruthenium electroreduction sweep onto Electrode GC-7. Curves III and IV show the second and third reduction sweeps. Sweep rate: 0.001 V s^{-1}.*

In Fig. 5-1, the linear sweep illustrated by Curve II commenced at 0.4 V_{SCE} and then scanned towards lower potentials. An initial upper potential (E_i) of 0.6 V_{SCE} was used in the second and third electroreduction sweeps (Curves III and IV) to ensure that the electroreduction onset was observed (i.e. in case the Ru^{II} reduction onset in these second or third sweep increased). Higher potentials were avoided to prevent the production of irreversible ruthenium oxides such RuO_2 that form at potentials above 0.7 V_{SCE} [*Szabó and Bakos, 1987*]. However, some irreversible ruthenium oxides may form at potentials as low as 0.56 V_{SCE} [*Stŕbac et al., 2001*]; the irreversible Ru_2O_3 species may even form at 0.5 V_{SCE} [*Lezna et al., 1983*].

The gradient of curves II to IV appears similar to that of the linear-sweep electroreduction of $Pt(NH_3)_4Cl_2$ (Fig. 4-1 in Chapter Four). It is possible that the sulphite ligands in $H_3Ru(SO_3)_2OH$ slow the reduction kinetics of this species in a

similar fashion to the amine ligands in $Pt(NH_3)_4Cl_2$, as reported by Penven *et al.* [*Penven et al., 1992*]. The electroreduction of ruthenium in the second and third sweeps (Curves III and IV in Fig. 5-1) appears to commence at the same potential as that for the initial sweep in $H_3Ru(SO_3)_2OH$ solution (Curve II), and the reduction current densities appear progressively stronger with each consecutive sweep (albeit only slightly). This is likely to indicate the formation of new ruthenium deposits during each reduction sweep (as opposed to the growth of ruthenium deposits). Ru^{II} reduction onto Ru is likely to occur with a lower overpotential (i.e. at a higher potential, the formation of Ru-Ru bonds being energetically favoured) *cf.* reduction onto GC, as in the case of $PtCl_6^{2-}$ electroreduction onto Pt^0 (refer to Fig. 4-2 in Chapter Four). The increase in the cathodic current density, j_c, from Curve II to Curve IV most probably results from the increase in electrode surface area (and therefore in the current density due to charging of the electrical double layer, j_{dl}) with more ruthenisation.

The slight increase in j_c between Curves II and IV in Fig. 5-1 might also be explained by the reduction of ruthenium surface oxides. Apart from irreversible oxides such as RuO_2 and Ru_2O_3 (the production of which is considered negligible in this potential range), hydroxide species are generally known to adsorb (reversibly) at around 0.2 V_{SCE} and higher potentials. These species form a non-stoichiometric Ru(OH) and $Ru(OH)_2$ oxide layer, approximately represented by Eqs. 5-3 and 5-4. It is difficult to determine at what potential ruthenium adsorbs hydroxide species due to hydrogen adsorption/desorption behaviour on ruthenium at these potentials. Some researchers believe $Ru(OH)_x$ begins to form at 0.16 [*Szabó and Bakos, 1987*] or even as low as 0.11 V_{SCE} [*Watanabe and Motoo, 1975*]. At any rate, some $Ru(OH)_x$ species will form on the surface of the Ru deposits during the initial high potentials of Curve III (Fig. 5-1), and these will be reduced at lower potentials, thus contributing to the cathodic current densities observed. A similar argument can explain the increased j_c observed in the linear sweep shown by Curve IV. The high initial potential of Curves III and IV (0.6 V_{SCE}) also increases the likelihood of significant $Ru(OH)_x$ formation, and at the slow sweep rate employed, 0.001 V s^{-1}, the ruthenised GC-7 electrode is held at potentials above 0.2 V_{SCE} for 400 s, considerable time to

allow adsorption of OH^- species. Since $Ru(OH)_x$ species may form at potentials close to, or even lower than the commencement of $H_3Ru(SO_3)_2OH$ electroreduction, it is difficult to completely avoid the formation of $Ru(OH)_x$ species[i].

$$Ru + H_2O \rightarrow Ru(OH) + H^+ + e^- \qquad (5\text{-}3)$$

$$Ru + 2H_2O \rightarrow Ru(OH)_2 + 2H^+ + 2e^- \qquad (5\text{-}4)$$

Furthermore, ruthenium is known to adsorb hydrogen (in similar fashion to platinum in acid media), and this reaction will also contribute to the cathodic current densities. The 'hydrogen region' on ruthenium, where $Ru\text{-}H_{ads}$ forms (Eq. 5-5) and is oxidised (Eq. 5-6), occurs in roughly the same potential range as on platinum, from – 0.24 to 0.0 V_{SCE} (i.e. 0.0 to 0.24 V_{RHE}). The effects of both H adsorption and $Ru(OH)_x$ reduction may also be responsible for the j_c fluctuations observed in the electroreduction sweeps (Curves II to IV). The roughness of j_c in the sweeps appears to increase with more ruthenisation (from Curve II to IV), further supporting this possibility. At any rate, it is probable that the increase in j_c from Curve II to IV results from the increased ruthenisation of the GC surface, and that $H_3Ru(SO_3)_2OH$ does not preferentially reduce onto Ru deposited from the same species, in comparison with the GC surface (otherwise the electroreduction onset would increase with further ruthenisation).

$$Ru + H^+ + e^- \rightarrow Ru\text{-}H_{ads} \qquad (5\text{-}5)$$

$$Ru\text{-}H_{ads} \rightarrow Ru + H^+ + e^- \qquad (5\text{-}6)$$

[i] It may be possible, however, that these surface species limit the growth of ruthenium particles due to the higher electrical resistance of the oxide film (refer to the Future Work section- Section 7.3.2).

Between 0.0 and – 0.15 V_{SCE} (in Curves II to IV of Fig. 5-1) a decrease in the linear-sweep gradient is observed, suggesting diffusion limitations in the $H_3Ru(SO_3)_2OH$ electroreduction. At potentials negative to – 0.15 V the gradient increases again, probably due to greater adsorption of protons (and this might also be supported by the increase in the j_c fluctuations). Sweeping to even lower potentials was avoided since the evolution of hydrogen on the ruthenium deposits would cause a significant increase in the cathodic current densities, obscuring the $H_3Ru(SO_3)_2OH$ electroreduction currents.

Curves II and III in Fig. 5-2 illustrate the slight scatter in the current densities of $H_3Ru(SO_3)_2OH$ electroreduction onto separately prepared GC electrodes. Curve II is a reproduction of Curve II in Fig. 5-1 (Electrode GC-7), and commenced from 0.4 V_{SCE}. The linear sweep shown by Curve III in Fig. 5-2 (Electrode GC-8) commenced from 0.5 V_{SCE}. The onsets for electroreduction are roughly equivalent, and the variation in current densities may have arisen from a slight difference in the initial surface areas of the GC electrodes (most likely caused by the preparation of new GC surfaces via polishing). This scatter of ~ 0.035 mA cm^{-2} at 0.0 V is negligible, especially in comparison with the large scatter in onset potentials observed for the $H_3Pt(SO_3)_2OH$ species, as discussed in Chapter Four (Fig. 4-6).

Curve III in Fig. 5-2 also shows $H_3Ru(SO_3)_2OH$ electroreduction at potentials within the region of hydrogen evolution (i.e. below – 0.24 V_{SCE}, or 0.0 V_{RHE}). Strong current densities resulting from this reaction may be observed at even higher potentials, (e.g. close to – 0.2 V_{SCE}). The hydrogen evolution reaction (HER) is known to occur more strongly at higher potentials on electroplated ruthenium compared with platinum [*Hadži-Jordanov et al., 1977*].

Additional potentiodynamic experiments in the ruthenium sulphite solution were performed to further investigate the electrochemistry of this ruthenium species, as shown in Fig. 5-3. GC-8 was initially ruthenised during the linear sweep shown by Curve III in Fig. 5-2 (shown again by Curve II in Fig. 5-3) and then experienced 5 more similar sweeps in the same $H_3Ru(SO_3)_2OH$ solution at different rates as shown

in Fig. 5-3 (a). A slight decrease in the reduction slope is observed below ~ 0.05 V, possibly resulting from diffusion limitations in the electroreduction of $H_3Ru(SO_3)_2OH$. This is particularly evident in the faster sweeps (Curves V to VII). At potentials below about – 0.2 V strong j_c is observed, originating from the hydrogen evolution reaction. Following the reduction sweeps shown in Fig. 5-3 (a), GC-8 was cycled in the ruthenium solution with a progressively increasing upper potential, Fig. 5-3 (b). For clarity, only two electroreduction CV scans (Curves IX and X) are shown in Fig. 5-3 (b) however, before Curve X was performed CVs scanned up to 0.5, 0.6, and 0.7 V. The reduction current densities progressively increased following these scans to higher potentials. 0.8 V was the highest upper potential used, and strong cathodic current densities may be observed below 0.2 V (Curve X). Some of this j_c is expected to arise from the reduction of surface oxides (in addition to further $H_3Ru(SO_3)_2OH$ reduction). Surface oxides may also form during the initial (higher potential) part of the [illegible] sweeps shown in Fig. 5-3 (a), and some of the j_c observed in these sweeps may result from oxide reduction in addition to ruthenium electroreduction.

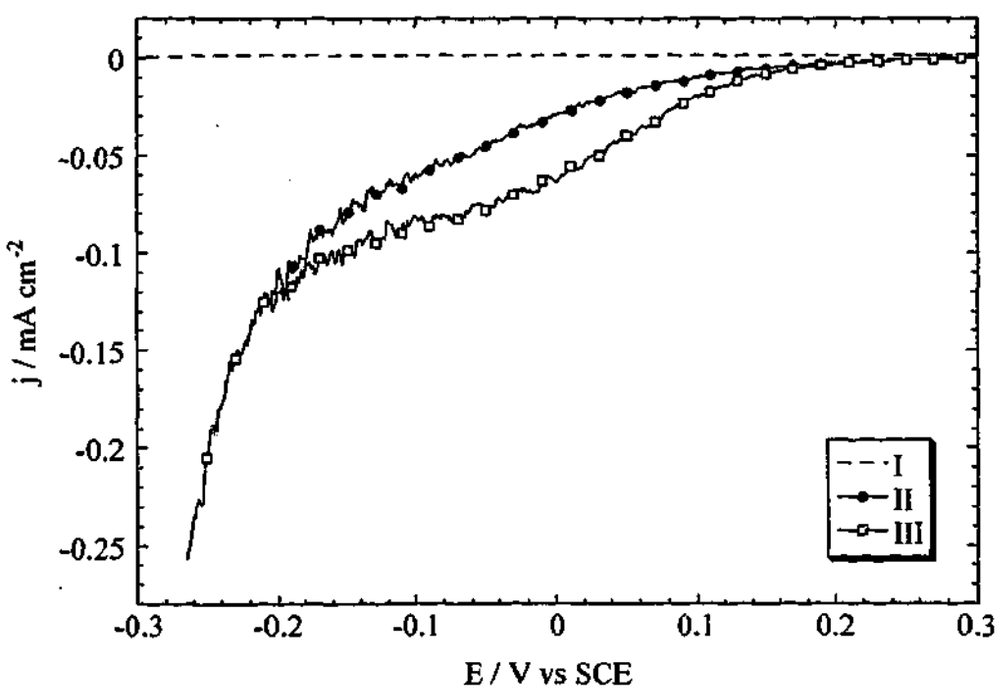

Fig. 5-2 *Initial potentiodynamic sweeps of GC electrodes in 0.01 M $H_3Ru(SO_3)_2OH$ + 0.5 M H_2SO_4 solution. Curve I is a GC baseline in 0.5 M H_2SO_4. Curves II and III illustrate the first ruthenium electroreduction sweeps onto Electrodes GC-7 and GC-8 respectively. Sweep rate: 0.001 V s^{-1}.*

Typical cyclic voltammograms of $H_3Ru(SO_3)_2OH$-ruthenised glassy carbon electrodes, are shown in Fig. 5-4. The GC-7 electrode was lightly ruthenised as shown in Fig. 5-1. The GC-8 electrode was ruthenised as shown by the linear-sweeps and CV scans in Fig. 5-3. Curves II and III are the second analysis CV scans of Ru/GC-7 and Ru/GC-8 in 0.5 M H_2SO_4. The ruthenium loading on Ru/GC-8 appears significantly greater than that on Ru/GC-7 (by at least a factor of 10, from a rough comparison of the $Ru(OH)_x$ current densities at ~ 0.3 V), as is expected from the greater electroreduction time experienced by Electrode GC-8. However, these ruthenised electrodes do not exhibit all the electrochemical features compared to electrodes prepared from $RuCl_3$ solution, for example the ruthenised platinum of Hadži-Jordanov *et al.* in Fig. 5-5. Nevertheless, in later SEM/EDXS analyses of similarly ruthenised CB-based electrodes (from $H_3Ru(SO_3)_2OH$ solution), the existence of Ru deposits was confirmed (refer to Section 5.2.4).

Current densities for the adsorption and desorption of atomic H on the ruthenium surface, Eqs. 5-4 and 5-5, may be observed at low potentials (i.e. below 0.2 V_{RHE}) in Fig. 5-5. However, in Fig. 5-4 no definite evidence of these processes is observed, apart from relatively minor cathodic current densities around – 0.1 V_{SCE}. In Fig. 5-5 increased j_c is observed following scans to potentials above ~ 0.6 V_{RHE} as $Ru(OH)_x$ species (formed above 0.2 V_{RHE}) are reduced. This was not observed on Electrode Ru/GC-8, which was scanned to 1.2 V as shown by Curve IV in Fig. 5-4 (b). However, slight increases in j_c were observed on similarly $H_3Ru(SO_3)_2OH$-ruthenised GC electrodes in scans over smaller potential ranges (e.g. Curve X in Fig. 5-3), most probably arising from $Ru(OH)_x$ reduction. A very strong oxidation process occurs at potentials above 0.15 V_{SCE} on the Ru/GC-8 electrode that is not observed in Fig. 5-5. At lower potentials, a cathodic spike may be observed in Fig. 5-4 that probably represents the evolution of hydrogen, although this reaction does not appear as strongly on the ruthenised electrode in Fig. 5-5.

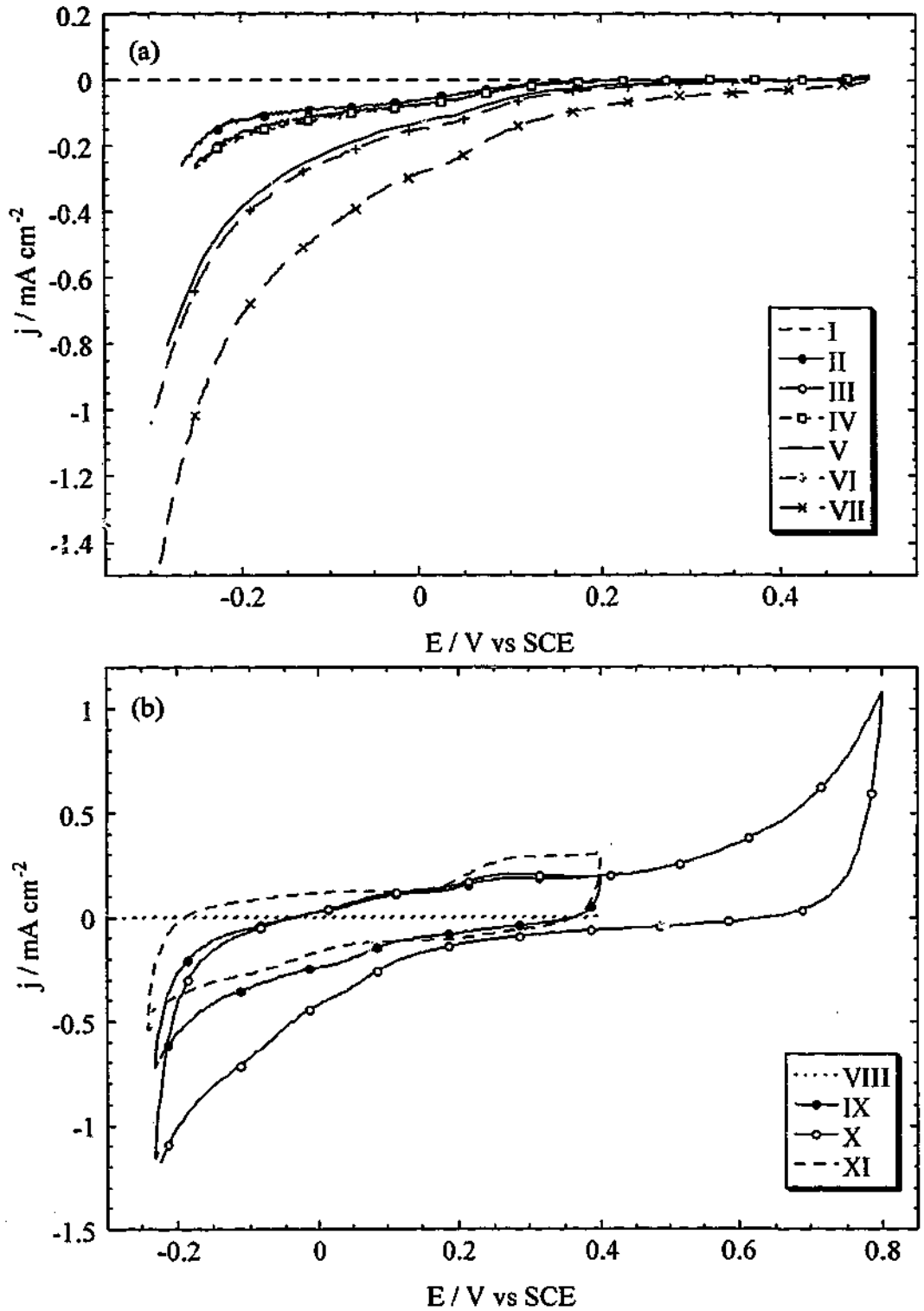

Fig. 5-3 *Potentiodynamic investigation of $H_3Ru(SO_3)_2OH$ and ruthenisation of GC-8 in $H_3Ru(SO_3)_2OH$ solution. (a) Linear-sweep study. Curve I is the baseline scan of GC-8 in 0.5 M H_2SO_4 at 0.001 V s^{-1}. Curves II to VII show sweeps in 0.01 M $H_3Ru(SO_3)_2OH$ + 0.5 M H_2SO_4 solution, at different rates; Curves II to IV at 0.001 V s^{-1}; Curves V and VI at 0.02 V s^{-1}; Curve VII at 0.05 V s^{-1}. (b) Further ruthenisation of Ru/GC-8 and study of $H_3Ru(SO_3)_2OH$ solution via cyclic voltammetry. Curve VIII is the baseline scan of GC-8 in 0.5 M H_2SO_4. Curves IX and X show CV scans of Ru/GC-8 in 0.01 M $H_3Ru(SO_3)_2OH$ + 0.5 M H_2SO_4 solution. Curve XI is the second analysis scan of Ru/GC-8 in 0.5 M H_2SO_4. Scanning rate (for Curves VIII to XI): 0.05 V s^{-1}.*

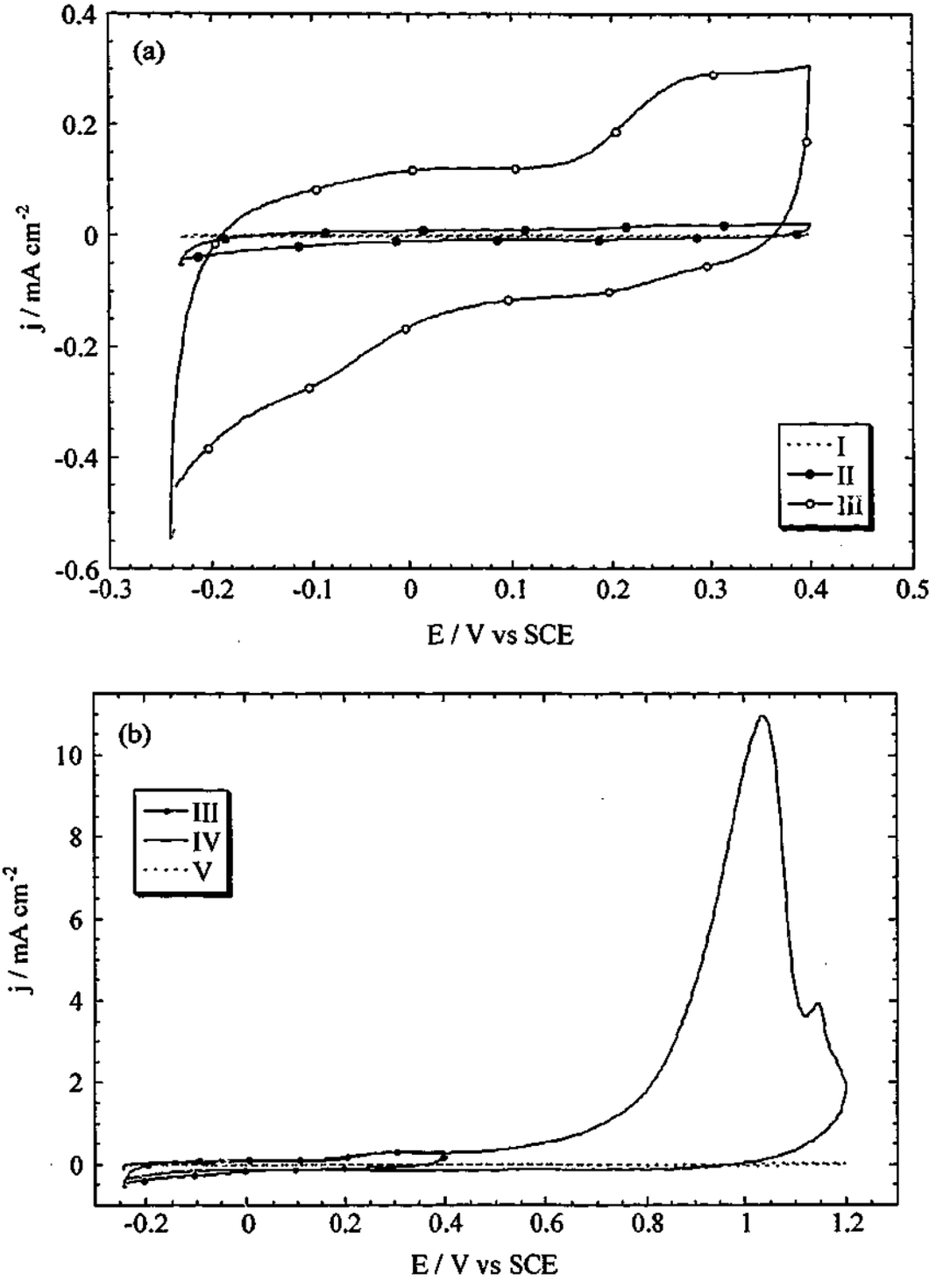

Fig. 5-4 *Potentiodynamic analyses of Electrodes Ru/GC-7 and Ru/GC-8, which were ruthenised as shown in Figs. 5-1 and 5-3 respectively. (a) Curve I is a GC baseline CV in 0.5 M H_2SO_4. Curves II and III show the second analysis scans of Ru/GC-7 and Ru/GC-8 in 0.5 M H_2SO_4 solution. (b) Further potentiodynamic analysis of Ru/GC-8. Curve III is displayed again for comparison. Curve IV was the first CV to be scanned to an upper potential of 1.2 V. Curve V was the next scan following Curve IV. Scanning rate: 0.05 V s^{-1}.*

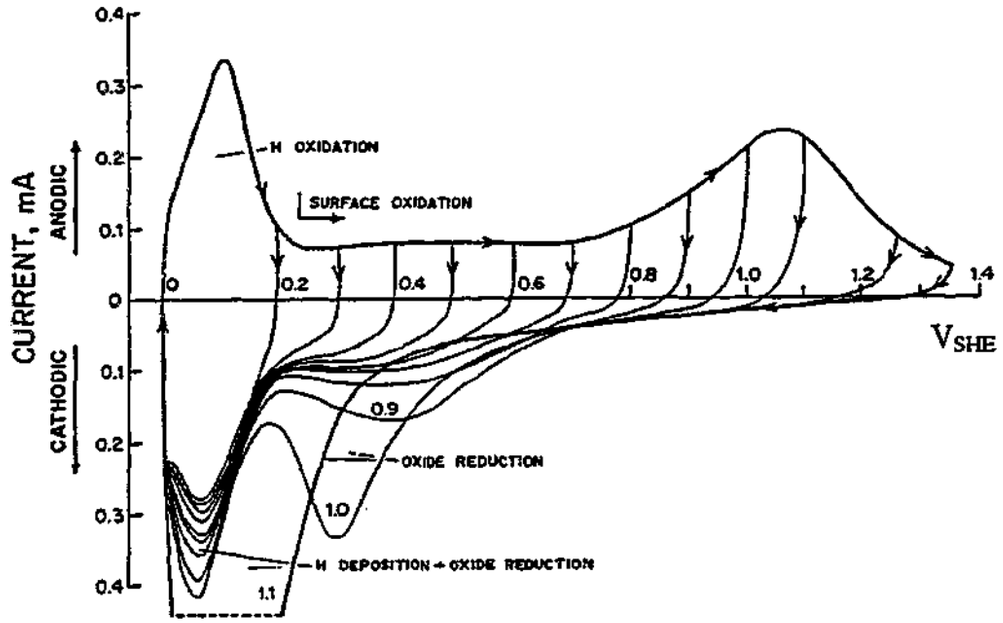

Fig. 5-5 Potentiodynamic analysis of a ruthenised Pt electrode, by Hadži-Jordanov et al. [Hadži-Jordanov et al., 1977]. Cyclic voltammograms of Ru/Pt electrode in 0.5 M H_2SO_4 at 25 °C, with progressively increasing upper potentials. Note: SHE scale. Scanning rate: 0.008 V s^{-1}.

Initially, the lack of a clear Ru-H_{ads} oxidation peak on the Ru/GC-7 electrode was thought to arise from the low ruthenium loading deposited on the glassy carbon. However, electrodes with higher ruthenium loadings (i.e. electrodes which had experienced longer electroreduction times) did not exhibit any H-oxidation behaviour either. A similar lack of the Pt-H_{ads} oxidation peak was noticed on electrodes platinised from $H_3Pt(SO_3)_2OH$ (which resulted from a poisoned Pt surface, as discussed previously in Chapter Four). Since platinum and ruthenium exhibit similar chemistry (being 'platinum group metals'), this lack of a 'H-region' in CV scans was not surprising, especially considering the identical ligands in both Pt and Ru sulphite species). However, the surface chemistry of the two metals can be significantly different, e.g. Ru adsorbs OH^- at much lower potentials (~ 0.4 V lower) *cf.* Pt, and Ru does not appear to adsorb methanol (or at least not at potentials below 0.5 V_{SCE} [*Gasteiger et al., 1993*]). Ruthenium is known to adsorb chloride ions [*Hadži-Jordanov et al., 1977*] and so it is possible that other complexing species

such as sulphite may be adsorbed on Ru. Thus, as in the case of platinum electroreduction from $H_3Pt(SO_3)_2OH$, ruthenium electroreduced from $H_3Ru(SO_3)_2OH$ may also be poisoned by sulphite or related species.

The strong oxidation current densities observed at potentials above 0.15 V_{SCE} in Curve III of Fig. 5-4 suggest the possibility of ruthenium surface poisoning. Hadži-Jordanov *et al.* [*Hadži-Jordanov et al., 1977*] studied the adsorption of chloride onto ruthenised electrodes and found that, similar to platinum electrodes, the adsorbed Cl^- prevented the surface oxide formation from occurring until higher potentials, obtaining a double-layer region (within which there was no overlap between H_{ads} oxidation and $Ru(OH)_x$ formation). A similar surface poisoning of the Ru/GC-8 electrode shown in Fig. 5-4 has probably occurred. The oxidation process at potentials above 0.15 V_{SCE} also coincides with that on the chloride-poisoned Ru [*Hadži-Jordanov et al., 1977*], which, in the latter work, was believed to represent OH^- replacement of adsorbed Cl^- species.

Further potentiodynamic scans of the Ru/GC-8 electrode were performed over a wider potential range as shown in Fig. 5-4 (b). This analysis was undertaken to determine whether electrochemical activation or 'cleaning' of the deposited ruthenium was possible (as it was for platinum electroreduced from $H_3Pt(SO_3)_2OH$ solution in Chapter Four). Scanning to higher potentials also provides an indication of the electrochemical stability of the Ru deposits. Curve IV in Fig. 5-4 shows the first CV scanned to an upper potential of + 1.2 V. A strong oxidation reaction is observed with a peak current density at around 1.0 V. These anodic current densities appear considerably stronger than those resulting from scanning over a similar range (e.g. 0.0 to 1.4 V_{RHE}) in Fig. 5-5. The scanning rate, υ, used by Hadži-Jordanov *et al.* [*Hadži-Jordanov et al., 1977*] in Fig. 5-5 is not as fast, however current densities generally vary in proportion to υ. Some electro-dissolution of Ru is expected from the scans passing to high potentials in Fig. 5-5, although most of the j_a results from formation of Ru_2O_3 and RuO_2 surface species (as is suggested by the approximately similar j_c area on the reverse sweep, resulting from the reduction of ruthenium surface oxides). In contrast, very little j_c is observed in Curve IV of

Fig. 5-4. Curve V of Fig. 5-4 immediately follows Curve IV and exhibits no features apart from the GC baseline. Hence it is likely that the Ru deposited onto GC-8 was completely electro-dissolved during Curve IV in Fig. 5-4 (possibly passing through higher oxide states). Since this is significantly different to the CV-analysed Ru in Fig. 5-5, the Ru electro-dissolution from Ru/GC-8 may have been enhanced by the poisoning species, similar to the increased corrosion of Ru observed in HCl solution [*Hadži-Jordanov et al., 1977*]. If a sulphite or related species is adsorbed to the Ru then it may facilitate more rapid Ru electro-dissolution via complexing the Ru. On platinum (as described in Chapter Four) the formation of the surface oxide layer is believed to help in the oxidation of adsorbed sulphide species and repeated scanning over a wide potential range, up to the region where oxygen evolution commences, greatly accelerates the cleaning process. However, ruthenium is known to be less stable at higher potentials *cf.* platinum, so a similar 'oxidative removal' of poisoning species from the Ru surface is probably not viable. Scans were also performed at low potentials (passing to potentials as low as – 0.5 V_{SCE}), to investigate whether the H2 evolution reaction (HER) on the Ru surface could aid in removing the poisoning species (e.g. via a 'reductive cleaning' process), without any apparent change in CV characteristics.

No improvements were found following *ca.* 20 similar CV scans on the electrode, and the only remaining features were the current density peaks for the oxidation and reduction processes of the GC surface functionalities (at around 0.4 and 0.3 V_{SCE} respectively) which increased with continued scanning. Time was also allowed for reduction of any ruthenium oxides using slow CV scans and potentiostatic holds at low potentials (e.g. 0.0, -0.2, -0.4 V_{SCE}), with no change in the CV features. After electrochemical cycling proved unsuccessful for cleaning Ru electrodeposited from $H_3Ru(SO_3)_2OH$, the effect of heating was studied. Another Ru/GC electrode was prepared in similar fashion, and then heated at 95°C for 20 h in air. Again, no change was observed in the resulting Ru/GC CV scans. Higher temperatures were not feasible due to concerns regarding the GC electrode thermal stability (e.g. possible delamination of the CTFE casing).

5.2.2 Potentiostatic Ru/GC Electrode Preparation

Reduction at a constant potential provides a straightforward electrodeposition method that bypasses the need to determine potential limits in potentiodynamic reduction and simplifies the tailoring of a desired metal loading. A brief investigation into ruthenium deposition from $H_3Ru(SO_3)_2OH$ solution under constant potential was performed. By electroplating ruthenium at one potential (as opposed to the linear-sweeps and CV scans performed in Section 5.2.1) greater control over the charge passed (which is related to the ruthenium loading deposited) may be achieved. Potentiostatic electrodeposition is also more likely to be used in electrode fabrication commercially, in large-scale processes. For catalyst electrodeposition into PEMFC and DMFC electrodes very low metal loadings are desired (as opposed to the films in common industrial electroplating). Furthermore, passing a desired amount of charge at a certain potential is preferred *cf.* galvanostatic methods for reproducible deposition (e.g. during galvanostatic deposition the electrode potential can drop to low voltages where hydrogen evolution may occur and affect the deposition).

According to Figs. 5-1, 5-2 and 5-3 it should be possible to potentiostatically reduce ruthenium from $H_3Ru(SO_3)_2OH$ solution at potentials negative to + 0.2 V. The rate of reduction will increase as the potential is decreased, as a greater overpotential is applied to the electrode, and the equilibrium of Eq. 5-1 will shift to the right (i.e. towards Ru deposition). However at low potentials, especially less than – 0.23 V, the HER takes place on the ruthenium surface and the cathodic current densities resulting from this vigorous reaction will interfere with those from the ruthenium reduction. If an estimate of the ruthenium loading is desired from the total charge passed in electrodeposition then these HER contributions should be avoided. The effects of H adsorption onto ruthenium (and also absorption into ruthenium) during reduction may also contribute to the cathodic current densities, although to a lesser extent. At potentials greater than 0.1 or 0.15 V, some anodic current densities may arise from the formation of $Ru\text{-}OH_{ads}$, although reduction at these potentials from the $H_3Ru(SO_3)_2OH$ species is unlikely due to low reduction rates.

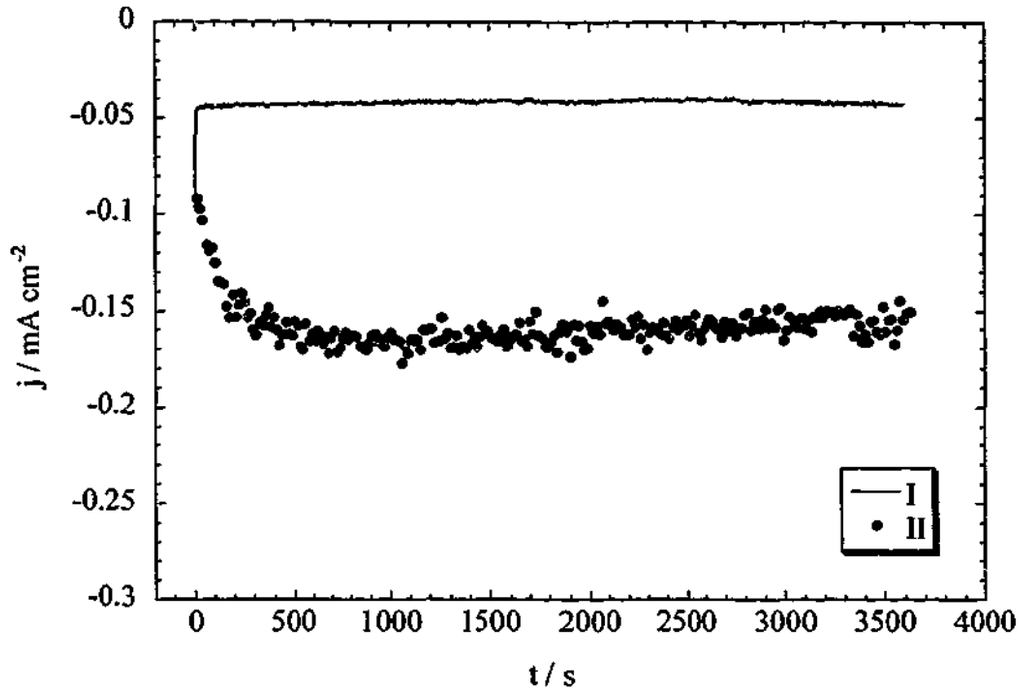

Fig. 5-6 *Current density-time transients for the potentiostatic reduction of ruthenium from a 0.01 M $H_3Ru(SO_3)_2OH$ + 0.5 M H_2SO_4 solution onto GC electrodes. Curve I shows the attempted ruthenisation of GC-9 at 0 V. Curve II shows the ruthenisation of GC-10 at – 0.2 V.*

Fig. 5-6 shows the current density-time (*j-t*) transients for Electrodes GC-9 and GC-10 in a 0.01 M $H_3Ru(SO_3)_2OH$ + 0.5 M H_2SO_4 solution at different potentials. Curve I shows the attempted ruthenisation of GC-9 at 0.0 V. In Figs. 5-1 and 5-2, some $H_3Ru(SO_3)_2OH$ reduction appears to occur at this potential (with reduction current densities of around – 0.03 to – 0.06 mA cm^{-2}, under linear sweep conditions at 0.001 V s^{-1}). A comparable current density of – 0.045 mA cm^{-2} was obtained in Curve I of Fig. 5-6. However, no traces of ruthenium were found during the subsequent CV analysis of GC-9 in 0.5 M H_2SO_4, even though this electrode was held at a potential of 0.0 V for 1 h. It is possible the amount of ruthenium deposited onto GC-9 was so little that the GC electrode j_{dl} obscured any ruthenium electrochemical features.

Curve II in Fig. 5-6 displays the ruthenisation of Electrode GC-10 at a lower potential (– 0.2 V). After about 5 min, the current density reaches a value of *ca.* – 0.15 mA cm^{-2}, which is roughly equivalent to the j_c observed at – 0.2 V in the linear-sweep reductions of $H_3Ru(SO_3)_2OH$ (Curves II to IV of Fig. 5-1). The fluctuations in the j_c over time may again be explained by the H-adsorption/desorption behaviour on the deposited ruthenium surfaces at these potentials. The slight decrease in the reduction current density over time in Curve II may have resulted from a slight decrease in the ruthenium ion concentration (in the electroplating solution) over the hour.

The potentiodynamic analysis of Ru/GC-10 is shown in Fig. 5-7. Ru/GC-10 exhibits similar electrochemical features to Ru/GC-8; the larger j_{dl} most probably indicates a higher Ru loading. The CV scan of Ru/GC-10 also exhibits greater current densities in the 'H region', but no strong H-adsorption/desorption peaks were found. A cathodic shoulder may be observed at – 0.1 V (which is less obvious on Ru/GC-8) which may represent some H_{ads} formation, but may have also arisen from the reduction in surface oxides. Again, the ruthenium on GC-10 is readily electro-dissolved on scanning to higher potentials (Curves III and IV in Fig. 5-7), but more scans were required before all of the Ru was removed, probably due to the higher ruthenium loading. After sweeping the electrode potential to 1.0 V for the first time (Curve III), strong cathodic current densities are observed in the reverse sweep, particularly at potentials below + 0.2 V. These are believed to result from the reduction of Ru_2O_3 and RuO_2 formed at high potentials, as was observed by Hadži-Jordanov *et al.* in Fig. 5-5.

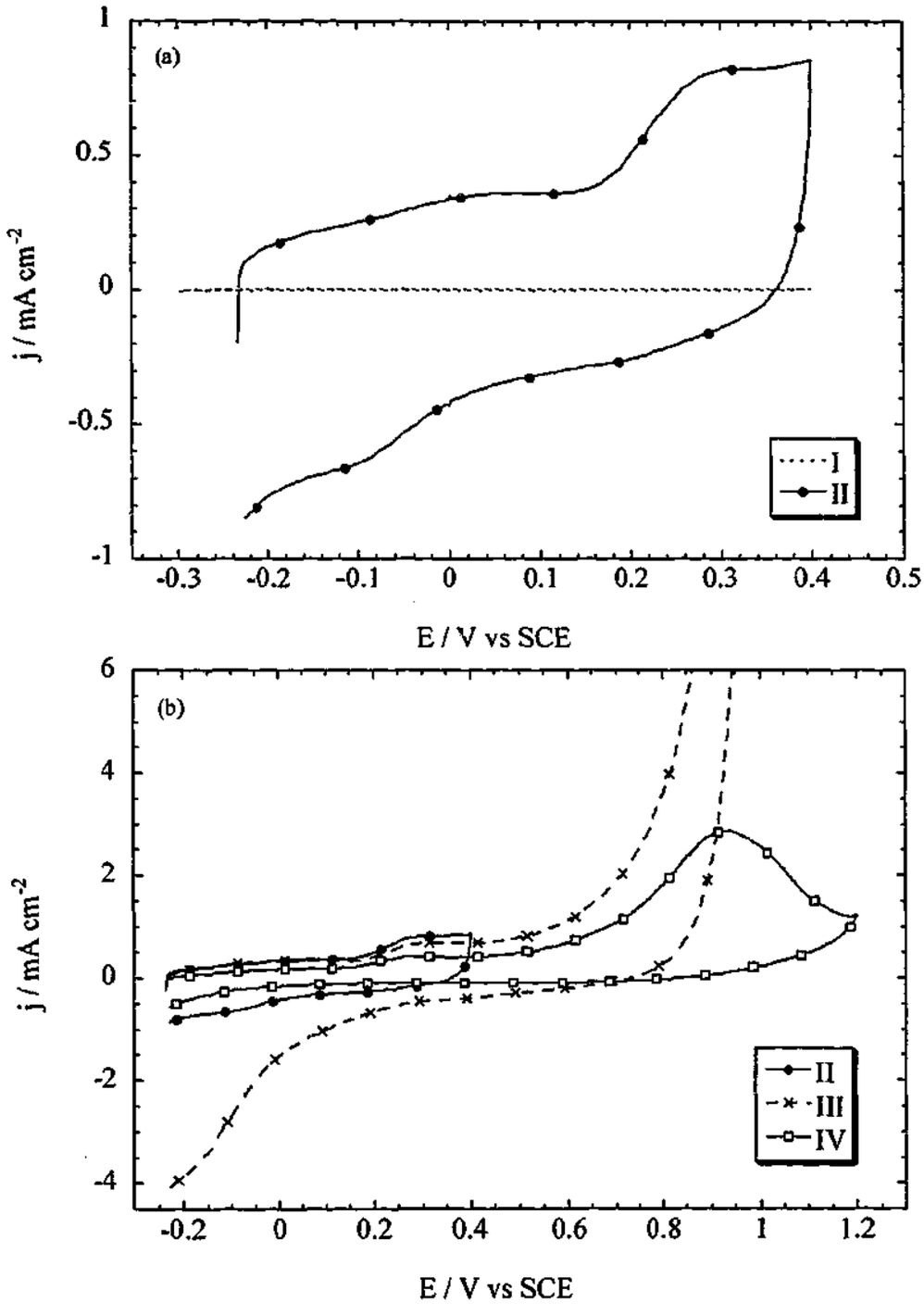

Fig. 5-7 *Potentiodynamic analysis of Ru/GC-10 in 0.5 M H_2SO_4 following potentiostatic ruthenisation as shown by Curve II in Fig. 5-6. (a) Curve I is the GC-10 baseline CV. Curve II shows the first analysis scan of the ruthenised electrode. (b) Curve III shows the seventh analysis scan of Ru/GC-10 and the first CV to scan to an upper potential of 1.0 V. Curve IV is the fifth CV to scan to an upper potential of 1.0 V. Curve II is displayed again for comparison. Scanning rate: 0.05 V s^{-1}.*

5.2.3 Electrodeposition Comparison with $RuCl_3$

The electrodeposition of ruthenium from the commonly available $RuCl_3$ species was investigated for comparison with both $H_3Ru(SO_3)_2OH$ electroreduction and the unusual potentiodynamic scans of $H_3Ru(SO_3)_2OH$-deposited ruthenium. The cleaning and electro-dissolution behaviour of $RuCl_3$-ruthenised GC electrodes was then studied.

Curves II and III in Fig. 5-8 illustrate the electroreduction of $RuCl_3$ onto GC electrodes. $RuCl_3$ electroreduction appears to commence at a higher potential *cf.* $H_3Ru(SO_3)_2OH$, at around 0.6 V_{SCE}, which is surprising because this potential is higher than 0.438 V_{SCE} which was calculated for the $RuCl_3 \rightarrow Ru$ reaction (Eq. 5-2 [*Bard, 1976*]). This discrepancy is probably explained by a higher valence of the ruthenium species in solution. The $RuCl_3$ dissolved to form a red-brown solution in 0.5 M H_2SO_4, indicative of a Ru^{IV} species according to Pourbaix [*Pourbaix, 1966*] and Bard [*Bard, 1976*]. This is further supported by the work of Chrzanowski and Wieckowski, who found that $RuCl_3$ formed the $[Ru^{IV}O(H_2O)_4]^{2+}$ species in solution [*Chrzanowski and Wieckowski, 1997*]. The theoretically calculated E° for $RuCl_3$, Eq. 5-2, was probably based on the Ru^{III} species. Unfortunately, the electroreduction of $RuCl_3$ and Ru^{IV} species has not been extensively studied before. The general appearance of Curves II and III in Fig. 5-8 is similar to that of $H_3Ru(SO_3)_2OH$ reduction (Curve IV), with an initial steep j_c gradient which then decreases at lower potentials, suggesting diffusion limitations (possibly with simultaneous j_a processes, such as $Ru(OH)_x$ formation). The gradient then increases at lower potentials, probably due to $Ru(OH)_x$ reduction and H adsorption processes at the deposited Ru surface. The initial j_c gradients of the first electroreduction sweeps (Curves II and IV) are not as steep *cf.* that of other species (e.g. H_2PtCl_6, which is readily reduced at around 0.1 V_{SCE} - see Fig. 4-1 in Chapter Four). The initial electroreduction gradients are similar to those during electroreduction sweeps of the $Pt(NH_3)_4^{2+}$ species, which is known to have slow reduction kinetics [*Penven et al., 1992*]. It is highly likely that the reduction kinetics of both ruthenium species may also be slow.

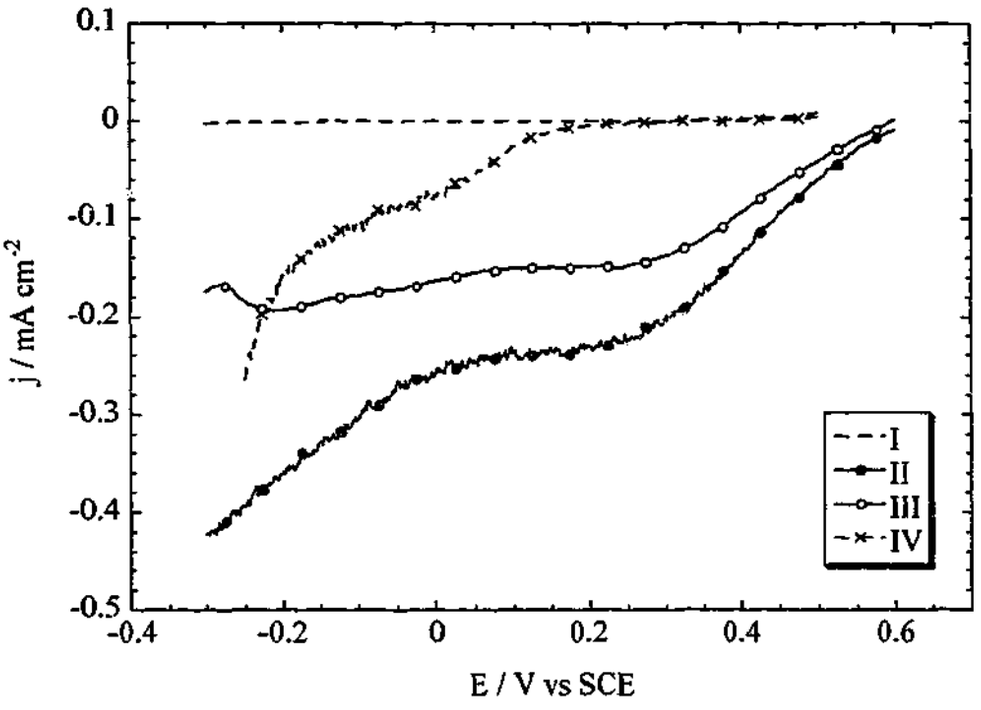

***Fig. 5-8** Linear-sweep electroreduction of ruthenium from a 0.01 M $RuCl_3$ + 0.5 M H_2SO_4 solution onto glassy carbon. Curve I is the GC-11 baseline in 0.5 M H_2SO_4. Curves II and III show the first and fifth ruthenium electroreduction sweeps from $RuCl_3$ solution onto Electrode GC-11. For comparison, Curve IV shows the first reduction sweep of ruthenium from $H_3Ru(SO_3)_2OH$ solution onto Electrode GC-8. Sweep rate: 0.001 V s^{-1}.*

In the subsequent CV-analysis of the $RuCl_3$-deposited Ru/GC-11 (ruthenised as shown by the linear-sweeps in Fig. 5-8), typical Ru electrochemical features such as those illustrated in Fig. 5-5 were not observed. This was surprising at first, however it transpires that the surface chemistry of Ru is highly sensitive to electroreduction potential. Strong H_{ads} behaviour (particularly the Ru-H_{ads} oxidation peak) is apparently only observed on Ru surfaces that have been electroplated at potentials where hydrogen evolves on Ru. The ruthenised electrode in Fig. 5-5 was actually deposited at a very low potential, – 0.2 V_{RHE} (i.e. – 0.44 V_{SCE}), at which potential hydrogen will evolve vigorously on Ru[ii]. Hadži-Jordanov *et al.* suggested that Ru

[ii] Incidentally, the majority of electrodeposited ruthenium reported in the literature was galvanostatically deposited (during which the WE potential may be forced to very low potentials to maintain the desired plating current - for example 100 mA cm^{-2}); well-defined H_{ads} regions are typically exhibited by such electrodes.

deposited within the HER region may have "*a more disordered or expanded ruthenium structure...that is capable of admitting atomic H with increased facility*" [*Hadži-Jordanov et al., 1977*].

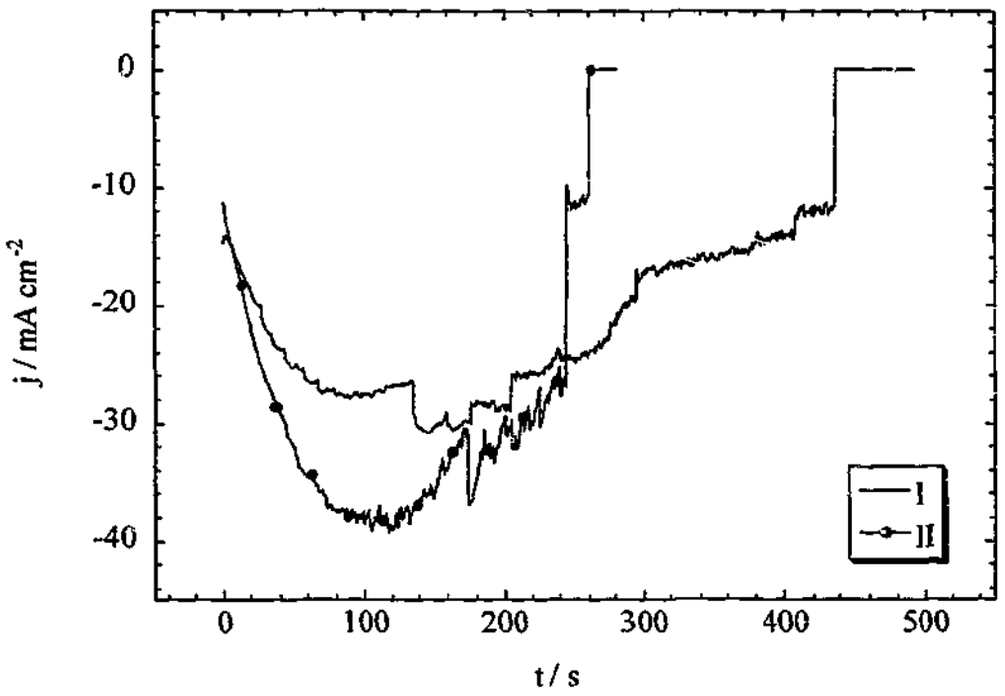

Fig. 5-9 *Potentiodynamic ruthenisation of GC electrodes at – 0.45 V. Curve I shows the j-t behaviour of Electrode GC-12 in 0.01 M $RuCl_3$ + 0.5 M H_2SO_4 solution. Curve II shows the ruthenisation of Electrode GC-13 in 0.01 M $H_3Ru(SO_3)_2OH$ + 0.5 M H_2SO_4 solution.*

GC electrodes were ruthenised from $RuCl_3$ and $H_3Ru(SO_3)_2OH$ solutions again, at potentials within the HER region (– 0.45 V_{SCE}, Fig. 5-9). In Fig. 5-9, the j_c may be observed to rapidly increase with time during both electroreductions (for the first 100 s) followed by a rapid decrease in reduction current density. The initial increase in j_c was believed to result from rapid Ru electroreduction combined with vigorous H_2 evolution on the WE surface at these low potentials. During the first minute of electroreduction, significant numbers of bubbles (most probably H_2) were observed to evolved from the WE surfaces. Some of these bubbles became trapped beneath the electrode surfaces (due to the configuration of the electrochemical cell), even

with high flow rates of N_2 purging. Eventually, these bubbles coalesced to form a large bubble on each electrode that covered the entire WE surface. The increase in trapped bubble size (and thus decrease in WE surface area in contact with solution) correlates with the decrease in electroreduction current densities shown in Fig. 5-9. The fluctuations in the *j-t* behaviour of the electrodes were observed to be related to bubble formation and removal of trapped bubbles. Ru electroreduction ceased following *ca.* 440 s (GC-12) and *ca.* 260 s (GC-13), when the electrochemical circuits were broken.

The potentiodynamic analysis of Electrodes GC-12 and GC-13 is shown in Fig. 5-10. Only the Ru deposited from the $RuCl_3$ species exhibited a Ru-H_{ads} oxidation peak (Curves IV-VI). The Ru-H_{ads} oxidation peak was observed following 15 scans of Ru/GC-12 over the same potential range (Curve IV); it is likely that the Ru surface was inhibited by adsorbed impurities in earlier scans (e.g. Curve III). The Ru deposited from $H_3Ru(SO_3)_2OH$ appeared to be poisoned again, regardless of the low reduction potential used (and deposition within the HER region). As in previous experiments, electrochemical cycling was unable to clean the Ru/GC-13 surface, and scans to high potentials again caused the dissolution of Ru. In another interesting comparison, the greater stability of the $RuCl_3$-ruthenised electrode (Ru/GC-12) is apparent in Fig. 5-10, since Ru loss via electrodissolution occurs more gradually during scans to high potentials (see Curves V and VI in Fig. 5-10).

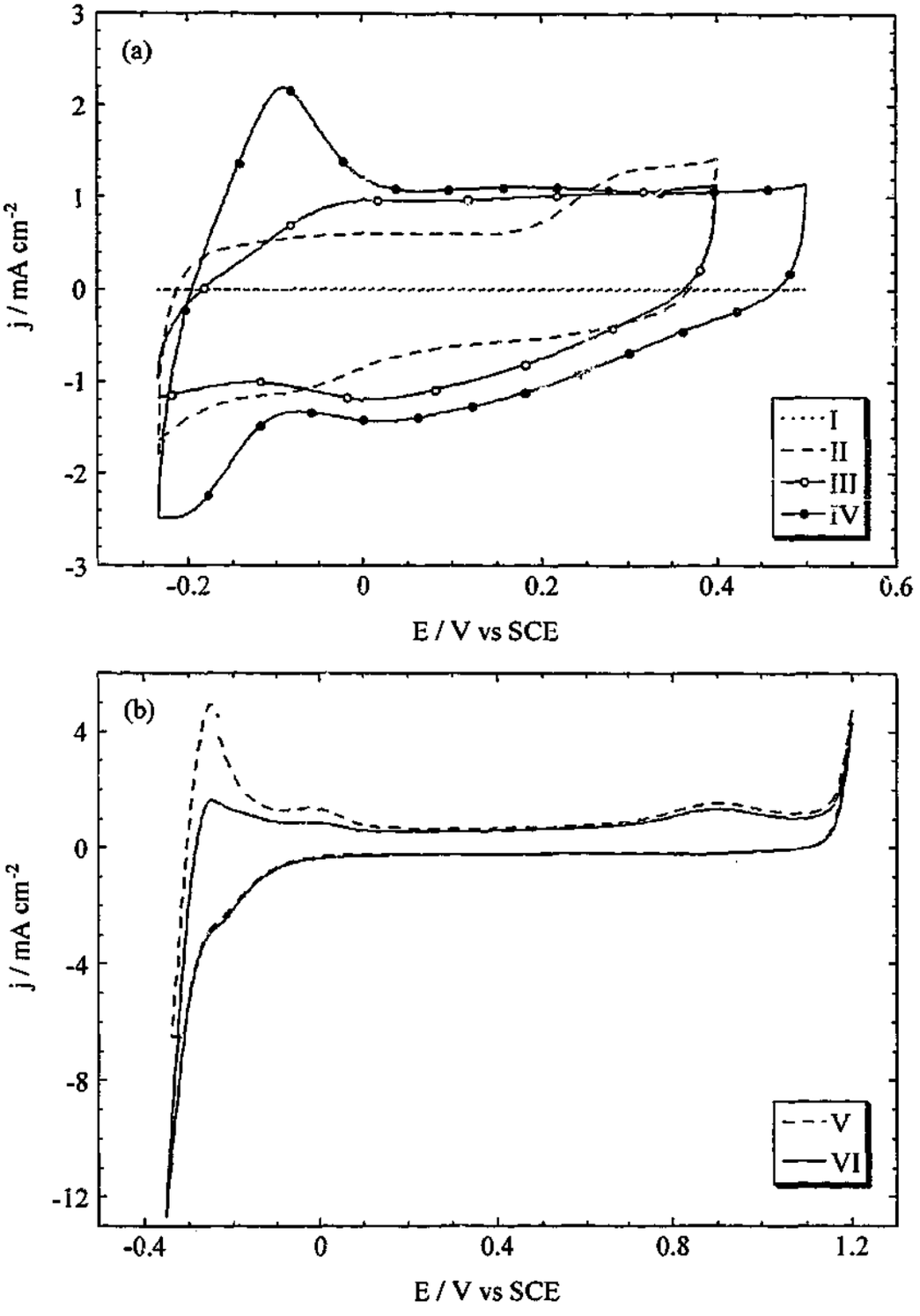

Fig. 5-10 *Potentiodynamic analysis (in 0.5 M H_2SO_4) of Ru/GC electrodes prepared potentiostatically at – 0.45 V as shown in Fig. 5-9. Curve I is a GC baseline. Curve II shows a typical CV scan of the Ru/GC-13 electrode that was ruthenised from $H_3Ru(SO_3)_2OH$ solution (Fig. 5-9). Curves III to VI show CV scans of the Ru/GC-12 electrode that was ruthenised from $RuCl_3$ solution (Fig. 5-9). Curve III is the second scan of Ru/GC-12 and Curve IV shows a scan of the same electrode following 15 cleaning scans (over the same potential range). Curves V and VI show the electrochemistry of Ru over a wider potential range. Scan rate: 0.05 V s^{-1}.*

5.3 Ru/CB Preparation

The ruthenisation of carbon-black (CB) based electrodes was also investigated using the $H_3Ru(SO_3)_2OH$ species, for completion and also for SEM/EDXS analyses. Electroreduction of $H_3Ru(SO_3)_2OH$ onto Electrode CB-4 was found to commence at a slightly higher potential (~ 0.1 V more positive) *cf.* electroreduction of the same species onto GC (e.g. Curve II in Fig. 5-11). CB-4 was further ruthenised in the same $H_3Ru(SO_3)_2OH$ solution (potentiostatically at – 0.45 V, i.e. within the HER region), as shown by Curve III in Fig. 5-11. Again, strong j_c was observed (with similar j_c values to those in Curve II of Fig. 5-9). However, the cathodic current density was not observed to similarly decrease, since the evolved H_2 could easily escape from the high surface-area CB-based electrode positioned vertically in the electrochemical cell. Fluctuations in the j_c may also be observed in Curve III of Fig. 5-11 as the electrode-solution interfacial area was altered by H_2 evolution.

Curve II in Fig. 5-12 shows a typical CV scan of the Ru/CB-4 electrode. Aside from larger current densities, this CV appears similar to the ruthenised GC electrodes in Figs. 5-3, 5-4 and 5-7. Thus, the Ru appears to be poisoned in a similar fashion to the GC-ruthenised electrodes. No potentiodynamic cleaning was attempted on this electrode, since it appeared similar to the Ru/GC electrodes previously prepared (and any Ru electrodissolution was undesirable prior to SEM/EDXS analyses).

An SEM micrograph of the freshly deposited Electrode Ru/CB-4 is shown in Fig. 5-13. The image was recorded using 'back scattered' electrons, which highlight changes in compositional differences across a sample surface. Similar to 'secondary electron' mode, the brighter regions represent elements of higher atomic mass; darker regions indicate either elements of lower atomic mass, or pores in the surface (from which backscattered electrons are not emitted).

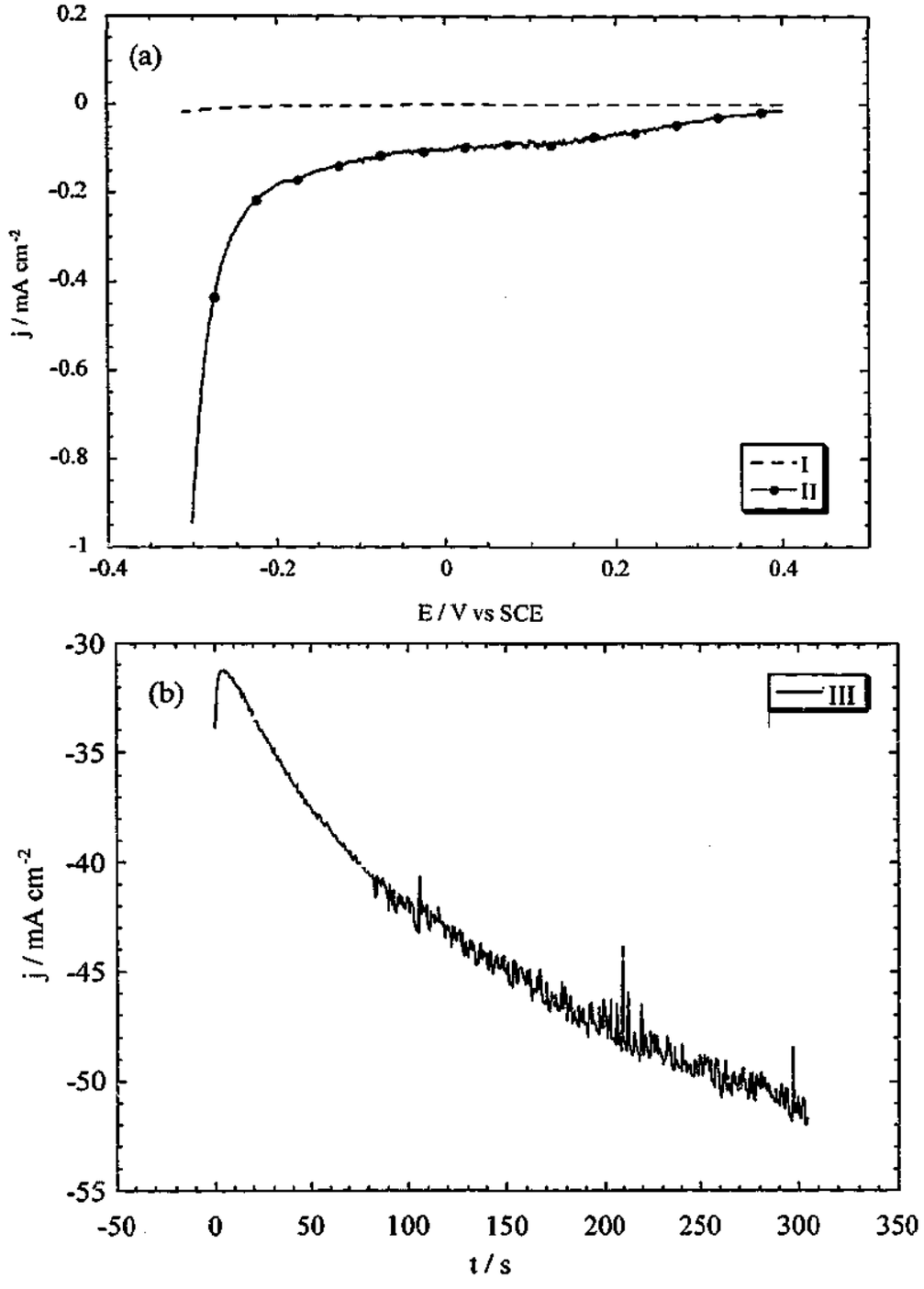

Fig. 5-11 *Linear-sweep and potentiostatic electroreduction of $H_3Ru(SO_3)_2OH$ onto a carbon-black (CB) based electrode. (a) Curve I is a baseline sweep of Electrode CB-4 in 0.5 M H_2SO_4. Curve II shows a linear-sweep of CB-4 in 0.01 M $H_3Ru(SO_3)_2OH$ + 0.5 M H_2SO_4 solution. Sweep rate: 0.001 V s^{-1}. (b) Curve III shows a current density-time transient for the potentiostatic reduction of ruthenium at – 0.45 V (from the same $H_3Ru(SO_3)_2OH$ solution) onto Electrode CB-4, following the linear-sweep shown by Curve II in (a).*

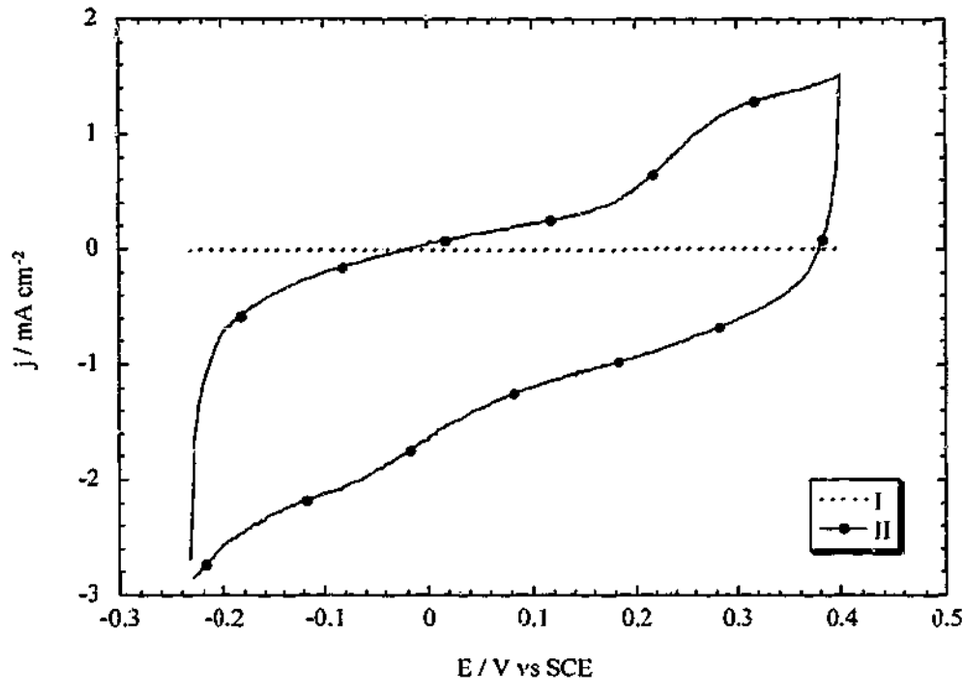

Fig. 5-12 *Potentiodynamic analysis of the Ru/CB-4 electrode prepared as shown in Fig. 5-11. Curve I is the CB-based electrode baseline CV scan in 0.5 M H_2SO_4. Curve II shows the third analysis scan of the ruthenised electrode. Scan rate: 0.05 V s^{-1}.*

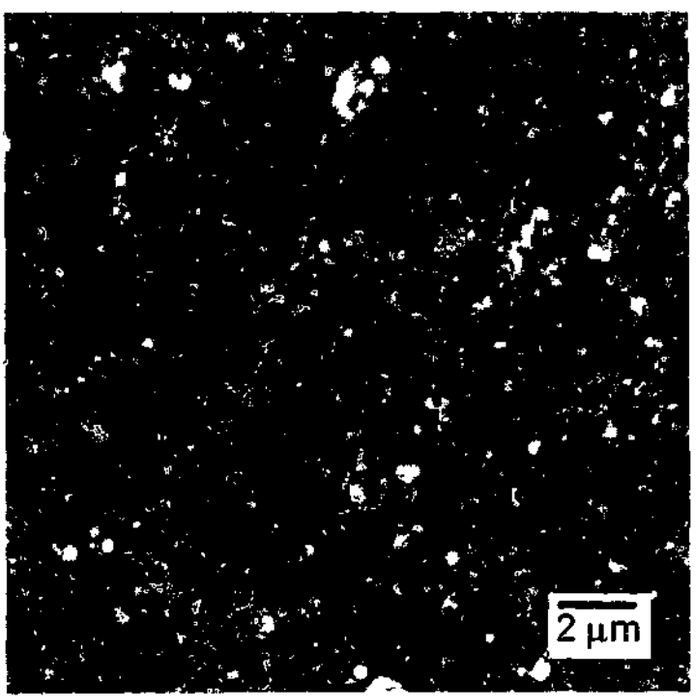

Fig. 5-13 *SEM micrograph (backscattered electron image) of the Ru/CB electrode ruthenised from $H_3Ru(SO_3)_2OH$ solution as shown in Fig. 5-11. The highly dispersed, bright particles are platinum as determined by EDXS (see Fig. 5-14).*

The brighter regions of the Ru/CB-4 electrode (in Fig. 5-13) were found to be rich in Ru and S, as determined from EDXS analysis, Curve I of Fig. 5-14. No Ru was found by EDXS in the darker electrode regions (Curve II); these areas displayed the presence of carbon and sulphur, although at low levels. The relative intensity in the darker region is considerably less, most probably due to the reduced electron scattering abilities of the lighter elements in these areas. The carbon and oxygen peaks do not show up as strongly as expected, since these lighter elements are less stable in the electron beam (even at the relatively low accelerating voltage of 20 kV). The Ru particle size is difficult to ascertain from the SEM micrograph, however it appears that the particles are up to 500 nm in diameter. Whether these particles are in agglomerate form and/or have highly roughened surfaces (e.g. in a 'sponge-like' form [*Hadži-Jordanov et al., 1977*]), resulting from the low electrodeposition potential is unknown.

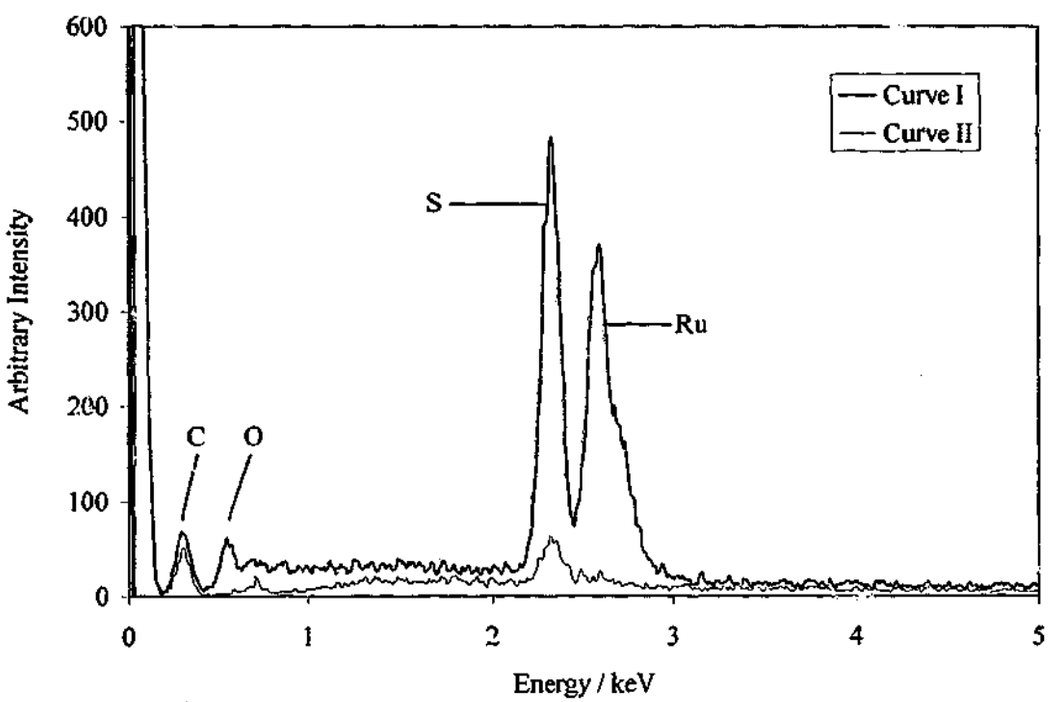

Fig. 5-14 *EDXS analysis of the Ru/CB-4 electrode ruthenised from $H_3Ru(SO_3)_2OH$ solution as shown in Fig. 5-11. Curve I was recorded in an electrode region with a high density of 'bright' particles, cf. Curve II which was recorded in a region lacking bright particles.*

5.4 PtRu Preparation

The preparation of PtRu binary catalysts was investigated via a number of different methods. Initial experiments were undertaken to determine whether the $H_3Ru(SO_3)_2OH$ species could be electroreduced onto platinum and supported platinum electrodes, i.e. the preparation of Ru/Pt and Ru/Pt/GC. These multi- and partial-ruthenium monolayers were then characterised electrochemically. Co-electrodeposition of PtRu catalysts onto GC electrodes was then investigated and the resulting metallised electrodes electrochemically analysed. Additionally, the oxidation of methanol solution was also investigated on some catalysts.

The dispersion of Ru atoms across a platinum or supported platinum electrode surface provides a useful model surface, and presumably has nearly identical properties to the surface of a PtRu alloy. The fractional coverage of ruthenium and platinum surface sites is of major importance since it effectively determines the catalytic activity for a given reaction (at a particular catalyst loading and temperature). Some researchers [*Fujiwara et al., 1999; Souza et al., 1997; Gasteiger et al., 1994; 1993*] have co-deposited PtRu or ruthenised platinum electrodes to differing extents to investigate the optimal Ru surface coverage for Pt-CO_{ads} or methanol oxidation reactions. A partially ruthenised surface exhibits similar electrochemistry to a PtRu alloy- i.e. the electrochemical features of both metals are apparent using potentiodynamic techniques.

For the successful co-electrodeposition of PtRu, reduction of both metal ions onto either a Pt, Ru or carbon surface site is essential, so a simple way to determine whether the deposition of a PtRu co-deposit is possible (by using the $H_3Ru(SO_3)_2OH$ species and a Pt species) is to test the success of $H_3Ru(SO_3)_2OH$ electroreduction onto a Pt surface. Moreover, a Pt substrate may aid in the cleaning of the poisoning species on the Ru surface. A 2.0 mm diameter Pt disc electrode (embedded in a CTFE cylinder) was used for the readily reproducible, well-characterised Pt surface.

Fig. 5-15 shows the electroreduction of $H_3Ru(SO_3)_2OH$ onto a Pt electrode, Pt-1, and the subsequent electrochemical analysis of the ruthenised electrode. Curve I shows the first of three linear-sweeps of Pt-1 in $H_3Ru(SO_3)_2OH + H_2SO_4$ solution, between 0.4 and – 0.3 V_{SCE}. The electroreduction onset appears to commence immediately on scanning towards negative potentials, and is ~ 0.2 V higher *cf.* the reduction onset observed for this Ru species on a GC electrode (Figs. 5-1 and 5-2). In the analysis of the Ru/Pt-1 electrode, electrochemical evidence of Ru is observed at potentials greater than ~ 0.2 V (similar to that in Fig. 5-4). The platinum surface appears to be poisoned (as observed in the H_{ads} region), which is expected since it is partially covered by a ruthenium deposit. However, this ruthenium layer was electrochemically unstable (even without scanning to potentials more positive than 0.4 V) and these features are short-lived.

Similar results were found with the ruthenisation of Pt/GC electrodes from $H_3Ru(SO_3)_2OH$ solution. No difference in electrochemical features were observed with higher Ru-loadings, except that higher loadings dominated the electrochemistry of the electrode- a typical example is shown in Fig. 5-16. Again, the ruthenium remained in a poisoned state (unchanged by the platinum substrate). No evidence of platinum surface electrochemistry was observed until all of the Ru had been electrodissolved. This was surprising, since in other work the surface electrochemical features of both Ru and Pt were observed in binary PtRu deposits [*Frelink et al., 1995; Gasteiger et al., 1993*]; surface fractions may even be estimated from CV curves [*Souza et al., 1997*]. For example, Fig. 5-17 illustrates the effect of Ru surface coverage on PtRu catalysts [*Gasteiger et al., 1993*].

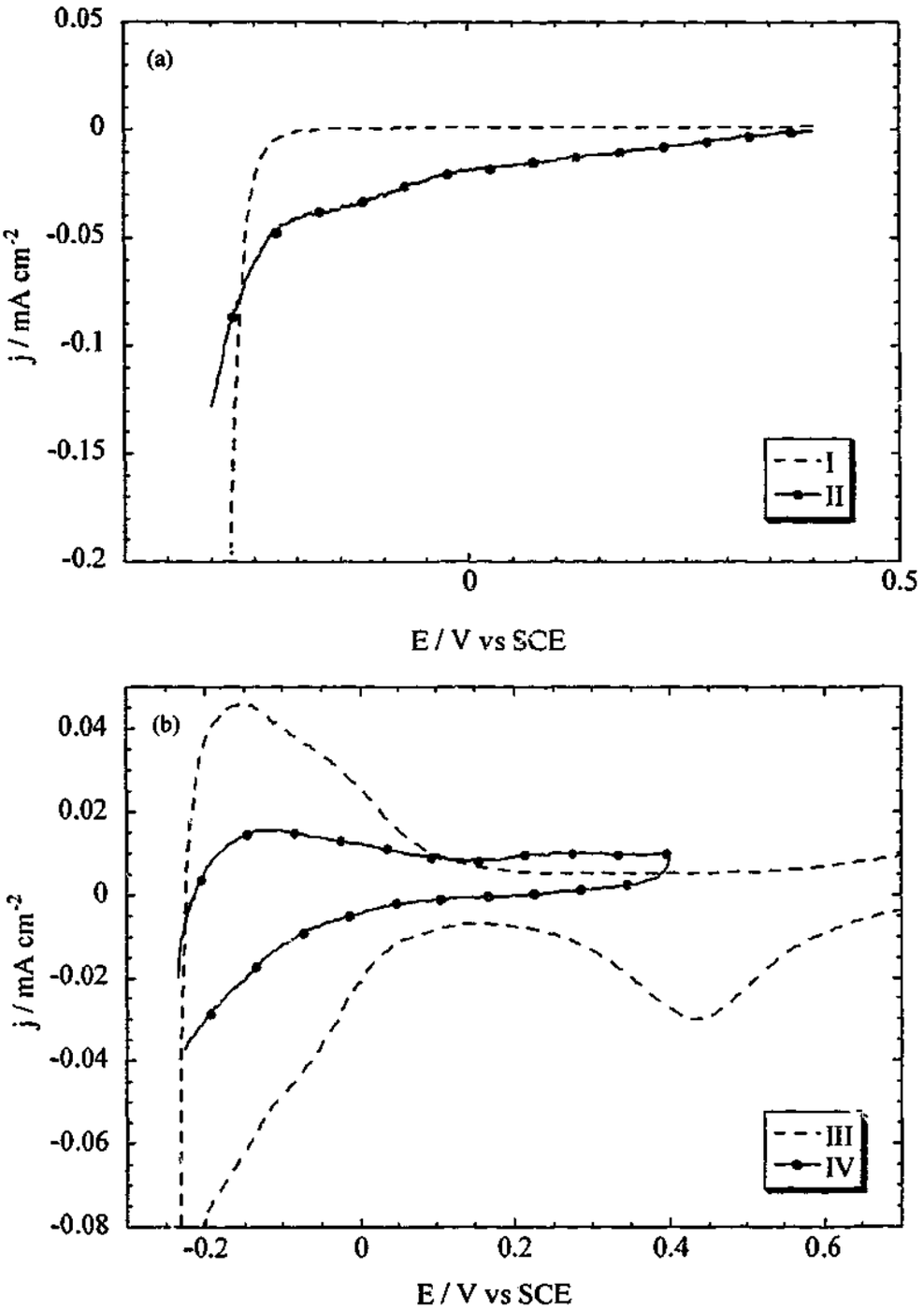

Fig. 5-15 *Ruthenisation of a platinum electrode and analysis. (a) Curve I shows the Pt-1 baseline sweep in 0.5 M H_2SO_4. Curve II shows the linear-sweep electroreduction of ruthenium from a 0.01 M $H_3Ru(SO_3)_2OH$ + 0.5 M H_2SO_4 solution onto Pt-1. Sweep rate: 0.001 V s^{-1}. (b) Curve IV shows a cyclic voltammogram of the resulting Ru/Pt-1 electrode, in comparison to a CV of Pt-1 prior to ruthenisation, Curve III. Scanning rate: 0.05 V s^{-1}.*

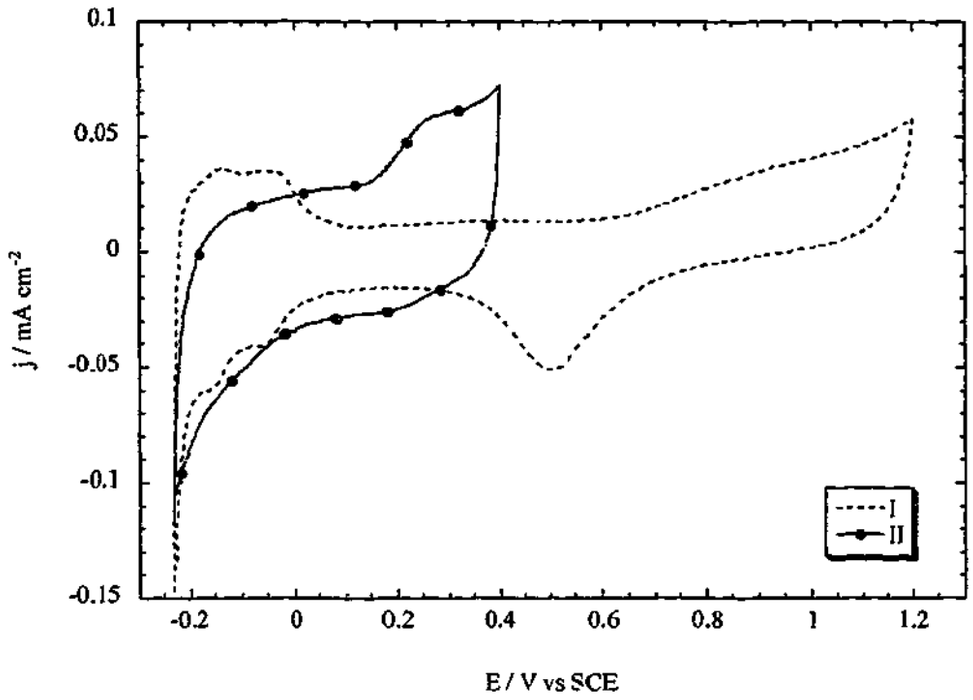

Fig. 5-16 *Cyclic voltammograms of Electrodes Pt/GC-14 and Ru/Pt/GC-14. Curve I is a baseline scan of Pt/GC-14 in 0.5 M H_2SO_4. This electrode was ruthenised in a 0.1 M $H_3Ru(SO_3)_2OH$ + 0.5 M H_2SO_4 solution at – 0.2 V for 600s. Curve II illustrates a CV scan of the resulting electrode (Ru/Pt/GC-14) in 0.5 M H_2SO_4. Scanning rate: 0.05 V s^{-1}.*

The oxidation of methanol was investigated as a rapid way to determine whether the catalyst was in fact 'alloy-like' at the surface. For example, higher current densities and/or a lower overpotential for methanol oxidation should be observed if both Pt and Ru surface sites exist (and are connected on the electrode surface).

In Fig. 5-18, CV scans of Electrode Ru/Pt/GC-14 are shown in sulphuric acid and methanol solution before and after ruthenisation in $H_3Ru(SO_3)_2OH$ solution. The presence of Ru on the Pt/GC-14 surface was not found to enhance methanol electro-oxidation, as is shown by Curve IV. In fact, the onset for methanol oxidation did not change and the oxidation current densities were actually lower *cf.* those in the non-ruthenised electrode (Curve II). The reduction in j_a could possibly be explained by the loss of Pt surface area following ruthenisation (i.e. by Ru coverage). Electrode Ru/Pt/GC-14 was gradually scanned in a methanol + sulphuric acid solution over

the same potential range, until the CV scan shown by Electrode Pt/GC-14 (Curve II) was restored. At no point did the ruthenium appear to be cleaned, and the oxidation of methanol was not enhanced beyond the behaviour shown in Curve II.

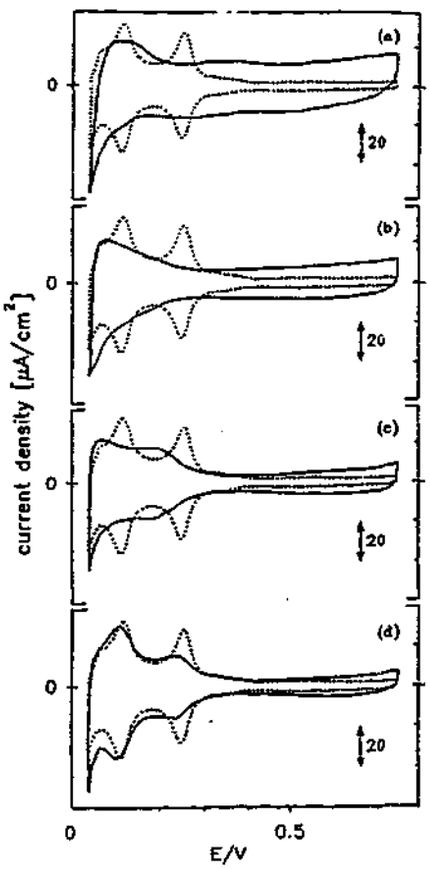

Fig. 5-17 Cyclic voltammograms of sputtered PtRu alloy electrodes (on Pt), by Gasteiger et al. In each of (a) to (d) a background Pt CV scan is shown (broken curve) and a CV scan of a PtRu electrode with a Ru surface coverage of 100, 46, 33 and 7 at%, respectively [Gasteiger et al., 1993]. Scanning rate: 0.05 V s^{-1}.

Essentially, these studies show that the ruthenisation of a platinum-based electrode is reasonably complicated. These experiments were intended to illuminate suitable conditions for use in PtRu co-electrodeposition, and also aid in the electrochemical analysis of the mixed metal surface. In any case, it was shown that $H_3Ru(SO_3)_2OH$ could be electroreduced onto platinum, which is important for the preparation of the binary catalyst system (provided the Ru surface can be successfully cleaned).

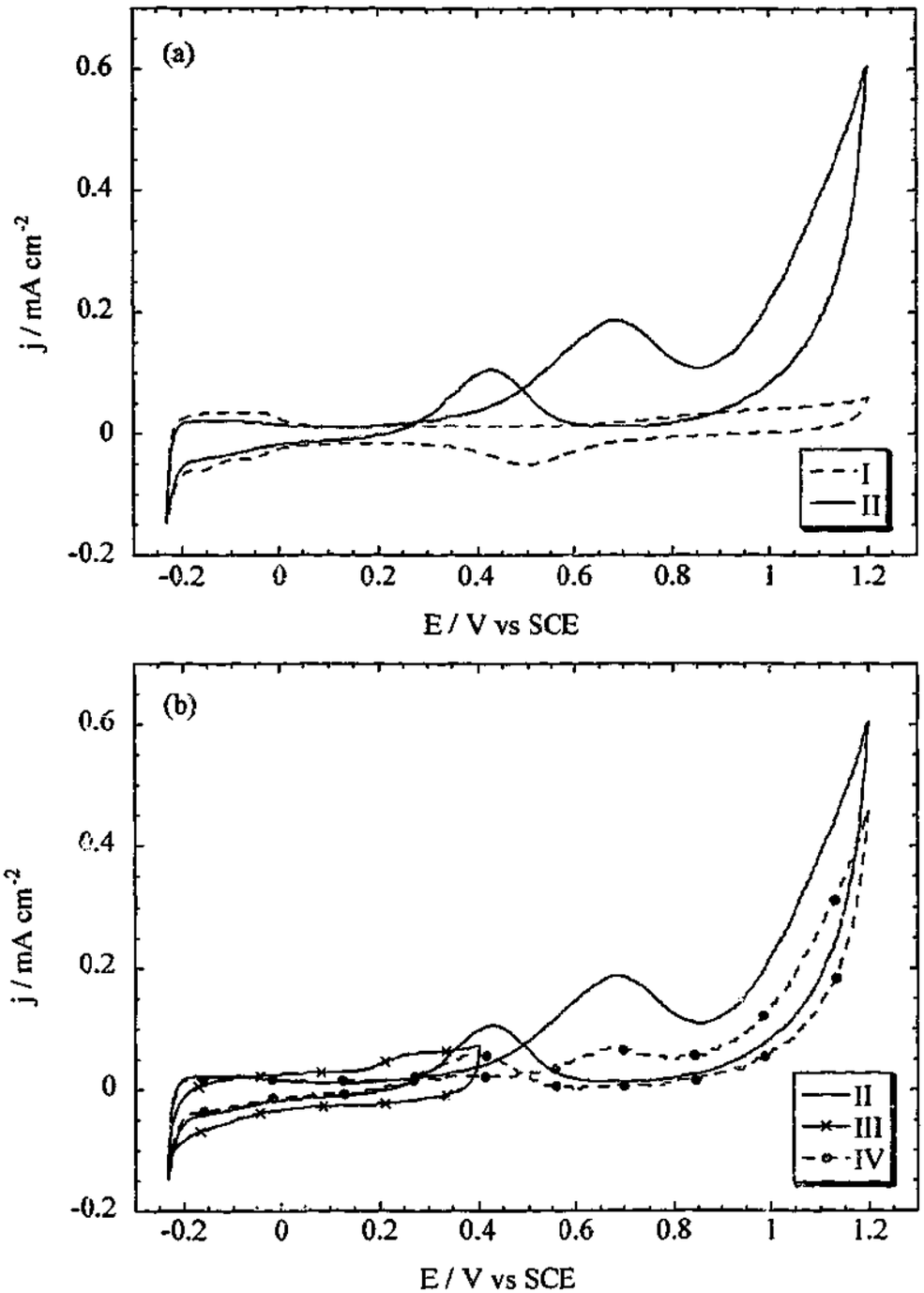

Fig. 5-18 Cyclic voltammograms of Electrodes Pt/GC-14 and Ru/Pt/GC-14 in methanol and acid solutions. (a) Curve I is a baseline scan of Pt/GC-14 in 0.5 M H_2SO_4. Curve II shows a CV scan of the same Pt/GC-14 in a 0.5 M H_2SO_4 + 5.0 M methanol solution. (b) Curve III is a baseline scan of the ruthenised Pt/GC electrode (i.e. Ru/Pt/GC-14) in 0.5 M H_2SO_4. Curve IV shows a CV scan of the same Ru/Pt/GC-14 in a 0.5 M H_2SO_4 + 5.0 M methanol solution. Curve II is shown again for comparison. Scanning rate: 0.05 V s^{-1}.

Theoretically, the co-electrodeposition of the two sulphite species, $H_3Ru(SO_3)_2OH$ and $H_3Pt(SO_3)_2OH$ could produce an ideal catalyst, since this avoids PtRu contamination with chloride species. The co-electrodeposition of these two sulphite species was attempted because the mixture of both metal complexes may affect the electrodeposition behaviour. It was also thought possible that $H_3Pt(SO_3)_2OH$ electroreduction might occur at more positive potentials onto the Ru deposits, since the reduction of platinum onto ruthenium should take place at a lower overpotential *cf.* the GC substrate.

A $H_3Ru(SO_3)_2OH$ and $H_3Pt(SO_3)_2OH$ solution (0.005 M concentrations of each species in 0.5 M H_2SO_4) was electrodeposited onto Electrode GC-15 electrode via three linear-sweeps in the range + 0.4 to – 0.5 V. The CV analysis of the resulting GC-15 appeared very similar to the ruthenised glassy carbon electrodes prepared in Figs 5-4 and 5-7. In addition, on scanning this electrode to higher potentials large oxidation current densities were observed (especially at potentials > 0.6 V), strongly suggesting the dissolution of ruthenium, as was observed in Figs. 5-4 and 5-7. No electrochemical evidence of platinum was found on GC-15, either throughout the potentiodynamic analysis, or following the eventual ruthenium removal (via electro-oxidation). The lack of platinum evidence was surprising, but it is possible that not enough time was allowed at lower potentials (where the electroreduction of $H_3Pt(SO_3)_2OH$ is significant).

5.5 Summary

Ruthenium was successfully electrodeposited from the $H_3Ru(SO_3)_2OH$ species onto both GC and CB-based electrodes. The resulting ruthenium deposits were found to be poisoned, possibly by a sulphide or related species, in a similar fashion to the platinum deposited from $H_3Pt(SO_3)_2OH$ solution. However, it was not possible to remove poisons from the $H_3Ru(SO_3)_2OH$-deposited Ru via the potentiodynamic cycling method used in Chapter Four. Refer to Chapter Seven for more extensive conclusions of this chapter and also possibilities for future studies on related work.

Chapter Six

Catalyst Deposition via Impregnation/Electroreduction

6.1 Chapter Overview

A major problem in PEMFC and DMFC electrodes is the low utilisation of noble metal catalysts (as was outlined in Section 1.3.2.2 of Chapter One). This may result in reduced fuel cell performance (e.g. thicker catalyst layers may be required, which increases the *iR*-drop across the cell). In addition, low catalyst utilisation is certainly not cost effective.

As described in Chapter One, low utilisation of Pt and PtRu catalysts may arise in a couple of ways. If the noble metal catalysts are deposited as large particles onto the carbon-black support, then a high proportion of catalyst atoms will be contained within the particle, and will thus be unable to participate in the fuel cell reactions (which occur at the catalyst surface). Ideally, these expensive catalysts will have a maximised specific surface area, *S* (i.e. a high surface-area per mass of catalyst particle). Low catalyst utilisation may also result from the positioning of catalyst particles throughout the catalyst layer. It is essential for the catalyst particles to be located in the 'three-phase reaction zones' (or 3PRZs) for the catalyst surface to be utilised. Chapter One offers a more thorough explanation of fuel cell catalysis.

Catalyst electroreduction has been investigated by a number of researchers and shown to be promising for the fabrication of fuel cell electrodes (Section 1.3.3.4 of Chapter One). The H_2PtCl_6 and $RuCl_3$ species have been studied the most extensively. In some cases, the unique chemistry of the within Nafion-bound catalyst layers has been utilised to preferentially deposit catalyst particles in 3PRZ regions, such as in work by Taylor *et al.* [*Taylor et al., 1992*]. The size of the electrodeposited particle however, is another issue, and alternative approaches may be required.

In Chapter Four, a catalyst deposition technique was investigated which showed the potential to limit the growth of platinum particles during electroreduction. It was called the 'poisoning' method, since the deposited platinum surface appeared to be covered by a strongly adsorbing species, or poison, during the electroreduction of

$H_3Pt(SO_3)_2OH$. Very few electrochemical features of the resulting Pt/GC and Pt/CB electrodes prepared in this manner correlated with those of typical Pt electrodes. The Pt particles were eventually cleaned via extensive electrochemical cycling, oxidatively removing the impurities. This poisoning method was then trialled on a similar ruthenium species, $H_3Ru(SO_3)_2OH$, but without any conclusive success (Chapter Five).

In this Chapter, the catalysation of fuel cell electrodes was approached from a different perspective. Catalyst utilisation should be greatly enhanced if small Pt (and PtRu) particles are deposited only in the 3PRZ regions. A couple of methods were investigated to achieve this. Catalyst was impregnated into 'fuel cell type' electrodes by mixing a platinum salt into the catalyst layer ink (Section 6-2), and also via an ion-exchange of platinum cations into the Nafion within the catalyst layer (Section 6.3).

6.2 The Impregnation and *In Situ* Electroreduction (IISE) Method

6.2.1 Introduction

The "Impregnation and *In Situ* Electroreduction" (IISE) method was developed in an attempt to maximise the proportion of catalyst contained within the 3PRZ regions of fuel cell electrodes. The 'impregnation' step involved mixing a known amount of catalyst solution into the catalyst layer ink before application to the electrode. The catalyst ions are then expected to be contained within the hydrophilic Nafion 'inverse micelles' (see Fig. 1-6 in Chapter One) in the catalyst layer. The electroreduction of these catalyst ions was then carried out *in situ* in the Fuel Cell Test Station (refer to Chapter Three). The objective was to use Nafion as the only electrolyte (i.e. the Nafion contained within both electrodes and also the separating Nafion membrane). In this way, electroreduction of catalyst ions is expected only at

carbon surfaces with $-SO_3H$ group access (the ionic pathway is required in order to conserve charge, i.e. to complete the electrochemical circuit). The carbon particles would also have to be electrically connected to the electrode in order for catalyst electroreduction to occur.

This IISE method is expected to be superior to catalyst electroreduction in a platinum-impregnated electrode immersed into e.g. H_2SO_4 solution, since it is possible for platinum ions to be electrodeposited onto carbon surfaces without Nafion contact (the charge being conserved by the liquid electrolyte). This could occur if sufficient time is allowed in the H_2SO_4 solution before reduction, enabling the diffusion of platinum ions out of the Nafion micelles.

6.2.2 Preliminary Experiments and Conditions

Initially, the deposition of platinum from H_2PtCl_6 solution was investigated using the IISE method. A CB-based electrode, CB-5, was prepared with a Nafion[i]:Vulcan ratio of 1:8.5. The Nafion/Vulcan catalyst layer also contained ~ 38 wt% H_2PtCl_6, to approximate a commonly used supported platinum loading of 20 wt% Pt/Vulcan. The catalyst layer ink was applied to the electrode and dried until 0.5 mg cm^{-2} of the H_2PtCl_6-containing catalyst layer had been applied (i.e. an equivalent loading of ~ 90 μg cm^{-2} platinum metal).

The membrane-electrode assembly (MEA) was prepared next. The working electrode (WE, i.e. CB-5 containing the H_2PtCl_6), was placed on one side of a cleaned Nafion 117 membrane, and a counter electrode (CE) was placed on the opposite side. The CE was prepared as a conventional fuel cell electrode, using ~ 0.5 mg cm^{-2} Pt catalyst (using a 20 wt% Pt/Vulcan commercial catalyst, from E-TEK, Inc.) mixed with 9 wt% Nafion ionomer; this ink was applied to the Toray carbon-paper base of

[i] The Nafion amount is always given in 'dry mass' (using the 5 wt% Nafion ionomer solution- refer to Chapter Three).

the electrode. Refer to Chapter Three for a more detailed description of fuel cell electrode preparation.

The platinised nature of the CE was important for two main reasons. This electrode was used as a reference electrode (RE) in addition to a CE, since achieving adequate electrolyte contact with a typical reference electrode such as the SCE is not ensured with the thin (125 μm) solid, Nafion membrane electrolyte. The other reason for utilising a conventional PEMFC electrode as the CE (and RE) was to enable calculation of the platinum surface-area in CB-5 (the WE) during subsequent potentiodynamic analysis. The available platinum surface-area under PEMFC conditions (i.e. using the Nafion electrolyte throughout the catalyst layer and MEA) is effectively the most useful measure of catalyst utilisation.

The MEA was next sandwiched between the graphite flow field blocks in the Test Station (e.g. similar to Fig. 1-3 in Chapter One), foregoing the normal hot-pressing of the two electrodes to the membrane. The hot-pressing stage was avoided to prevent any possible decomposition of the $PtCl_6^{2-}$ species at higher temperatures. Kinoshita and Stonehart [*Kinoshita and Stonehart, 1977*] describe a commonly used 'impregnation technique' to prepare supported catalysts, which involved soaking a carbon support in a platinum solution followed by heating at 260°C in air for 3 hours to decompose the platinum ions, forming metallic Pt on the carbon surface. Although it seems unlikely for $PtCl_6^{2-}$ decomposition to occur under the usual hot-pressing conditions (temperatures of up to 125°C, applied for ~ 2 min), this stage was nevertheless avoided. The strong clamping of the MEA inside the Fuel Cell Test Station was expected to enable sufficient electrolytic contact between the catalyst layer and the Nafion 117 membrane.

Humidified nitrogen and hydrogen were supplied to the WE (Electrode CB-5) and the CE/RE, respectively, for 15 min to allow Nafion hydration (to ensure ionic transport through the membrane and both electrodes all three components must be hydrated). Longer humidification times were avoided since this may allow time for diffusion of platinum ions from CB-5 into the Nafion 117 membrane (due to the high

concentration gradient of platinum ions). A potential of – 2.0 V (versus the CE/RE) was applied for 60 s to the CB-5 WE via a potentiostat. The potential of the CE/RE was expected to be at that for the standard hydrogen electrode (SHE), since at this electrode H_2 was supplied under ambient conditions and the platinised electrode is present in a strong acidic electrolyte. Hence a potential of *ca.* – 2.2 V_{SCE} (0.0 V_{SHE} equates to *ca.* – 0.24 V_{SCE}) was applied to the WE to facilitate platinum electroreduction. This low potential was used with the intention to rapidly electrodeposit the $PtCl_6^{2-}$ species without allowing time for diffusion of any $PtCl_6^{2-}$ ions to more 'favourable' reduction sites (e.g. deposited platinum particles).

In the subsequent analysis of the WE (CB-5), no voltage-current performance was observed in the Fuel Cell Test Station. CB-5 was used as the anode with humidified H_2 reactant, and the CE/RE as the cathode with humidified O_2 (flow rates were approximately 100 mL min^{-1}). It was not possible to draw any current from the cell. This indicates that the cell was not actually operating, i.e. no H^+ or electron flow occurred. The cell was probably limited either through poor ionic conductivity or lack of reactions occurring at the electrodes.

Following the fuel cell performance test using CB-5 as the anode, a potentiodynamic analysis was performed on the electrode in the Test Station. Again, similar to in the electroreduction step, humidified N_2 was passed through the CB-5 WE compartment, both to hydrate the Nafion and to degas the electrode (mainly to purge oxygen from the electrode). The CE/RE was maintained under a stream of humidified H_2. Gas flow rates were again ~ 100 mL min^{-1}. *In situ* CV scans were at first scanned over the normal range, e.g. between 0.0 and 1.2 $V_{CE/RE}$ (i.e. using a voltage scale with respect to the Pt/C CE/RE under H_2 flow, which approximates to V_{SHE}), but no electrochemical evidence of platinum was observed. The initial potential, E_i, was moved to progressively more negative values, until Curve I in Fig. 6-1 was obtained. Curve I shows the initial CV scan from an E_i of – 1.5 $V_{CE/RE}$, and displays possible signs of O_2 evolution at high potentials, possible H_2 evolution at low potentials and a cathodic shoulder at *ca.* – 0.5 $V_{CE/RE}$. Curves II and III in

Fig. 6-1 are the 5th and 6th scans following Curve I, and show a slight oxidation peak arising at *ca.* –1.4 $V_{CE/RE}$.

At an E_i of – 1.5 V_{SHE} a clean, platinised electrode will evolve considerable amounts of H_2 in acidic media (and accordingly, strong cathodic current densities, j_c, are observed around the E_i in Fig. 6-1). In a positive-potential scan at this scanning rate (0.1 V s^{-1}), an E_i of even say – 0.01 V_{SHE} will produce significant anodic current densities for the oxidation of evolved H_2 at the Pt surface. This might explain the slight oxidation peak (or step) observed at ~ –1.4 $V_{CE/RE}$ in Curves II and III, however at such an extreme low potential much stronger current densities would be expected. This peak appears to be overwhelmed by cathodic current densities, possibly from continued $PtCl_6^{2-}$ reduction or the reduction of other species, e.g. O_2.

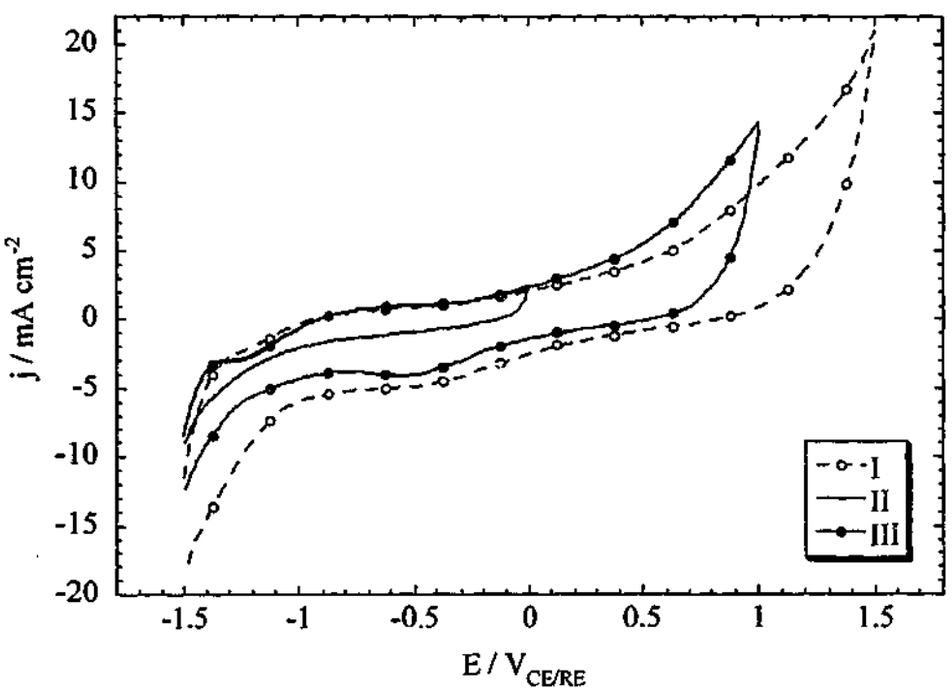

Fig. 6-1 *Potentiodynamic analysis of the IISE-platinised electrode, CB-5. In situ CV scans were performed in the Fuel Cell Test Station, using the pre-platinised cathode as the CE and RE. Curve I is the first scan over this range, Curve II the fifth and Curve III the sixth. The voltage scale used in this figure is with respect to the CE/RE (see text). Scanning rate: 0.1 V* s^{-1}.

The cathodic shoulder occurring at ~ – 0.5 $V_{CE/RE}$ (or V_{SHE}) in Curves I and III of Fig. 6-1 appears similar to the electroreduction of PtO_2. The j_c for PtO_2 reduction are observed most significantly between 0.9 and 0.5 V_{SHE} on a typical Pt electrode, however, in Curves I and III of Fig. 6-1, the cathodic shoulder occurs at much lower potentials, between *ca.* – 0.3 and – 0.7 $V_{CE/RE}$. Another interesting observation is the lack of such a shoulder in Curve II. Curve II is not scanned to as high an upper potential *cf.* Curves I and III and the missing cathodic shoulder is probably best explained by the formation of very little PtO_2 during the positive-potential sweep (and thus the negligible PtO_2 reduction observed in the negative sweep).

At any rate, these observations suggest the presence of metallic platinum deposits in the CB-5 electrode. Further analyses were not performed in the Fuel Cell Test Station due to a number of concerns, including in particular, uncertainty in the exact potential of the CE/RE. Electrochemical 'cleaning' of the electrode is also more likely to be successful in aqueous solution, where any impurities such as Cl^- ions may be easily removed from the CB-5 electrode (into the bulk solution). Another concern was the cause of the cathodic spikes that appeared at low potentials (in the Test Station). Determining whether this j_c was arising from further $PtCl_6^{2-}$ reduction or from O_2 reduction is easiest performed in a well-degassed aqueous solution (without possible interactions from other fuel cell components[ii]).

The CB-5 electrode was then potentiodynamically investigated in 0.5 M H_2SO_4. Since the electrode was not designed for analysis in aqueous solution, part of the 4 cm^2 square-shaped electrode was held between two pieces of Toray carbon-paper which were connected to the potentiostat. The blank Toray pieces were used to provide a 'non-wettable' electrical connection to the electrode (to maintain the whole electrode in solution whilst keeping the potentiostat connection above solution). Curve I in Fig. 6-2 illustrates a CV scan of CB-5 in acid solution.

[ii] Electrochemical analysis of the CB-5 electrode in H_2SO_4 solution was perceived to be simpler than fuel cell testing, where other MEA components may interfere with the fuel cell performance. Typically, in analysing fuel cell MEAs, a several hours of operation is performed whilst monitoring the voltage-current density characteristics before steady state conditions are achieved. 'Cleaning' of the catalysts in the electrodes and equilibration of other electrode components may occur in this initial testing period.

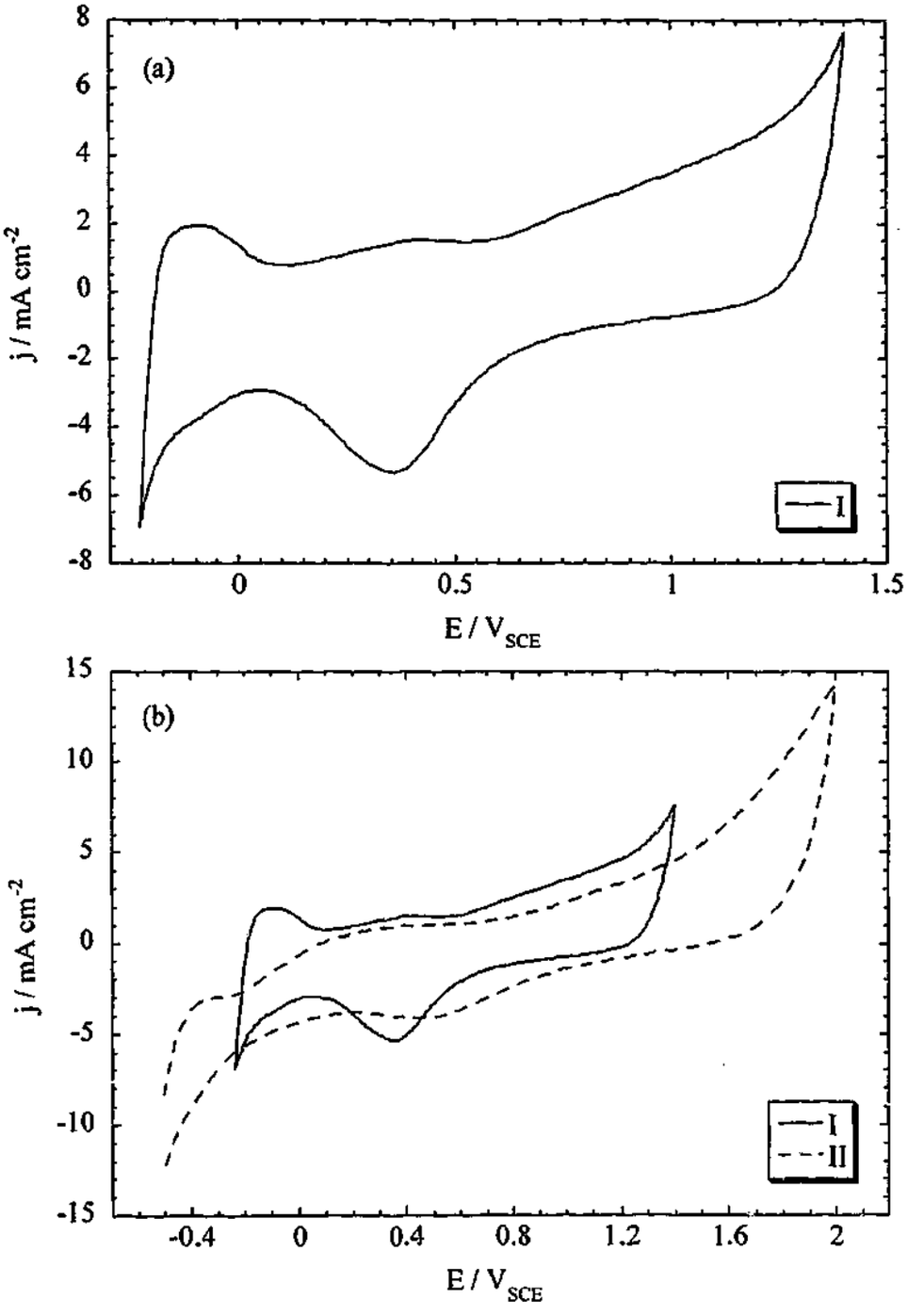

Fig. 6-2 *Potentiodynamic analysis of the IISE-platinised electrode, CB-5. (a) Analysis in 0.5 M H_2SO_4 solution. The CV scan shown by Curve I was performed after ca. 30 similar scans. SCE scale used. (b) Comparison of CV scans in acid solution and in the Fuel Cell Test Station. Curve I is shown again for comparison. Curve II shows an In situ scan performed in the Test Station, using the pre-platinised cathode as the CE and RE (a reproduction of Curve III from Fig. 6-1). The voltage scale of Curve II has been adjusted for clarity of comparison (see text). Scanning rate: 0.1 V s^{-1}.*

Curve II in Fig. 6-2 is a reproduction of Curve III presented already in Fig. 6-1, and is provided for a comparison of CB-5 CV scans in the different electrolytes. The voltage scale shown for this scan was adjusted for easier comparison with Curve I, by increasing the whole voltage scale of Curve II by 1.0 V. The electrochemical features of platinum in Curves I and II appear to be in roughly the same potential regions. The most striking difference between the two curves is the hydrogen adsorption/desorption characteristics.

It was previously considered that perhaps other reactions occurring at the low electroreduction potential in the Test Station (especially the evolution of H_2, and also the reduction of any O_2 left in the porous CB-5) could have dominated at the expense of $PtCl_6^{2-}$ reduction. However, the initial CV scans in H_2SO_4 solution were actually similar to the scan shown by Curve I in Fig. 6-2. The Pt-H_{ads} oxidation peak area increased with further scanning, until Curve I was recorded, at which point the peak area was relatively constant. Apart from this typical cleaning of the platinised electrode, no evidence of additional platinum ion reduction (e.g. strong j_c) was observed in the initial scans in H_2SO_4 solution. This suggests that all the $PtCl_6^{2-}$ ions had been electroreduced whilst in the Test Station. The lack of fuel cell performance and platinum activity observed in the *in situ* CV scans might then be attributed to poisoning of the catalyst with chloride and possibly other species, which could presumably only be removed in the bulk H_2SO_4 solution.

6.2.3 Summary of the IISE Method

The IISE method appears to have been successful as far as performing $PtCl_6^{2-}$ electroreduction *in situ* within the Fuel Cell Test Station. However, the subsequent operation of the IISE-platinised CB-5 electrode in the Test Station proved inconclusive. Some electrochemical evidence of platinum was found on the CB-5 electrode during *in situ* CV scans, and this was later confirmed in potentiodynamic experiments in 0.5 M H_2SO_4.

Due to the complicated nature of this experiment, a number of possibilities were considered to help explain the lack of fuel cell performance. Typical causes of fuel cell failure are poor ionic contact or poor reaction kinetics at the electrodes (either may limit the whole cell). Since CV scans were successfully performed in the Test Station, it may be concluded that H^+ transport between the WE and CE/RE occurred, and thus the Nafion electrolyte throughout the MEA was hydrated (at least to some extent). The CE/RE is unlikely to have been a significantly limiting cell component (excluding typical polarisation losses), especially at the high platinum loading of 0.5 mg cm^{-2}. Hence the most likely explanation for the observed poor fuel cell performance is that the CE-5 anode was not completely operational.

The CB-5 electrode was then either insufficiently platinised, or the platinum within CB-5 was poisoned. The platinum loading of 90 μg cm^{-2} applied to CB-5 (in the catalyst layer ink) is relatively low, however loadings as low as 50 μg cm^{-2} have yielded high performance in PEMFCs [*Appleby, 1995*]. The H_2 oxidation reaction at the anode (where CB-5 was being trialled, following electroreduction) is extremely facile on Pt. The possibility of some $PtCl_6^{2-}$ ions remaining after the electroreduction step was also considered. 60 s at *ca.* – 2.2 V_{SCE} should have been more than sufficient for the electroreduction of this species (*cf.* the strong reduction current densities observed at much higher potentials, e.g. Curve IV in Fig. 5-11). Nor was any evidence of further platinum electroreduction found during the initial CV scans in H_2SO_4 solution[iii].

Therefore, the poisoning of platinum deposits by the by-product chloride ions and other species is the most likely cause of cell failure (and the minimal platinum electrochemical evidence observed during the *in situ* CV scans). During the initial scans in H_2SO_4 solution the platinum in CB-5 was found to be poisoned, but no more than is typical for a platinum electrode in e.g. adsorbing species from a normal laboratory atmosphere. Following 10- 20 CV scans over the potential range used in

[iii] It is also possible that $PtCl_6^{2-}$ ions might have been trapped in regions with poor ionic transport, or possibly even in regions lacking an electronic pathway (e.g. if ions had diffused into the Nafion membrane during the 15 min of MEA humidification). However, the lack of strong j_c to represent further platinum electroreduction in the initial acid solution analyses undermines this possibility.

Fig. 6-2 (a) the Pt-H_{ads} oxidation peak area appeared relatively constant, indicating the platinum surface was free from impurities. The same platinum deposits in CB-5 appear to have remained poisoned throughout the *in situ* experiments and were cleaned much more readily in H_2SO_4 solution.

During the *in situ* CV scans, the lack of any current densities for either Pt-H_{ads} or H_2 oxidation processes suggests that the platinum surface was affected by adsorbed impurities. A Pt electrode is typically 'cleaned' of impurities by cycling between the H_2 and O_2 evolution potentials for at least 10 min, if a rate of 0.1 V s^{-1} is used (i.e. after 20 scans) [*Will, 1965*]; see also Section 2.4 in Chapter Two. No improvement was observed following this procedure during the *in situ* CV scans. Cl^- ions will be present in the CB-5 electrode following $PtCl_6^{2-}$ reduction, and chloride has been shown to strongly adsorb onto the Pt surface, preventing the adsorption of oxygen-containing species at low potentials [*Skou, 1973; Bagotzky et al., 1970*]. This is known as 'chloride blocking', and results in decreased Pt-H_{ads} oxidation. Other species such as sulphide are also known to poison platinum surfaces [*Chin and Howard, 1986; Gerischer, 1975; Loucka, 1971*] and reduce the Pt-H_{ads} oxidation peak area. During the *in situ* experiments, it may have been impossible for complete Pt cleaning without a bulk liquid solution to remove the poisoning ions, particularly given that the poisons are likely to be anions and are expected to be excluded from the Nafion cation-exchange electrolyte.

The surface-area of platinum in Electrode CB-5 was calculated from a CV performed at 0.05 V s^{-1} in the 0.5 M H_2SO_4 solution, the scan recorded *ca.* 30 scans following Curve I in Fig. 6-2 (to ensure platinum surface cleanliness and stability). From the area under the Pt-H_{ads} oxidation peak, a surface-area of 14.5 cm^2 Pt cm^{-2} was found (i.e. 14.5 cm^2 Pt per square centimetre of electrode). A platinum specific surface-area (S) was estimated at 16.1 $m^2 g^{-1}$ Pt, using the platinum loading of ~ 90 μg cm^{-2} in CB-5 (as determined from the amount of H_2PtCl_6-containing catalyst layer ink applied to the electrode). A platinum particle diameter of 17.4 nm was then estimated from the Pt specific surface-area and Eq. 1-16 (Chapter One), assuming homogeneously dispersed, spherical particles. This particle size is not ideal for use

in PEMFC electrodes (values of the order of 1-2 nm are preferred) but nevertheless this illustrates a potential method of electrochemical catalyst deposition. In the following section an alternative electrodeposition method is described.

6.3 The Ion-Exchange and Electroreduction (IEE) Method

6.3.1 Introduction

Due to the complications with the 'IISE' method a new direction was investigated. CB-based electrodes were again 'impregnated' with platinum ions, but the electroreduction of these ions was performed in H_2SO_4 solution. This was expected to enable the rapid deposition of all platinum ions, without the Nafion-electrolyte concerns (i.e. whether the Nafion was sufficiently hydrated). Electroreduction in solution also enabled the use of a known, reliable RE potential (using the saturated calomel electrode, SCE). Furthermore, instead of impregnating $PtCl_6^{2-}$ species and assuming that these will predominantly exist in the hydrophilic electrode regions, a cationic species, $Pt(NH_3)_4^{2+}$, was used which is known to undergo an ion-exchange for the protons in the $-SO_3H$ groups of Nafion [*Delime et al., 1998; Sheppard et al., 1998; Millet et al., 1995; 1989; Liu et al., 1992*].

6.3.2 IEE Concept

The $Pt(NH_3)_4Cl_2$ species dissociates to form the $Pt(NH_3)_4^{2+}$ cationic species in aqueous media which may be ion-exchanged for the sulfonic acid protons in Nafion, Eq. 6-1, as shown by [*Millet and Delime*]. Platinum cations may thus be ion-exchanged into the Nafion electrolyte within a preformed catalyst layer of a CB-based electrode, and subsequently electroreduced onto nearby carbon particles, Eq. 6-2 (where R represents a Nafion polymer segment). In this process, it is

expected that the platinum deposits that form will be available for fuel cell catalysis, as explained below.

$$R\text{-}(SO_3H)_2 + Pt(NH_3)_4^{2+} \rightarrow R\text{-}(SO_3)_2Pt(NH_3)_4 + 2H^+ \qquad (6\text{-}1)$$

$$R\text{-}(SO_3)_2Pt(NH_3)_4 + C + 2e^- + 2H^+ \rightarrow Pt/C + R\text{-}(SO_3H)_2 + 4NH_3 \qquad (6\text{-}2)$$

To satisfy the electroreduction step, the platinum particles deposited in this procedure must be electrically connected through the carbon particle network to the porous carbon (gas diffusion) backing of the electrode. It is believed that any such platinum deposited would be accessible to the Nafion electrolyte from which it was reduced, thus forming the three-phase reaction zones required for fuel cell operation.

A reasonably high concentration of $Pt(NH_3)_4^{2+}$ solution (0.1 M) is used in this procedure, to ensure an equilibrium shift towards significant ion-exchange. An immersion time of 1.0 h is used to ensure maximum ion-exchange. Furthermore, a low voltage (– 1.0 V_{SCE}) is applied to the electrode during the electroreduction (for 60 s) to increase the reduction kinetics and inhibit diffusion of platinum ions through the Nafion to any existing platinum nuclei (i.e. to limit particle growth).

It is also possible to achieve a desired platinum loading using this IE method by repeating the ion-exchange/reduction process any number of times. Once the platinum has been electroreduced in H_2SO_4, the Nafion is returned to its original protonated form and may be ion-exchanged again, as shown by Millet *et al.* [*Millet et al., 1989*].

Providing a small platinum particle size can be maintained, high platinum utilisations should be realised in PEMFC catalyst layers prepared via this method. On achieving higher platinum utilisations, cost reductions in fuel cell stacks may be

envisaged through the use of less platinum, or improved fuel cell performances may result under certain conditions, e.g. by preparing thinner catalyst layers.

This IE method was only studied on CB-based electrodes, since Nafion is required for the ion-exchange and preparing reproducible Nafion coatings on GC electrodes (i.e. with accurate weights and thicknesses) was difficult. $Pt(NH_3)_4Cl_2$ was the only noble metal species investigated for the ion-exchange, but this method is expected to be suitable for any cationic species.

The concentration of Nafion throughout the catalyst layer was varied to investigate the effect this had on the extent of platinisation and also the size of the resulting platinum particles. Additional Nafion ionomer was applied to the catalyst layers to increase the amount of platinum ion-exchanged into the electrodes (i.e. to enhance the overall effect of the method). This additional Nafion was also applied in differing amounts to investigate the effect of Nafion loading on the specific surface area, S (in $m^2\ g^{-1}$) of the resulting platinum deposits. The solvent was again removed from the electrodes.

6.3.3 Comparison of IEE and IISE Methods

The benefits of this 'ion-exchange and electroreduction' (IEE) method appear superior to those of the 'IISE' approach. Neither method can theoretically prevent the diffusion of Pt ions from the catalyst layer into either Nafion or H_2SO_4 electrolytes, since equilibrium dictates the diffusion of platinum ions towards the less-concentrated medium (and the tendency for diffusion will commence once the electrode and electrolyte come into contact). However, the IEE method has a great potential to limit any Pt ion diffusion if the reduction potential, E_{red}, is applied immediately after electrode immersion into H_2SO_4 solution. The liquid electrolyte will rapidly contact all of the hydrophilic Nafion and Pt ion regions after electrode immersion (allowing for the rapid application of the E_{red}), whereas in the case of the IISE method, the Nafion electrolyte in all three MEA components require hydration

in order for any electroreduction to take place. Hence the 15 minutes allowed for humidification in the IISE attempt[iv].

The main advantage of the IISE method (if complications with electrolyte hydration, RE potential and degassing are ignored) is that, in theory Pt ions without -SO_3H group access cannot be electroreduced. Thus all Pt reduced this way should automatically exist in 3PRZ regions. However, this does not necessarily yield high utilisations since large platinum particles may yet form and, furthermore, any platinum existing in regions lacking -SO_3H access will be 'wasted' (and the platinum ion will not be able to migrate). In the IEE method, it is possible that Pt might be ion-exchanged into an -SO_3H ionic group that exists in an isolated portion of Nafion (and having no Nafion ionic contact, this platinum would also be 'wasted' under fuel cell conditions). However, the likelihood of this occurring appears very small: the 10 wt% Nafion is thoroughly mixed throughout the catalyst layer suspension, sufficient to adequately bind the fine carbon-black particles on drying.

More practical advantages of the IEE method include greater flexibility, such as in performing simple electrochemical-analyses (and potentiodynamic cleaning or electrode washing, if necessary) of the platinised CB electrode. Performing further IEE platinisation processes is also more straightforward with the IEE method. In comparison with the IISE method, considerable care is required in dismantling the Test Station and MEA, and even so the catalyst layer may have adhered to the Nafion 117 membrane during experimentation[v]. The IISE-prepared electrode may then be CV-analysed in solution (providing an additional section of electrode exists for potentiostat connection) and any Cl^- ions may be removed via electrochemical

[iv] It might be possible to circumvent this IISE drawback by applying the desired reduction voltage once the MEA is connected and held within the Test Station, during the degassing/humidification of the MEA- refer to the Future Work section (Section 7.4.2 of Chapter Seven). In this way, the E_{red} could be applied for as long as necessary to electroreduce all Pt ions. However, during the degassing/humidification stage a significant proportion of current may be consumed by e.g. O_2 reduction at the WE and, perhaps more worryingly, the reference potential of the CE may alter as the air is gradually replaced with N_2. In the IEE method, degassing (of both the WE and H_2SO_4 solution) is easily performed and the constant reference potential of the SCE is assured.

[v] Of course, if a desired platinum loading was initially applied to the electrode, further platinisation via the IISE-method would not be necessary.

cycling[vi]. CV-analysis may be performed in the Test Station, but the electrochemistry of the WE may be obscured by low performance of other fuel cell components (e.g. poor gas diffusion into electrodes, Nafion hydration, temperature, CE/RE operation and potential, etc.).

6.3.4 IEE-Platinised Electrodes

The initial objective was to verify the operation of the IEE method (refer to Section 6.3.2 for detailed theory and conditions). Assuming that all platinum cations are exchanged into the $-SO_3H$ groups, and the electroreduction step is sufficiently rapid (to prevent significant Pt diffusion), small particles of platinum are expected to be deposited. Depending on the desired platinum surface-area, further IEE platinisation processes may be performed to increase the platinum loading on the electrode (as outlined in Section 6.3.2). The success and viability of such additional platinisations is another feature of the IEE method to be investigated.

The process of platinum ion-exchange into fuel cell electrodes is expected to be affected by the amount of Nafion electrolyte within the electrodes. If the $Pt(NH_3)_4Cl_2$ solution concentration is maintained constant, more platinum cations are expected to be ion-exchanged into the Nafion sulphonic acid groups (in an electrode) if a high loading of Nafion is used. This may be one method of controlling the extent of $Pt(NH_3)_4^{2+}$ impregnation into the fuel cell electrodes. Moreover, it should be possible to illustrate the operation of the IEE method by platinising electrodes of varying Nafion loading.

Hence the effect of the Nafion electrolyte on the IEE process was studied. Three electrodes were prepared with high catalyst layer loadings (applying an additional milligram of the 10 wt% Nafion/Vulcan ink, not containing platinum) *cf.*

[vi] It may be feasible to soak the Nafion 117 membrane in, for example, 0.5 M H_2SO_4 and then water to help remove other ions (including Cl^-) without dismantling the delicate MEA.

conventional fuel cell electrodes, to allow a greater extent of $Pt(NH_3)_4^{2+}$ ion-exchange and thus higher Pt loadings, to enable easier characterisation of the Pt CV features. Additional Nafion ionomer solution was also applied to each of the electrodes, in differing amounts, Table 6-1. The total amount of Nafion is expected to effectively determine the quantity of exchanged Pt^{2+} ions, and consequently the resulting platinum loading on the electrode. The concentration of Nafion (in wt%) in each electrode is also given in Table 6-1.

Characteristic	*CB-6*	*CB-7*	*CB-8*
Geometric Area (cm^2)	4.8	4.8	4.8
Catalyst Layer (mg cm^{-2})*	3.2	3.2	3.2
Total Nafion (mg cm^{-2})	0.50	0.71	1.17
Total Nafion (wt%)	15	20	29

Table 6-1 *Characteristics of Electrodes CB-6, CB-7 and CB-8 prior to platinisation via the IEE method.*
**Loading excluding the mass of platinum.*

The cyclic voltammograms in Fig. 6-3 illustrate the platinum electrodeposited after one IEE process. These CVs were recorded after *ca.* 25 cycles over a similar range. For clarity, only Electrodes CB-6 and CB-7 are shown in Fig. 6-3. A larger double-layer capacitance is observed for Electrode CB-7, due to the higher Nafion loading in this electrode (and possibly also from a greater mass of platinum deposited).

Negligible hydrogen adsorption/oxidation behaviour was observed when sweeping the potential of the IEE-platinised Electrodes CB-6, CB-7 and CB-8 from – 0.232 V_{SCE} to more positive values (the current from these reactions is most likely to have been obscured by the large double-layer charging in each electrode). Therefore, to illustrate the presence of platinum in the electrodes, the cyclic voltammograms were scanned from – 0.25 V_{SCE}. The anodic peaks at *ca.* – 0.15 V_{SCE}

are not seen in the electrode baseline scans before platinisation, and have most probably resulted from the oxidation of molecular hydrogen (formed at –0.242 V_{SCE} and below) on the platinum nuclei. The strong current densities observed at the potential extremities in Fig. 6-3 (presumably representing the evolution of H_2 and O_2) also suggest the presence of Pt in the electrodes, as does the slight peak at ~ 0.2 V_{SCE}, possibly indicating the reduction of PtO_2.

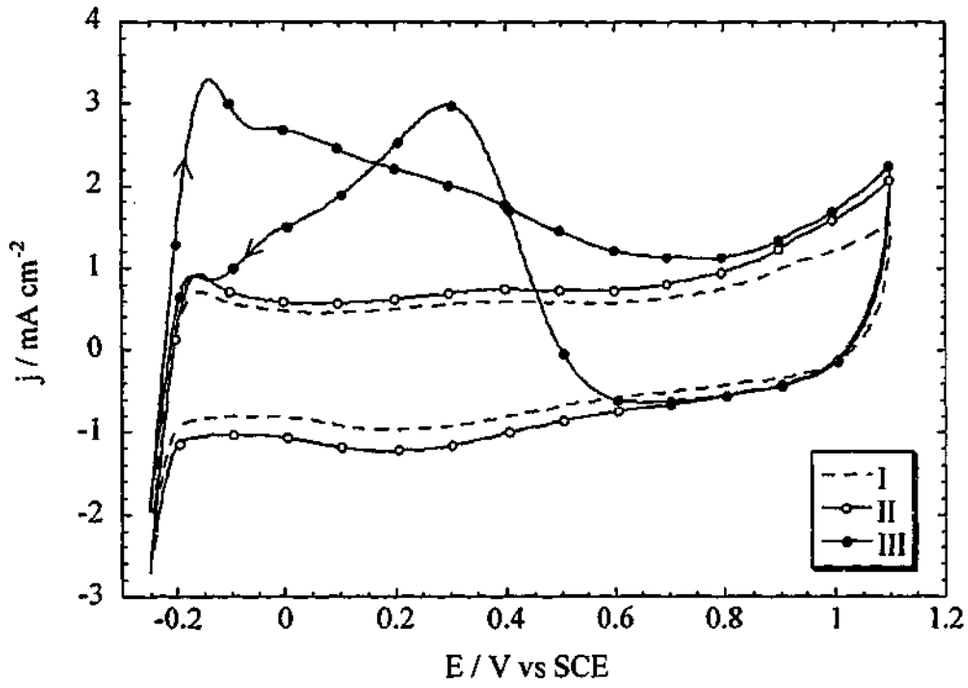

Fig. 6-3 *Potentiodynamic analysis of electrodes CB-6 and CB-7 in 0.5 M H_2SO_4 following one IEE platinisation process. Curve I shows a CV scan of CB-6, Curves II and III are scans of CB-7. Hydrogen was bubbled under Electrode CB-7 before and throughout the CV shown by Curve III. The initial potential, E_i, used for all scans was – 0.25 V. Scanning rate: 0.05 V s^{-1}.*

As further evidence to support the platinum content of the electrodes, CB-7 was scanned over the same range in the 0.5 M H_2SO_4 solution with hydrogen gas bubbling under the electrode surface (Curve III in Fig. 6-3, performed after Curve II). The hydrogen was bubbled at a high rate of ~ 100 mL min^{-1} and a great proportion was probably not oxidised (e.g. by passing around the electrode) however, from a qualitative viewpoint the electrode may be observed to readily

catalyse the oxidation of H_2. Strong anodic current densities, j_a, for H_2 oxidation are observed initially, as CB-7 is scanned from – 0.25 V. At potentials greater than ~ 0.6 V_{SCE} the additional j_a (i.e. *cf.* Curve II) becomes negligible, most likely due to the formation of PtO_2 on the platinum surface at around 0.6 V_{SCE} and higher potentials (*cf.* Fig. 2-3 in Chapter Two). On the reverse sweep (towards lower potentials) H_2 oxidation commences again below 0.6 V_{SCE}, concomitant with PtO_2 reduction. This last observation provides further evidence for the presence of platinum in Electrode CB-7, and the ill-defined cathodic peaks at *ca.* 0.2 V_{SCE} in Curves I and II of Fig. 6-3 are therefore indeed believed to represent the electroreduction of surface PtO_2 species. The gradual decrease in j_a in both the forward and reverse sweeps (below 0.6 V_{SCE}) following the initial H_2 oxidation peak is most probably explained by diffusion limitations of the H_2 transport into the electrode.

Since very little platinum appeared to be deposited in one IEE process (judging from the negligible Pt surface-area obtained[vii]) further IEE-platinisations of the CB-6, CB-7 and CB-8 electrodes were performed. Fig. 6-4 illustrates a series of IEE-platinisations of Electrode CB-6. Curve II shows a CV of Pt/CB-6 after the second IEE-platinisation, in which little change in the Pt-H_{ads} region is observed. The electrode electrochemistry appears to remain dominated by the large j_{dl} of the carbon-based electrode.

The Pt/CB-6 electrode appears more platinised following 5 IEE processes (Curve III of Fig. 6-4). The Pt-H_{ads} oxidation peak increased with the additional platinisation stages, as was expected. The surface-area is expected to increase at low levels of platinisation as small particles grow and more particles are formed. It is not until higher platinum loadings that particles reach a size where a substantial number of Pt atoms are contained within the particle with respect to those on the surface (and Pt utilisation decreases).

[vii] I.e. estimated from the area under the Pt-H_{ads} oxidation peak, which is directly related to the Pt surface-area when scanned from an E_i of – 0.232 V_{SCE}.

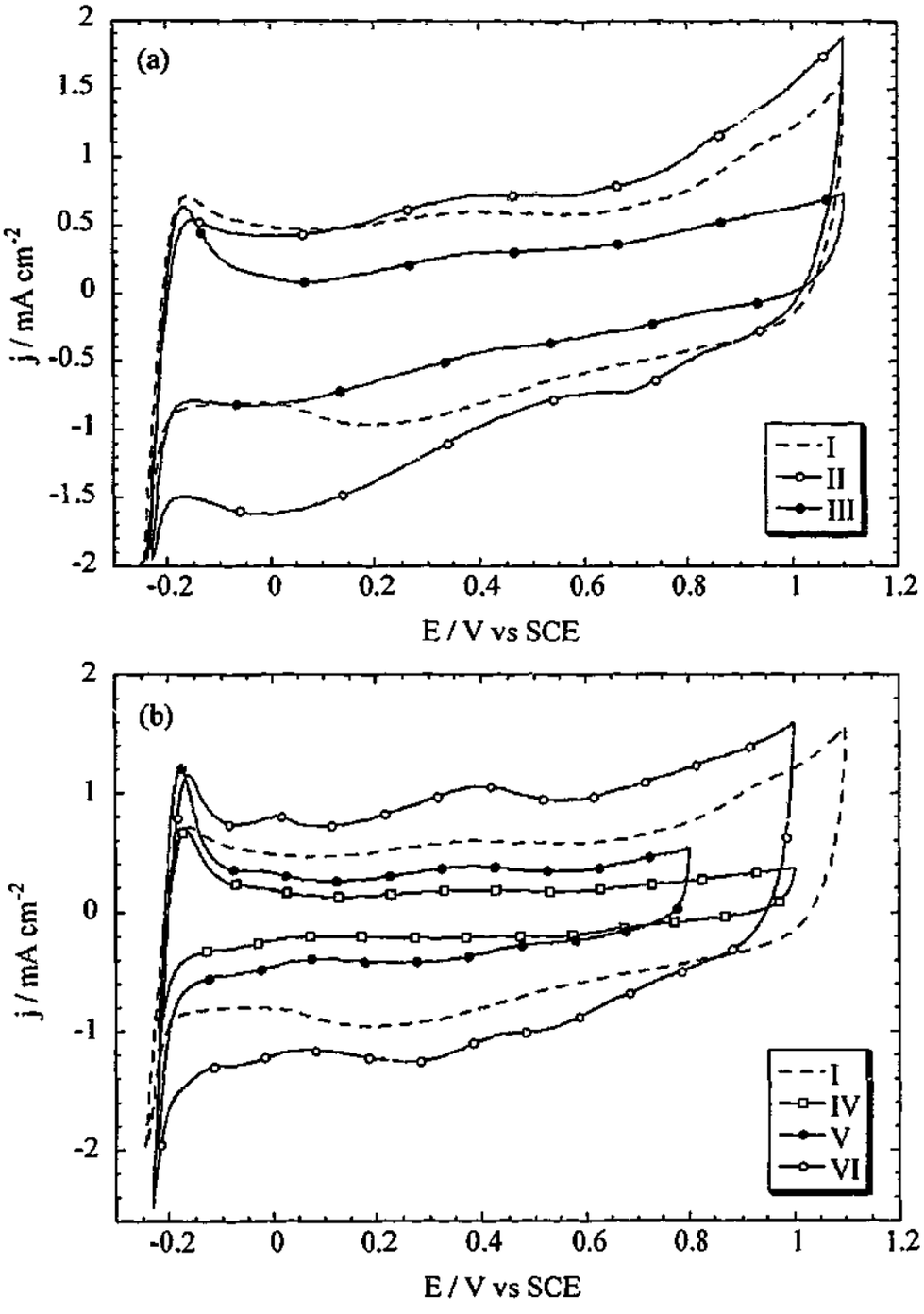

Fig. 6-4 *Potentiodynamic analyses of Electrode Pt/CB-6 following a series of IEE platinisation processes. Curves I to V represent CV scans of the Pt/CB-6 electrode following 1, 2, 5, 10 and 20 IEE platinisation processes, respectively. Curves VI shows a scan of the same electrode following 20 IEE processes and further electrochemical cycling (i.e. recorded after ~ 60 scans following Curve V). Note that the initial potential, E_i, in Curves I to III was – 0.25 V_{SCE} and the E_i in Curves IV to VI was – 0.232 V_{SCE}. Scanning rate: 0.05 V s^{-1}.*

Curves I to III of Fig. 6-4 were scanned from an initial potential of – 0.25 V_{SCE} to qualitatively illustrate the increase in platinum surface-area with more IEE processes. Very little electrochemical evidence of platinum was observed when scanning from – 0.232 V_{SCE}, even following 5 platinisation stages (Curve III), so the lower E_i was used. The large double-layer charging of the electrodes at these low Pt loadings is believed to have obscured the platinum features, as has been observed in other high surface-area fuel cell electrodes containing low Pt loadings [*Gloaguen et al., 1997*]. Increased Pt surface-area is expected to produce a greater peak area for the combined oxidation of both H_2 and Pt-H_{ads} (since a greater amount of H_2 will be evolved on a larger Pt surface).

Curves IV and V of Fig. 6-4 represent scans of the Pt/CB-6 electrode following 10 and 20 IEE-platinisation processes, respectively. These were scanned from a higher E_i of – 0.232 V_{SCE} (*cf.* the – 0.25 V_{SCE} used in Curves I to III) and show significant Pt-H_{ads} regions with respect to the electrode j_{dl}. No H_2 oxidation current densities are involved in these peaks[viii]. At platinisation levels above ~ 5 IEE processes, scans commencing from – 0.25 V_{SCE} were found to produce very large j_a (the oxidation peak predominantly consisting of H_2 oxidation). Fig. 6-5 illustrates this effect for all three IEE-platinised electrodes, with comparisons of the j_a peak area following 5 and 10 IEE processes (all scans commenced from an E_i of – 0.25 V_{SCE}). The basic trend of increasing j_a peak area with a greater number of IEE processes still holds true even from this low initial potential, regardless of the additional oxidation current densities generated. Hence, the level of platinisation of the electrodes (as roughly judged by the surface-area) appears to have increased with each additional IEE processes. In addition, Fig. 6-5 illustrates the improvement in definition of the Pt-H_{ads} region, with the peak representing the oxidation of the more strongly adsorbed protons, at *ca.* 0.0 V_{SCE}, developing superior definition with higher levels of platinisation (from 5 to 10 platinisation processes).

[viii] It should be noted that some of the results presented in a paper related to this work [S.D. Thompson, L.R. Jordan, M. Forsyth, *Electrochim. Acta.* **46** (2001) 1657-1663; Appendix A] incorrectly calculated Pt surface-areas from CV scans using an E_i of – 0.25 V. The possibility of conflicting anodic current densities for the oxidation of evolved H_2 (following scans to potentials more negative than – 0.24 V_{SCE}) was not initially expected. The basic trends reported remain the same.

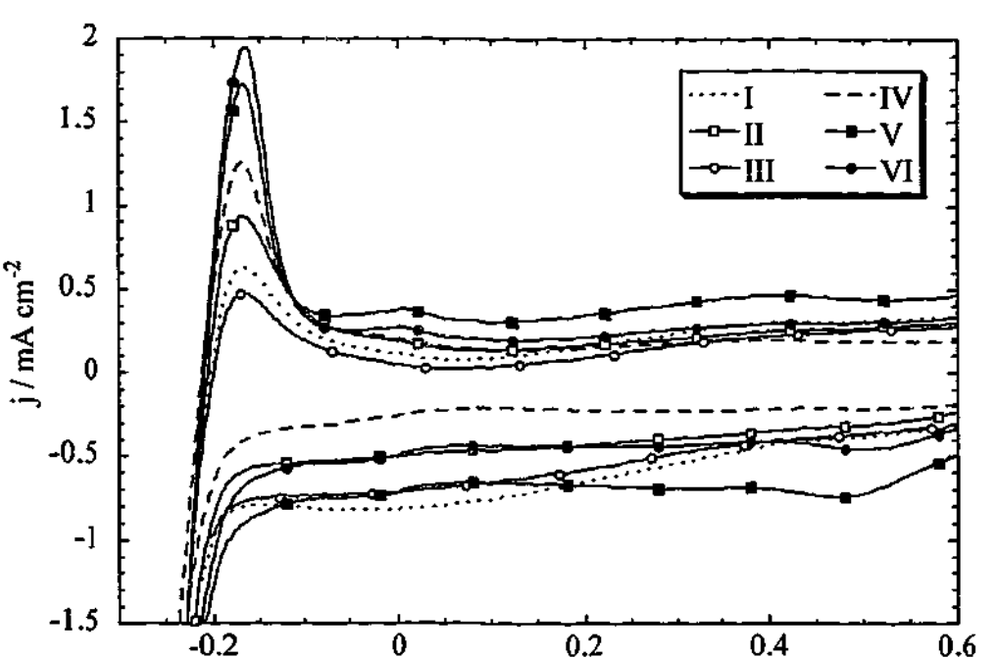

***Fig. 6-5** Potentiodynamic analyses of Electrodes Pt/CB-6, Pt/CB-7 and Pt/CB-8 following 5 and 10 IEE platinisation processes. Scans commenced from – 0.25 V. Curves I, II and III represent CV scans of the Pt/CB-6, Pt/CB-7 and Pt/CB-8 electrodes following 5 IEE processes; Curves IV, V and VI of the same electrodes after 10 IEE processes. Only a segment of the CV scans are illustrated to enhance the clarity in the Pt-H_{ads} region, however these were scanned over the typical voltage range, such as used in Fig. 6-4. Scanning rate: 0.05 V s^{-1}.*

There appears to be a slight decrease in the area of the Pt-H_{ads} oxidation peaks between Curves V and VI of Fig. 6-4 (both at 20 IEE processes). Curve VI displays more defined features *cf.* Curve V, especially in the Pt-H_{ads} region. Additionally, a cathodic peak at ~ 0.5 V_{SCE} may be observed in Curve VI, which most probably results from PtO_2 reduction (there is slight evidence for this in Curve V). The larger peaks (anodic at ~ 0.4 V_{SCE}, cathodic at ~ 0.3 V_{SCE}) in both curves most likely represent the formation and reduction of surface oxide functionalities on the carbon-black surface. The potential ranges for these carbon surface oxidation/reduction peaks are in agreement with those reported by Gloaguen *et al.* using electrodes containing the same carbon-black (Vulcan XC-72R). By the time Curve VI was performed, the Pt/CB-6 electrode would have experienced a considerable amount of potentiodynamic scanning, gradually increasing the number of e.g. carboxylic and phenol-type surface groups [*Kinoshita, 1988*].

Interestingly, the double layer charging of Pt/CB-6 appears to have decreased between Curves I and III in Fig. 6-4. The j_{al} decreases further between Curves III and IV, before increasing by Curve V and again by Curve VI. This fluctuation might be explained by insufficient wetting of the electrode (and therefore less electrode surface-area for the H_2SO_4 solution to contact, i.e. less charging capacitance). Alternatively, the continued wetting and drying of the electrodes may lead to internal rupturing of the catalyst layers (e.g. from the expansion/contraction of the hygroscopic Nafion electrolyte). Similar Nafion-bound carbon-black electrodes prepared by Wilson and Gottesfeld [*Wilson and Gottesfeld, 1992, in J. Appl. Electrochem.*] were found to swell when used as the cathode in a PEMFC, presumably as water was produced in the O_2 reduction reaction, causing discontinuities in the electronic and ionic pathways. The layers used by Wilson and Gottesfeld contained *ca.* 25 wt% Nafion (*cf.* 15 to 29 wt% used in this IEE method). However, the production of water within the catalyst layer is different to the absorption of water from immersing the catalyst layer in aqueous solution (and the former may cause greater localised swelling, so rupturing may have been a more significant issue in their work[ix]). With regards to the possible catalyst layer rupturing in this IEE work, if this was indeed the case, parts of the electrode may lose electronic contact, and be held together by the Nafion binding electrolyte. However, once an electrode is placed in the Test Station, significant pressure is applied to seal the reactant compartments against the electrodes, and under compaction all the platinum within the catalyst layer may be electrically accessible. At any rate, in Curves I to VI of Fig. 6-4, the features representing platinum surface electrochemical processes may be observed to gain definition following more IEE processes, regardless of the j_{al} of the electrode.

[ix] Another preparation [*Wilson and Gottesfeld, 1992, in J. Appl. Electrochem.*] involved the melt-processing of Nafion-bound catalyst layers to the Nafion membrane prior to PEMFC tests. Elevated temperatures were used (e.g. 125-135 °C) and in later work the Nafion components were changed from the H^+ form to a Na^+ or tetrabutylammonium [*Wilson et al., 1995*] form, to withstand temperatures of up to 210 °C. The melt-processed catalyst layers with Nafion in the H^+ form were found to experience enhanced long term performance in the PEMFC Test Stations, but as a consequence of the higher temperature processing the number of sulphonic acid groups in Nafion were reduced from acid-catalysed degradation. Improved interfacial ionic bonding [*Wilson and Gottesfeld, 1992, in J. Electrochem. Soc.*] was thought to have been achieved in the MEAs utilising the alternative Nafion forms. Such adaptions should be possible with the IEE method (although the loss of sulphonic acid groups in Nafion would limit the extent of ion-exchange processes), refer to Chapter Seven.

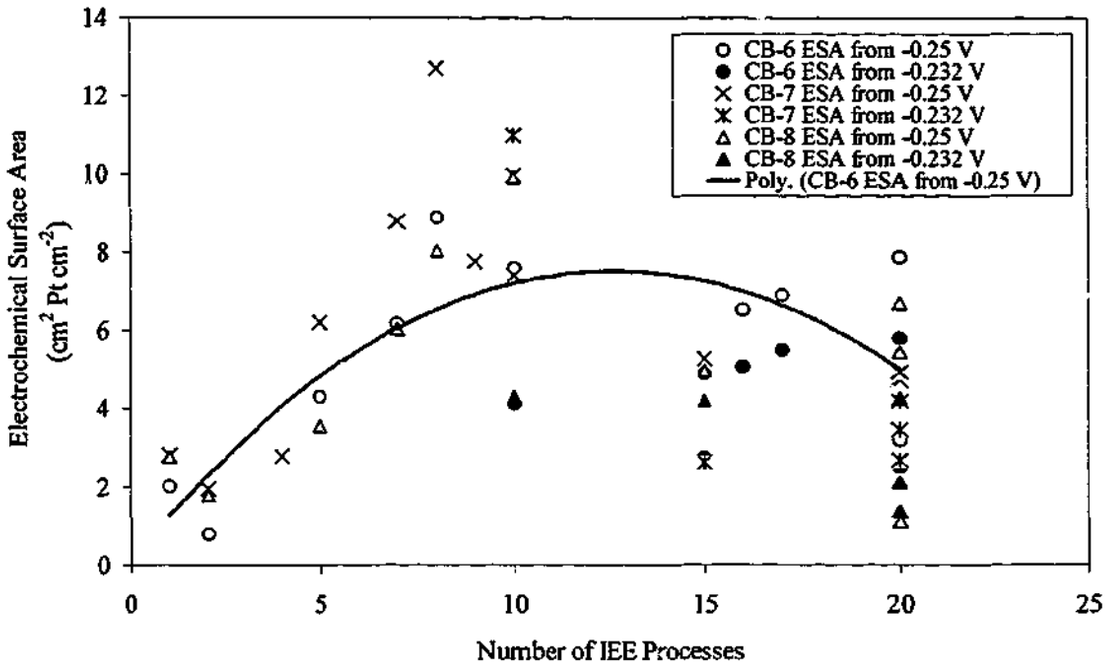

Fig. 6-6 *The relationship between the electrochemical surface-area of Pt in Electrodes CB-6, CB-7 and CB-8 at varying degrees of platinisation (between 1 and 20 IEE processes). Note that the 'real' surface area is represented by data points using an E_i of – 0.232 V_{SCE}; the other data points represent estimates of the surface area calculated from CV scans using a lower E_i value (– 0.25 V_{SCE}). A second order polynomial fit is included to guide the eye over the Electrode CB-6 ESA estimates (open circles) which were calculated from an E_i of – 0.25 V_{SCE}.*

The relationship between the electrochemical surface-area (*ESA*) of platinum and the number of IEE platinisation processes performed on each of the three electrodes is shown in Fig. 6-6. Calculating the Pt surface-area at the low levels of platinisation (from an E_i of – 0.232 V_{SCE}) was not feasible in some cases. Instead, Fig. 6-6 contains some over-estimates of the Pt surface-area from CV scans using an E_i value of – 0.25 V_{SCE}. Although the j_{an} peak area of a CV scanning from an E_i more negative than – 0.232 V_{SCE} cannot be used to calculate the 'real' Pt surface-area (due to the additional j_a from H_2 oxidation), these over-estimates are provided to show the gradual increase in the Pt surface-area between 1 and 10 IEE platinisation processes. The 'real' Pt *ESA* is shown by measurements with E_i = – 0.232 V.

The trends in Fig. 6-6 clearly show the increase in Pt *ESA* with additional IEE-platinisation processes, up to around 10 processes. At the low platinisation extents

(below 10 IEE processes) the gradual increase in the estimated Pt surface-area may be observed from the polynomial fit provided for Electrode CB-6 (which is similar to the *ESA* trends of the other two electrodes from E_i values of – 0.25 V_{SCE}), even if the actual *ESA* values are arbitrary. The *ESA* values for the fit were calculated from CV scans using an E_i of – 0.25 V_{SCE} (since these data points exist over the whole IEE range). It should again be noted that the actual Pt *ESA* will be lower than that plotted from scans using E_i = – 0.25 V_{SCE}.

The platinum *ESA* in each electrode appears to have stabilised (e.g. between 10 and 15 IEE processes) and then gradually decreased up until 20 IEE processes, Fig. 6-6. In fact, given the scatter in the *ESA* values, the *ESA* for each electrode appears relatively stable above *ca.* 10 IEE processes. A gradual stabilisation (or a lessening of the increase in Pt *ESA* with each IEE processes) was expected, since continued platinum electrodeposition will eventually lead to particulate growth, and at a certain point the increase in *ESA* relative to the total *ESA* may be negligible. In fact, it may be possible to experience a reduction in the total Pt *ESA* (e.g. by the agglomeration of smaller particles causing a loss in surface-area).

It is difficult to determine an obvious distinction between the *ESA* trends for the three electrodes shown in Fig. 6-6. Higher Nafion-loadings would be expected to yield greater amounts of platinum at a given number of IEE processes performed, since more $Pt(NH_3)_4^{2+}$ ions may be ion-exchanged into the electrodes in each IEE process. Platinum loadings cannot be determined from the *ESA* values, although generally, lower surface-areas will be obtained from electrodes with higher Pt loadings (above a certain loading) due to more particle agglomeration and growth. This is highlighted by commercially available Pt/C, where a 10 wt% Pt/C catalyst has an average particle size of ~ 1.5- 1.8 nm, *cf.* a particle size of 2.2 nm for a 30 wt% supported Pt loading [*Stonehart, 1990*]. At the higher loaded carbon support, greater agglomeration of Pt particles occurs, reducing the overall Pt surface-area [*ibid.*]. This effect may be observed for Electrode CB-8 in Fig. 6-6, where the platinum *ESA* is generally lower irrespective of the number of IEE processes *cf.* that found in the other electrodes with lower Nafion-loadings.

From the discussion above, the *ESA* of Pt in Electrode CB-8 would be expected to reach a maximum at a lower number of IEE processes, *cf.* the other electrodes. A reasonable trend cannot be extracted from the data presented in Fig. 6-6. Nevertheless, the lower Pt *ESA* in Electrode CB-8 after 20 IEE processes suggests this could be the case.

There appears a great deal of scatter in Fig. 6-6, which is probably accounted for by the susceptibility of platinum *ESA* on electrochemical cycling. Initially, at least 5- 10 CV scans (at 0.05 V s^{-1}) are required to clean the platinum surface of any adsorbed impurities [*Will, 1965*]. Once a clean Pt surface is obtained, further scanning over a reasonable potential range, e.g. between the hydrogen and oxygen evolution regions, will gradually cause roughening and faceting (the promotion of certain crystallographic faces with respect to others) of the platinum surface, possibly from the electrodissolution/re-deposition of surface atoms [*Egli et al., 1993; Triaca and Arvia, 1990; Visintin et al., 1989; Chialvo et al., 1983*]. These processes will thus affect the platinum *ESA* calculated.

Furthermore, the j_{dl} of the electrode may fluctuate over time, depending on the degree of oxidation of the carbon surface. At high platinisations in Fig. 6-6, the electrodes would have experienced a great deal of electrochemical cycling, and the additional j_{dl} thus generated may obscure some of the Pt features, possibly contributing to the decrease in the *ESA*. This effect may be observed by comparing Curves V and VI in Fig. 6-4. Both curves represent scans of the Pt/CB-6 electrode following 20 IEE processes, however before Curve VI was recorded *ca.* 60 scans over the same potential range were performed[x].

Table 6-2 presents the Pt *ESA* and loading characteristics of the three electrodes. It is clear from the platinum loadings, *W* (determined by AAS) that the amount of Nafion in the catalyst layer does affect the platinisation of the electrodes, as

[x] After Curve V, but before Curve VI was performed Electrode Pt/CB-6 was immersed in hot (80-90 °C) sulphuric acid solution (1.0 M) for 1 h. This was performed in order to ensure any remaining Pt cations were removed before AAS analysis and also to help cleanse the electrode.

expected. This appears to confirm the hypothesis that more Pt ions will be impregnated in higher Nafion-loading electrodes. This finding also supports the idea that the IEE method facilitates 'customisation' of the platinum loading in an electrode.

Characteristic	*CB-6*	*CB-7*	*CB-8*	*G-1*[a]	*G-2*[a]	*G-3*[a]
Geometric Area (cm^2)	4.8	4.8	4.8	-	-	-
Catalyst Layer ($mg\ cm^{-2}$)[b]	3.20	3.23	3.15	-	-	-
Total Nafion (wt%)**	15	20	29	50	50	50
ESA ($cm^2\ Pt\ cm^{-2}$)[c]	5.79	4.18	4.25	-	-	-
W ($\mu g\ Pt\ cm^{-2}$)[d]	54.3	75.2	76.1	3.0	32	39
S ($m^2\ Pt\ g^{-1}$)[f]	10.7	5.56	5.58	64	19	15
d (nm)[e]	26.2	50.4	50.2	4.5	14.0	18.5

Table 6-2 *Characteristics of the IEE-platinised electrodes and some comparisons with similar electrodes by Gloaguen et al. [Gloaguen et al., 1997].*

[a]*Electrodes electrochemically platinised [Gloaguen et al., 1997] from 0.002 M K_2PtCl_6 + 0.1 M H_2SO_4 solution. Electrodes consisted of ~ 5 μm layers of 50 wt% Nafion/C , deposited onto a glassy carbon substrate. The carbon-black (Vulcan XC-72) loadings in these layers ranged between 340-565 $\mu g\ cm^{-2}$.*
[b]*Loading excluding the mass of platinum.*
[c]*ESA and S values are based on the best reproducible CV scans following 20 IEE-platinisation processes. These are slightly lower cf. a paper published from this work, as explained in Footnote viii.*
[d]*The platinum loading was determined from the amount of deposited metal on the electrodes following 20 IEE processes by AAS (the electrodes were immersed in 1.0 M H_2SO_4 at 80- 90 °C for 1 h prior to AAS analysis to ensure no platinum cations remained in the Nafion electrolyte).*
[e]*Average Pt particle size determined from Eq. 1-16 (Chapter One). These particle sizes are larger than those reported elsewhere, see Footnote viii.*

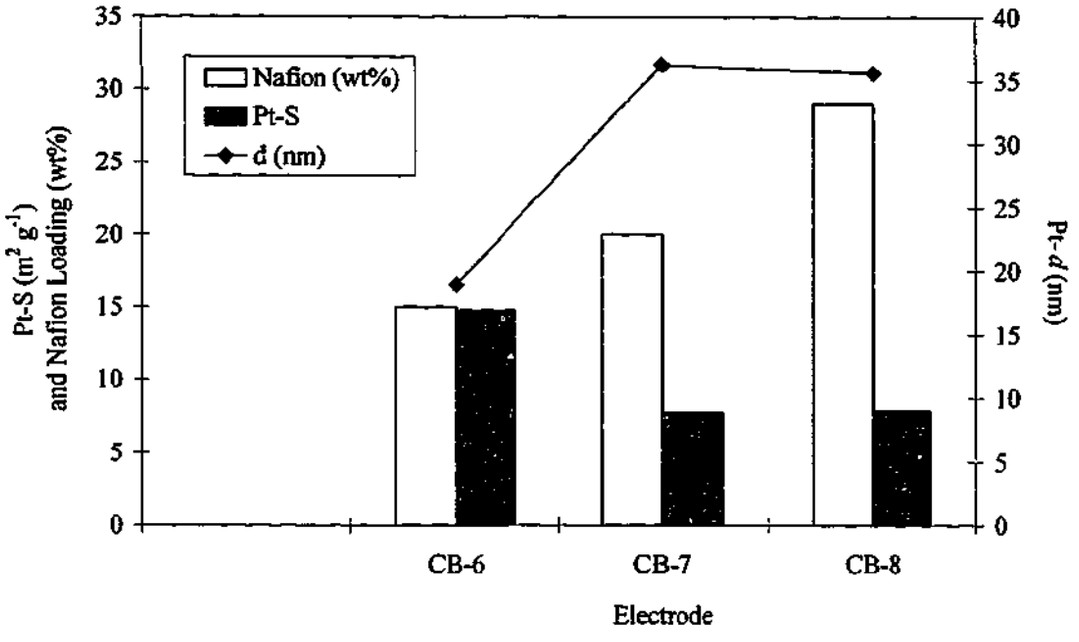

Fig. 6-7 The relationship between the specific surface-area, S, and particle diameter, d, of the platinum deposits in the IEE-platinised electrodes.

The specific surface-area, *S*, values in Table 6-2 indicate that a low Nafion loading is preferable for the IEE method of platinisation. It is believed that less platinum particle growth is allowed at low Nafion loadings, since less platinum can be exchanged into the electrode. This process may be imagined as an electroreduction from a dilute solution in which the platinum cations are constrained from widespread diffusion (by virtue of the ion-exchange followed by the rapid electroreduction). Fig. 6-7 illustrates this effect, where smaller platinum particles are produced at lower Nafion loadings (e.g. in Electrode CB-6).

Electrode CB-6 shows the highest level of platinum surface-area for a given mass and is thus the most likely to achieve the highest utilisation under fuel cell conditions. Furthermore, lower concentrations of Nafion within the catalyst layer may be more desirable (e.g. for achieving better cell performance) possibly by facilitating more rapid gas transport to the supported catalyst particles. Typically, between 25 and 50 wt% Nafion is used in PEMFC catalyst layers [*Wilson et al., 1995*]; DMFC catalyst layers may have as little as 7 wt% Nafion [*Ren et al., 1996*].

Fuel cell performance is usually improved at low current densities with higher Nafion-loadings in the catalyst layer (where contact to a greater number of Pt particles is facilitated). However, at high current densities a lower Nafion-loading is preferred to enable rapid gas transport and minimise any water flooding effects at the cathode. Therefore, depending on the desired operating conditions of the fuel cell (e.g. high fuel efficiency at low current densities, or high power at intermediate current densities), differing concentrations of Nafion may be optimal in catalyst layers. Thin catalyst layers could be prepared for IEE-platinisation similar to those that have been used by other researchers [*Wilson and Gottesfeld, 1992, in J. Appl. Electrochem.*], since at high current densities the majority of the current is believed to be generated near the membrane side of the catalyst layer [*Bockris and Srinivasan, 1969*]. In turn, the IEE-platinisation conditions could be adapted, to minimise platinum particulate growth. A further point is that via the IEE method, all deposited platinum should be in the 3PRZ regions of the electrode, thus maximising the utilisation of the available platinum surface area. The only potential losses in Pt utilisation would then arise from particle size.

Some promise for attaining higher platinum utilisations (i.e. depositing even smaller platinum particles) via the IEE method is indicated in the comparison with the work of Gloaguen *et al.* [*Gloaguen et al., 1997*]. These researchers platinised electrodes of similar composition (Electrodes G-1 to G-3 in Table 6-2) from a K_2PtCl_6 solution, and at low platinum loadings achieved very high *S* values. On the electrodes containing high Pt loadings (32 and 39 μg cm^{-2} on Electrodes G-2 and G-3), specific surface areas of 19 and 15 m^2 g^{-1} were obtained respectively [*ibid.*], which are comparable to the ~ 11 m^2 Pt g^{-1} achieved on Electrode CB-6 (with 54 μg Pt cm^{-2}). At very low Pt-*W* (3 μg Pt cm^{-2} on Electrode G-1) an *S* of 64 m^2 g^{-1} was reported [*ibid.*]. It is likely that if similar low Pt loadings were deposited via the IEE method much higher specific surface areas could be attained (since the possibility of particle growth/agglomeration is lessened).

A further point to make between the comparison of results reported by Gloaguen *et al.* and those for the IEE-platinised electrodes (CB-6 to CB-8 in Table 6-2) is that in

the former work the Pt *ESA* was calculated from CO_{ads} coulometry. This provides greater accuracy in determining the charge passed, since a sharp peak (at *ca.* 0.6-0.8 V_{SCE}) is observed from which the double-layer charging of the electrode is easier to subtract. In addition, a higher carbon loading was used in the IEE Electrodes (by around a factor of 5) and the higher C_{dl} may have obscured more of the Pt-H_{ads} features *cf.* those observed by *Gloaguen et al.* Accordingly, the Pt *ESA* for Electrodes CB-6 to CB-8 might be considerably larger than the values presented in Table 6-2.

In most of the CV scans performed on the IEE-platinised electrodes the maximum E_u was 0.8 V, to avoid too much oxidation of the carbon surface. Significant oxidation of the Vulcan XC-72 carbon-black occurs above ~ 0.8 V_{SCE} [*Kinoshita, 1988*]. However, scans to higher potentials (up to 1.2 V_{SCE}) were found to greatly improve the Pt-H_{ads} area and definition of the whole platinum 'CV fingerprint' (and were therefore performed at each IEE platinisation level, for example, observe the potential ranges in Fig. 6-4). It is possible that given time, scanning to e.g. 0.7 or 0.8 V_{SCE} would eventually lead to cleaned, reproducible Pt features. The formation of PtO_2 on the platinum surface occurs just below this E_u (at around 0.6 V_{SCE} and higher potentials) and the oxidation/reduction of the Pt surface layer is a well-known electrochemical method used for cleaning platinum and platinised electrodes [*Will, 1965*]. However, a full PtO_2 monolayer does not typically form by ~ 0.8 V_{SCE}, and for complete Pt surface cleaning higher E_u values are required. If strongly adsorbing species are introduced to the solution (e.g. sulphur-containing species, such as those discussed in Chapter Four) then scanning to higher potentials, at least 1.2 V_{SCE}, appears necessary. Moreover, if the upper scanning potential was limited to 0.75 V_{SCE}, the greater number of scans required to fully clean the Pt deposits may also result in considerable oxidation of the carbon surface (which occurs at *ca.* 0.4 V_{SCE}, Fig. 6-4), so that no benefit would be gained over using the lower E_u.

The additional exchange/reduction processes might not be necessary once an ideal combination of the Nafion loading and the $Pt(NH_3)_4^{2+}$ solution concentration is found. For example, higher concentrations of platinum solutions (for increased ion-

exchange) may be used with low Nafion loadings, to achieve a desired platinum loading. The application of a known Pt-W to electrodes for IEE-platinisation is also possible- refer to the Future Work section (Section 7.4.2) in Chapter Seven. Alternatively, the use of more exchange/reduction processes may prove beneficial in terms of producing a greater dispersion of platinum deposit.

The scanning electron micrograph in Figure 6-8 shows a high dispersion of platinum particles in the catalyst layer of Electrode Pt/CB-6. The platinum particle size however, appears quite large (on the order of several hundred nanometers) which does not agree with the estimated average particle size, *d*, from the AAS and surface-area analyses. This may be due to the aggregation of platinum particles into clusters such as observed by Ye and Fedkiw [*Ye and Fedkiw, 1996*]. These workers found that platinum particles observed with SEM were almost two orders of magnitude larger than the particle size calculated from the specific surface area, and TEM was used to show the dendritic nature of the platinum clusters.

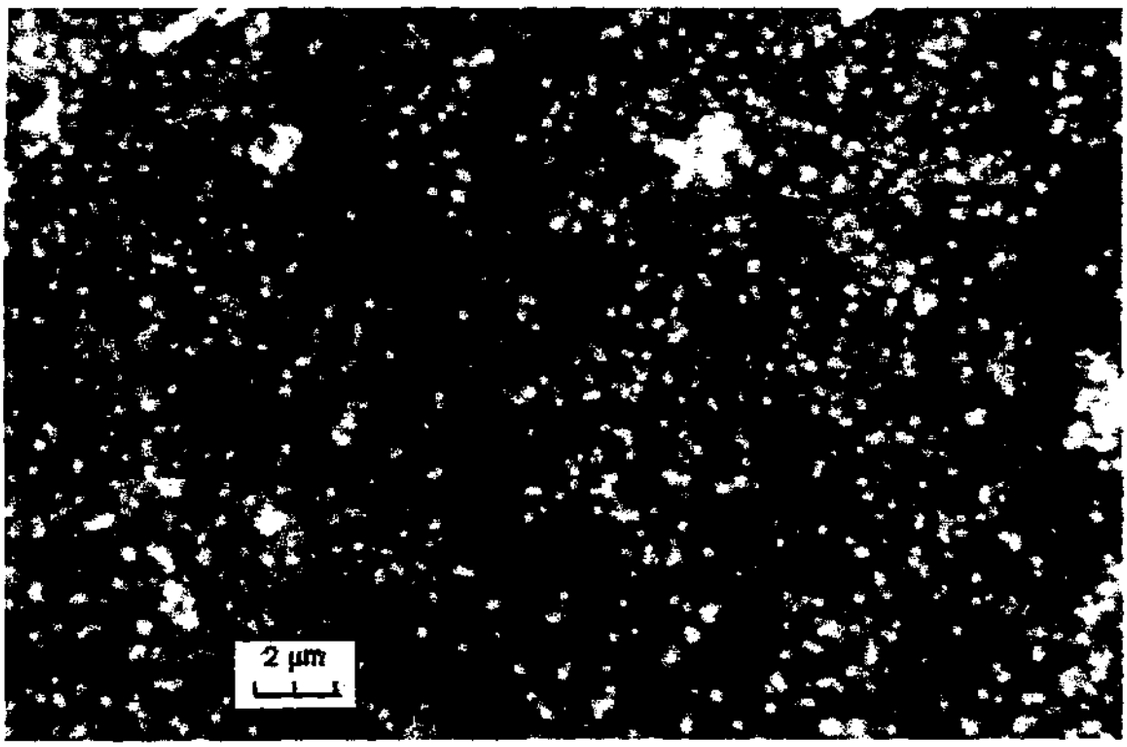

Fig. 6-8 *SEM image of Electrode Pt/CB-6. The highly dispersed, bright particles are platinum as determined by EDXS.*

A further point to note is that the $Pt(NH_3)_4^{2+}$ species has been reported to have very slow reduction kinetics [*Penven et al., 1992*], and it is possible that these electrodes may not have received enough time to completely electroreduce all of the ion-exchanged platinum. If this were the case, it may account for the low platinum surface areas observed during the initial ion-exchange/reduction processes. Alternatively, a certain amount of deposited platinum may be required in the electrodes before the hydrogen adsorption/desorption peaks begin to appear [*Lin-Cai and Pletcher, 1983*].

It is also possible that not all of the platinum deposited was impregnated into the electrodes via ion-exchange. Some $Pt(NH_3)_4^{2+}$ species may have existed in the hydrophilic Nafion micelles along with the Cl^- counterions. Previously (in the initial stages of this work, especially following the problems encountered in the IISE experiment under fuel cell conditions), anions were thought to be excluded from the cation-exchange membrane. This would effectively allow only cation impregnation into the Nafion-bound electrode, and to maintain charge balance in Nafion, the cations would have to be exchanged for the $-SO_3H$ protons. This is not the case, for example, the $PtCl_6^{2-}$ anion has been successfully electrodeposited onto carbon through Nafion films [*Gloaguen et al., 1997; Ye and Fedkiw, 1996; Itaya et al., 1986*]. In the work of Gloaguen *et al.*, a lower H_2SO_4 solution concentration (0.1 M) was used to decrease the amount of sulphate ions within the Nafion regions of electrodes, enabling an increased $PtCl_6^{2-}$: SO_4^{2-} ratio in the electrode. Hence, in this work, a small number of Cl^- ions may exist in the electrode (and thus along with some $Pt(NH_3)_4^{2+}$ ions which are not in an ion-exchanged form) however, the actual number of these additional ions is expected to be minimised in comparison with the work of Gloaguen *et al.*, due to exclusion by the higher concentration (0.5 M) of SO_4^{2-} ions.

If anions can impregnate Nafion, then the $Pt(NH_3)_4^{2+}$ within the CB electrodes in this study is not necessarily completely in the ion-exchanged form, some may exist in 'solution' form (in the Nafion micelles). The higher Pt-loading found in Electrodes CB-7 and CB-8 is then not exclusively assignable to a greater extent of

platinum ion-exchange, it may also have arisen from greater platinum impregnation in general throughout these electrodes. The extent of ion-exchange possible within Nafion will depend on the platinum solution concentration, equilibration time and the number of $-SO_3H$ groups in the electrode. The latter is most important in this work since the first two conditions are maintained constant.

The 'equivalent weight' (EW) of Nafion is given as 1100 g per mole of $-SO_3H$ groups. In 1 cm^2 of a CB-based electrode (with a 2.28 mg Nafion/Vulcan conventional catalyst layer loading), 0.228 mg (10 wt%) is Nafion, and in this electrolyte there is approximately 1.25×10^{17} sulphonic acid groups. Theoretically, the maximum number of $Pt(NH_3)_4^{2+}$ species ion-exchangeable into the electrodes is equivalent to half the number of $-SO_3H$ groups, to balance charge (one Pt^{2+} per two H^+). Thus, in one IEE process, a maximum of 6.6×10^{17} $Pt(NH_3)_4^{2+}$ species may be ion-exchanged into Electrode CB-6, i.e. 0.21 mg of metallic Pt. It is clear from the platinum loadings in Table 6-2 (CB-6 has a Pt-*W* of 0.054 mg cm^{-2}, i.e. ~ 0.26 mg of Pt in total) that the maximum possible number of platinum cations were not exchanged and electroreduced in each of the 20 IEE processes.

In fact, it appears as though around one-twentieth of the maximum number of $Pt(NH_3)_4^{2+}$ species may be deposited in each IEE process, assuming a roughly equal number exchange in each process. This is not surprising, since the number of $Pt(NH_3)_4^{2+}$ ions that may be impregnated into an electrode will be constrained by the equilibrium that forms between ion-exchanged platinum and platinum ions in the bulk immersion solution. At higher platinum solution concentrations, more platinum cations are expected to diffuse into the electrode. An advantage of ion-exchanging only a small proportion of the available $-SO_3H$ groups (e.g. about 5%, if the above discussion is correct) is that most, if not all of the platinum cations are in the ion-exchanged form.

Electrode CB-6 appears to have been platinised the most desirably, exhibiting the highest *S* and lowest *d* values (Fig. 6-7). This was not surprising, since the electrodes with higher Nafion loadings are expected to be impregnated by greater

amounts of platinum during each IEE process, and above a certain number of IEE processes the growth/agglomeration of Pt particles may lead to a stabilisation or loss in Pt *ESA*. It is probably not feasible to use less than *ca.* 10-15 wt% Nafion in the catalyst layers, predominantly because high levels of ionic conductivity are desirable, but also since the Nafion acts as a binder for the layer. In earlier PEMFC electrode fabrication, between 25 and 50 wt% PTFE was commonly used to bind the catalyst layer [*Wilson and Gottesfeld, 1992, in J. Appl. Electrochem*] and the layer was subsequently impregnated with Nafion solution. The later replacement of PTFE by Nafion was found to greatly enhance cell performance (as outlined in Section 1.3.3.1 of Chapter One); PTFE is occasionally used in cathode catalyst layers (to help with water flooding at high current densities). Thus, it is possible to further reduce the Nafion content of catalyst layers for platinisation via the IEE method, however, this may cause a reduction in fuel cell performance, or else could allow the preparation of very thin catalyst layers with less *iR*-drop polarisation.

6.4 Summary

Two methods were investigated for the direct platinisation of fuel cell electrodes. The IISE Method (Section 6.2) illustrated the potential for electrodepositing platinum within an assembled PEMFC. Cleaning or activation of the IISE-deposited platinum was found to be necessary. In the second technique, the IEE Method (Section 6.3), an ion-exchange process was used to enable selective platinum electrodeposition within 3PRZ regions of PEMFC electrodes. The preparation of electrodes with low platinum loadings is possible via the IEE Method, and following further optimisation, this method could prove viable for producing PEMFC electrodes.

Chapter Seven

Conclusions and Future Work

7.1 Chapter Overview

Chapter Seven summarises the main findings from the investigations pursued in this dissertation and provides suggestions of possible experiments and related avenues that may be explored in follow-up work. The main objective throughout this work was to develop alternative methods for the catalysation of PEMFC and DMFC electrodes, primarily through the use of electrodeposition. A few methods were investigated, and a large number of possible future methods have been discovered (via the relatively wide-ranging studies presented in Chapters Four to Six).

7.2 Poisoning During Pt Electrodeposition

7.2.1 Summary of Pt Poisoning Conclusions

- Platinum was successfully electrodeposited from a $H_3Pt(SO_3)_2OH$ solution onto both GC and CB-based electrodes. The success in platinising the Nafion-bound 'fuel cell type' electrodes from this species is important since (i) fuel cell electrodes may be prepared in this direct way, and (ii) this implies that the $H_3Pt(SO_3)_2OH$ species (e.g. as $Pt(SO_3)_2^{2-}$) is probably able to penetrate the thin Nafion films binding carbon black particles (i.e. these anionic species are not excluded from the cation-exchange membrane).

- Reasonably low potentials (*ca.* – 0.45 V_{SCE}) were required to facilitate the electroreduction of platinum from $H_3Pt(SO_3)_2OH$ solution (*cf.* ~ + 0.2 V_{SCE} for H_2PtCl_6).

- The platinum electrodeposited from $H_3Pt(SO_3)_2OH$ solution was found to be strongly poisoned and could be 'cleaned' of the adsorbed species by potentiodynamic cyclic between the potentials of hydrogen and oxygen evolution. Faster cleaning was achieved if CVs were scanned to slightly higher

potentials, up to around 1.4 V_{SCE} (scanning to higher potentials risked the loss of platinum via electrodissolution). With this higher upper potential, Pt deposits were cleaned in 20- 50 CV scans, depending on platinum loading.

- Since sulphite, SO_3^{2-}, ligands are present in the platinum complex, it is likely that these will be released once the Pt is reduced. These ligands may adsorb onto the platinum deposits, or more likely, will become reduced to sulphide, S^{2-}, species at the low potentials used for $H_3Pt(SO_3)_2OH$ electroreduction; these S^{2-} species may then adsorb onto the platinum deposits.

- Further evidence for the 'sulphite/sulphide poisoning of Pt' hypothesis was observed in the similar poisoning of Pt in $NaHSO_3$ solution (i.e. with SO_3^{2-} ions). Following these experiments, potentiodynamic cycling was required to restore the clean Pt surface in the same way as for Pt electrodeposited from $H_3Pt(SO_3)_2OH$ solution.

- Pt particles electrodeposited from $H_3Pt(SO_3)_2OH$ solution appear relatively small (diameters of ~ 50 nm from SEM analysis), suggesting that this poisoning has limited Pt particulate growth during electrodeposition to some extent. It was not possible to confirm this particle size from the electrochemical measurements since the charge passed during electrodeposition most probably contains contributions from other competing reactions (such as hydrogen evolution and sulphite reduction).

- Following these studies, the catalysation of pre-fabricated fuel cell electrodes by direct electrodeposition of $H_3Pt(SO_3)_2OH$ (and subsequent electrochemical cleaning), this 'Pt poisoning' method appears straightforward and promising for potential fuel cell production. Increased platinum utilisation may be realised under fuel cell conditions, if small platinum particles with a high surface roughness could be electrodeposited into the active regions of electrodes. The limitation of Pt particulate growth during electrodeposition could be enhanced in further work, possibly via methods suggested in the following section.

7.2.2 Potential Future Experiments with Pt Poisoning

i. The extent of platinum poisoning over time could be studied. Pt could be potentiostatically electrodeposited onto separate electrodes for different lengths of time, and the resulting deposits could then be investigated. It would be interesting to know whether slightly larger Pt particles were deposited over longer electroreduction times, i.e. whether particle growth is still possible. If this was found to be the case, smaller platinum particles might be achievable via shorter electroreduction times. The addition of more sulphite or sulphide to the solution (e.g. via $NaHSO_3$) may also aid in the production of smaller Pt particles.

ii. It may prove useful to develop alternative methods for removing the sulphide or sulphite species, such as heating at elevated temperatures in e.g. oxidising or reducing atmospheres (where SO_2, SO_3 or H_2S products may result). This possibility is more significant in the case of Ru electrodeposited from $H_3Ru(SO_3)_2OH$, and is discussed further in Section 7.3.2.

iii. Further experimental work relating to the 'Pt poisoning' method could include the investigation of other ions or molecules that may adsorb onto Pt surfaces (for limiting/preventing Pt growth during electrodeposition). Unsaturated organic molecules such as ethylene (C_2H_4) and acetylene (C_2H_2) are known to adsorb onto gold [*Hodgson et al., 1999; Zinola and Castro Luna, 1998*]. These gases could potentially be bubbled into a solution during platinisation. Acetylene would probably adsorb the most strongly, however great care would be required with this reactive gas. The removal of any of these adsorbing species may however prove difficult. Electrochemical cycling may be successful for removing the adsorbed gases. Heating of ethylene or acetylene adsorbents in air or hydrogen may also help to remove these molecules.

iv. With electrodeposition into CB-based electrodes, the effect of 'pre-immersion' time before electrodeposition could be investigated further. Greater time for equilibration of the $H_3Pt(SO_3)_2OH$ species (e.g. the $Pt(SO_3)_2^{2-}$ ions) in the Nafion electrolyte may prove beneficial, possibly enabling more Pt electrodeposition. The dispersion of Pt particles throughout the electrode might also be enhanced. For example, a procedure could involve a series of equilibration steps, separated by rapid electroreduction pulses.

7.3 Ruthenium Electrodeposition

7.3.1 Summary of Ru Electrodeposition Conclusions

- Ruthenium was electrodeposited from $H_3Ru(SO_3)_2OH$ solution onto Pt, GC and CB-based electrodes at *ca.* 0.2 to 0.3 V and more negative potentials. Contrary to ruthenisation from other species (e.g. $RuCl_3$) electrodeposition of $H_3Ru(SO_3)_2OH$ at potentials within the H_2 evolution region did not result in Ru deposits exhibiting Ru-H_{ads} oxidation behaviour.

- Unfortunately, it was not possible to clean the poisoning species from the Ru electrodeposited from $H_3Ru(SO_3)_2OH$ solution via the electrochemical means investigated. The potentiodynamic cycling regime successfully used for cleaning Pt deposited from $H_3Pt(SO_3)_2OH$ proved ineffective for $H_3Ru(SO_3)_2OH$-deposited Ru. This was believed to occur because the electrodissolution of Ru occurred at potentials negative to the oxidation potential of the poison. Evolving hydrogen on the ruthenised electrode surface during potentiostatical holds at low potential was not found to decrease the poisoning (e.g. via H_2S formation).

- A CB-based electrode was successfully ruthenised from $H_3Ru(SO_3)_2OH$ solution, however the Ru was poisoned in similar fashion to the ruthenised GC electrodes. Thus, there is potential to prepare fuel cell electrodes from this species, provided

an efficient cleaning method was developed. The Ru particles were found to be highly dispersed across the CB electrode surface, although the average particle size (up to 500 nm) was reasonably large. A number of large agglomerates were observed in the SEM micrograph, suggesting that the smaller particles may also exist as agglomerates. At any rate, the Ru particle size could be further reduced with an optimisation of the electrodeposition method.

- The attempted electrodeposition of PtRu (from either both sulphite complexes, or from $H_3Ru(SO_3)_2OH$ and H_2PtCl_6) produced mixed results. The presence of platinum on the electrodes did not aid in the electrochemical cleaning of the poisoned Ru (from $H_3Ru(SO_3)_2OH$ solution). At no stage were electrochemical features of both Pt and Ru visible in a CV scan at the same time. It is probable that the Ru remained poisoned whilst on the electrodes, and the large j_{ai} (obscuring any platinum electrochemistry and representing the poisoned Ru) was not removed until all of the Ru had dissolved. The platinum was probably never completely cleaned (as evidenced by the lack of a Pt-H_{ads} region in the CV scans) until all of the Ru and poisoning species had been electrodissolved.

- Furthermore, the binary PtRu-catalysed electrodes (from the respective platinum and ruthenium sulphite species) did not exhibit superior activity for methanol-oxidation *cf.* Pt. In fact, the activity was lowered with the presence of the poisoned Ru.

- Following the 'Ru electrodeposition from $H_3Ru(SO_3)_2OH$ solution' studies, it is clear that this method is not yet feasible for PtRu catalysation of fuel cell electrodes. However, if the Ru surface could be 'cleaned' in an effective manner without loss of Ru, then this method could prove very promising (e.g. for achieving small PtRu particles, possibly with a higher utilisation under fuel cell conditions). The Ru-loading and particle size could be optimised.

7.3.2 Potential Future Ru Electrodeposition Experiments

i. The development of alternative methods for the removal of sulphides and related species from ruthenium surfaces that do not cause Ru dissolution would prove highly beneficial. Possible methods include reduction via bubbling hydrogen or e.g. hydrazine (or by evolving hydrogen at low potentials for a long time, or possibly even via immersion in reducing solutions such as $NaBH_4$). The use of ultrasonication and/or elevated temperatures with or without any of the above methods may also prove beneficial. Temperatures of 90-100 °C for long periods (~ 20 h) did not yield any change in poisoned Ru/GC electrodes, but perhaps temperatures over ~ 500 °C may help to remove the poisons. High temperatures in an H_2 atmosphere (similar to the cleaning/reduction step of the PtRu/C supported catalyst produced via the method of US Patent 4,044,193 [*Petrow and Allen, 1977*]) may also prove successful. Another possibility for ruthenium cleaning is the oxidation of poisoning species in O_2 or air at high temperatures, although this may risk the production of higher Ru-oxides, e.g. RuO_2 (which may be difficult to reduce back to Ru metal).

ii. Again, similar to (iii) in Section 7.2.2, ethylene or acetylene could be adsorbed onto Ru surfaces (assuming these species adsorb onto Ru), during the electroreduction of Ru from an e.g. $RuCl_3$ (or $Ru(NO)(NO_3)_3$ solution). These might prove more effective blocking agents to particle-growth, which might also be removed more readily (and ideally without Ru loss).

Continued Investigations into PtRu Binary Catalyst Electrodeposition:

iii. The preparation of binary PtRu electrodeposits might be possible by using the IEE Method, following optimisation of the relative concentrations of $Pt(NH_3)_4^{2+}$ and a Ru cationic species (to attain catalysts with the desired surface ratio of each metal). The potential variations are discussed in Section 7.4.3.

iv. It may also be possible that the adsorbed oxides on the Ru surface at low potentials could limit the growth of Ru particles due to the higher electrical resistance of the oxide film. This could be investigated by Ru reduction onto Ru electrodes at low potentials (< 0.1 V_{SCE}) and at higher potentials, e.g. 0.4 V_{SCE}, where $Ru(OH)_2$ species exist. The use or formation of Ru_2O_3 or RuO_2 surfaces is probably not useful though, since these higher oxides are difficult to reduce (i.e. reduction potentials above ~ 0.6- 0.7 V_{SCE} are not advisable).

7.4 IISE & IEE Methods

7.4.1 Summary of IISE Method Conclusions

- Platinum was successfully electroreduced from H_2PtCl_6 directly within a PEMFC-type electrode via the IISE Method.

- Several obstacles were encountered during the IISE process, including uncertainty over the exact potential of the counter electrode.

- Cleaning or activation of the IISE-deposited platinum was necessary, and was found to be easiest once the electrode was removed from the MEA. Further development of the method was abandoned in favour of the more robust IEE Method.

- Nevertheless, the IISE Method illustrated the possibility of electrodepositing platinum within an assembled PEMFC. With further optimisation, this method could prove useful for preparing fuel cell electrodes.

7.4.2 Summary of IEE Method Conclusions

- Following 20 Ion-Exchange/ Electroreduction (IEE) processes, low Pt loadings of 50-80 μg cm^{-2} were successfully deposited (as determined from AAS).

- Increased Pt loadings were found in electrodes containing a higher Nafion wt%, as expected. This is likely to have resulted from a greater extent of platinum cations being ion-exchanged (and subsequently electroreduced) during each IEE process into the electrodes containing a greater proportion of Nafion.

- The average Pt particle diameters in the electrodes were found to be between 26 and 50 nm. It is expected that smaller particles could be deposited with further optimization of the method (e.g. a higher ion-exchange per process combined with fewer processes for an equivalent platinum loading).

- The smallest average Pt particle size deposited (26 nm) is a factor of 10 times greater than a typical catalyst available from E-TEK, Inc. However, the surface of all Pt particles deposited using the IEE method is expected to be available under fuel cell conditions, increasing the platinum utilisation.

- Hence, the IEE Method may prove a viable catalysation approach for fuel cell electrodes. Smaller Pt deposits could probably be prepared under optimised conditions. For example, higher solution concentrations combined with shorter immersion times and a reduced number of IEE processes. Alternatively, lower platinum solution concentrations could be used with more IEE processes (although this may increase particle growth).

7.4.3 Potential Future IISE & IEE Experiments

Further optimisation of the IEE Method:

i. Lower Pt loadings could be deposited, which might enable smaller Pt particles. However, the electrochemical features and surface-area of such electrodes will be even more obscured by the j_{dl} of the CB-based electrode. Other methods, such as the electro-oxidation of an adsorbed carbon monoxide layer [*Gloaguen et al., 1997*] may allow the estimation of Pt electrochemical surface-area (for very low Pt loadings).

ii. The effect of the number of IEE processes on platinum loading could be investigated, for optimisation of the method. Establishing if a linear relationship exists between Pt loading and the number of processes may prove useful. If this is not the case, then a change in conditions of the IEE method may be beneficial (e.g. by altering the Pt solution concentration, ion-exchange time, electroreduction time, etc.).

iii. The pH of the ion-exchanging solution could also be adjusted to manipulate the extent of ion-exchange (by altering the equilibrium of protons in the Nafion electrolyte). For example, a higher proportion of exchanged Pt is expected with an increased pH. Higher Pt concentrations within the electrode may be beneficial in creating a greater number of Pt nuclei, relative to an electrode with an equivalent Pt-loading (which has experienced more IEE processes).

iv. The application of a desired loading (e.g. of $Pt(NH_3)_4^{2+}$) onto CB electrodes before electrodeposition is also possible. The catalyst species could be applied, e.g. via pipette, to the CB-based electrode (and the CB electrode could be maintained in a hydrated form to maximise the diffusion of catalyst ions throughout the electrode). Alternatively, the catalyst species could be applied to the electrode in the catalyst layer ink, as in the case of the 'In Situ' study of Chapter Six (with e.g. $PtCl_6^{2-}$, but this is equally possible with $Pt(NH_3)_4^{2+}$).

Combinations of Electrodeposition Methods:

v. The utilisation of the catalyst poisoning technique (Chapter Four) could also be investigated in combination with the IEE method, to aid in limiting Pt particulate growth. For example, the platinum deposits in the electrode could be poisoned following each IEE process (as the electrode is further platinised), so that growth of the existing deposits is minimised, and then the newly ion-exchanged platinum is expected to form new nuclei throughout the electrode. This approach may also be used with (iv) above, where known amounts of platinum are applied in several stages (and electrodeposition and poisoning processes are performed between each stage).

vi. A PtRu co-electrodeposition method using the IEE technique may be possible, with cationic Pt and Ru species. The relative concentration of each metal species in solution would require optimisation to achieve a desired Pt:Ru ratio. Two-step IEE-catalysation procedures could also be investigated for PtRu deposits. For example, a CB-based electrode could be platinised, cleaned and analysed. Ru could be then be electroreduced onto the electrode. A large proportion of this Ru is expected to reduce onto lower overpotential Pt surfaces *cf.* the carbon substrate.

The 'In Situ' (IISE) Catalyst Electrodeposition Method:

vii. The IISE Method could be simplified in a DMFC Test Station, since the DMFC typically experiences fewer problems with membrane hydration. Although methanol crossover and the effects of methanol during electroreduction (e.g. methanol may also act as a poisoning species on platinum) would have to be considered. It may be feasible to integrate the SCE reference electrode into the cell, to measure/apply the WE potential with more accuracy. If the SCE is inserted into the MEA, ionic contact with the Nafion may be difficult to

maintain. This will depend on the amount of water contained within the membrane.

viii. Catalyst ion-exchange could also be used in combination with the IISE approach. The desired loading (of Pt or PtRu) may be tailored by applying solution to the CB-based electrode, as described in (iv) above, or by application in the catalyst layer ink. Cleaning of the deposited catalysts remains an issue, but it may be possible to heat the entire MEA in e.g. sulphuric acid for an extended period, to wash out most impurities and reaction by-products. Alternatively, electrochemical cycling (within the MEA) may be possible, e.g. with part of the MEA immersed in H_2SO_4 solution.

ix. The removal of the catalysed WE from the MEA is not an ideal approach, since delamination of the WE may occur (onto the Nafion membrane). However, this would allow a much simpler WE cleaning process and the Nafion membrane/CE part of the MEA could then be washed and used again. Ideally, the WE removal would be avoided, allowing hot pressing of the MEA (i.e. to facilitate maximum ionic contact between the membrane and the Nafion within the WE catalyst layer, increasing the 3-phase-reaction-zone area in the WE). If the catalysed WE is not easily cleaned within the MEA, then careful removal of the WE may be the only option. The WE could then be readily electrochemically cycled in H_2SO_4 solution (and the electrochemical surface-area of Pt could easily be calculated).

Appendices

Appendix A

Articles Arising from this Work

1. "Platinum electrodeposition for polymer electrolyte membrane fuel cells," S.D. Thompson, L.R. Jordan, M. Forsyth, *Electrochim. Acta.* **46** (2001) 1657-1663.

2. "Platinum electrodeposition from $H_3Pt(SO_3)_2OH$ solutions," S.D. Thompson, L.R. Jordan, A.K. Shukla, M. Forsyth, *J. Electroanal. Chem.* **515** (2001) 61-70.

PERGAMON

Electrochimica Acta 46 (2001) 1657–1663

ELECTROCHIMICA Acta

www.elsevier.nl/locate/electacta

Platinum electrodeposition for polymer electrolyte membrane fuel cells

Scott D. Thompson, Larry R. Jordan, Maria Forsyth *

School of Physics and Materials Engineering, Monash University, Wellington Road, Clayton, Vic. 3800, Australia

Received 8 August 2000; received in revised form 25 October 2000

Abstract

A novel electrodeposition technique for preparing the catalyst layer in polymer electrolyte membrane fuel cells has been designed, which may enable an increase in the level of platinum utilisation currently achieved in these systems. This method consists of a two-step procedure involving the impregnation of platinum ions into a preformed catalyst layer (via an ion-exchange into the Nafion polymer electrolyte), followed by a potentiostatic reduction. The concentration of Nafion within the catalyst layer was found to have a significant bearing on the size of the platinum deposits. The preparation of catalyst layers containing a desired platinum loading should also be possible using this method. Surface areas of the platinum deposits were determined using cyclic voltammetry. The prepared catalyst was compared with a conventional electrode made from E-TEK Pt/C. Scanning electron microscopy was used to investigate the dispersion of the platinum particles. Platinum loadings were determined quantitatively by atomic absorption spectroscopy.

Keywords: Platinum utilisation; Electrodeposition; PEMFC catalyst layer; Nafion ion-exchange; $Pt(NH_3)_4Cl_2$

1. Introduction

Fuel cells are receiving increased recognition as notable alternatives to our present power sources because they exhibit high operational efficiencies and impressive environmental acceptability. Polymer electrolyte membrane fuel cells (PEMFCs) have great potential for use both in stationary power generation (e.g. under combined heat and power operation) and as vehicular power sources. One challenge facing PEMFCs, however, is to improve the utilisation of platinum within the catalyst layer which should ultimately allow a reduction in the platinum loading at a given fuel cell performance.

Ideally, all of the platinum contained within a PEMFC catalyst layer would be active for the hydrogen oxidation and oxygen reduction reactions. For this to be the case, the fuel or oxidant must react at the interfacial region between the polymer electrolyte (e.g. Nafion) and the platinum catalyst. This is known as the three-phase reaction zone. The electrode should be suitably fashioned to allow fast access of the reactant into this zone and furthermore, for a reaction to occur, the electrolyte/catalyst interface must enable the transfer of both protons and electrons.

The conventional platinum-supported-on-carbon (Pt/C) catalyst may be prepared at a small particulate size, e.g. 1.5–1.8 nm via the 'sulfito route' [1], but ensuring polymer electrolyte contact to all of these platinum particles remains a major problem. The most common method for fabricating the PEMFC catalyst layer is to mix the Pt/C agglomerates with solubilised polymer electrolyte (such as Nafion ionomer) and apply

* Corresponding author. Tel.: +61-39-9054939.
E-mail address: maria.forsyth@spme.monash.edu.au (M. Forsyth).

0013-4686/01/$ - see front matter

this paste to a porous carbon support. However, up to 90% of the platinum atoms in such electrodes may be inactive [2]. Platinum particles deposited within the porous carbon nanostructure may be inaccessible to the polymer electrolyte (Fig. 1). For example, the sulfonic acid micelles which facilitate proton transport through Nafion have an approximate diameter of 4 nm [3] and would be excluded from carbon pores with diameters less than 4 nm. The area of the three-phase reaction zone may be extended by increasing the amount of polymer electrolyte throughout the catalyst layer, but too much polymer coverage may restrict gas access to some platinum particles (especially at high reaction rates). Even if only ca. 50% of platinum atoms are on the surface of these 1.5–1.8 nm particles [1] and are able to participate in the fuel cell reactions, still a substantial mass of platinum may be utilised.

The electrodeposition of platinum has been studied by a number of researchers, with the main intention of depositing small platinum particles at the polymer electrolyte/electrode interface. Platinum has been electroreduced from solution onto glassy carbon substrates [4–6], at carbon/Nafion interfaces [7–11] and into PEMFC electrodes [8–13]. In particular, the electroreduction of platinum from chloroplatinic acid, H_2PtCl_6, has been investigated most thoroughly [4,5,7,8,12,13]. Most notable of these studies is the work of Choi et al. [13], who recently demonstrated the ability to produce ca. 1.5 nm platinum deposits in a preformed electrode using a pulse electrodeposition technique. However, these pulse-platinised electrodes may face the same problem of poor polymer contact as in the case of conventional electrode fabrication.

The cationic platinum salt, $Pt(NH_3)_4^{2+}$ has been used by a few researchers for depositing platinum. Verbrugge [9] investigated platinum electrodeposition from dilute $Pt(NH_3)_4Cl_2$ solutions into preformed catalyst layers and succeeded in depositing most platinum in ca. 10 μm region at the Nafion membrane/electrode interface. An indication of platinum particle size or dispersion was not given, so the possible utilisation of the platinum deposited via this method is uncertain. Taylor and co-workers [10,11] electrodeposited a cationic platinum species into electrodes from solution through a Nafion film and a particle size of 2–3.5 nm was achieved. A ten-fold increase in mass activity was reported in comparison to an E-TEK platinum colloid, which was believed to result from an increase in platinum utilisation.

Platinum has been ion-exchanged into Nafion films from $Pt(NH_3)_4^{2+}$ species and then reduced chemically to produce platinum deposits at the film surfaces [14–17]. Low platinum loadings were possible in some of these methods (e.g. 0.5 mg cm^{-2}), but a small proportion of platinum was lost as isolated particles within the Nafion membrane. $Pt(NH_3)_4^{2+}$ has also been ion-ex-

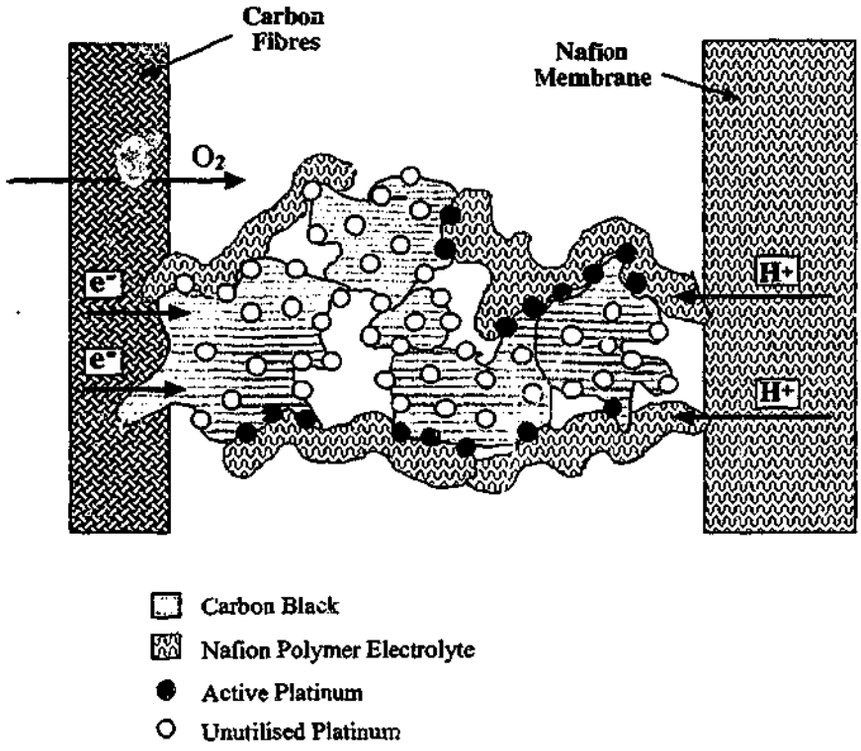

Fig. 1. Schematic diagram of a conventional PEMFC catalyst layer where up to 90% of the platinum may be unutilised.

changed into the surface oxides of a carbon-black [18,19] and then heated in air to form platinum oxides which were subsequently electroreduced. A high surface area resulted from this technique, ca. 100 $m^2 g^{-1}$. However, neither of these ion-exchange methods would be expected to enhance the contact of both carbon and Nafion to each platinum particle deposited.

2. Concept

In the present work, platinum cations were ion-exchanged for the sulfonic acid protons in the Nafion electrolyte within the preformed catalyst layer (Eq. (1)) and subsequently electroreduced onto nearby carbon particles (Eq. (2)):

$$R-(SO_3H)_2 + Pt(NH_3)_4^{2+} \rightarrow R-(SO_3)_2Pt(NH_3)_4 + 2H^+ \quad (1)$$

$$R-(SO_3)_2Pt(NH_3)_4 + C + 2e^- + 2H^+ \rightarrow Pt/C + R-(SO_3H)_2 + 4NH_3 \quad (2)$$

where R = Nafion.

To satisfy the electroreduction step, the platinum particles deposited in this procedure must be electrically connected through the carbon particle network to the porous carbon (gas diffusion) backing of the electrode. It is believed that any such platinum deposited would be accessible to the Nafion electrolyte from which it was reduced, thus forming the three-phase reaction zones required for fuel cell operation.

A high concentration of $Pt(NH_3)_4^{2+}$ solution is used in this procedure to ensure an equilibrium shift towards significant ion-exchange. Furthermore, a reasonably low voltage is applied to the electrode during the electroreduction to increase the reduction kinetics and inhibit diffusion of platinum ions through the Nafion to any existing platinum nuclei (i.e. to limit particle growth). It is also possible to achieve a desired platinum loading using this method by repeating the ion-exchange/reduction process any number of times. Once the platinum has been electroreduced in H_2SO_4, the Nafion is returned to its original protonated form and may be ion-exchanged again as shown by Millet et al. [15].

Provided a small platinum particle size can be maintained, high platinum utilisations should be realised in PEMFC catalyst layers prepared via this method. On achieving higher platinum utilisations, cost reductions in fuel cell stacks may be envisaged through the use of less platinum, or improved fuel cell performances may result under certain conditions, e.g. by preparing thinner catalyst layers.

3. Experimental

$Pt(NH_3)_4Cl_2$ and a 5 wt% Nafion ionomer solution were purchased from Aldrich. Ultrapure water (Milli-Q water treatment system) was used throughout. 5 cm^2 electrodes (non-platinised) were prepared for the ion-exchange/electrodeposition experiments. Catalyst layer loadings of 3.2 mg cm^{-2} were applied to carbon paper substrates from an ultrasonically homogenised ink containing 10 wt% Nafion (dry mass):Vulcan in isopropyl alcohol and water. Vulcan XC-72R carbon black was purchased from Cabot and Toray, TGPH-120 carbon paper was purchased from E-TEK Inc. The electrodes were allowed to dry at room temperature and were then heated at 90°C for 1 h in air to ensure that all the solvent had evaporated.

Additional Nafion ionomer was applied to the catalyst layers to increase the amount of platinum ion-exchanged into the electrodes (i.e. to enhance the overall effect of the method). This additional Nafion was also applied in differing amounts to investigate the effect of Nafion loading on the specific surface area, S (in $m^2 g^{-1}$) of the resulting platinum deposits. The solvent was again removed from the electrodes. A 4 cm^2 electrode prepared in the same fashion, with 20 wt% Pt/Vulcan catalyst from E-TEK Inc. (in place of the uncatalysed Vulcan in the electrodeposited electrodes) was also prepared for comparison.

The cation-exchange was carried out by immersing hydrated catalyst layers in a 0.1 M $Pt(NH_3)_4Cl_2$ solution for 1 h (to ensure equilibrium). Following this process, the electrodes were rinsed with water and held at a potential of -1.0 V (versus the SCE) for 10 min in 0.5 M H_2SO_4.

A number of ion-exchange/electroreduction processes were performed on each electrode (up to 20) to increase the platinum loading. The surface area was checked on a regular basis using cyclic voltammetry (CV). Potentiostatic deposition and CV experiments were performed in a three-electrode cell under a nitrogen atmosphere with a platinum coil counter electrode and a saturated calomel electrode (SCE) as the reference. CV scans for platinum surface area analyses were performed between -0.232 and $+1.0$ V at both 0.05 and 0.1 $V s^{-1}$. Electrochemical surface area (ESA) was calculated from the charge passed ($Q_H = 210$ μC cm^{-2}) in oxidising a full monolayer of adsorbed hydrogen atoms ($Pt-H_{ads}$). Platinum loadings of the three electrodeposited electrodes were determined by AAS. A known Pt-loading was applied to the E-TEK electrode from the 20 wt% Pt/C catalyst. The specific surface area, S, was calculated from the ESA:Pt-loading ratio. Platinum particle diameters, d, were calculated assuming homogeneously dispersed spherical particles [8],

$$d = (65 \times 10^3)(S\rho)^{-1}$$

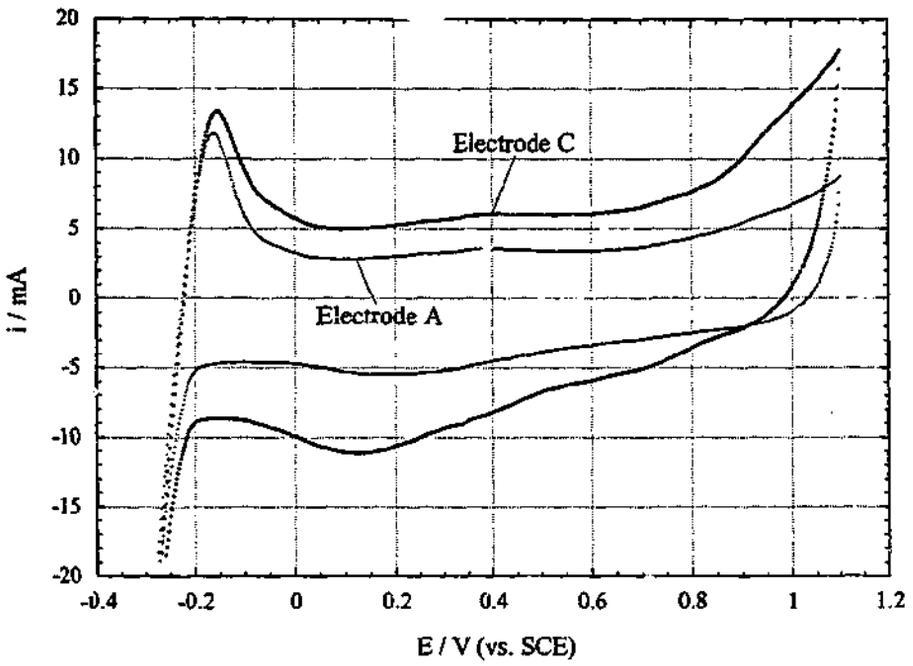

Fig. 2. Cyclic voltammograms of electrodes A and C after one ion-exchange/electroreduction process. These scans were performed at 0.05 V s^{-1} in 0.5 M H_2SO_4. The CVs commenced from −0.3 V (versus SCE) to illustrate the presence of platinum in the electrodes and are shown here only from −0.28 V (at potentials below −0.28 V the sharp cathodic spike continues).

where ρ is the density of platinum, 21.4 g cm^{-3}.

The dispersion of the platinum nuclei was investigated by scanning electron microscopy (SEM) and energy dispersive X-ray spectroscopy (EDXS) was used to confirm the platinum composition of the deposits.

4. Results and discussion

The cyclic voltammograms in Fig. 2 illustrate the platinum electrodeposited after one ion-exchange/electroreduction process. These CVs were recorded after ca. 30 cycles over a similar range. Table 1 shows the characteristics of the three electrodes. For clarity, only electrodes A and C are shown in Fig. 2. A larger double-layer capacitance is observed for electrode C due to the higher Nafion loading in this electrode (and possibly also from a greater mass of platinum deposited). Negligible hydrogen adsorption/oxidation behaviour was observed when sweeping from −0.232 V to more positive potentials, and the current from these reactions is probably obscured by the large double-layer charging in each electrode. To illustrate the presence of platinum in the electrodes, the CVs were scanned from −0.3 V. The large anodic peaks at ca. −0.15 V are not seen in the electrode baseline CVs before platinisation and are likely to have resulted from the oxidation of molecular hydrogen (formed at −0.242 V and below, versus the SCE) on the platinum nuclei.

Table 1
Electrode characteristics

Characteristic	Electrodeposited electrodes[a]			Standard 20% Pt/C
	A	B	C	E-TEK
Total Nafion (wt%)	15	20	29	9
ESA (cm^2 Pt cm^{-2})	22	19	10	325
Pt-loading (μg Pt cm^{-2})	39	54	54	500
S (m^2 Pt g^{-1})	55	36	19	65
d (nm)	5.1	7.8	15	4.3

[a] Measurements conducted on the electrodes after 20 ion-exchange/electroreduction processes.

Fig. 3 shows the cyclic voltammograms of the electrodeposited electrodes after 20 ion-exchange/electroreduction processes. These CV scans all exhibit the characteristic platinum surface reactions as observed on single crystal platinum electrodes [20]. An additional anodic peak is observed at about +0.4 V, due to the oxidation of the surface oxide groups on the carbon, in agreement with Gloaguen et al. [8]. This peak has become larger throughout the number of platinisation processes, most probably resulting from the gradual oxidation of the carbon surface during the surface area CVs conducted after each deposition. The corresponding reduction peak for these carbon surface oxides occurs at ca. +0.22 V. The cyclic voltammograms for each of these electrodes exhibit a gradual increase in the $Pt-H_{ads}$ oxidation peak area between 10 and 20 ion-exchange/reduction processes. However, an accurate determination of the platinum surface area after only a few processes was not possible due to the large amount of double-layer charging in the electrodes.

It is clear from Table 1 that the amount of Nafion in the catalyst layer does affect the platinum electrodeposition, which was expected from the cation-exchange. The specific surface area (S) values in Table 1 indicate that a low Nafion loading is preferable. It is believed that less platinum particle growth is allowed at low Nafion loadings, since less platinum can be exchanged into the electrode. This process may be imagined as an electroreduction from a dilute solution in which the platinum cations are constrained from widespread diffusion (by virtue of the ion-exchange followed by the rapid electroreduction). Fig. 4 illustrates this effect, where smaller platinum particles are produced at lower Nafion loadings.

The specific surface area values in Table 1 indicate the potential for attaining high utilisations of the platinum catalyst deposited via this method. Electrode A shows the highest level of platinum surface area for a given mass (approaching that of the E-TEK electrode) and thus is most likely to achieve the highest utilisation under fuel cell conditions. Furthermore, lower concentrations of Nafion within the catalyst layer may be more desirable (e.g. for achieving better cell performance) by allowing easier gas access to the supported catalyst particles.

The additional exchange/reduction processes may be unnecessary once an ideal combination of the Nafion loading and the $Pt(NH_3)_4^{2+}$ solution concentration is found. For example, higher concentrations of platinum solutions (for increased ion-exchange) may be used with low Nafion loadings to achieve a desired platinum loading. Alternatively, the use of more exchange/reduction processes may prove beneficial in terms of limiting particle growth or in producing a greater dispersion of the platinum deposit.

The SEM micrograph in Fig. 5 shows a high dispersion of platinum particles in the catalyst layer of electrode A. The platinum particle size, however, appears quite large (of the order of several hundred nanometers) which does not agree with the calculated particle

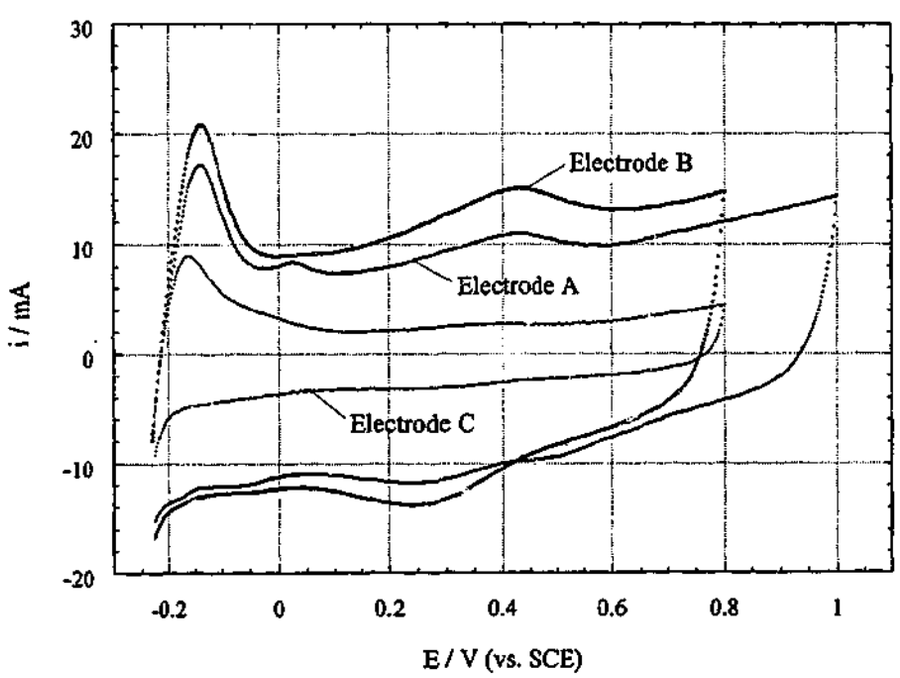

Fig. 3. Cyclic voltammograms of the electrodeposited electrodes after 20 ion-exchange/electroreduction processes. The scan rate was 0.1 $V\,s^{-1}$ and scans commenced from −0.232 V (versus SCE).

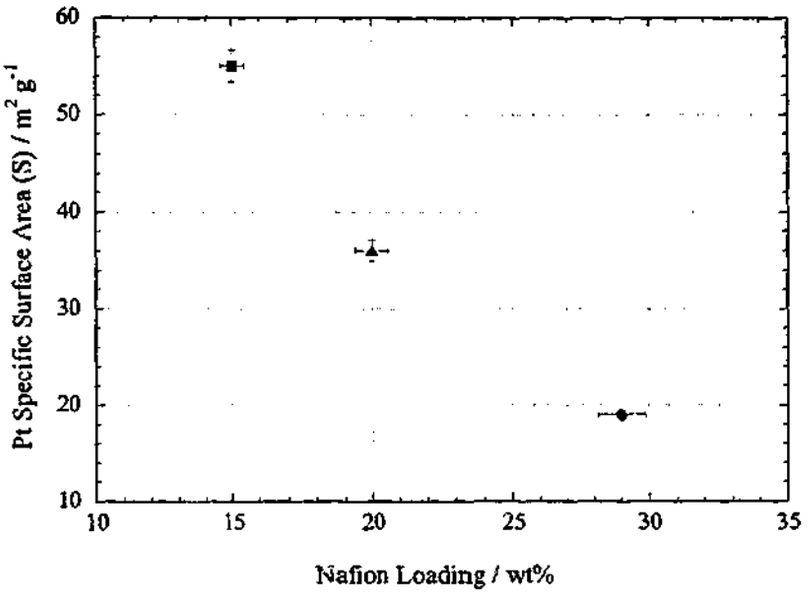

Fig. 4. The effect of Nafion loading on the surface area of the electrodeposited platinum: electrode A (■); electrode B (▲); and electrode C (●).

size from the AAS and surface area analyses. This may be due to the aggregation of platinum particles into clusters such as observed by Ye and Fedkiw [21]. These workers found that platinum particles observed with SEM were almost two orders of magnitude larger than the particle size calculated from the specific surface area, and TEM was used to show the dendritic nature of the platinum clusters.

The $Pt(NH_3)_4^{2+}$ species has been reported to have very slow reduction kinetics [22] and it is possible that these electrodes may not have received enough time to completely electroreduce all of the ion-exchanged platinum. If this were the case, it may account for the low platinum surface areas observed during the initial ion-exchange/reduction processes. Alternatively, a certain amount of deposited platinum may be required in the electrodes before the hydrogen adsorption/desorption peaks begin to appear [6].

5. Conclusions

In this work we have demonstrated the operation of this cation-exchange/electroreduction method. Im-

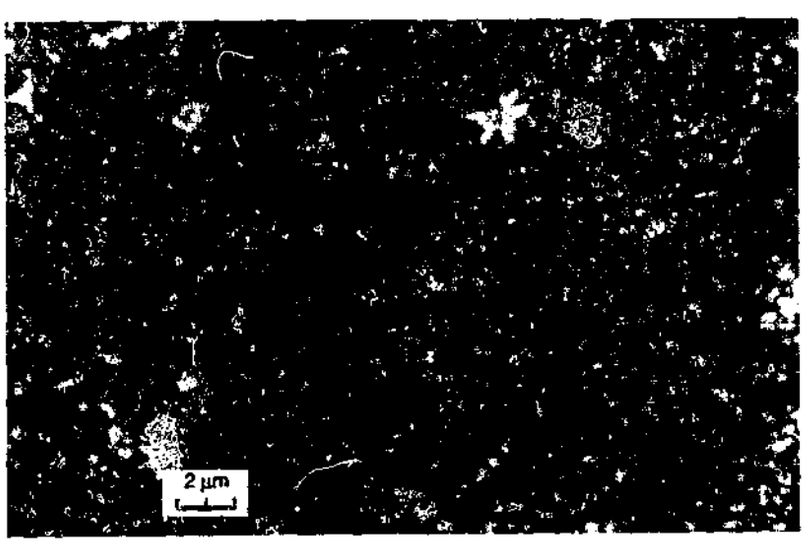

Fig. 5. SEM image of electrode A. The highly dispersed bright particles are platinum as determined by EDXS.

proved platinum utilisation may be enabled in PEMFC electrodes prepared using this technique, via increasing the Nafion/platinum interfacial region throughout the catalyst layer. The high specific surface areas of the electrodeposited platinum indicate the potential for achieving high platinum utilisations. Electrode A, with the lowest Nafion loading, exhibited the greatest platinum surface area for a given mass and is thus most likely to achieve the highest utilisation under fuel cell conditions among the electrodes. This suggests that lower Nafion loadings may limit the growth of platinum particles.

The effect of the platinum solution concentration and its bearing on the amount of platinum exchanged and deposited is currently under investigation. Catalyst layers containing even lower Nafion loadings are also being studied in conjunction with the use of additional exchange/reduction processes. The time allowed for the ion-exchanging process is another variable and shorter times are being trialed.

References

[1] P. Stonehart, Ber. Bunsen-Ges. Phys. Chem. 94 (1990) 913.
[2] S. Srinivasan, O.A. Velev, A. Parthasarathy, D.J. Manko, Appleby, space electrochemical research and technology (SERT) 1991, NASA Conference Publication 3125, April 9–10, 1991.
[3] C.H. Hamann, A. Hamnett, W. Vielstich, Electrochemistry, Weinheim/Wiley/VCH, New York, 1998.
[4] K. Shimazu, D. Weisshaar, T. Kuwana, J. Electroanal. Chem. 223 (1987) 223.
[5] K. Shimazu, K. Uosaki, H. Kita, J. Electroanal. Chem. 256 (1988) 481.
[6] J. Lin-Cai, D. Pletcher, J. Electroanal. Chem. 149 (1983) 237.
[7] K. Itaya, H. Takahashi, I. Uchida, J. Electroanal. Chem. 208 (1986) 373.
[8] F. Gloaguen, J.-M. Léger, C. Lamy, J. Appl. Electrochem. 27 (1997) 1052.
[9] M.W. Verbrugge, J. Electrochem. Soc. 141 (1994) 46.
[10] E.J. Taylor, E.B. Anderson, N.R.K. Vilambi, J. Electrochem. Soc. 139 (1992) L45.
[11] N.R.K. Vilambi, E.B. Anderson, E.J. Taylor, US patent 5,084,144, 1992.
[12] M.P. Hogarth, J. Munk, A.K. Shukla, A. Hamnett, J. Appl. Electrochem. 24 (1994) 85.
[13] K.H. Choi, H.S. Kim, T.H. Lee, J. Power Sources 75 (1998) 230.
[14] R. Liu, W.-H. Her, P.S. Fedkiw, J. Electrochem. Soc. 139 (1992) 15.
[15] P. Millet, M. Pineri, R. Durand, J. Appl. Electrochem. 19 (1989) 162.
[16] P. Millet, F. Andolfatto, R. Durand, J. Appl. Electrochem. 25 (1995) 227 (see also p. 233).
[17] F. Delime, J.M. Léger, C. Lamy, J. Appl. Electrochem. 28 (1998) 27.
[18] K. Kinoshita, P. Stonehart, Modern Aspects of Electrochemistry, vol. 12. Plenum Press, New York, 1977.
[19] K. Kinoshita, Carbon: Electrochemical and Physiochemical Properties, Wiley, New York, 1998.
[20] F.G. Will, J. Electrochem. Soc. 112 (1965) 451.
[21] J.-H. Ye, P.S. Fedkiw, J. Electrochim. Acta 41 (1996) 221.
[22] R. Le Penven, W. Levason, D. Pletcher, J. Appl. Electrochem. 22 (1992) 415.

ELSEVIER

Journal of Electroanalytical Chemistry 515 (2001) 61–70

Journal of Electroanalytical Chemistry

www.elsevier.com/locate/jelechem

Platinum electrodeposition from $H_3Pt(SO_3)_2OH$ solutions

S.D. Thompson [a], L.R. Jordan [a], A.K. Shukla [b], M. Forsyth [a,*]

[a] *School of Physics and Materials Engineering, P.O. Box 69M, Monash University, Victoria 3800, Australia*
[b] *Solid State and Structural Chemistry Unit, Indian Institute of Science, Bangalore 560012, India*

Received 3 April 2001; received in revised form 21 August 2001; accepted 9 September 2001

Abstract

In this work, an investigation into the electrochemistry of $H_3Pt(SO_3)_2OH$ is reported. Platinum was electroreduced from a solution of this complex acid onto glassy carbon (GC) in preliminary experiments and then onto carbon-black (CB) based electrodes as used in polymer electrolyte membrane fuel cells (PEMFCs). The electrodeposited platinum is believed to be poisoned by a sulphide or retained sulphite species. Platinised electrodes were electrochemically cycled between the hydrogen and oxygen evolution potentials in H_2SO_4 solution in order to activate the platinum and obtain a reproducible surface area. Strong oxidation and reduction currents were observed during the potentiodynamic cycling treatments indicating gradual removal of the poisoning species. For a comparison, the poisoning effect of sulphite was investigated on both smooth platinum and Pt/GC electrodes using 1 M $NaHSO_3$ solution. The Pt and Pt/GC electrodes were instantly deactivated in $NaHSO_3$ solution and were cleaned in a manner akin to the Pt/GC electrode prepared from electroreduction of $H_3Pt(SO_3)_2OH$. The platinum redox behaviour and surface area of these sulphite-poisoned electrodes was fully recoverable using the same potentiodynamic cycling treatment. Brief electrodeposition comparisons with other platinum species, viz. H_2PtCl_6 and $Pt(NH_3)_4Cl_2$, are also presented. The platinised electrodes were characterised by cyclic voltammetry, scanning electron microscopy (SEM), and energy dispersive X-ray spectroscopy (EDXS).

Keywords: Platinum electrodeposition; $H_3Pt(SO_3)_2OH$; Sulphito route; Glassy carbon; Carbon-black; Cyclic voltammetry

1. Introduction

High surface area platinum catalysts are used in a number of devices including sensors and polymer electrolyte membrane fuel cells (PEMFCs). For a high utilisation of this noble metal (i.e. the amount of platinum surface area available for reactions relative to the mass of platinum) it is essential to prepare platinum deposits of maximum specific surface area. Accordingly, platinum particles are usually deposited onto a high surface area carbon-black to limit particle agglomeration.

A common method for platinising electrodes is via the chemical reduction of readily available platinum salts such as H_2PtCl_6 or $Pt(NH_3)_4Cl_2$ by $NaBH_4$. Platinum has been deposited onto or into the polymer electrolyte membrane to produce Pt/PEM electrodes using the impregnation–reduction method [1–4]; generally, large platinum particles and films are produced using this method. $NaBH_4$ has also been used to reduce H_2PtCl_6 [5] and to reduce thermally decomposed H_2PtCl_6 [6] onto activated carbon surfaces. Unsupported platinum alloy particles have also been prepared by borohydride reduction [7], whereby the particles are precipitated out of solution and may be made into an electrode using the decal transfer process [8].

Another common way of preparing platinum supported on carbon (Pt/C) with a high specific surface area is via a colloidal method such as the 'sulphito route' [9,10]. In an early stage of this method, chloride is removed from H_2PtCl_6 by converting this platinum salt into $Na_6Pt(SO_3)_4$. The removal of chloride species from PEMFC catalysts is necessary since chloride is known to poison platinum and decrease the adsorption of oxygen, methanol [11], and glucose [12]; chloride is even believed to corrode platinum in acidic media [13].

* Corresponding author. Tel.: +61-3-9905-4939; fax: +61-3-9905-4940.
E-mail addresses: scott.thompson@spme.monash.edu.au (S.D. Thompson), maria.forsyth@spme.monash.edu.au (M. Forsyth).

0022-0728/01/$ - see front matter
PII: S0022-0728(01)00637-4

Meta-stable platinum oxide colloids are then prepared from $Na_6Pt(SO_3)_4$, which precipitate onto suspended carbon-black particles, followed by chemical reduction, e.g. by H_2, to produce the supported Pt/C catalyst [9]. An average platinum particle diameter of 1.5–1.8 nm may be prepared via the sulphito route, although even with particles this small only half of the platinum atoms are at the surface [10] and available to participate in reactions.

Not only is a small particle size desirable for catalytic operation in electrochemical sensors and PEMFCs, but it is also essential for these platinum particles to be located in the three-phase reaction zones. These zones occur throughout the electrode where the electrically connected catalyst (via the carbon network) is in contact with the polymer electrolyte, and this catalyst must also be easily accessed by the reacting species. Catalyst layers are conventionally prepared by drying an ink consisting of Pt/C mixed with a solubilised form of the polymer electrolyte, e.g. Nafion®, onto either the electrode or the polymer membrane, however this method does not ensure polymer contact to all of the platinum particles. Electrodeposition offers an alternative method for preparing active Pt/C catalysts through which greater selectivity may be exercised in the placement of platinum particles into a preformed electrode. However, maintaining a small particle size is a major issue during electrodeposition since after the formation of the initial platinum particles, further platinum reduction onto these is usually favoured.

A number of researchers have studied the electroreduction of platinum from solution onto glassy carbon (GC) substrates [14–19] and into PEMFC electrodes [20–25]. Platinum particles of less than 20 nm have been electrodeposited from $PtCl_6^{2-}$ solutions [14,17–20,25], including the preparation of 1.5 nm sized platinum particles from H_2PtCl_6 solution by Choi et al. [25] using a pulsed-electroreduction method. Under certain conditions, electrodeposition may enable accurate control over the platinum loading deposited onto an electrode. Loadings of 10 $\mu g\,cm^{-2}$ or lower [14,15,17,18,20] and loadings of up to 750 $\mu g\,cm^{-2}$ [14,15,17–20,22–24] have been successfully prepared. The selective electroreduction of platinum at polymer electrolyte | carbon interfaces (to produce the three-phase reaction zones) has also been attempted [17,20,22–24,26]. Taylor and coworkers [23,24] prepared 2–3.5 nm sized platinum particles by electroreducing a cationic platinum salt into a Nafion®-bound carbon-black layer. $Pt(NH_3)_4^{2+}$ has been ion-exchanged into a Nafion® containing electrode followed by electroreduction by Thompson et al. [26]. Verbrugge [22] also explored the selective electroreduction of $Pt(NH_3)_4^{2+}$ into electrodes by utilising the unique chemistry of the carbon | Nafion® interface.

In this paper, we report the platinisation of glassy carbon and carbon-black based electrodes from $H_3Pt(SO_3)_2OH$ solution. The $H_3Pt(SO_3)_2OH$ compound was initially chosen for platinising electrodes because all chloride ions are removed during its preparation [9] and this should enable the preparation of a 'cleaner' platinum catalyst with a higher chemical stability. In addition, to the knowledge of these authors the electrodeposition of this platinum species is the first ever reported in the literature. Surprising results were found, however, in preliminary $H_3Pt(SO_3)_2OH$ electrodeposition experiments, where the resulting platinum deposits appeared to be poisoned. It was then postulated that the species adsorbing on the platinum deposits might, in fact, limit the growth of these particles during the electrodeposition step. Preliminary results of this potential 'poisoning method' are also presented. In addition, comparisons of platinum electrodeposition from aqueous solutions of H_2PtCl_6 and $Pt(NH_3)_4Cl_2$ are provided.

2. Experimental

All electrochemical experiments were performed in a three-electrode cell at room temperature. The cell consisted of a working electrode, a counter electrode (platinum wire, ca. 2 cm immersed in solution), and a saturated calomel reference electrode (SCE, Radiometer). The SCE was separated from the cell by a support tube (Bioanalytical Systems, Inc.) similar to a Luggin capillary, which was filled with 0.5 M H_2SO_4. The glass frit at the base of the SCE tube was spaced at a distance roughly twice its diameter from the working electrode surface. Glassy carbon (GC, BAS Inc.), platinum (Pt, BAS Inc.), or carbon-black (CB) based working electrodes were used. All potentials are reported on the SCE scale. High purity nitrogen was used to flush gases from all solutions for at least 15 min before use and bubbling was continued for the duration of each experiment. Milli-Q water was used throughout in all solutions and rinsings.

GC electrodes were used in preliminary platinum electrodeposition investigations, since GC allows the preparation of a readily reproducible, low surface area carbon support. These GC electrodes (3 mm diameter, embedded in a CTFE[1] cylinder) were polished with a 0.05 μm Al_2O_3 suspension (BAS Inc.) and cleaned ultrasonically in Milli-Q for 5 min at room temperature before each experiment. Baseline cyclic voltammograms of the polished GC electrodes were then recorded in 0.5 M H_2SO_4 to ensure a smooth, reproducible surface (i.e. unchanged over five cyclic voltammograms at 50

[1] Chlorotrifluoroethylene fluoropolymer.

mV s^{-1}) without any evidence of platinum or surface oxide functionalities. These electrodes were scanned extensively in the range −0.23 to +1.2 V and repolished, if necessary. The GC electrodes were then repolished and cleaned ultrasonically before checking via cyclic voltammetry. At this final stage only five baseline CV scans were performed so as to avoid oxidation of the GC surface; in addition, the upper voltage was not allowed to exceed +0.4 V for the same reason. The platinum working electrode (2 mm diameter, embedded in a CTFE cylinder) was polished in a similar fashion to the GC electrodes, and the typical platinum redox behaviour was confirmed via cyclic voltammetry.

The CB based working electrodes were prepared with the conventional electrode design as used in PEMFCs. These electrodes consist of a catalyst layer supported on a diffusion layer, which is in turn supported on porous carbon paper. The catalyst layer is essentially a thin film of polymer electrolyte and carbon-black, which, in the case of the present work, is not platinised. Other than enhancing the diffusion of fuel cell gases into the catalyst layer, the diffusion layer acts as a micro-porous support to the catalyst layer and prevents penetration of the catalyst into the macro-porous carbon paper [27].

A backing layer ink was prepared by suspending 10 wt% PTFE (from a 60 wt% PTFE dispersion in water, Aldrich) and Vulcan XC-72R carbon-black (Cabot) in cyclohexane. This ink was ultrasonically homogenised for ca. 30 min, and a loading of 0.7 mg cm^{-2} was applied to the wet-proofed carbon paper (Toray TGPH-120, E-TEK Inc.). The electrode was dried at ca. 75 °C to constant weight, and then sintered at 350 °C for 30 min. Catalyst layer inks were prepared from a 5 wt% Nafion® solution (Aldrich) and Vulcan XC-72R carbon-black. 1 cm^2 electrodes (geometric area) were prepared by pipetting 2.3 mg cm^{-2} of this ink onto the sintered backing layers and drying the electrodes to correct weight. The ink comprised 10 wt% Nafion® (dry mass):Vulcan in isopropyl alcohol and water, and was ultrasonically homogenised prior to application. The electrodes were allowed to dry at room temperature and were then heated at 90 °C for 1 h to ensure that all the solvent had evaporated.

$Na_6Pt(SO_3)_4$ was prepared from H_2PtCl_6 (99.995%, Aldrich) according to US Patent 4,044,193 [9]. The insoluble white salt was rinsed copiously with warm Milli-Q water to remove any probable impurities such as chloride ions. $Na_6Pt(SO_3)_4$ was then dissolved in 0.5 M H_2SO_4 producing the complex platinum sulphite acid, $H_3Pt(SO_3)_2OH$ [9].

The redox behaviour of the platinum sulphite acid was first studied by cyclic voltammetry on both types of carbon working electrodes using a 0.01 M $H_3Pt(SO_3)_2OH$ in 0.5 M H_2SO_4 solution. Potentiostatic deposition was also performed on the GC and CB based working electrodes from the same platinum solution at low potentials.

After deposition, the platinised electrodes were rinsed in Milli-Q water and placed in 0.5 M H_2SO_4 for an initial investigation. A few cyclic voltammograms at 0.05 V s^{-1} from −0.23 to +1.2 V were performed to check for any reduction of platinum. The electrodes were then potentiodynamically cycled from −0.23 to +1.4 V at 0.05 or 0.5 V s^{-1} for 20–50 scans. Following this treatment, the platinum was again investigated. This two-step procedure was repeated until a reproducible platinum surface area was acquired, i.e. by observing the anodic current peaks resulting from the oxidation of the adsorbed hydrogen monolayer on the platinum surface (Pt–H_{ads}). High flow rates of nitrogen were used to purge solutions of possible gases, e.g. SO_x, H_2S, formed during these cycling treatments, and the 0.5 M H_2SO_4 solution was changed and the electrodes and cell were rinsed at several stages throughout the cycling procedures.

In addition, a solution of 1 M $NaHSO_3$ was prepared in Milli-Q water (ionic strength = 1 M) for a brief investigation into the electrochemistry of sulphite on both smooth Pt and Pt/GC electrodes. 0.01 M solutions of $Pt(NH_3)_4Cl_2$ (99.99%, Aldrich) and H_2PtCl_6 in 0.5 M H_2SO_4 were also prepared for electrodeposition comparisons.

The platinised CB based electrodes were also investigated by scanning electron microscopy (SEM) on a JEOL-840A instrument at an accelerating voltage of 20 kV. Energy dispersive X-ray spectroscopy (EDXS) was used to confirm the platinum composition of the deposits.

3. Results and discussion

Potentiodynamic sweeps illustrating platinum electroreduction onto glassy carbon electrodes from 0.01 M solutions of $H_3Pt(SO_3)_2OH$, $Pt(NH_3)_4Cl_2$, and H_2PtCl_6 in 0.5 M H_2SO_4 are shown in Fig. 1. The platinum sulphite acid reduces onto GC at potentials negative to −0.4 V (Curve II). This onset potential is also observed in the case of $H_3Pt(SO_3)_2OH$ electroreduction onto carbon-black based electrodes (Curve VI in the inset) and the reduction currents are roughly three orders of magnitude greater (cf. Curve II) resulting from the larger surface area of carbon available for platinum deposition. The existence of platinum deposits on the electrodes was confirmed in later analyses from the typical platinum CV 'fingerprint' scans in sulphuric acid [28] and also by EDXS.

$H_3Pt(SO_3)_2OH$ appears to be very stable in comparison with the other two platinum species. $PtCl_6^{2-}$ is readily electroreduced onto GC at potentials negative to +0.2 V (Curve IV in Fig. 1) in agreement with the

literature [17,19]. The $Pt(NH_3)_4^{2+}$ species has not been studied as extensively as chloroplatinic acid and the electroreduction of this species is known to be slow [29] but $Pt(NH_3)_4^{2+}$ appears to reduce at potentials below 0 V (Curve II). The substitution of ammonia ligands for chlorides is known to increase the stability of platinum species [30]. The complexing ability of sulphite probably contributes to the high chemical stability observed for $H_3Pt(SO_3)_2OH$.

Numerous studies reported in the literature have investigated the electroreduction of platinum from $PtCl_6^{2-}$ solutions onto carbon substrates [17,19]. It is well documented that once platinum nuclei have been deposited, further platinum deposition will take place onto existing platinum nuclei since this facilitates reduction at a lesser overpotential in comparison with the carbon substrate. This leads to a positive shift in the onset potential for $PtCl_6^{2-}$ reduction (by 0.2–0.3 V [17,19]) in CV scans following the initial reduction scan. However, in contrast to platinum reduction from $PtCl_6^{2-}$ solutions, no significant change in the onset potential is observed when platinising GC from $H_3Pt(SO_3)_2OH$ solution, which suggests that $H_3Pt(SO_3)_2OH$ does not reduce onto platinum deposits formed from the same platinum species.

A small degree of scatter (~ 0.05 V) was observed between the onset potentials of the initial reduction scans of $H_3Pt(SO_3)_2OH$ onto freshly polished GC electrodes. These minor variations in onset potentials can probably be explained by hydrogen evolving on the initial platinum deposits since pure platinum electrodes in acidic solutions rapidly evolve hydrogen at potentials negative to -0.25 V resulting in strong cathodic currents. It was also found that the electroreduction onset potential was very sensitive to minute traces of platinum remaining on the GC electrodes after polishing. Even if CV scans of polished GC electrodes displayed no platinum oxidation/reduction behaviour nor hydrogen adsorption/desorption reactions, baselines such as Curve I were recorded in 0.5 M H_2SO_4. Trace amounts of platinum will result in strong cathodic currents, probably from hydrogen evolution, and if $H_3Pt(SO_3)_2OH$ is reduced onto such electrodes slightly higher onset potentials are observed.

In a further contrast between platinum electrodeposition from $H_3Pt(SO_3)_2OH$ and $PtCl_6^{2-}$ solutions, no evidence of platinum was observed when GC electrodes were cycled at 0.02 V s^{-1} in the $H_3Pt(SO_3)_2OH + H_2SO_4$ solution regardless of the number of reduction cycles performed. In the case of platinum electroreduction from $K_2PtCl_6 + H_2SO_4$ solution, Pt–H_{ads} oxidation peaks appear on the return sweep of all CV scans [17,19].

The electroreduction reaction of $H_3Pt(SO_3)_2OH$ might be described by Eq. (1). The production of sulphite ions (SO_3^{2-}) or other sulphur-containing species during platinisation may lead to the poisoning of platinum nuclei by sulphide (S^{2-}) ions, a known platinum poison [31–33]. Sulphide ions could result from the reduction of sulphite in accordance with Eq. (2) at potentials negative to -0.01 V [34]. Since this reaction would occur in the same potential region as $Pt(SO_3)_2^{2-}$

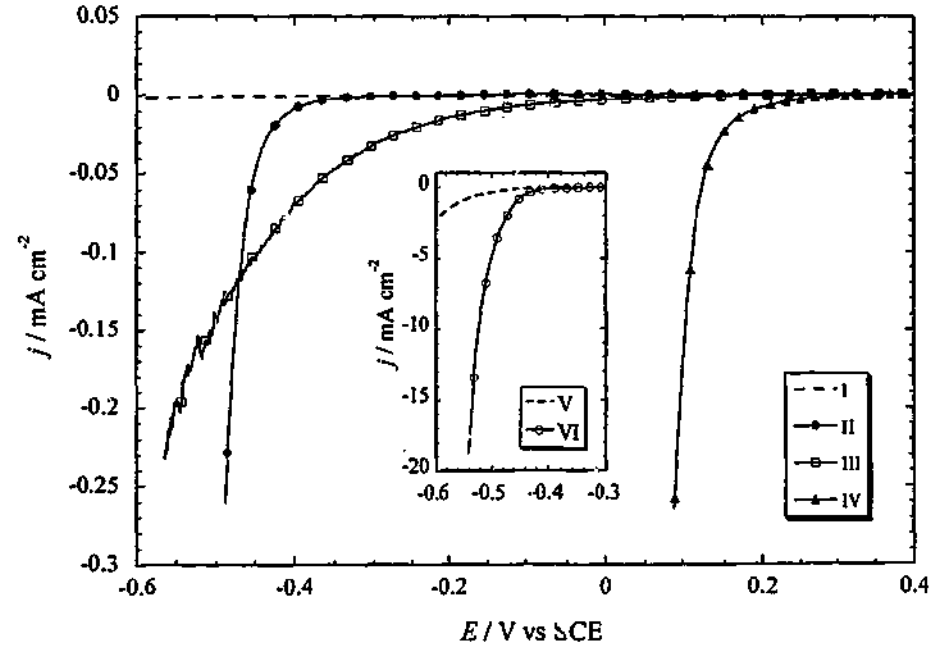

Fig. 1. Linear-sweep electroreduction of platinum from aqueous solutions onto GC and CB based electrodes. Curves I and V (inset) show the respective baselines of the GC and CB electrodes in 0.5 M H_2SO_4. Curves II–IV show platinum electroreduction onto GC from 0.01 M solutions of $H_3Pt(SO_3)_2OH$, $Pt(NH_3)_4Cl_2$ and H_2PtCl_6 in 0.5 M H_2SO_4, respectively. Curve VI (inset) shows platinum electroreduction from a 0.01 M $H_3Pt(SO_3)_2OH + 0.5$ M H_2SO_4 solution onto a CB based electrode. Scan rate: 0.001 V s^{-1}.

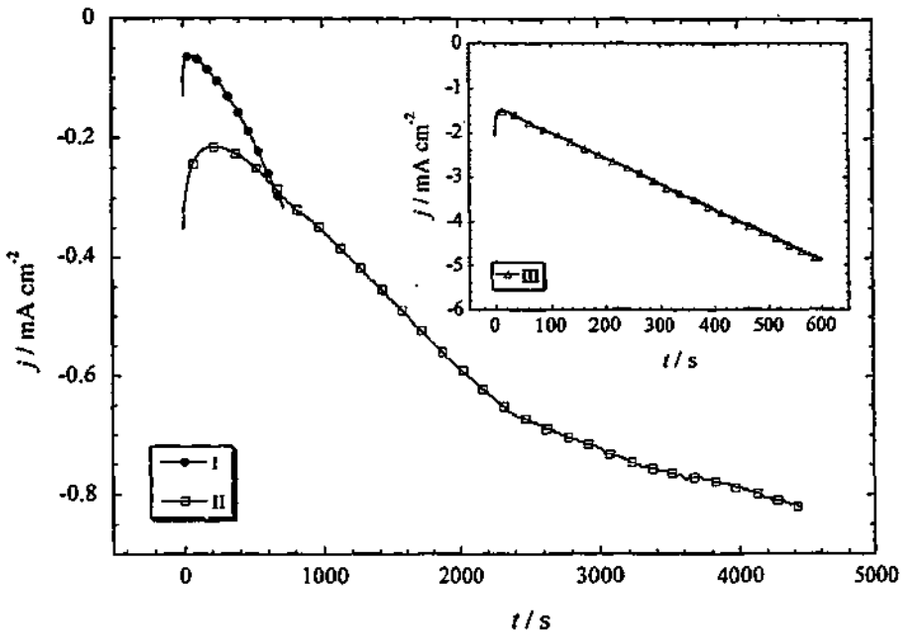

Fig. 2. Current density–time transients for the potentiostatic reduction of platinum at −0.45 V vs. SCE, from a 0.01 M $H_3Pt(SO_3)_2OH$ + 0.5 M H_2SO_4 solution: onto GC electrodes, 'GC1' and 'GC2' (Curves I and II), and onto a CB based electrode, 'CB1' (Curve III in the inset). Curves I and II were obtained under identical conditions from separately polished GC electrodes and highlight the reproducibility issues of $H_3Pt(SO_3)_2OH$ electrodeposition.

electroreduction it may occur concomitantly, and platinum could be poisoned immediately after deposition.

$$Pt(SO_3)_2^{2-} + 2e^- \rightarrow Pt^0 + 2SO_3^{2-} \quad (1)$$

$$SO_3^{2-} + 6e^- + 6H^+ \rightarrow S^{2-} + 3H_2O \quad (2)$$

Fig. 2 shows the current density–time (j–t) transients for the potentiostatic reduction of $H_3Pt(SO_3)_2OH$ onto both GC (Curves I and II) and CB based electrodes (Curve III shown as inset) at −0.45 V. This relatively low potential was used because at this potential the reduction of $H_3Pt(SO_3)_2OH$ appears significant (compare the reduction current density in Curve II of Fig. 1 with the GC baseline, Curve I). The three curves in Fig. 2 have an unusual appearance on comparison with previous studies of $PtCl_6^{2-}$ electroreduction [20,21], where the long-term reduction current has been shown to be constant over time. On the other hand, curves I–III display a marked increase in the cathodic current density over time, which suggests other reactions are occurring simultaneously with the platinum electroreduction. Additional cathodic current may have arisen from hydrogen evolving on the deposited platinum. Another reaction, which could contribute to the cathodic currents along with platinum reduction and hydrogen evolution, is the reduction of sulphite to sulphide according to Eq. (2).

Fig. 3 shows the CV analysis of a Pt/GC electrode which was platinised as shown by Curve II in Fig. 2. A longer time for reduction was allowed compared with Curves I and III, to enable a higher platinum loading. Curve I in Fig. 3 shows the second cyclic voltammogram in 0.5 M H_2SO_4 at 0.05 $V s^{-1}$ which was scanned to an upper potential of + 1.4 V. Several scans were performed before Curve I with upper potentials less than + 1.4 V but these did not show any evidence of characteristic platinum surface reactions. However, when the Pt/GC electrode was scanned from −0.3 V to more positive potentials, a sharp cathodic spike was observed followed by an anodic peak at potentials negative to 0 V. This cathodic spike most probably originated from hydrogen evolution and the anodic peak may have arisen from the oxidation of a small amount of either evolved or adsorbed hydrogen, and both of these anodic and cathodic currents suggest the presence of platinum. Clear signs of the deposited platinum are visible in Curve I (Fig. 3), in particular, the strong anodic peak between + 0.6 and + 1.3 V which is in the potential range for the formation of platinum surface oxides ($Pt–O_{ads}$), and also by the strong cathodic peak at + 0.45 V which normally represents the reduction of $Pt–O_{ads}$. Curve I also exhibits strong cathodic current densities between + 0.25 and -0.23 V, representing the reduction of some species. The current density spikes at around −0.23 and + 1.4 V are assigned to the evolution of hydrogen and oxygen, respectively.

Curve II in Fig. 3 displays the fifth cyclic voltammogram scanned to an upper potential of + 1.4 V, i.e. three scans after Curve I was recorded. In Curve II, the magnitudes of the strong oxidation and reduction current densities observed in Curve I have decreased and the $Pt–H_{ads}$ formation/oxidation peaks between −0.23

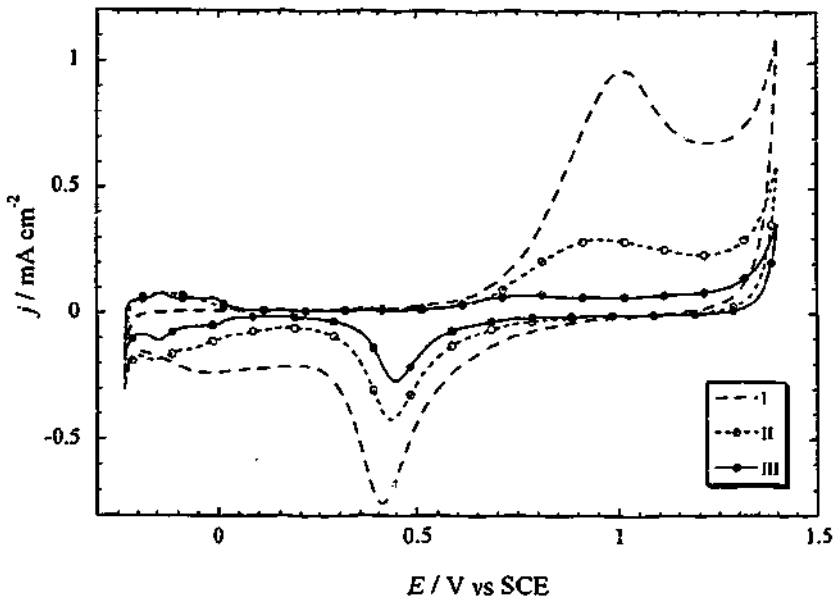

Fig. 3. Cyclic voltammograms in 0.5 M H_2SO_4 illustrating the cleaning of the Pt/GC electrode 'GC2' platinised as shown by Curve II in Fig. 2. Curve I shows the second CV scanning to a potential of +1.4 V, Curve II shows the fifth CV. Curve III was performed after 50 similar CV scans after resting in mQ water for 12 h, and shows the cleaned Pt/GC. Scan rate: 0.05 V s^{-1}.

and +0.1 V have become visible. Curve III in Fig. 3 shows a CV scan of the completely cleaned Pt/GC electrode which was recorded after a further 50 scans similar to those applied to produce Curve II, the final 10 scans of which were performed the following day after the electrode was rested overnight (~14 h) in Milli-Q water. This curve exhibits the typical platinum CV 'fingerprint' and all of the hydrogen and oxygen reactions on the platinum surface are clearly visible. After continued cycling of this Pt/GC electrode, no further increase in the platinum surface area was observed on comparison with Curve III. Instead, during this cycling procedure, the current density due to the electrical double-layer charging on the electrode (j_{dl}) gradually increased along with anodic and cathodic peaks at around +0.35 V, representing the oxidation and reduction of surface functionalities on the glassy carbon.

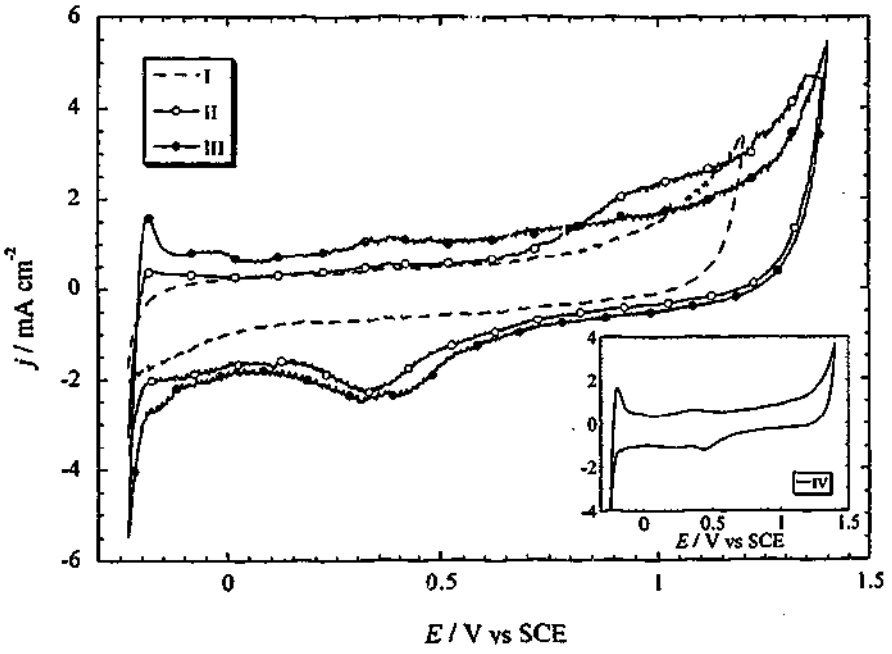

Fig. 4. Cyclic voltammograms in 0.5 M H_2SO_4 illustrating the cleaning of the Pt/CB electrode 'CB1' platinised as shown by Curve III (inset) in Fig. 2. Curve I shows the second CV scanning to a potential of +1.2 V, Curve II shows the second CV scanning to +1.4 V, and Curve III shows the cleaned Pt/GC, after 25 similar CV scans. Curve IV (inset) illustrates another cleaned Pt/CB electrode platinised in the same way. Scan rate: 0.05 V s^{-1}.

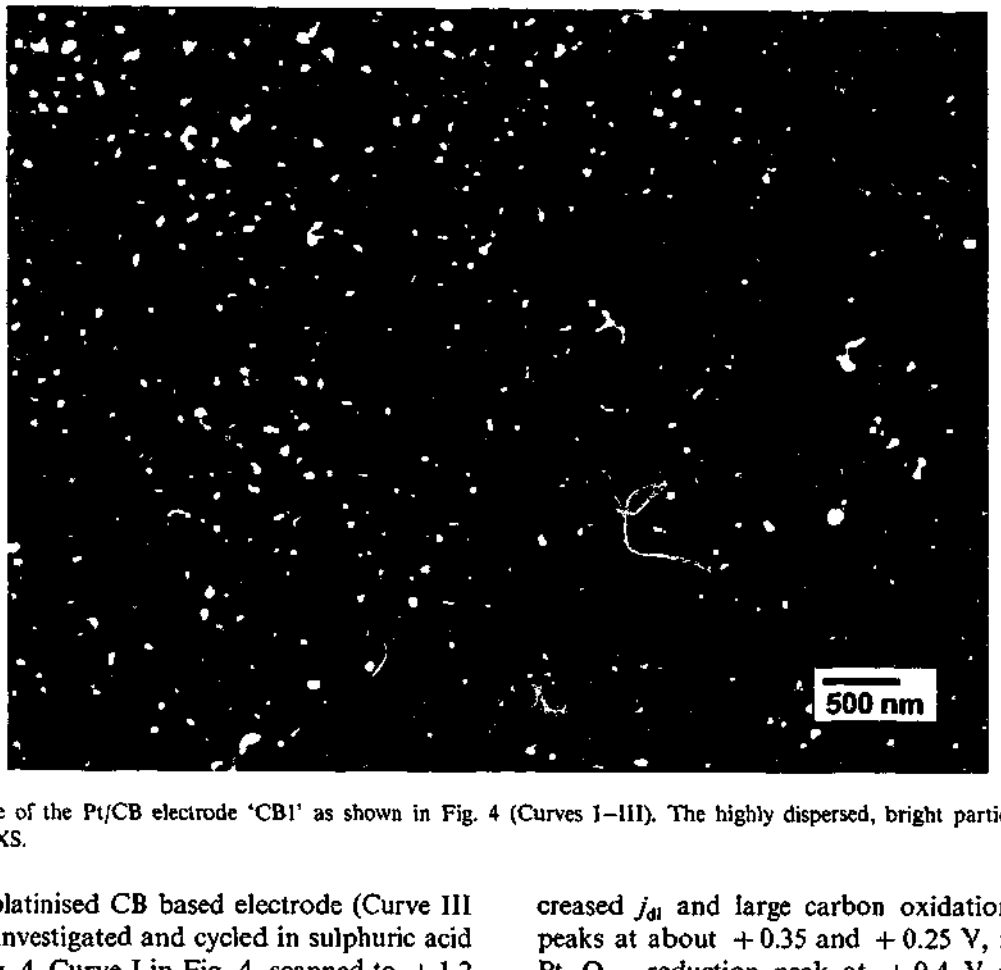

Fig. 5. SEM image of the Pt/CB electrode 'CB1' as shown in Fig. 4 (Curves I–III). The highly dispersed, bright particles are platinum as determined by EDXS.

Similarly, a platinised CB based electrode (Curve III in Fig. 2), was investigated and cycled in sulphuric acid as shown in Fig. 4. Curve I in Fig. 4, scanned to + 1.2 V, displays negligible platinum redox behaviour. Only the cathodic current densities at potentials less than 0 V and the anodic current densities at potentials greater than about + 0.8 V suggest any platinum presence. In the second CV scanned to + 1.4 V (Curve II), current density peaks in the regions for hydrogen and oxygen adsorption/desorption are visible. Curve III in Fig. 4 shows the cleaned Pt/CB electrode after 25 similar scans. Continued cycling was again performed on this electrode (cf. the Pt/GC electrode previously discussed) but no further increase in the platinum surface area was observed; the additional scans merely caused an increased j_{dl} and large carbon oxidation and reduction peaks at about + 0.35 and + 0.25 V, respectively. The $Pt-O_{ads}$ reduction peak at + 0.4 V merges with the reduction peak of the oxidised GC surface groups in Curve III. These separate cathodic peaks can be seen with more clarity in a CV scan of another Pt/CB electrode (Curve IV, inset to Fig. 4), which was platinised from $H_3Pt(SO_3)_2OH$ solution in the same way. The faster cleaning of the Pt/CB electrode compared with that of the Pt/GC electrode may be explained by the fact of less time for the potentiostatic deposition and possibly less time for the deposited platinum to be poisoned in the case of the Pt/CB electrode.

Fig. 5 displays a typical SEM micrograph of the cleaned Pt/CB electrode shown by Curve III in Fig. 4.

Table 1
Characteristics of the electrodes platinised from a 0.01 M $H_3Pt(SO_3)_2OH$ + 0.5 M H_2SO_4 solution at −0.45 V

Electrode	A_g/cm^2	t_{red}/s	Q_r/C	W/μg	A_r/cm^2	R_f	S/m^2 g^{-1}	d/μm
GC1	0.071	720	0.008	8.0	0.022	0.31	0.28	1.0
GC2	0.071	4450	0.18	180	0.082	1.2	0.046	6.1
CB1	1.0	600	1.8	1870	6.2	6.2	0.33	0.85

A_g, geometric area of the electrodes; t_{red}, time for potentiostatic reduction: Q_r, charge passed; W, platinum loading determined from the charge transferred (assuming a 2 electron transfer per platinum atom deposited); A_r, electrochemical surface area of the cleaned platinum determined from the charge passed in oxidising a full monolayer of adsorbed hydrogen, $Pt-H_{ads}$ (assuming $Q_{11} = 210$ μC cm^{-2}); R_f, roughness factor of the platinum deposits (i.e. the ratio of A_r to A_g); S, specific surface area (i.e. the ratio of A_r to W); d, estimate of the platinum particle diameter, assuming homogeneously dispersed spherical deposits [20], from the equation, $d = (6 \times 10^3)(S\rho)^{-1}$, where ρ is the density of platinum, 21.4 g cm^{-3}.

The bright particles throughout this image were confirmed to be platinum by EDXS analysis. The average platinum particle diameter is approximately 50 nm, considerably larger than desired. However, it may be possible to reduce this particle size under optimised conditions. It is also possible that these particles observed in the SEM micrograph are actually aggregates of smaller platinum particles [19].

Table 1 shows the characteristics of the GC and CB based electrodes which were platinised potentiostatically from a $H_3Pt(SO_3)_2OH$ solution at -0.45 V. As one can observe in this table, the specific surface areas (S) are quite low, and the estimates of the platinum particle diameters (d) are very large. In fact, the estimated platinum particle size for the CB1 electrode is around 20 times greater than the 50 nm approximate size observed in the SEM image of Fig. 5. On comparison with the GC electrodes, the d estimates appear up to two orders of magnitude greater than these particles observed in the CB based electrode. Unfortunately, SEM analysis was not possible with these platinised GC electrodes since removing such small deposits proved impossible, and cutting the electrodes shattered the surface of the GC. As discussed before, the deposition charge, Q_r, is thought to contain significant contributions from parasitic processes such as sulphite reduction and hydrogen evolution, and this may account for the large discrepancy. If an average platinum particle size of 50 nm is assumed, then an S value of 5.6 $m^2\,g^{-1}$ would be more representative of these electrodes. This value is still relatively low compared to a commercially available catalyst from E-TEK, Inc. [26].

On comparing the platinised GC1 and GC2 electrodes, the particle size does appear to increase with an increase in the platinum loading, which suggests the poisoning process may not completely prevent particle growth (although the calculation of d is dependent on W which is unlikely to be accurate given the above discussion). Indeed, from Fig. 5 some particle growth is evident. The lower S value for the GC2 electrode compared to GC1 is also uncertain, since one cannot be sure how much of the deposition charge is from platinum reduction. The platinum surface area (A_r) of GC2 is not much larger than that of GC1. It is possible that if the GC2 electrode was well platinised and poisoned, and could therefore not facilitate further platinum reduction, then the remaining charge could have arisen largely from other reactions such as hydrogen evolution.

Attempts were made to deposit Pt at higher potentials, including -0.2, 0, $+0.1$ V, but even when the voltage was applied for up to 1 h no evidence of platinum was found after the subsequent potential cycling of the electrodes. Since the platinum loadings calculated from the j–t transients are prone to overestimation, the roughness factor provides more information on the platinum deposits. The R_f for a 20 wt% Pt/C E-TEK catalyst was found in other work to be 325 [26] which is considerably greater than that of 6.2 for the CB1 electrode. The R_f for the CB1 electrode compares more favourably with the work of Gloaguen et al. [20], where platinum loadings into Nafion®-bound CB electrodes ranged between 3 and 39 $\mu g\,cm^{-2}$ with roughness values between 1.9 and 5.9, respectively.

The gradual increase in the platinum surface area as represented by the $Pt–H_{ads}$ oxidation peak during the scanning between -0.23 and $+1.4$ V appears to indicate the activation of the platinum surface. In addition, the strong anodic and cathodic currents in the regions of $+1.0$ and $+0.2$ V, respectively, in Figs. 3 and 4 were observed to decrease with more potential cycling and this also appears representative of the gradual platinum cleaning. Similar oxidation and reduction currents have been observed with sulphide-poisoned platinum electrodes in both H_2SO_4 and H_3PO_4 solutions [32,33].

Hence, from the various phenomena observed throughout this $H_3Pt(SO_3)_2OH$ electrodeposition study and, in particular, the unaltered onset for reduction and the required activation of the deposited platinum via potential cycling, it would appear that a passivation process is occurring on the platinum deposited from $H_3Pt(SO_3)_2OH$ solution. It is possible that the deposited platinum may have retained some sulphite ligands or adsorbed these after reduction. According to Eq. (2) and at these low potentials, the adsorbed species is likely to be sulphide. The effect of sulphite ions on both smooth platinum and Pt/GC electrodes was investigated in separate experiments using a 1 M $NaHSO_3$ solution. Platinum poisoning was evident in the first CV scans of each electrode by the complete lack of hydrogen adsorption and oxidation peaks. The electrodes remained poisoned after rinsing in Milli-Q water and being transferred to sulphuric acid solution for analysis. Again, the reduction of sulphite to sulphide is likely to have occurred during these experiments in $NaHSO_3$ solution where the electrodes were scanned to -0.23 V. Whilst cycling the poisoned electrodes in 0.5 M H_2SO_4, oxidation and reduction current densities similar to those in Fig. 3, Curve II were observed. However, after 10 sweeps in the -0.23 to $+1.2$ V range, the platinum surface had almost completely recovered as is observed from the restoration of the typical platinum CV 'fingerprint'. Similarly to the previous discussion, the additional anodic and cathodic current is believed to correspond to the oxidative/reductive removal of the adsorbed species which in this case is either sulphite or sulphide ions.

The potentiodynamic cycling of the electrodes platinised from $H_3Pt(SO_3)_2OH$ solution was found to be

the most effective method for activation, compared with either static potential approaches or heating the platinised electrodes. A minor improvement was observed in the Pt–H_{ads} oxidation peak area after applying potentials of +1.0 or +1.2 V to the Pt/GC electrode for 5–10 min. However, sweeping from -0.23 to +1.2 V at 0.05 $V s^{-1}$ for the same duration appeared to clean platinum more rapidly. Potentiostatic holds at −0.2 or −0.3 V for the same time yielded negligible improvement. Similar findings have been observed in the work of Loucka [33] who attempted to oxidise a poisoning sulphur species from platinum by holding the electrode potential at 1.35 V for 10 min. Loucka found that the sulphur was not completely removed from the electrode even though the currents for sulphur oxidation had fallen to zero and cycling was required for complete platinum activation. Alternating polarisation approaches have also been used to activate platinum, e.g. switching the potential of a platinum electrode between +0.07 and +1.27 V in presence of sulphite ions [35]. In addition, no effect was found in this work from heating Pt/GC electrodes poisoned in $NaHSO_3$ solution, even when they were heated for up to 15 h in air at 100 °C.

Furthermore, cleaning was observed to occur more rapidly when an upper potential of +1.4 V was used whereby the maximum oxidation of the poisoning species is attained in each cycle. The oxidation probably proceeds via the formation of Pt–O_{ads}, where strong anodic current densities are observed at potentials positive to +0.6 V (Curve I in Fig. 3). It is known that sulphide adsorbs onto platinum and may be removed by being initially oxidised to elemental sulphur followed by further oxidation by oxygen evolution to SO_4^{2-}, $S_2O_6^{2-}$, and $S_2O_3^{2-}$ ions [31] or to SO_4^{2-} and SO_3 species [33]. The Pt electrode remains passivated due to a thin oxide layer and must then be reduced. At high surface coverages of adsorbed sulphur, it is necessary to repeat these oxidation and reduction steps, i.e. to cycle the electrode potential in order to remove all of the poisoning species completely.

Faster scanning rates, e.g. 0.5 $V s^{-1}$, were found to enhance slightly the cleaning time (i.e. the time of cycling required until clean platinum deposits were obtained) of the platinised electrodes. However, scanning at rates faster than 0.5 $V s^{-1}$ or to potentials greater than +1.4 V was avoided since this resulted in an apparent loss in the platinum surface area, i.e. a decrease in the Pt–H_{ads} oxidation peak area. In the work of Loucka [33] the rate of potential scanning was found to have no effect on the cleaning of sulphide-poisoned platinum, where scanning rates were varied between 6.7×10^{-3} $V s^{-1}$ and 30 $V s^{-1}$. Cycling to potentials negative to −0.3 V was also avoided in this work since this merely resulted in a large amount of evolved hydrogen and negligible improvement in activating the platinum deposits. It should also be noted that these activated Pt/GC and Pt/CB electrodes were analysed again a day later and several weeks later after resting in Milli-Q water and the final platinum surface area was reproducible. Any faceting or roughening caused by the electrochemical cycling is therefore discounted and the increase in platinum surface area is believed to be wholly due to the cleaning process.

4. Conclusions

The potentiodynamic sweeping of platinum electrodes between the hydrogen and oxygen evolution potentials is a standard electrochemical procedure [28] and provides a clean, reproducible platinum surface. In this work, however, a greater number of potential sweeps were required in order to obtain a reproducible platinum surface. It is believed that this resulted from a poisoning species (possibly sulphide or sulphite) which was gradually removed via the cycling regime.

During the electroreduction of $H_3Pt(SO_3)_2OH$, the poisoning effect may prove beneficial in limiting platinum particle growth, and could result in the deposition of very small, dispersed particles. This poisoning effect is being investigated further by surface techniques such as X-ray photoelectron spectroscopy. In addition, the electrodeposition of the meta-stable platinum oxide colloid [9] is currently being attempted and the selective deposition of small particles preferably less than 2 nm at the three-phase reaction zones may yield improvements in platinum utilisation.

This potentiodynamic cycling procedure for activating platinum may also be used to reactivate fuel cell electrodes poisoned by impurities in gas streams. The platinum may be poisoned by sulphur impurities such as H_2S in hydrogen produced from reformed fossil fuels or, in the case of the direct methanol fuel cell (DMFC) platinum may be poisoned by sulphur impurities in the methanol supply. The preferred use of 'logistics' fuels such as diesel by the defence force also encounters the issue of platinum deactivation via adsorbed sulphides and it is possible that an electrochemical cycling procedure, similar to that used in this work and elsewhere [32,33], could be useful to reactivate fuel cell electrodes in the field.

References

[1] F. Delime, J.M. Léger, C. Lamy, J. Appl. Electrochem. 28 (1998) 27.
[2] S.-A. Sheppard, S.A. Campbell, J.R. Smith, G.W. Lloyd, T.R. Ralph, F.C. Walsh, Analyst 123 (1998) 1923.
[3] P. Millet, F. Andolfatto, R. Durand, J. Appl. Electrochem. 25 (1995) 233.

[4] R. Liu, W.-H. Her, P.S. Fedkiw, J. Electrochem. Soc. 139 (1992) 15.
[5] D.K. Rogers, US Patent, 4,379,034, 1983.
[6] A.K. Shukla, R. Manoharan, Indian Patent, 170,423, 1992.
[7] K.L. Ley, R. Liu, C. Pu, Q. Fan, N. Leyarovska, C. Segre, E.S. Smotkin, J. Electrochem. Soc. 144 (1997) 1543.
[8] M.S. Wilson, S. Gottesfeld, J. Appl. Electrochem. 22 (1992) 1.
[9] H.G. Petrow, R.J. Allen, US Patent, 4,044,193, 1977.
[10] P. Stonehart, Ber. Bunsenges. Phys. Chem. 94 (1990) 913.
[11] V.S. Bagotzky, Yu.B. Vassilyev, J. Weber, J.N. Pirtskhalava, J. Electroanal. Chem. 27 (1970) 31.
[12] E.M. Skou, Acta. Chem. Scand. 27 (1973) 2239.
[13] A.N. Chemodanov, Ya.M. Kolotyrkin, Proceedings of the 3rd European Symposium on Corrosion Inhibitors, Ferrara, Italy, 1970, p. 49.
[14] K. Shimazu, K. Uosaki, H. Kita, J. Electroanal. Chem. 256 (1988) 481.
[15] K. Shimazu, D. Weisshaar, T. Kuwana, J. Electroanal. Chem. 223 (1987) 223.
[16] J. Lin-Cai, D. Pletcher, J. Electroanal. Chem. 149 (1983) 237.
[17] K. Itaya, H. Takahashi, I. Uchida, J. Electroanal. Chem. 208 (1986) 373.
[18] A.A. Mikhaylova, O.A. Khazova, V.S. Bagotzky, J. Electroanal. Chem. 480 (2000) 225.
[19] J.-H. Ye, P.S. Fedkiw, Electrochim. Acta 41 (1996) 221.
[20] F. Gloaguen, J.-M. Léger, C. Lamy, J. Appl. Electrochem. 27 (1997) 1052.
[21] M.P. Hogarth, J. Munk, A.K. Shukla, A. Hamnett, J. Appl. Electrochem. 24 (1994) 85.
[22] M.W. Verbrugge, J. Electrochem. Soc. 141 (1994) 46.
[23] E.J. Taylor, E.B. Anderson, N.R.K. Vilambi, J. Electrochem. Soc. 139 (1992) L45.
[24] N.R.K. Vilambi, E.B. Anderson, E.J. Taylor, US Patent 5,084,144, January 28, 1992.
[25] K.H. Choi, H.S. Kim, T.H. Lee, J. Power Sources 75 (1998) 230.
[26] S.D. Thompson, L.R. Jordan, M. Forsyth, Electrochim. Acta 46 (2001) 1657.
[27] L.R. Jordan, A.K. Shukla, T. Behrsing, N.R. Avery, B.C. Muddle, M. Forsyth, J. Appl. Electrochem. 30 (2000) 641.
[28] F.G. Will, J. Electrochem. Soc. 112 (1965) 451.
[29] R. Le Penven, W. Levason, D. Pletcher, J. Appl. Electrochem. 22 (1992) 415.
[30] A.J. Bard, in: A.J. Bard (Ed.), Encyclopedia of the Electrochemistry of the Elements, vol. 6, Marcel Dekker, New York, 1976 (Ch. 4).
[31] H. Gerischer, in: A.J. Bard (Ed.), Encyclopedia of the Electrochemistry of the Elements, vol. 4, Marcel Dekker, New York, 1975 (Ch. 6).
[32] D.-T. Chin, P.D. Howard, J. Electrochem. Soc. 133 (1986) 2447.
[33] T. Loucka, J. Electroanal. Chem. 31 (1971) 319.
[34] G. Valensi, J. van Muilder, M. Pourbaix, in: A.J. Bard (Ed.), Encyclopedia of the Electrochemistry of the Elements, vol. 4, Marcel Dekker, New York, 1975 (Ch. 6).
[35] K.I. Rosental', V.I. Veselovskij, Zh. Fiz. Khim. 27 (1953) 1163.

Appendix B

Air Pollution Sources, Health Effects and Possible Control Measures

Pollutant	*Sources*	*Effects*	*Prevention and Control*
Ozone (O_3)	Formed when reactive organic gases (ROG) and nitrogen oxides react in the presence of sunlight. ROG sources include any source that burns fuels (e.g., gasoline, natural gas, wood, oil); solvents; petroleum processing and storage; and pesticides	Breathing difficulties, lung tissue damage, damage to rubber and some plastics.	Reduce motor vehicle reactive organic gas (ROG) and nitrogen oxide emissions through emissions standards, reformulated fuels, inspections programs, and reduced vehicle use. Limit ROG emissions from commercial operations and consumer products. Limit ROG and NO_x emissions from industrial sources such as power plants and refineries. Conserve energy
Respirable Particulate Matter (PM_{10})	Road dust, windblown dust, agriculture and construction, fireplaces. Also formed from other pollutants (acid rain, NO_x, SO_x, organics). Incomplete combustion of any fuel.	Increased respiratory disease, lung damage, cancer, premature death, reduced visibility, surface soiling.	Control dust sources, industrial particulate emissions, wood burning stoves and fireplaces. Reduce secondary pollutants which react to form PM_{10}. Conserve energy

Fine Particulate Matter ($PM_{2.5}$)	Fuel combustion in motor vehicles, equipment, and industrial sources; residential and agricultural burning. Also formed from reaction of other pollutants (acid rain, NO_x, SO_x, organics).	Increases respiratory disease, lung damage, cancer, premature death; reduced visibility; surface soiling.	Reduce combustion emissions from motor vehicles, equipment, industries, and agriculture and residential burning. Precursor controls, like those for ozone, reduce fine particle formation in the atmosphere.
Carbon Monoxide (CO)	Any source that burns fuel such as automobiles, trucks, heavy construction equipment and farming equipment, residential heating.	Chest pain in heart patients, headaches, reduced mental alertness	Control motor vehicle and industrial emissions. Use oxygenated gasoline during winter months. Conserve energy.
Nitrogen Dioxide (NO_2)	See Carbon Monoxide	Lung irritation and damage. Reacts in the atmosphere to form ozone and acid rain	Control motor vehicle and industrial combustion emissions. Conserve energy.
Lead	Metal smelters, resource recovery, leaded gasoline, deterioration of lead paint	Learning disabilities, brain and kidney damage	Control metal smelters, No lead in gasoline. Replace leaded paint with non-lead substitutes.
Sulfur Dioxide (SO_2)	Coal or oil burning power plants and industries, refineries, diesel engines	Increases lung disease and breathing problems for asthmatics. Reacts in the atmosphere to form acid rain.	Reduce the use of high sulfer fuels (e.g., use low sulfer reformulated diesel or natural gas). Conserve energy.

Visibility Reducing Particles	See $PM_{2.5}$	Reduces visibility (e.g., obscures mountains and other scenery), reduced airport safety, lower real estate value	See $PM_{2.5}$
Sulfates	Produced by the reaction in the air of SO_2 (see SO_2 sources), a component of acid rain	Breathing difficulties, aggravates asthma, reduced visibility	See SO_2
Hydrogen Sulfide	Geothermal power plants, petroleum production and refining, sewer gas	Nuisance odor (rotten egg smell), headache and breathing difficulties (higher concentrations)	Control emissions from geothermal power plants, petroleum production and refining, sewers, sewage treatment plants

Table B.1 *Air pollution sources, health effects and possible control measures. Taken from the California Air Resources Board URL [CARB, 2003].*

Appendix C

PEMFC-Powered Prototype EVs

DaimlerChrysler

DaimlerChrysler unveiled the first fuel cell-powered modern vehicle in 1994. The prototype NECAR1 (New Electric Car) was essentially a large on-board laboratory (with ~ 800 kg of energy producing components) contained within a Mercedes-Benz transporter. Two years later, the NECAR2 prototype was demonstrated. A 50 kW PEMFC operating on H_2 powered this 6-seater Mercedes-Benz V-class vehicle. It achieved a top speed of 110 km h^{-1} and a driving range of 250 km (approximately equivalent to the range of a typical battery-powered EV). In 1997 the NEBUS (New Electric Bus) was demonstrated in small bus fleets. By the time the NECAR4 prototype (successor to the NECAR2) was completed in 1999, the fuel cell drive system had been sufficiently compacted to enable locating it in the floor of the Mercedes-Benz A-class vehicle. The NECAR4 EV operated on liquid hydrogen, achieved a top speed of 145 km h^{-1}, a range of 450 km and could accommodate up to 5 passengers [*DaimlerChrysler URL*]. In terms of acceleration, the NECAR4 could achieve a speed of 56 km h^{-1} in 6 seconds from a stationary position [*Koch, 1999*]. However, the cost of the NECAR4 was estimated at more than US$ 100000 in 1999 [*Koch, 1999*].

To enable fuel versatility, DaimlerChrysler also demonstrated a methanol-powered fuel cell EV, the NECAR3, in 1997. Methanol was reformed on-board to H_2 for PEMFC operation. Only 2 passengers could fit in the A-class vehicle due to the volume consumed by the 50 kW PEMFC system and large reformer, however it could travel about 400km and achieved a top speed of 120 km h^{-1}. The NECAR5 presented in November 2000 was the technological successor to the NECAR3. In

this modified EV, the methanol reformer was located beneath the car along with the PEMFC stack and electric drive system, allowing a smaller vehicle. The NECAR5 recently established a long-distance driving record of 5250 km for a fuel cell-powered vehicle. It was driven across the USA in 2002, from San Francisco to Washington, passing through snowy mountainous terrain over 2600 m in elevation, as well as through normal city traffic.

Toyota

Toyota has been involved in hybrid-PEMFC development since 1992. In 1997, Toyota unveiled their FCHV (fuel cell hybrid vehicle) in a RAV4 model 'SUV' (sports utility vehicle). Similar to DaimlerChrysler's NECAR3 (also demonstrated in 1997), the PEMFC stack operated on hydrogen reformed from methanol on-board the FCHV [*Kreith et al., 1999*]. The latest FCHV prototype consists of a 90 kW Toyota-developed PEMFC stack combined with a 109 hp electric motor in the RAV4 SUV. The PEMFC operates on hydrogen stored on board in four tanks (stored at 350 bar). The FCHV has a driving range of almost 300 km, a top speed of over 150 km h^{-1} and achieves 100 km per gallon petrol equivalent.

It is interesting that the newer PEMFC EV prototypes from both Toyota and DaimlerChrysler are fueled by hydrogen stored on-board, after both companies successfully displayed methanol reformate-fueled EVs in 1997 [*Kreith et al., 1999*]. This is possibly because EVs operating on methanol reformate are not classified as ZEVs, or possibly because of the lower fuel conversion efficiencies of such cells combined with a reformer- *ca.* 27% (*cf.* ~17% for the internal combustion engine) [*ibid.*].

Honda

Honda started fuel cell research in 1989 and have developed the FXC fuel cell-hybrid prototype. The FXC is a 4-seating EV with a 78 kW PEMFC stack and an 80 hp electric motor. The FXC also uses an ultracapacitor to store regenerative power[1]. The PEMFC operates on hydrogen (3.75 kg of H_2 stored at 350 bar), which apparently has a refueling time of only 3-5 min. The vehicle can achieve a top speed of 150 km h^{-1} and a range of 270 km. Honda also set up a solar-powered hydrogen refueling station at their Torrance, California headquarters in August 2001.

DaimlerChrysler, Toyota and Honda have all announced trials for small fleets of their 'market ready' EVs for testing under normal driving conditions around the world. In November 2002, DaimlerChrysler announced plans for testing 60 hybrid fuel cell cars for in the US, Europe, Japan and Singapore [*Hydrogen Fuel Cell Letter, 2002*]. On the 2 December 2002, both Toyota and Honda presented PEMFC-hybrid vehicles to the University of California (two of six EVs) and the Los Angeles City Hall (the first of five EVs), respectively [*ibid.*].

Ford

In August 1999, the Ford Motor Company opened the first hydrogen filling station in North America, in Dearborn, Michigan. The station reportedly cost $1.5 million [Garsten, *1999*]. The hydrogen station is for refueling Ford's P2000 and FCV prototype fuel cell cars. The Focus FCV has a Ballard 900 series stack and a driving range of 160 km. The Ford Motor Company is committed to a limited production of FCV vehicles by 2004.

[1] i.e. the power lost during breaking, around 50% of which may be harnessed on-board by an electric motor. Most EVs are expected to make use of this energy-saving functionality.

Ford have been developing their P2000 vehicle, having three prototypes- two hybrids (powered by a conventional engine and with batteries) and one PEMFC powered EV. The LSR hybrid is reportedly 40% lighter than the average mid-sized family sedan, and has a fuel efficiency of more than 60 miles to the gallon (using a small high-power battery to store additional energy); the PTH hybrid has more on-board batteries, making it heavier, but enabling an increase of 10% in fuel efficiency. The third alternative version of the P2000 incorporates a hydrogen-fueled PEMFC. The fuel cell-powered P2000 has a maximum speed of over 128 km h^{-1} and a driving range of around 160 km, powered by a Ballard Mark 700 series PEMFC stack [*Ford URL*].

General Motors

The Hy-Wire concept vehicle from GM is a further evolution of the Autonomy design, in a 5-seater sedan. An eleven-inch aluminium chassis is reported to contain the compressed hydrogen, PEMFC stack and all technical components. This 'skateboard'-like chassis will provide a low center of gravity and is believed to allow for large 'economies of scale', since 2 to 3 basic platforms can be used for the whole range of General Motors vehicles [*Hydrogen Fuel Cell Letter, 2002*].

The Hy-Wire is powered by a 94 kW PEMFC stack, situated near the radiator at the rear of the vehicle. The fuel cell operates an electric motor that drives the front wheels (future expectations include 'hubmotors' on each wheel, possibly enabling 4-wheel steering). The EV achieves a 100 km range at present, on 3 hydrogen tanks (at 350 bar; 700 bar tanks are currently under consideration). Refueling takes 5 min. The same fuel cell system achieved 160 km h^{-1} in the Zafira-based HydroGen 3 in 2001 [*Hydrogen Fuel Cell Letter, 2002*].

References

References

ABS (Australian Bureau of Statistics) URL=http://www.abs.gov.au, last updated 2 February 2001.

ADL (Arthur D. Little) Inc., "Cost Analysis of Fuel Cell System for Transportation, Baseline System Cost Estimate," 2000, URL=http://www.ott.doe.gov/pdfs/baseline_cost_model.pdf.

Appleby, A. J., US Pat. 4,610,938 (Sept. 9, 1986).

Appleby, A. J., *J. Power Sources* **53** (1995) 187.

Appleby, A. J., *Phil.Trans.R.Soc.Lond.A* **354** (1996) 1681.

Austin, L. G., "Fuel Cells: A Review of Government-Sponsored Research, 1950-1964," NASA SP-120, Washington, D.C., National Aeronautics and Space Administration, 1967.

Bagotzky, V. S., Vassilyev, Yu. B., Weber, J., and Pirtskhalava, J. N., *J. Electroanal. Chem.* **27** (1970) 31.

Bard, A. J., (Ed.), "Encyclopedia of the Electrochemistry of the Elements," vol. 6, Marcel Dekker, Inc., New York, 1976, Ch. 4.

Beden, B., Kadirgan, F., Lamy, C. and Leger, J. M., *J. Electroanal. Chem.* **127** (1981) 75.

Bockris, J. O'M., and Srinivasan, S., "Fuel cells: Their Electrochemistry," New York, McGraw-Hill, 1969.

Burns, L., Hydrogen Fuel Cell Letter, September 2002,
URL=http://www.hfcletter.com.

Cameron, D. S., *Platinum Metals Review* **41** (1997) 171.

CARB (California Air Resources Board) Fact Sheets, "California's Zero Emission Vehicle Program," 6 December 2001; "Zero Emission Vehicle Program Changes," 10 December 2001; "Local, State and Federal Zero-Emission Vehicle Incentives," 7 November 2002; "Fuel Cell Electric Vehicles," 30 May 2002;
URL=http://www.arb.ca.gov.

Castro Luna, A. M., Camara, G. A., Paganin, V. A., Ticianelli, E. A. and Gonzalez, E. R., *Electrochem. Comm.* **2** (2000) 222.

Cattaneo, C., Sanchez de Pinto, M. I., Mishima, H., López de Mishima, B. A., Lescano, D. and Cornaglia, L., *J. Electroanal. Chem.* **461** (1999) 32.

Chemodanov, A. N. and Kolotyrkin, Ya. M., Proc. 3rd European Symp. on Corrosion Inhibitors, Ferrara, Italy, (1970) 49.

Chialvo, A. C., Triaca, W. E. and Arvia, A. J., *J. Electroanal. Chem.* **146** (1983) 93.

Chin, D.-T. and Howard, P. D., *J. Electrochem. Soc.* **133** (1986) 2447.

Choi, K. H., Kim, H. S. and Lee, T. H., *J. Power Sources* **75** (1998) 230.

Choose Positive Energy URL=http://www.choose-positive-energy.org/.

Chrzanowski, W. and Wieckowski, A., *Langmuir* **13** (1997) 5974.

Commons, C., Jarrett, S., McKenzie, C., Moseley, W., Porter, M. and Williamson, M., "Heinemann Chemistry Two," 3rd ed., Melbourne, Chemistry Education Association, 1999.

Cramm, S., Friedrich, K. A., Geyzers, K.-P., Stimming, U., and Vogel, R., *Fresenius J. Anal. Chem.* **358** (1997) 189.

DaimlerChrysler, URL=http://www.daimlerchrysler.com/.

Delime, F., Léger, J. M. and Lamy, C., *J. Appl. Electrochem.* **28** (1998) 27.

Dickson, A., Thorpe, S., Harman, J., Donaldson, K. and Tedesco, L., "Australian Energy Outlook to 2019-20," ABARE (Australian Bureau of Agricultural and Resource Economics) Conference Paper 2001.27, ABARE project 1171, presented at the Australian Institute of Energy National Conference, Sydney, 22-23 November 2001, URL=http://www.abareconomics.com.

Egli, W. A., Visintin, A., Triaca, W. E. and Arvia, A. J., *Appl. Surf. Sci.* **68** (1993) 583.

E-TEK Company Catalog, 1996.

EVAA (Electric Vehicle Association of the Americas), "State laws and Regulations Impacting Electric Vehicles," 31 October 2002, URL=http://www.evaa.org/evaa/pages/state_enact.html.

Ford URL=http://www.ford.com/en/vehicles/specialtyVehicles/environmental/fuelCell/fordP2000.htm

Frelink, T., Visscher, W., and van Veen, J. A. R., *Surf. Sci.* **335** (1995) 353.

Fujiwara, N., Friedrich, K. A. and Stimming, U., *J. Electroanal. Chem.* **472** (1999) 120.

Garsten, E., "Ford opens first North American hydrogen fueling station," August 16 1999, URL=http://www.cnn.com/US/9908/16/fuel.cell.car/index.html.

Gasteiger, H. A., Marković, N., Ross, Jr., P. N. and Cairns, E. J., *J. Phys. Chem.* **97** (1993) 12020.

Gasteiger, H. A., Marković, N., Ross, Jr., P. N. and Cairns, E. J., *J. Electrochem. Soc.* **141** (1994) 1795.

Gerischer, H., in Bard, A. J. (Ed.), "Encyclopedia of the Electrochemistry of the Elements," vol. 4, Marcel Dekker, Inc., New York, 1975, Ch. 6.

Gloaguen, F. , Léger, J.-M. and Lamy, C., *J. Appl. Electrochem.* **27** (1997) 1052.

Greenpeace, URL=http://archive.greenpeace.org/~climate/climatemain.shtml.

Gottesfeld, S., "The Polymer Electrolyte Fuel Cell: Materials Issues in a Hydrogen Fueled Power Source," Los Alamos National Laboratory (LANL), URL=http://education.lanl.gov/resources/h2/gottesfeld/education.html.

Hamann, C. H., Hamnett, A. and Vielstich, W., "Electrochemistry," New York, Wiley-VCH, 1998.

Hadži-Jordanov, S., Angerstein-Kozlowska, H., Vuković, M. and Conway, B. E., *J. Phys. Chem.* **81** (1977) 2271.

Hatfield, C. B., *Nature* **387** (1997) 121.

Hepel, M., *J. Electrochem. Soc.* **145** (1998) 124.

Hodgson, A. W. E., Jacquinot, P., Jordan, L. R. and Hauser, P. C., *Anal. Chim. Acta* **393** (1999) 43-48.

Hogarth, M. P., Munk, J., Shukla, A. K. and Hamnett, A., *J. Appl. Electrochem.* **24** (1994) 85.

Hydrogen Fuel Cell Letter, URL=http://www.hfcletter.com.

IEA, "Renewables in Global Energy Supply: An IEA Fact Sheet," International Energy Agency, November 2002, URL=http://www.iea.org.

IPCC (Intergovernmental Panel on Climate Change), "Summary for Policymakers (Climate Change 2001: Synthesis Report)," a summary of the Third Assessment Report, 2001, URL=http://www.ipcc.ch/.

IPCS, "IPCS News: The Newsletter of the International Programme on Chemical Safety," Issue 2, October 1992, URL=http://www.who.int/pcs/newsletter/ipcs-02.pdf.

Itaya, K., Takahashi, H. and Uchida, I., *J. Electroanal. Chem.* **208** (1986) 373.

James, M., Stokes, R., Ng, W. and Moloney, J., "Chemical connections 2: VCE Chemistry Units 3 & 4," 2nd ed., Milton Queensland, John Wiley & Sons Australia Ltd., 2000.

Jordan, L. R., Shukla, A. K., Behrsing, T., Avery, N. R., Muddle, B. C. and Forsyth, M., *J. Appl. Electrochem.* **30** (2000) 641.

Kable, M., "Car Wars: Why Fuel Cells Will Win Out," *The Australian*, 17 June 1999, pp. 31-34.

Kerr, R. A., *Science* **281** (1998) 1128.

Kinoshita, K. and Stonehart, P., "Modern Aspects of Electrochemistry," Vol. 12, Plenum Press, New York, 1977.

Kinoshita, K., "Carbon: Electrochemical and Physiochemical Properties", New York, Wiley, 1988.

Koch, K., "DaimlerChrysler introduces car powered by fuel cells," March 17 1999, URL= http://www.cnn.com/NATURE/9903/17/fuel.cell.car/.

Koponen, U., Peltonen, T., Bergelin, M., Mennola, T., Valkiainen, M., Kaskimies, J. and Wasberg, M., *J. Power Sources* **86** (2000) 261.

Kreith, F., Potestio, D. S. and Kimbell, C., "Ground Transportation for the 21st Century," N.Y., The American Society of Mechanical Engineers, 1999.

Ley, K. L., Liu, R., Pu, C., Fan, Q., Leyarovska, N., Segre, C. and Smotkin, E. S., *J. Electrochem. Soc.* **144** (1997) 1543.

Lezna, R. O., De Tacconi, N. R. and Arvía, A. J., *J. Electroanal. Chem.* **151** (1983) 193.

Lin, W. F., Zei, M. S., Eiswirth, M., Ertl, G., Iwasita, T. and Vielstich, W., *J. Phys. Chem. B* **103** (1999) 6968.

Lin-Cai, J. and Pletcher, D., *J. Electroanal. Chem.* **149** (1983) 237.

Liu, R., Her, W.-H. and Fedkiw, P. S., *J. Electrochem. Soc.* **139** (1992) 15.

Lomborg, B., "The Skeptical Environmentalist," Cambridge, UK, Cambridge University Press, 2001.

López de Mishima, B. A., Mishima, H. T. and Castro, G., *Electrochim. Acta* **40** (1995) 2491.

Loucka, T., *J. Electroanal. Chem.* **31** (1971) 319.

Mabbott, G. A., *J. Chem. Ed.* **60** (1983) 697.

McEvoy, A. J., "Fuel Cell Technology Status and Prospects for EPFL Part-I," URL=http://dcwww.epfl.ch/icp/ICP-2/fcell1.html.

McNicol, B. D., Rand, D. A. J. and Williams, K. R., *J. Power Sources* **83** (1999) 15.

McMichael, A. J., *British Medical Journal* **325** (2002) 1465.

Mikhaylova, A. A., Khazova, O. A. and Bagotzky, V. S., *J. Electroanal. Chem.* **480** (2000) 225.

Millet, P., Andolfatto, F. and Durand, R., *J. Appl. Electrochem.* **25** (1995) 227; 233.

Millet, P., Pineri, M. and Durand, R., *J. Appl. Electrochem.* **19** (1989) 162.

Moore, W. J., "Basic Physical Chemistry," New Jersey, Prentice/Hall International Inc., 1983.

Motavalli, J., "Forward Drive," San Francisco, Sierra Club Books, 2000.

O'Connell, P. J., O'Sullivan, C. K. and Guilbault, G. G., *Analytica Chimica Acta* **373** (1998) 261.

Oniciu, L., "Fuel Cells," Kent, UK, Abacus Press, 1976.

Pachauri, R. K., Chairman of the IPCC (Intergovernmental Panel on Climate Change), Keynote Address, World Summit on Sustainable Development, Johannesburg, 1 September 2002, URL=http://www.ipcc.ch/.

Passalacqua, E., Lufrano, F., Squadrito, G., Patti, A. and Giorgi, L., *Electrochim. Acta* **43** (1998) 3665.

Penven, R. L., Levason, W. and Pletcher, D., *J. Appl. Electrochem.* **22** (1992) 415.

Petrow, H. G. and Allen, R. J., US Patent 4,044,193, 1977.

Pianin, E., Washington Post, New York Times, as reported in The Age, "Celebrated Author Accused of Bias," 9 January 2003, p. 7.

Pourbaix, M., "Atlas of Electrochemical Equilibria in Aqueous Solutions," 1st ed., London, Pergamon Press, 1966.

Raistrick, I. D., US Pat. 4,876,115 (Oct. 24, 1989).

Ravikumar, M. K. and Shukla, A. K., *J. Electrochem. Soc.* **143** (1996) 2601.

Reddington, E., Sapienza, A., Gurau, B., Viswanathan, R., Sarangapani, S., Smotkin, E. S. and Mallouk, T. E., *Science* **280** (1998) 1735.

Ren, X. and Gottesfeld, S., *J. Electrochem. Soc.* **148** (2001) A87.

Ren, X., Wilson, M. S. and Gottesfeld, S., *J. Electrochem. Soc.* **143** (1996) L12.

Richarz, F., Wohlmann, B., Vogel, U., Hoffschulz, H. and Wandelt, K., *Surf. Sci.* **335** (1995) 361.

Rogers, D. K., US Patent 4,379,034, 1983.

Rosental', K. I., Veselovskij, V. I., *Zh. Fiz. Khim.* **27** (1953) 1163.

Savadogo, O., *J. New. Mat. Electrochem. Systems (I)* (1998) 47.

Sheppard, S.-A., Campbell, S. A., Smith, J. R., Lloyd, G. W., Ralph, T. R. and Walsh, F. C., *Analyst* **123** (1998) 1923.

Shimazu, K., Weisshaar, D. and Kuwana, T., *J. Electroanal. Chem.* **223** (1987) 223.

Shimazu, K., Uosaki, K. and Kita, H., *J. Electroanal. Chem.* **256** (1988) 481.

Shiroishi, H., Sayama, H., Moroi, T. and Kaneko, M., *J. Electroanal. Chem.* **502** (2001) 132.

Shukla, A. K. and Manoharan, R., Indian Patent 170,423, 1992.

Shukla, A. K., Ravikumar, M. K. and Gandhi, K. S., *J. Solid State Electrochem.* **2** (1998) 117.

Skou, E. M., *Acta Chem. Scand.* **27** (1973) 2239.

Souza, J. P. I., Botelho Rabelo, F. J., de Moraes, I. R. and Nart, F. C. *J. Electroanal. Chem.* **420** (1997) 17.

Srinivasan, S., Velev, O. A., Parthasarathy, A., Manko, D. J. and Appleby, A. J., "Space Electrochemical Research and Technology (SERT) 1991," NASA Conference Publication 3125 (1991).

Stonehart, P., *Ber. Bunsenges. Phys. Chem.* **94**, (1990) 913.

Strbac, S., Maroun, F., Magnussen, O. M. and Behm, R. J., *J. Electroanal. Chem.* **500** (2001) 479.

Szabó, S. and Bakos, I., *J. Electroanal. Chem.* **230** (1987) 233.

Taylor, E. J., Anderson, E. B. and Vilambi, N. R. K., *J. Electrochem. Soc.* **139** (1992) L45.

Thomas, S. and Zalbowitz, M., "Fuel Cells- Green Power," Los Alamos National Laboratory (LANL) URL=http://education.lanl.gov/resources/fuelcells/.

Tremiliosi-Filho, G., Kim, H., Chrzanowski, W. Wieckowski, A., Grzybowska, B. and Kulesza, P., *J. Electroanal. Chem.* **467** (1999) 143.

Triaca, W. E. and Arvia, A. J., *J. Appl. Electrochem.* **20** (1990) 347.

Uchida, M., Aoyama, Y., Eda, N. and Ohta, A., *J. Electrochem. Soc.* **142** (1995) 463; 4143.

UNESCO (United Nations Educational, Scientific and Cultural Organization), "Fuel Cells: Trends in Research and Applications," (Ravello, Italy, 10-14 June 1985), Primart, Paris, 1985, pp.34-6.

US EPA (Environment Protection Agency), "Vehicle Fuels and the 1990 Clean Air Act," EPA 400-F-920015, August 1994, Fact Sheet OMS-13, URL=http://www.epa.gov/ otaq/13-fuels.htm.

Valensi, G., van Muilder, J., Pourbaix, M., in Bard, A. J. (Ed.), "Encyclopedia of the Electrochemistry of the Elements," vol. 4, Marcel Dekker, Inc., New York, 1975, Ch. 6.

Verbrugge, M. W., *J. Electrochem. Soc.* **141** (1994) 46.

Vigier, F., Gloaguen, F., Léger, J.-M. and Lamy, C., *Electrochim. Acta.* **46** (2001) 4331.

Vilambi, N. R. K., Anderson, E. B. and Taylor, E. J., US Patent, 5,084,144, 1992.

Visintin, A., Canullo, J. C., Triaca, W. E. and Arvia, A. J., *J. Electroanal. Chem.* **267** (1989) 191.

Vuković, M., *J. Chem. Soc. Faraday Trans.* **86** (1990) 3743.

Watanabe, M. and Motoo, S., *J. Electroanal. Chem.* **60** (1975) 267.

White, J. H. and Sammells, A. F., *J. Electrochem. Soc.* **140** (1993) 2167.

WHO (World Health Organisation), Environmental Health URL=http://www.who.int/environmental_information/index.html.

Will, F. G., *J. Electrochem. Soc.* **112** (1965) 451.

Williams, J. O. and Mahmood, T., *Applications of Surface Science* **6** (1980) 62.

Wilson, M. S. and Gottesfeld, S., *J. Appl. Electrochem.* **22** (1992) 1.

Wilson, M. S. and Gottesfeld, S., *J. Electrochem. Soc.* **139** (1992) L28.

Wilson, M. S., Valerio, J. A. and Gottesfeld, S., *Electrochim. Acta* **40** (1995) 355.

Sheik Yamani (to Reuters), 25 June 2000, URL=http://www.cbsnews.com/stories/2000/06/25/world/printable209367.shtml.

Ye, S., Vijh, A. K. and Dao, L. H., *J. Electrochem. Soc.* **143** (1996) L7.

Ye, J.-H. and Fedkiw, P. S., *Electrochim. Acta.* **41** (1996) 221.

Zinola, C. F. and Castro Luna, A. M., *J. Electroanal. Chem.* **456** (1998) 37-46.